Fall 2011

Assessment of co-processing of cellulose II and silicon dioxide as a platform to enhance excipient functionality

Jhon Jairo Rojas Camargo
University of Iowa

ASSESSMENT OF CO-PROCESSING OF CELLULOSE II AND SILICON DIOXIDE AS A PLATFORM TO ENHANCE EXCIPIENT FUNCTIONALITY

by

Jhon Jairo Rojas Camargo

An Abstract
Of a thesis submitted in partial fulfillment
of the requirements for the Doctor of
Philosophy degree in Pharmacy
in the Graduate College of
The University of Iowa

December 2011

Thesis Supervisor: Professor Douglas R. Flanagan

ABSTRACT

This thesis project studied microcrystalline cellulose II (CII), a polymorphic form of cellulose, which has lower mechanical properties, less plastic deformation, higher elastic recovery and faster disintegration properties than microcrystalline cellulose I (CI). Also, the effects of processing and silicification on CII materials were investigated.

Particle modification through spray drying, wet granulation and spheronization was employed to improve CII performance. Spray-drying (SDCII) and wet granulation (WGCII) produced materials with no difference in mechanical or disintegration properties from unprocessed CII, but did show an increase in density and particle flow. Conversely, spheronization (SPCII) showed the poorest mechanical properties compared to CII. Further, SDCII showed better dilution potential than CII. Thus the advantages of SDCII were apparent when it was mixed with a poorly compressible drug (acetaminophen) because fibrous CII was converted to spheroidal particles through spray drying. The rapid disintegration of SDCII and CII compacts was due to water wicking through capillaries followed by compact bursting. Compacts of ibuprofen mixed with SDCII and Avicel® PH-102 had comparable disintegration rates and release profiles compared to ibuprofen formulated with commercial disintegrants and Avicel® PH-102, especially at levels ≥10% w/w.

Adding fumed silica into CII particles through spray drying, wet granulation (WGCII) and spheronization (SPCII) at 2-20% w/w was also studied. Silicification increased physical properties such as true density, Hausner ratio, porosity, ejection force and specific surface area of SDCII and WGCII. Other properties such as bulk and tap densities were reduced due to the amorphous and light character of fumed silica. Spheronized CII showed no change in these properties with silicification. Silicification diminished lubricant sensitivity with magnesium stearate due to the competition of SiO_2 with magnesium stearate to coat CII particles.

Silicification also decreased the affinity of CII for water only at the 20% w/w level due to the few silanol groups available for water interaction compared to surface hydroxyl groups on CII alone. Particle size modification of CII was process-dependent

rather than silicification-dependent. Additionally, silicification decreased the apparent plasticity and elastic recovery of SDCII and WGCII when compacted. The former effect along with increased powder porosity increased surface area and compressibility of SDCII and WGCII. Compact tensile strength of silicified CII materials was in the order: spray-dried > wet granulated > spheronized. This order was due to the combined effect of particle morphology and how fumed silica was incorporated and distributed within CII particles. Silicification did not affect the rapid disintegration properties of CII. Thus, diphenhydramine HCl and griseofulvin tablets prepared with silicified CII had faster disintegration and release than those prepared with commercial silicified CI (Prosolv®). Moreover, CII beads containing diphenhydramine HCl or griseofulvin had faster release profiles compared to beads prepared with Prosolv® SMCC 50 or Avicel® PH-101. This behavior showed that rapid disintegration is an intrinsic property of CII.

Compact tensile strength decreased more for unsilicified CI and CII compacts stored at ≥75% RH, while silicified CI and CII compacts lost less tensile strength under the same conditions. Reprocessed CI materials containing acetaminophen (1:1mixtures) lost 35-72% of their original strength compared to silicified CII materials (15-25% loss) indicating more particle interaction upon recompression.

Abstract Approved:

_____

Thesis Supervisor

_____

Title and Department

_____

Date

ASSESSMENT OF CO-PROCESSING OF CELLULOSE II AND SILICON DIOXIDE AS A PLATFORM TO ENHANCE EXCIPIENT FUNCTIONALITY

by

Jhon Jairo Rojas Camargo

A thesis submitted in partial fulfillment
of the requirements for the Doctor of
Philosophy degree in Pharmacy
in the Graduate College of
The University of Iowa

December 2011

Thesis Supervisor: Professor Douglas R. Flanagan

Graduate College
The University of Iowa
Iowa City, Iowa

CERTIFICATE OF APPROVAL

_____

PH.D. THESIS

_____

This is to certify that the Ph.D. thesis of

Jhon Jairo Rojas Camargo

has been approved by the Examining Committee for the thesis requirement for the Doctor of Philosophy degree in Pharmacy at the December 2011 graduation.

Thesis Committee:

_____
Douglas R. Flanagan, Thesis Supervisor

_____
Dale Eric Wurster

_____
Jennifer Fiegel

_____
Maureen D. Donovan

_____
Mickey L. Wells

To my parents Lucia and Jairo and my siblings Lucy, Zaira and Jose.

Anyone who has never made a mistake has never tried anything new.

Albert Einstein (1879-1955)

ACKNOWLEDGMENTS

I would like to thank the following people because they were essential to me, fulfilling my academic and professional goals during my doctorate studies:

First my first adviser, Dr. Vijay Kumar, I express to him my deepest gratitude for his teaching, philosophy and wise counseling. His guidance, support and availability were crucial in my studies, especially in times of discouragement and frustration. Throughout out all these years he was a good model of honesty, discipline, humbleness, hard work and diplomacy. Thanks for teaching me these important virtues that have transformed my life at The University of Iowa. I would like to thank Dr. Flanagan for taking over my thesis providing the final changes, comments and scientific critique to promote this document.

I also want to thank the committee members of my thesis: Dr. Donovan, Dr. Fiegel, Dr. Flanagan, Dr. Wells and Dr. Wurster. I appreciate their time and commitment provided to this thesis. I am very pleased and honored by their presence and the quality time they spent in evaluating the results hereby presented. Their expertise, feedback and suggestions have been valuable and contributed to my scientific development. I give special thanks to Dr. Wurster for allowing me to use equipment in his laboratory. I also express my gratitude to Dr. Poust for serving in my comprehensive examination committee. I also thank Dr. Carvajal and Dr. Smith at Purdue University for their help and guidance during my visit to Purdue to conduct extrusion-spheronization experiments. I also appreciate the excellent training given by Mr. Nessler and Dr. Swenson in the scanning electron microscopic and X-rays laboratories, respectively.

I would like to acknowledge all the faculty members of the Division of Pharmaceutics and Translational Therapeutics for their technical teaching, which promotes scientific development, critical thinking and a problem solving base. It

transformed my vision of the role of pharmaceutics and physical pharmacy for drug development. I also appreciate their financial support and the initial support provided by University of Antioquia, especially to Professors Tobon and Bedoya. I also express my gratitude to Dr. Reist for his trust, support and teaching me the value of professionalism and personalized pedagogy in the Pharmacy Practice Laboratory.

I also thank not only all the members of my research group, but my friends in the College of Pharmacy, especially Dr. Ira Buckner, Bhavik Bhatt, Ross Friedman, Stacy Ross, Dave Bress, Baltazar Silvan and Allan Raymond for their friendship and assistance in my project. I also thank my friends in the College of Medicine and Departments of Chemistry and Spanish for making my life pleasant, their friendship, acceptance and showing me the cultural values of this great nation.

TABLE OF CONTENTS

LIST OF TABLES x

LIST OF FIGURES xiii

LIST OF ABBREVIATION xx

CHAPTER

I INTRODUCTION..... 1

Solid Dosage Forms 1
Direct Compression (DC) 3
Attributes of an Ideal Direct Compression Excipient 5
Direct Compression Excipient Examples 7
Need for New Excipients..... 9
New Excipients Sources..... 13
Particle Engineering as Source of New Excipients..... 16
Excipient Co-Processing as a Source of New Excipients 19
Role of Material Science in Co-processing 20
Co-Processed Excipients 21
Powder Compaction and Particle Bonding..... 26
Powder Consolidation Models..... 27
Factors that Affect the Mechanical Properties of Powders 31
Cellulose II Allomorph as a Direct Compressive Agent..... 31
Spray Drying to Engineer Functional Properties of Cellulose ... 36
Amorphous SiO_2 as a Co-Processing Agent for CII..... 36
Co-processing of Cellulose with Fumed Silica 37

II OBJECTIVES 39

Primary Objective # 1 39
Specific Objectives..... 39
Primary Objective # 2..... 40
Specific Objectives..... 40
Primary Objective # 3..... 40
Specific Objectives..... 40

III EXPERIMENTAL SECTION..... 42

Materials 42
Methods 44
Preparation of Unprocessed Cellulose II Powders (CII) ... 44
Preparation of Spray-Dried Cellulose II (SDCII)..... 44
The Spray Drying Process 44
Statistical Experimental Protocol..... 46
Pilot Scale Preparation of SDCII Powder..... 49

Particle Size and Particle Size Distribution Analyses of SDCII 50
Moisture Content (MC) 51
Fumed Silica Content 51
Fourier-Transform Infrared Spectroscopy (FT-IR) 52
Swelling Studies (Swelling Value) 52
Water Uptake Analysis of SDCII and CII 53
CII-SiO_2 Composites Prepared by Spray Drying 53
CII-SiO_2 Composites Prepared by Wet Granulation 55
CII-SiO_2 Composites Prepared by Spheronization 56
Preparation of Excipient-Griseofulvin and Excipient-Diphenhydramine·HCl Beads by Spheronization 56
Particle Size and Particle Size Distribution of Composite Materials 57
True Density Determination 58
Bulk/Tap Densities, Powder Porosity and Hausner Ratio 58
Powder Flow Measurements 60
Degree of Crystallinity (DC) 60
Degree of Polymerization 62
Water Sorption Analysis 63
Surface Area Measurements 65
Scaning Electron Microscopy (SEM) 68
Energy Dispersive X-ray Spectroscopy (EDX) 68
Tableting Properties 68
Cylindrical Compacts and Determination and Compact Porosity 68
Compact Water Sorption Ratio 70
Compressibility Analysis 70
Kawakita Analysis 71
Compact Elastic Relaxation 71
Tablets for Disintegration Studies 72
Ibuprofen Dissolution Studies 72
Compact Crushing Strength 74
Dilution Potential of SDCII and CII 75
Lubricant Sensitivity of CII and SDCII 75
Lubricant Sensitivity of CII-SiO_2 Composites 75
Load-Deflection Curves and Diametric Compression of CII:SiO_2 Composites 76
Compact Friability 77
Beads Friability 78
Disintegration Studies 78
Griseofulvin Release Studies 79
Diphenhydramine·HCl Release Studies 80
Preparation of Square Compacts 81
Load-Deflection Curves and Brittle Fracture Index 82
Stress-Strain Curves of Compacts 82
Cylindrical Compacts for Moisture Sorption Studies 85
Mechanical Properties of the Compacts Stored as a Function of Humidity 85
Preparation of the Relative Humidity Chambers 85
Compacts Reprocessability 87

Compacts Specific Surface Areas 87

IV RESULTS AND DISCUSSION 90

Preparation and Tableting Properties of SDCII for Direct Compression 90
Cellulose II Preparation (CII) 91
Spray-Dried Cellulose II Preparation (SDCII) 97
Fractional Factorial Study of Spray Drying Conditions 99
Box Behnken Design for Spray Drying Optimization 104
Carbohydrate Excipient Powder Properties 111
Compression and Compaction Characteristics of Carbohydrate Excipients 121
Lubricant Sensitivity 133
Compact Disintegration 136
Evaluation of Disintegration Properties of CII, SDCII and Commercial Disintegrants 139
Powder Properties 140
CII-SiO_2 Composites 166
Preparation and Characterization 166
Powder Properties 173
Particle Size Distribution 173
Morphological Characterization 176
Principal Component Analysis 198
Water Sorption Characteristics 203
Swelling Studies 215
Tableting Properties 217
Compaction Characteristics 217
Load-Deformation Curves and Diametral Compression Test 226
Compression Characteristics 230
Heckel Analysis 230
Kawakita Analysis 235
Compact Elastic Recovery 239
Lubricant Sensitivity to Magnesium Stearate 240
Compact Disintegration 244
Bead Friability and Disintegration 249
Diphenhydramine HCl and Griseofulvin Beads Preparation with Cellulosic Excipients 252
Drug Release Studies from Beads of Cellulosic Excipients 254
Dissolution of Diphenhydramine HCl Compacts 259
Dissolution of Griseofulvin Compacts 262
Further Compact Studies 265
Compacts at Different Relative Humidities 266
Brittle Fracture Index 271

V CONCLUSIONS 280

Future Directions 285

APPENDIX A. CALIBRATION CURVES FOR DRUGS EMPLOYED IN DISSOLUTION STUDIES……...….286

APPENDIX B. ANOVA TEST FOR PARTICLE SIZE OF CII AQUEOUS DISPERSIONS…….……289

The ANOVA Test Results……....290

APPENDIX C. RESPONSE SURFACE ANALYSIS OF THE TENSILE STRENGTH AS A FUNCTION OF RELATIVE HUMIDITY AND TIME …….292

Modeling Tensiles Strength Data According to a Response Surface Methodology…… ..... …293

APPENDIX D. TENSILE STRENGTH OF REPROCESSED MATERIALS…….307

Reprocessing Susceptibility ..... ….308
Tukey Test for the Tensile Strength of Reprocessed Materials ..... ….312

REFERENCES……315

LIST OF TABLES

Table		
I-1.	Direct Compression Excipients: Advantages and Disadvantages	10
I-2.	Commercial and Investigational Co-processed Cellulosic Excipients	22
I-3.	Salient Feasures of Co-Processed Cellulosic Excipients	23
III-1.	List of the Materials Employed	42
III-2.	Tablet Compositions	73
III-3.	Composition of Compacts Made with Ibuprofen and Disintegrants	73
III-4.	Salt Solutions for Relative Humidity Chambers	86
IV-1.	Crystallinity and Degree of Polymerization of CII and Cotton Linter	96
IV-2.	Effect of Homogenization and Colloid Mill on Particle Size	98
IV-3.	CII Spray Drying Conditions and Results from the Fractional Factorial Design for Yield and Particle Size	100
IV-4.	Coefficient Estimates and *t-test* Results from the Fractional Factorial Design for Yield and Particle Size	101
IV-5.	Spray Drying Conditions and Results for Box Behnken Design (BBD)	106
IV-6.	Coefficient Estimates and t-test Results from Box Behnken Analysis for Yield	107
IV-7.	Analysis of Variance from Box Behnken Analysis	109
IV-8.	Validation of the Box Behnken Model for Yield under Optimal Operating Conditions	110
IV-9.	FT-IR Bands Obtained for Cellulosics and their Assignments	114
IV-10.	Carbohydrate Excipient Powder Properties	117
IV-11.	Out-of-Die Heckel Results	123
IV-12.	Powder Properties of CII, SDCII and Commercial Disintegrants	143
IV-13.	Disintegrant Effects on Properties of Ibuprofen Compacts	162

IV-14. Geometric Mean Diameter of Cellulosic Composites and Commercial Cellulose I Materials 169

IV-15. Powder Properties of CII, Spray-Dried Materials and Prosolv® SMCC 50 (silicified microcrystalline cellulose I) 192

IV-16. Powder Properties of CII, Wet Granulated Materials and Prosolv® SMCC 90 (silicified microcrystalline cellulose I) 193

IV-17. Powder Properties of CII, Spheronized Materials and CP-203® (spheronized microcrystalline cellulose I) 194

IV-18. Parameters Obtained from the GAB Model for the Spray-Dried Materials and Prosolv® SMCC 50 (silicified microcrystalline cellulose I) 206

IV-19. Parameters Obtained from the GAB Model for Wet Granulated Materials and Prosolv® SMCC 90 (silicified microcrystalline cellulose I) 207

IV-20. Parameters Obtained from the GAB Model for Spheronized Materials and CP-203® (spheronized microcrystalline cellulose I) 210

IV-21. Parameters from the Leuenberger Model for CII, Spray-Dried, Wet Granulated CII:SiO_2 and Prosolvs® (silicified microcrystalline cellulose I) Materials 220

IV-22. Heckel Parameters for CII, Spray-Dried and Wet Granulated CII:SiO_2 Materials and Prosolv® (silicified microcrystalline cellulose I) 232

IV-23. Kawakita Parameters for CII, Spray-Dried and Wet Granulated CII:SiO_2 Materials and Prosolv® (silicified microcrystalline cellulose I) . 238

IV-24. Bead Friability and Disintegration of CII, Spheronized CII:SiO_2 and CP-203® (spheronized microcrystalline cellulose I) 250

IV-25. Properties of Diphenhydramine HCl or Griseofulvin Cellulosic Beads 253

IV-26. Mechanical Properties Derived from the Stress-Strain Curves of the Square Compacts (3.84 cm^2) of Cellulose II and Commercial Cellulose I (Avicel® and Prosolv®) 273

IV-27. Bonding Specific Surface Area (1.1 cm dia. round compacts) of Cellulose II and Commercial Cellulose I (Avicel® and Prosolv®) 279

B1. ANOVA Test for Cellulosic Dispersions (see Table IV-2) 291

C1. Coefficients of the Quadratic Model from Response Surface Analysis for Tensile Strength as a Function of RH and Time 295

C2. ANOVA Analysis for Response Surface Methodology for Tensile Strength as a Function of RH and Time 298

D1. ANOVA Table and Tukey Test for Tensile Strength of Reprocessed Cellulose II and Commercial Cellulose I (Avicel® and Prosolv®) Materials 313

LIST OF FIGURES

Figure		Page
I-1.	Deformation Mechanism upon Compression	8
I-2.	Material Effects on Derived Formulation Properties	14
I-3.	Various Heckel Plots: (A) Plastic Material at Two Size Fractions; (B) Fragmenting Material; (C) Mixture of Wax and Lactose Reaching Complete Densifications at Low Pressures (adapted from Fassihi, 1988)	29
I-4.	Scheme for Producing Cellulose Allomorphs	33
I-5.	Conformations of Cellulose I (A) and Cellulose II (B) (adapted from Klemm et al., 1998a)	34
I-6.	SEM of Fumed Silica Aggregates at 110,000 Magnification (adapted from Cabot Corp, 2004)	38
I-7.	Hydrogen Bonding between SiO_2 and Water (Adapted from Cabot Corp, 2004)	38
III-1.	Yamato Spray-Drier	45
III-2.	Schematic of an Air-Atomizing Nozzle	47
III-3.	Schematic of the Water Uptake Set-up	54
III-4.	Typical Powder X-ray Diffractogram of Cellulose II Showing Crystalline and Amorphous Regions	61
III-5.	Typical Stress-Strain Curves for Brittle (blue line) and Plastic Materials (purple line)	83
IV-1.	Powder XRD of CII Lots and Cotton Linter	93
IV-2.	Cellulose Hydrolysis Mechanism (adapted from Xiang et al., 2003)	95
IV-3.	Microstructure and Accessibility of Cellulose Microfibrils (adapted from Paako, 2010)	96
IV-4.	Plot for Yield Obtained from the Box Behken Design. Constant Factors: 0.44 m^3/min Drying Air Speed; 1.0 kg-f/cm^2 Atomization Air Pressure; 2.0 mL/min Feed Flow Rate; 711 µm Spray Nozzle Diameter. The Yellow Region of the Plot Represents the Optimal Temperature and Feed Concentration Ranges to Produce SDCII > 70% Yields	109

IV-5. Chemical Structure of: (A) CII, SDCII and Avicel® PH-102; (B) Starch 1500®; (C) Fast Flo® 316 Made with ChemSketch® v. 11.01 (advanced Chemical Development, Inc, Toronto) 112

IV-6. FT-IR Spectra of Carbohydrate Excipients: CII, SDCII, Fast Flo® 316 (lactose monohydrate), Starch 1500® (pregelatinized starch) and Avicel® PH-102 (microcrystalline cellulose I) 113

IV-7. Powder X-rays Diffractograms of Carbohydrate Excipients: CII, SDCII, Fast Flo® 316 (lactose monohydrate), Starch 1500® (pregelatinized starch) and Avicel® PH-102 (microcrystalline cellulose I)..... 116

IV-8. SEMs of SDCII and CII at 400X and 3,000X..... 118

IV-9. SEMs of Fast Flo® 316, Avicel® PH-102 and Starch 1500® at 400X and 3,000X..... 119

IV-10. Heckel Plots (out-of-die) for: (A) SDCII (spray-dried cellulose II) and unprocessed cellulose II (CII); (B) Fast Flo® 316 (lactose monohydrate), Starch 1500® (pregelatinized starch) and Avicel® PH-102 (microcrystalline cellulose I). Y-Axis Corresponds to the Inverse of Logarithm of Porosity..... 122

IV-11. Cross-sectional Images of CII and SDCII at: (A) 10 MPa; (B) 120 MPa; (C) 260 MPa Compression Pressures at 350X (scale bar, 100 µm)..... 127

IV-12. Cross-sectional Images of Commercial Carbohydrate Compacts at: (A) 10 MPa; (B) 120 MPa; (C) 260 MPa Compression Pressures at 350X (scale bar, 100 µm) 128

IV-13. Crushing Strength of Carbohydrate Excipient Compacts: CII, SDCII, Fast Flo® 316 (lactose monohydrate), Starch 1500® (pregelatinized starch) and Avicel® PH-102 (microcrystalline cellulose I)..... 130

IV-14. Friability of Carbohydrate Excipient Compacts: CII, SDCII, Fast Flo® 316 (lactose monohydrate), Starch 1500® (pregelatinized starch) and Avicel® PH-102 (microcrystalline cellulose I)..... 132

IV-15. Dilution Potential of Carbohydrate Excipient Compacts: CII, SDCII, Fast Flo® 316 (lactose monohydrate), Starch 1500® (pregelatinized starch) and Avicel® PH-102 (microcrystalline cellulose I)..... 132

IV-16. Sensitivity of Carbohydrate Excipient Compacts to Magnesium Stearate CII, SDCII, Fast Flo® 316 (lactose monohydrate), Starch 1500® (pregelatinized starch) and Avicel® PH-102 (microcrystalline cellulose I)..... 135

IV-17. Disintegration Profiles of Carbohydrate Excipient Compacts: CII, SDCII, Fast Flo® 316 (lactose monohydrate), Starch 1500® (pregelatinized starch) and Avicel® PH-102 (microcrystalline cellulose I)..... 137

IV-18. Chemical Structures of Disintegrants Made with ChemSketch v. 11.01 (Advanced Chemistry Development, Inc, Toronto, Canada)..... 141

IV-19. PXRD Characterization of Disintegrants: Ac-Di-Sol® (sodium carboxymethyl cellulose), Polyplasdone® XL (crospovidone) and Primojel® (sodium starch glycolate)..... 141

IV-20. SEM Images of Water Wicking Materials at 400X and 10,000X Magnifications..... 144

IV-21. SEM Images of Swelling Disintegrants at 400X and 10,000X Magnifications..... 145

IV-22. Swelling Values of SDCII, CII and Commercial Disintegrants: Ac-Di-Sol® (sodium carboxymethyl cellulose), Primojel® (sodium starch glycolate) and Polyplasdone® XL (crospovidone) 147

IV-23. Water Uptake of SDCII, CII and Commercial Disintegrants: Ac-Di-Sol® (sodium carboxymethyl cellulose), Primojel® (sodium starch glycolate) and Polyplasdone® XL (crospovidone) 149

IV-24. Disintegration Time/Crushing Strength Ratio as a Function of Compact Porosity of: Ac-Di-Sol® (sodium carboxymethyl cellulose), Primojel® (sodium starch glycolate) and Polyplasdone® XL (crospovidone) 152

IV-25. Disintegration Time of Compacts in Distilled Water and 0.1 N HCl of: Ac-Di-Sol® (sodium carboxymethyl cellulose), Primojel® (sodium starch glycolate) and Polyplasdone® XL (crospovidone) 155

IV-26. Disintegrant Level Effects on Disintegration Time of Direct Compression Excipients: (A) SDCII (spray-dried cellulose II) and (B) CII (unprocessed cellulose II) 157

IV-27. Disintegrant Level Effects on Disintegration Time of Direct Compression Excipients: (A) Polyplasdone® XL (crospovidone) and (B) Ac-Di-Sol® (sodium carboxymethyl cellulose) and (C) Primojel® (sodium starch glycolate)..... 158

IV-28. Effect of Disintegrant Levels on the Ibuprofen Release Profiles (A) 5%; (B) 10%; (C) 20% of: Ac-Di-Sol® (sodium carboxymethyl cellulose), Primojel® (sodium starch glycolate) and Polyplasdone® XL (crospovidone)..... 164

IV-29. Powder X-ray Diffractograms of CII, Prosolv® SMCC 50 (silicified microcrystaline cellulose I) and Spray-Dried Materials..... 170

IV-30. Powder X-ray Diffractograms of CII, Prosolv® SMCC 90 (silicified microcrystaline cellulose I), and Wet Granulated Materials..... 171

IV-31. Powder X-ray Diffractograms of CII, CP-203® (spheronized microcrystalline cellulose I) and Spheronized Materials..... 172

IV-32. Particle Size Distribution of CII, CII-SiO_2 Composites, Prosolv® (silicifed microcrystalline cellulose I) and CP-203® (spheronized cellulose I) Determined by Sieve Analysis 174

IV-33. Log-Probability Plots of CII-SiO_2 Materials and Commercial Cellulosic Materials (produced by the Minitab® software)..... 175

IV-34. SEMs of CII and Commercial Products: Prosolv® (silicifed microcrystalline cellulose I), CP-203® (spheronized cellulose I) at 50X and 10,000X 177

IV-35. EDS Showing SiO_2 Distribution on the Surface of Prosolv® (silicifed microcrystalline cellulose I) at 1,400X..... 178

IV-36. SEMs of Spray-Dried CII with Various Ratios of SiO_2 at 50X..... 180

IV-37. SEMs of Spray-Dried CII with Various Ratios of SiO_2 at 10,000X 181

IV-38. EDS Images Showing SiO_2 Distribution of on the Surface of SD-CII:SiO_2 Composites 182

IV-39. SEMs of Wet Granulated CII:SiO_2 Composites at 50X 184

IV-40. SEMs of Wet Granulated CII:SiO_2 Composites at 10,000X 185

IV-41. EDS Showing SiO_2 Distribution on the Surface of Wet Granulated CII:SiO_2 Composites 186

IV-42. SEM Microphotographs of Spheronized Products at 50X 188

IV-43. SEM Microphotographs of Spheronized Products at 10,000X 189

IV-44. SiO_2 Distribution (red spots) in: (A) Spheronized Bead Core; (B) Bead Surface 190

IV-45. Loading Plot of Measured Properties of CII and CII:SiO_2 Composites 200

IV-46. PCA Score Plot of Measured Properties of CII and CII:SiO_2 Composites..... 202

IV-47. Fitted Water Sorption Isotherms of the Spray-Dried Materials According to the GAB Model 204

IV-48. Fitted Water Sorption Isotherms of the Wet Granulated Materials According to the GAB Model 204

IV-49. Fitted Water Sorption Isotherms of the Spheronized Materials According to the GAB Model 209

IV-50. Effect of Silicification on the Specific Surface Area of CII 214

IV-51. Swelling Values of CII, Spray-Dried Materials and Prosolv® SMCC 50 (silicified microcrystalline cellulose I) 216

IV-52. Swelling Values of CII, Wet Granulated Materials and Prosolv® SMCC 90 (silicified microcrystalline cellulose I) 216

IV-53. Swelling Values of CII, Spheronized Materials and CP-203® (spheronized cellulose I) 218

IV-54. Tensile Strength of Compacts Made of CII, Spray-Dried CII:SiO_2 Materials and Prosolv® SMCC 50 (silicified microcrystalline cellulose I) 219

IV-55. Tensile Strength of Compacts Made of CII, Wet Granulated CII:SiO_2 Materials and Prosolv® SMCC 90 (silicified microcrystalline cellulose I) 222

IV-56. Crushing Strength of Compacts Made of CII, Spheronized Materials and CP-203® (spheronized cellulose I) 225

IV-57. Load-Deformation Curves of CII, Spray-Dried Materials and Prosolv® SMCC 50 (silicified microcrystalline cellulose I) Made at 120 MPa 227

IV-58. Load-Deformation Curves of the CII, Wet Granulated Materials and Prosolv® SMCC 90 (silicified microcrystalline cellulose I) Made at 120 MPa 227

IV-59. Heckel Plots for CII, Spray-Dried Materials and Prosolv® SMCC 50 (silicified microcrystalline cellulose I) 231

IV-60. Heckel Plots for CII, Wet Granulated Materials and Prosolv® SMCC 90 (silicified microcrystalline cellulose I) 231

IV-61. Kawakita Plots for CII, Spray-Dried Materials and Prosolv® SMCC 50 (silicified microcrystalline cellulose I) 237

IV-62. Kawakita Plots for CII, Wet Granulated Materials and Prosolv® SMCC 90 (silicified microcrystalline cellulose I) 237

IV-63. Elastic Recovery for CII, Spray-Dried CII:SIO_2 and Prosolv® SMCC 50 (silicified microcrystalline cellulose I) 241

IV-64. Elastic Recovery for CII, Wet Granulated CII:SIO_2 and Prosolv® SMCC 90 (silicified microcrystalline cellulose I) 241

IV-65. Lubricant Sensitivity (LSR) of CII, Spray-Dried Materials and Prosolv® SMCC 50 (silicified microcrystalline cellulose I) 243

IV-66. Lubricant Sensitivity (LSR) of CII, Wet Granulated Materials and Prosolv® SMCC 90 (silicified microcrystalline cellulose I) 243

IV-67. Effect of Blending Time on Lubricant Sensitivity of CII:SIO_2 Materials and Prosolv® (silicifed microcrystalline cellulose I) 245

IV-68. Disintegration Properties for CII, Spray-Dried CII:SIO_2 and Prosolv® SMCC 50 (silicified microcrystalline cellulose I)..... 247

IV-69. Disintegration Properties for CII, Wet Granulated CII:SIO_2 and Prosolv® SMCC 90 (silicified microcrystalline cellulose I)..... 247

IV-70. Disintegration Properties of Compacts Prepared with CII, Spheronized CII:SIO_2 and CP-203® (spheronized microcrystalline cellulose I)..... 248

IV-71. SEMs (60X) of CII, Spheronized CII:SIO_2 and CP-203® (spheronized cellulose I) Beads After Disintegration 251

IV-72. Dissolution Profiles of Diphenydramine HCl from Cellulosic Beads. Conditions: Apparatus 1 (baskets), 100 rpm, Time of 60 Minutes in 500 mL of Distilled Water. Drug Content, 25 mg 256

IV-73. Dissolution Profiles of Griseofulvin from Cellulosic Beads. Conditions: Apparatus 2 (paddles), 50 rpm, Time of 4.5 Days in 1,000 mL of Distilled Water Containing 5.4 mg/mL of Sodium Lauryl Sulfate, Drug Content, 125 mg 258

IV-74 Compact Dissolution Profiles of Diphenydramine HCl from CII, Spray-Dried Materials and Prosolv® SMCC 50. Conditions: Apparatus 1 (baskets), 1000 rpm, Time of 60 Minutes in 50 mL of Distilled Water, Drug Content, 25 mg 260

IV-75 Compact Dissolution Profiles of Diphenydramine HCl from CII, Wet Granulated Materials and Prosolv® SMCC 90. Conditions: Apparatus 1 (baskets), 1,000 rpm, Time of 60 Minutes in 500 mL of Distilled Water, Drug Content, 25 mg 261

IV-76 Compact Dissolution Profiles of Griseofulvin from CII, Spray-Dried Materials and Prosolv® SMCC 50. Conditions: Apparatus 2 (paddles), 75 rpm, Time of 90 Minutes in 1,000 mL of 40 mg/mL Sodium Lauryl Sulfate Media. Drug Content, 125 mg..... 263

IV-77 Compact Dissolution Profiles of Griseofulvin from CII, Wet Granulated Materials and Prosolv® SMCC 90. Conditions: Apparatus 2 (paddles), 75 rpm, Time of 90 Minutes in 1,000 mL of 40 mg/mL Sodium Lauryl Sulfate Media, Drug Content, 125 mg..... 264

IV-78 Water Sorption of 1.3 cm Round Compacts of Cellulose and Commercial Cellulose I (Avicel® and Prosolv®) Stored at Different Relative Humidities at 25 ºC..... 267

IV-79 Variation of 1.3 cm Round Compact Porosity of Cellulose II and Commercial Cellulose I (Avicel® and Prosolv®) with Relative Humidity at 25 ºC..... 268

IV-80	Radial Tensile Strength of 1.3 cm Round Compacts of Cellulose and Commercial Cellulose I (Avicel® and Prosolv®) Stored at Different Relative Humidities at 25 °C	270
IV-81	Stress-Strain Curves of Square Compacts of Cellulose and Commercial Cellulose I (Avicel® and Prosolv®)	276
IV-82	Change in Specific Surface Area with Compression Pressure (1.1 cm dia. round compacts) of CII and Commercial Cellulose I (Avicel® and Prosolv®)	278
V-1	Effect of Processing on the Powder Properties of CII	283
V-2	Effect of Silicification on the Tableting Properties of CII	284
A1	Ibuprofen HPLC Calibration Curve at 221 nm in pH 7.2 Phosphate Buffer	287
A2	Griseofulvin UV Calibration Curve at 291 nm in Methanol:Water (4:1)	287
A3	Diphenhydramine HCl HPLC Calibration Curve at 254 nm in Distilled Water	288
C1	Response Surface Plots for Tensile Strength of Cellulosic II Materials as a Function of RH and Time	296
C2	Response Surface Plots for Tensile Strength of Unsilicified (Avicel®) and Silicified (Prosolv®) Cellulosic I Materials as a Function of RH and Time	297
D1	Radial Tensile Strength of Processed and Reprocessed Round Compacts of Acetaminophen:Excipient (1:1) for Cellulosic CII and Commercial (Avicel® and Prosolv®) Materials	310
D2	Decrease in Compact Strength with Reprocessing for Cellulosic CII and Commercial (Avicel® and Prosolv®) Materials	311

LIST OF ABBREVIATIONS

Abbreviation	Name
CII	Cellulose II as Produced from Cotton Linter
DC	Degree of Crystallinity
DP	Degree of Polymerization
MC	Moisture Content
MCC	Microcrystalline Cellulose
SDCII	Spray-Dried Cellulose II
WGCII	Wet Granulated Cellulose II
SPCII	Spheronized Cellulose II
SD-CII:SiO_2(98:2)	Spray-dried Cellulose II and Silicon Dioxide at a 98:2 Ratio
SD-CII:SiO_2(95:5)	Spray-dried Cellulose II and Silicon Dioxide at a 95:5 Ratio
SD-CII:SiO_2(90:10)	Spray-dried Cellulose II and Silicon Dioxide at a 90:10 Ratio
SD-CII:SiO_2(80:20)	Spray-dried Cellulose II and Silicon Dioxide at a 80:20 Ratio
WG-CII:SiO_2(98:2)	Wet Granulated Cellulose II and Silicon Dioxide at a 98:2 Ratio
WG-CII:SiO_2(95:5)	Wet Granulated Cellulose II and Silicon Dioxide at a 95:5 Ratio
WG-CII:SiO_2(90:10)	Wet Granulated Cellulose II and Silicon Dioxide at a 90:10 Ratio
WG-CII:SiO_2(80:20)	Wet Granulated Cellulose II and Silicon Dioxide at a 80:20 Ratio
SP-CII:SiO_2(98:2)	Spheronized Cellulose II and Silicon Dioxide at a 98:2 Ratio
SP-CII:SiO_2(95:5)	Spheronized Cellulose II and Silicon Dioxide at a 95:5 Ratio
SP-CII:SiO_2(90:10)	Spheronized Cellulose II and Silicon Dioxide at a 90:10 Ratio
SP-CII:SiO_2(80:20)	Spheronized Cellulose II and Silicon Dioxide at a 80:20 Ratio
RH	Relative Humidity
PCA	Principal Component Analysis
CP-203®	Spheronized Cellulose I Named Celphere-203®
IT	Inlet Air Temperature
C	Feed Concentration
FR	Feed Flow Rate
AA	Atomization Air Pressure
DA	Drying Air Speed
ND	Nozzle Diameter
Y	Powder Yield
PS	Mean Particle Size
D_0	Densification by Die Filling
D_a	Combined Densification by Die Filling and Particle Rearrangement
D_b	Densification by Particle Rearrangement
SMCCII	Silicified Microcrystalline Cellulose II

CHAPTER I

INTRODUCTION

Solid Dosage Forms

Currently, more than 80% of all dosage forms on the market are comprised of tablets because they (i) are easy to dispense, (ii) offer dosage accuracy, (iii) present lower likelihood of toxicity compared to parenteral dosage forms due to their reduced bioavailability, (iv) are tamper resistant compared to capsules, and (v) offer better stability to heat and moisture compared to liquid and semi-solid formulations (Jivraj et al., 2000).

The International Pharmaceutical Excipient Council (IPEC) defines an excipient as *any substance other than the active drug or prodrug that is included in the pharmaceutical process or is contained in a finished pharmaceutical dosage form*. There is a broad range of excipients that can be used for making solid dosage forms. Based on their chemical nature, they can be classified as natural (such as cellulose, starch, chitosan, etc.), inorganic (such as dicalcium phosphate), synthetic (such as polyvinylpyrrolidone) and semisynthetic (such as hydroxypropyl cellulose) excipients. Cellulose, starch, lactose, mannitol, sorbitol, and dicalcium phosphate are some of the most common excipients employed for tableting. Direct compression (DC), wet granulation (WG), dry granulation (DG), and extrusion/spheronization (SP) are processes used to prepare a blend of the active pharmaceutical ingredient (API) and the excipient(s) prior to converting into a tablet or capsule dosage form. Direct compression is a simple and economical method by which compacts are made directly from a powder blend of API and the excipients.

In wet granulation, the API is mixed with a wet binder (often starch) and other excipients and then sequentially passed through sieves to obtain granules suitable for tableting (Allen et al., 1999). Wet granulation is the most common technique for tableting, since it allows a large number of drugs to be compacted in a wide range of doses. Nevertheless, when wet granulation is employed, batch to batch reproducibility might be difficult to achieve, especially when employing a highly soluble API. In such cases, the API may migrate from the core to the surface during drying. Further, segregation might occur during unit operations, such as blender-to-bin transfer, and bin-to-tablet press transfer. Such segregation could affect the uniformity of the dose. This problem could also be present in direct compression if there is a large difference between densities of the powder mixture (Hedden et al., 2006).

The dry granulation process involves the preparation of a dry blend of the API and excipients followed by precompression of the powder with high pressure rollers employing from 1 to 6 tons of force to form ribbons (roller compaction), which are then milled and sized. If needed, a dry binder and/or a lubricant are added and the mixture is compressed into a tablet.

In the extrusion/spheronization process, the API is blended with the excipients, followed by the addition of a wetting agent or a binder in an appropriate liquid (water or ethanol). The resulting plastic mass is extruded to form a noodle-like extrudate. The extrudate is then converted to beads with a spheronizer. The beads are dried and coated, if necessary, before putting them into capsules or making tablets (Soh et al., 2008).

Typically, the first three processes require the addition of several specialized excipients, such as a binder (compact forming material), filler (diluent), a disintegrant (facilitating compact disintegration) and a glidant/lubricant (improves powder flow and reduces friction with punch-die tooling). Among all the above mentioned methods direct

compression is the simplest, fastest and more economical method to study the tableting behavior of new excipients alone or in mixtures with drugs. Presented below is a brief overview of the direct compression process.

Direct Compression (DC)

In a 1993 survey of 58 pharmaceutical companies in the US about the selection of a tableting process, 41.5% of the companies indicated that direct compression was their preferred method. On the contrary, 1.5% indicated that they never used direct compression and 15.5% indicated that direct compression was not appropriate for their APIs. The other 41.5% indicated that they used both direct compression and wet granulation processes (Shangraw and Demarest, 1993). However, a recent report states, around 80% of the new drug application (NDA) projects employ wet granulation. The decision is driven by timelines rather than costs, since this is the most likely process to succeed. Employing direct compression which might appear as a rapid formulation procedure may have a higher chance to failure since it might not work for poorly compressible drugs with challenging physicochemical properties (McCormick, 2005).

Less than about 20% of APIs can be compressed directly into tablets (Harden et al., 2004). For some APIs, such as ethynylestradiol (dose = 25 µg), levothyroxine (dose = 50 µg), glimepiride (dose = 2 mg) the dose is too small to be able to be compressed into a tablet directly without needing a filler. To facilitate their handling during manufacture, ease of administration and to achieve the targeted content uniformity, it is recommended that the tablet thickness and weight should be kept above 2 mm and above 50 mg, respectively. Thus, diluents are used, usually from 5 to 80% of the tablet weight (Lachman et al., 1986). They are added to formulations to increase bulkiness of compacts, but sometimes they are added to improve cohesion, allow compression, enhance flow, and adjust tablet weight (Swarbrick and Boylan, 1986).

The dilution potential of an excipient is influenced by the compressibility of the API. It corresponds to the amount of excipient incorporated with a drug without losing its functional properties, such as compactibility or compressibity (Allen et al., 1999).

In the direct compression process, API and excipients are blended together and then compressed into tablets. Direct compression (DC) is gaining popularity since compared to current APIs, the emerging new molecules are usually sensitive to moisture, oxidation and heat, making wet granulation less attractive (Avachat and Ahire, 2007). Thus, DC is ideal for moisture and heat sensitive APIs, such as aspirin. It presents few stability issues, involves few excipients and requires less multifunctional excipients. Changes in dissolution profiles and the possibility of microbial growth on storage are also less likely to occur in tablets made by DC than in those prepared by wet granulations. Compacts made by DC disintegrate into primary particles, rather than granules, and hence, can provide faster API release (Saha and Shahiwala, 2009). The main advantage of DC over other tablet manufacturing methods is its simplicity, since it requires few unit operations and utilizes much less, energy, making the process more economical (Bolhuis and Chowhan, 1996).

Direct compression is highly influenced by the material characteristics, such as flowability, compressibility and dilution potential, since ~70% of commercial formulations contain excipients at higher fractions than APIs. Thus, an ideal DC excipient enables one to prepare compacts with APIs even at levels lower than 50% excipient (Jacob et al., 2007).

Since most poorly compressible drugs are limited to a maximum loading of 30% in a formulation, direct compression is not recommended for these materials. It is also not suitable for poorly flowing powdered drugs since they may agglomerate or segregate during manufacture (Shangraw and Demarest, 1993). In addition, problems, such as

weight variation and content uniformity, might occur because most filler-binders commercially available have limited dilution potential. For instance, acetaminophen, which has poor flow, compressibility, compactibility and low density is not recommended for DC (Bolhuis and Chowhan, 1996).

Even the choice of excipient grade can cause problems in DC. Choosing an improper grade of excipient could lead to segregation and greater lubricant sensitivity (Almaya and Aburub, 2008). For example, Avicel® PH-200 (dia. 180 µm) is more affected by addition of magnesium stearate than Avicel® PH-101 (dia. 50 µm) and Avicel® PH-102 (dia. 100 µm) because it has more regularly-shaped particles which are covered easily by magnesium stearate leading to less particle bonding. Further, large differences between the excipients and API particle shape and size may lead to inconsistent die filling, preferred orientations in particle bonding, non-homogeneous particle slippage and differences in pressure transmission within the powder bed, all resulting in tablet lamination and capping. Lamination corresponds to the separation of a compact into two or more distinct horizontal layers, whereas capping occurs when the upper or lower segment of the compact separates horizontally from the main body (Chow et al., 2008).

Attributes of an Ideal Direct Compression Excipient

The manufacture of a tablet dosage form usually involves a binder, filler, glidant (flow enhancer), disintegrant and lubricant. Functionality describes the activity of an excipient. A multifunctional excipient is defined as a material that has more than one functional property. A glidant improves flowability of the powder mixture; while a lubricant is added to reduce the friction between the powder and tablet tooling. The latter also enhances tableting efficiency and reduces punch-and-die wear. The filler (diluent) is used to increase the bulk of the tablet or capsule to the desired size/volume, easing

compact handling and administration. A binder allows the formation of granules or tablets of adequate tensile strength, whereas the use of a disintegrant allows the tablet break into particles when it comes in contact with water. Compressibility is expressed as the relative volume reduction of the powder bed in response to the applied pressure, and compactibility is the ability to form a compact with sufficient strength when a compression force is applied (Allen et al., 1999). Loading capacity or dilution potential is defined as the minimum amount of the excipient that when mixed with a drug shows no change in its compressibility, flow rate, and ability to form hard compacts at low pressures (Flores et al., 2000).

In order to ensure a robust and successful manufacture of tablets, a direct compression (DC) excipient ideally should possess the following characteristics: excellent compressibility, adequate powder flow, resistance to segregation during handling and storage, fast compact disintegration, a broad range of bulk densities, low sensitivity to lubricants, it should also be easily scaled up and allow higher drug loading even at low usage levels and it should not have a complex production (Jacob et al., 2007; Zeleznik and Renak, 2005).

In addition, a DC multifunctional excipient should preferably have the following characteristics (Thoorens et al., 2008; Chang and Chang, 2007):

1. Physiologically safe and it should not affect drug bioavailability;
2. Be physically and chemically stable to heat, moisture and air;
3. Not adversely affect the functional properties of other excipients and the API;
4. Be compatible with the packaging material(s);
5. Have a particle size that matches the active ingredient;
6. Good compactibility even in high speed tableting machines (low dwell times);
7. Ability to be reworked without loss of flow or compactibility;

8. Be cost effective and available preferably from multiple suppliers;

9. Have pleasant organoleptic properties, be well characterized and accepted by the industry and regulatory agencies;

10. Not contribute to the microbiological load of the formulation;

11. Preferably white.

A compendial excipient is a well characterized material other than the active ingredient, which possesses the desirable purity, strength and quality requirements specified by the United States Pharmacopoeia-National Formulary (USP/NF). Currently, several DC excipients are commercially available. However, most of them lack multifunctional characteristics. Hence, in recent years, several blends of two or more excipients with different properties to complement/improve their functionality have become commercially available (Garr and Rubinstein, 1991).

Direct Compression Excipient Examples

Materials, by virtue of their response to applied forces, can be classified as elastic, plastic, or brittle materials (Figure I-1). Generally, materials are not entirely elastic, plastic or brittle, but have some of all three characteristics. Thus, pharmaceutical materials may exhibit all three types of behavior, with one type being the predominant response. Opposed to brittle materials, a ductile material can withstand large deformations without breaking. Brittleness is caused by progressive failure along weak points in the crystals, whereas ductility favors sliding of crystal planes. Ductility and brittleness favor bonding because new surfaces are produced and, consequently, an increase in contact area between particles occurs during compression.

Picker developed a three dimensional model based on compression pressure, dwelling time and porosity data to characterize tableting behavior of pharmaceutical materials (Picker, 2004).

Plastic material	Brittle material
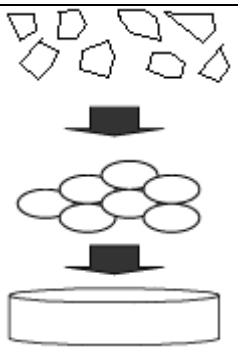	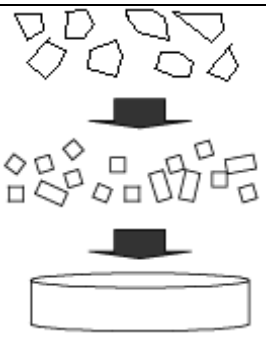
• Usually makes strong compacts • Elastic recovery may cause compact lamination and capping • Lubricant sensitive	• Compacts are not very strong • Does not exhibit elastic recovery and shows less dependence on the machine speed • Lubricant insensitive

[a] For completely elastic materials if the load upon compression is removed, the compact expands resulting in the individual original particles (Adapted from Nachaegari and Bansal, 2004).

Figure I-1. Deformation Mechanism upon Compression[a]

Based on the observed ability of the materials for densification, Picker ranked the ductility of some excipients as: maize starch > potato and pregelatinized starches ≅ maltodextrin > microcrystalline cellulose ≅ α-lactose monohydrate > xylitol ≅ maltose ≅ mannitol ≅ sodium carboxymethyl cellulose > dicalcium phosphate. The advantages and disadvantages of some common direct compression excipients are presented in Table I-1.

Need for New Excipients

In the recent past, few new excipients have been introduced into the market. The development of new excipients so far has been market driven (i.e., excipients are developed in response to market demand) rather than marketing driven (i.e., excipients are developed first and market demand created through marketing strategies). One reason for this lack of new excipients is the relatively high cost involved in excipient development, including the toxicological tests. However, with the increasing number of new drug moieties with varying physicochemical, pharmacokinetic, permeation and stability properties, there is a growing interest among formulators to search for new excipients that have minimal scale-up problems, low manufacturing costs, and little environmental impact (Marwaha et al., 2010). Other factors driving the search for new excipients are:

- The growing popularity of the direct compression process and demands for an ideal filler-binder that can replace two or more excipients avoiding the need for multiple excipients (i.e., disintegrant, lubricant, glidant, etc.).
- The increasing speed capabilities of tablet presses, which require excipients to maintain good compressibility and low weight variation even at short dwell times.
- Shortcomings of existing excipients, such as loss of compaction upon wet granulation, high moisture sensitivity and poor die filling as a result of agglomeration.

Table I-1. Direct Compression Excipients: Advantages and Disadvantages.

	Advantages	Disadvantages
α-Lactose	• Has good flow and is unreactive with moisture sensitive drugs (Whiteman and Yarwood, 1988). • It has good tableting properties and high dilution potential (Bolhuis et al., 2004).	• Reacts with amines and alkaline materials. β-lactose has poor flowability, and can pick up moisture easily (Whiteman and Yarwood, 1988). • Compressibility decreased at >5% moisture content (Bolhuis et al., 2004).
Pregelatinized starch	• Inexpensive, shows good flow and renders a homogeneous distribution of API during wet granulation (Klinger et al., 1986). • It has self-lubricant properties (Rahmouni et al., 2002). • Used in wet granulation, direct compression, capsule and bead formulations (Van Veen et al., 2005).	• It is highly sensitive to lubricant (Jahn and Steffens, 2005) and at high compression speeds suffers from capping (Alderborn and Nyström, 1996). • It shows a slow disintegration (Almaya and Aburub, 2008).
Microcrystalline cellulose	• Moisture content of <7% in the product eases slippage of individual crystals upon compression and avoid capping tendency (Jivraj et al., 2000). • Has good compactibility and compressibility (Jivraj et al., 2000).	• Compactibility is adversely affected when processed by wet granulation (Sherwood and Becker, 1998). • It is expensive and shows poor flow (Gustafsson, 2000). • Magnesium stearate leads to compact capping and lamination. It requires disintegrants and suffers from strain rate sensitivity (Moreton, 2008).
Dicalcium phosphate	• It is inexpensive. The anhydrous and hydrated forms can be used for direct compression and wet granulation (Miyazaki et al., 2009). • It is relatively insensitive to alkaline lubricants (Doldan et al., 1995).	• It requires the addition of lubricants and disintegrants and its tablets possess high porosity. On storage, compacts become hard delaying dissolution times, specifically when stored at low RH (Doldan et al., 1995).

Table I-1: Continued

Mannitol	• It has a cooling sensation in the mouth. It is less hygroscopic (<1%) than sorbitol (Ashok and Mahesh, 2006). • The granular form has the best flow and binding properties (Kim et al., 1998). • The α-form has the best compactibility and flow. Compact disintegration takes ~9 min (Yu et al., 1999).	• It is more expensive than sorbitol. It is available in three polymorphic forms (α, β, and γ). Flow and binding properties of all three forms depend on the recrystallization conditions during its manufacture (Yoshinari et al., 2003)
Dextrose	• It has sweet taste and renders good mouth feeling (Stout et al, 1991). • Direct compression produces stronger compacts over wet granulation (Olmo and Ghaly, 1999). • Dextrose is soluble in water and, hence, its tablets do not disintegrate, but dissolve (Olmo and Ghaly, 1999).	• On storage, compact disintegration and hardness increases, while, friability decreases. It is highly hygroscopic, and reacts with amine groups. It has poor compactibility at > 9% moisture content (Olmo and Ghaly, 1999). • An equal mixture of the anhydrous and monohydrate forms improves compactibility (Hebeda, et al, 1979).
Lactate	• It is 40% more sweet compared to sucrose and does not contribute to blood glucose levels. It has a low caloric value (Eroma et al., 2003). • It is employed in chewable tablets. It shows poor hygroscopicity, good flow and is lubricant insensitive (Eroma et al., 2003).	• It forms less strong compacts, but possesses lower capping tendency compared to mannitol and sorbitol (Bolhuis, et al., 2009).

Table I-1: Continued

Maltose	• It is non-hygroscopic and insensitive to magnesium stearate (Nehete et al., 1992). • It makes strong chewable compacts (Muzikova and Balharkova, 2008). • It is 33% sweeter than sucrose. Its compacts are non-friable and disintegrate < 9 min (Bowe et al., 1997).	• It could increase the glucose levels in diabetic patients (Bowe et al., 1997).
Sorbitol	• It is used for making lozenges, chewable, and orally disintegrating tablets. It exists in the α, β, γ, and δ forms (Guyot-Hermann and Draguet-Brughmans, 1985) • The γ form is the most stable and presents the best compaction, disintegration and dissolution characteristics. It is lubricant insensitive (Reiff et al., 1986).	• Storage at > 65% RH induces liquefaction and at low RH recrystallization, causing tablet hardening and instability of moisture sensitive drugs. It also clumps in the feed of the hopper and sticks to the surface of the die during tableting at RH > 50% (Lieberman, et al, 1990).
Sucrose	• It is used for wet granulation and has good flow (Behzadi et al., 2006). • It serves as an excellent taste masking agent (Mullarney et al., 2003).	• It has poor compactibility (Behzadi et al., 2006).

- The lack of excipients that address the needs of a patient, with a specific disease state such as those with diabetes, hypertension, and lactose and/or sorbitol sensitivity.
- The ability to modulate the solubility, permeability, or stability of drug molecules.

New Excipient Sources

Excipients with improved functionality can be obtained by developing a new chemical entity, new grades of existing materials or their combinations (Moreton, 1996). An excipient is only considered novel when it is a new chemical entity, a new route of administration is created by its use, a physical/chemical modification of an existing excipient is formed, a co-processed mixture of existing excipients is developed, or a food additive is used for the first time for oral drug administration (Larner et al., 2006). In the last three decades, new grades of existing excipients have been developed, but only a few novel excipients have been introduced in the market (Chang and Chang, 2007).

New grades of existing excipients can be achieved by modifying fundamental properties, leading to improved derived (functional) properties (Block et al., 2009; Reimerdes, 1993). Fundamental characteristics, such as morphology, particle size, shape, surface area, porosity and density all determine excipient functional properties, such as flowability, compressibility, compactibility, dilution potential, disintegration, and lubrication potential as depicted in Figure I-2. Any new chemical entity being developed as an excipient must undergo various stages of regulatory approval aimed at addressing issues of safety and toxicity, which is a lengthy and costly process. The requirements of purity, safety, and functionality of the excipients are established and harmonized by the International Pharmaceutical Excipients Council (IPEC).

In addition, like active ingredients, the excipient must undergo a phase of development, which shortens the market exclusivity period making the investment less attractive.

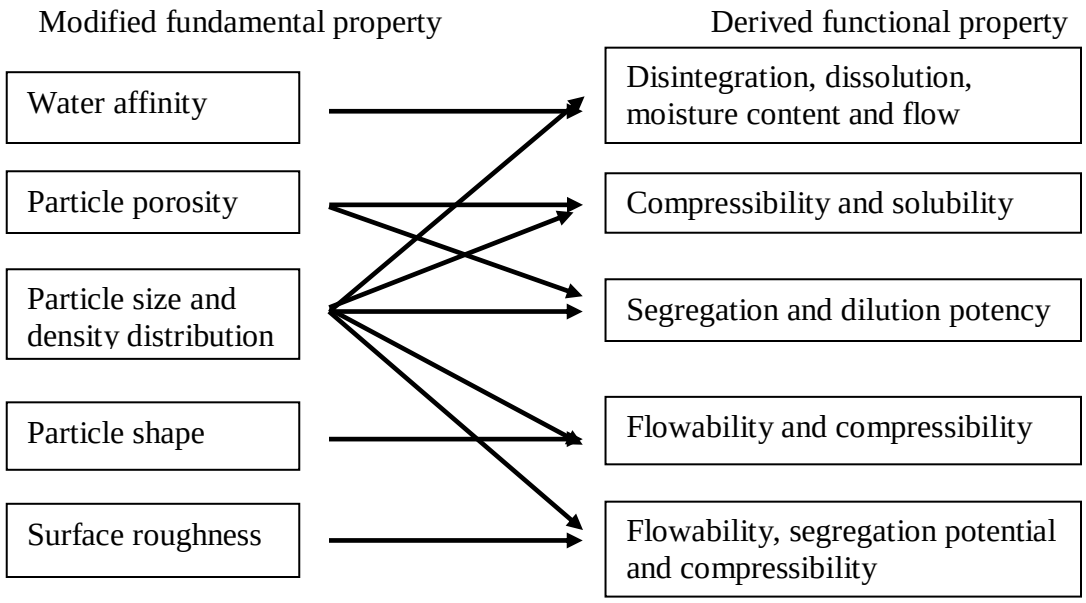

Figure I-2. Material Effects on Derived Formulation Properties.

One of the solutions was to develop drug products jointly, in which a new excipient becomes part of the new drug application. Thus, the combined expertise of pharmaceutical and excipient companies can lead to the development of tailor-made innovative excipients. For example, CyDex Pharmaceuticals (Lenexa, KS) and Pfizer (New York, NY) worked collaboratively to obtain the approval of a solubilizer for IV applications (Marwaha et al., 2010).

In the past four decades, excipients have been physically or chemically engineered for developing new grades, such as pregelatinized starch, Avicel® PH-101, PH-102, and PH-200 (FMC Biopolymers, Newark, DE), spray-dried lactose (Foremost Farms, Baraboo, WI) and crospovidone (Polyplasdone® XL and Polyplasdone® XL-10, International Specialty Products, Wayne, NJ). However, functionality can be improved only to a certain extent, because of the limited range of possible modifications that restricts functionality (Nachaegari and Bansal, 2004). Powder density and particle size could be altered to achieve better flow. However, when one attribute is improved, another may be compromised (i.e., flow of Avicel® PH-200 is improved 1.6 fold at the expense of its compactibility and vice versa for Avicel® PH-101) (Lerk et al., 1974; Taylor et al., 2000). However, in the case of native starches, thermal treatment led to an improved binder property (pregelatinized starch), attributable to the partially hydrolyzed nature of the granules which made them more hydrophilic (Klinger et al., 1986). Pregelatinization also provided other functionalities, such as excellent flow, self-lubrication, improved use as a filler in hard gelatin capsules (5-75%), and a better binder in wet granulation (5-20%). Further, this material has improved use as a dry binder for roller compaction and direct compression applications and as a disintegrant in tablets (5-10%) (Ashish and Neves, 2006).

Particle Engineering as a Source of New Excipients

Solids are characterized by three levels of state: molecular, particle, and bulk. Changes in one level are reflected in other levels. Thus, excipient functionality can be improved by modifying any of the three levels.

The molecular level comprises the arrangement of individual molecules in the crystal lattice and includes changes, such as polymorphism, pseudopolymorphism, and the amorphous state. The molecular level can be modified by changing the arrangement of molecules in the crystal lattice, generating new allomorphs, pseudopolymorphs, or making a material more amorphous by a chemical treatment (crosslinking). Varying the crystal lattice arrangement by adjusting parameters, such as crystallization and drying conditions often can create a particle with different properties.

One example of how a variation in the polymorphic form changes the functional properties of a material is lactose. Lactose exist in two forms, α-lactose and β-lactose. α-lactose monohydrate has good flow, small surface pore area, but poor binding properties. Anhydrous α-lactose, on the other hand, has a larger pore area, excellent binding properties (4 times larger), keeping the good flow characteristics. Further, different from the regular structure of α-lactose crystals, β-lactose has a granular form consisting of aggregates of small crystals with better binding properties (Lerk, 1993).

Other modifications at the molecular level involve chemical reactions or crosslinking of the excipient with a low molecular weight substance. These processes are expensive and usually require a need for solvent recovery and determination of residual solvents. Further, crosslinking agents are often toxic and leave traces of by-products (impurities) that could be harmful or degrade *in vivo* to toxic products. For example, MCC, starch, chitosan, lactose, and other sugars can be easily cross-linked with glutaraldehyde in a complex etherification reaction. However, glutaraldehyde also self-

polymerizes, leading to the formation of undesirable by-products, which are difficult to remove (Rasmussen and Albrechtsen, 1974). Further, carboxymethylation of potato starch (ether synthesis) followed by neutralization with citric acid produces a superdisintegrant (sodium starch glycolate). Similarly, another type of starch crosslinking produced hydroxyethyl starch, useful for parenteral applications. Cellulose derivatives, such as ethyl cellulose, methyl cellulose and hydroxypropylmethyl cellulose are also chemically modified excipients (Krassig, 1996).

The particle level comprises individual fundamental particle properties, such as morphology, particle size, shape, surface area, porosity, and density. At the particle level, individual particles can be modified by physical processing such as spray drying, wet granulation, crystallization, etc; or co-processing of the excipient with other inert materials. Co-processing is based on the concept of excipient interaction at the sub-particle level. It provides a functional synergy as well as masking the undesirable properties of the individual components (Block et al., 2009). Particles of the minor component can be incorporated either on the surface, or within the core of the excipient particles. This process requires homogenization of the excipients, followed by a co-processing step. As long as the two materials comply with the compendial requirements, the co-processed product does not need toxicity studies required for a new chemical entity.

At the bulk level, larger scale arrangements of the materials are involved. This level is of importance during the drug development stage and implies, for example, a dry blend of two or more excipients in a particular ratio. This level is composed of an ensemble of particles and governs functional properties, such as flowability, compressibility, compactibility, dilution, disintegration and lubrication potential, which are critical factors in the excipient's performance. This level can be modified by changing

particle interaction in the bulk state. The resulting blends will exhibit intermediate properties between those of the two parent materials. In a few cases, the magnitude of these properties is non-ratio-dependent (Nachaegari and Bansal, 2004). Particle size, particle size distribution and bulk density of the materials should be similar to prevent segregation during manipulation, handling and storage of the product, and batch-to-batch variability problems (Levin, 2006).

In the design and development of a drug product, it is not uncommon to use two or more excipients/coadjuvants to obtain a mixture with adequate tableting properties. The properties of such blends can result in either synergistic or antagonistic effect(s) with respect to various tableting properties (Lerk et al., 1974). For example, a dry blend can be used to formulate rapidly disintegrating tablets for a mixture of Prosolv® SMCC 90, mannitol and a poorly soluble drug (loratadine) compressed at low pressures. Prosolv® can adsorb a sufficient quantity of fine dust of the fast dissolving excipient (mannitol). The resulting compacts are able to disintegrate within 60 sec after contact with water or saliva (Beso and Sirca, 2006).

In a few cases, the API can be dispersed among the excipients in a liquid followed by spray drying to form a more homogeneous blend. For example, acetaminophen can be spray-dried with maltodextrin in water to produce oblong, free flowing particles with good compactibility. In this case, the binary mixture has good compactibility, but its compacts show a capping tendency (Gonnissen et al., 2008). Sometimes it is advisable to diminish the undesirable effects of adjuvants in the bulk simply by changing blending time (i.e., the negative effect of hydrophobic magnesium stearate on plastically deforming materials can be decreased by decreasing the blending time to < 5 min) (Jivraj et al., 2000).

Excipient Co-Processing as a Source of New Excipients

Over the years, the strategy for developing co-processed excipients has gained importance. However, the development of such combinations is a complex process because one excipient may interfere with the existing functionality of the other excipient. Co-processing was initially used by the food industry to improve stability, wettability, and solubility and to enhance the gelling properties of food ingredients, such as co-processed glucomannan and galactomannan (Modliszewski and Ballard, 1996). Excipient co-processing in the pharmaceutical industry originated in the early 1990s with the introduction of co-processed microcrystalline cellulose and calcium carbonate (Auguello et al., 1998a).

Excipient co-processing could lead to the formation of materials with superior properties compared to simple physical mixtures (gravity driven blending) of components. The aim of co-processing is to obtain a product with added value by a balance of its functionality and production costs. An excipient of reasonable price, such as a diluent, has to be combined with another functional material in order to obtain an integrated product with superior functionality than the simple blend of components. The randomized embedding of the components in the particles minimizes anisotropic behavior, such that deformation during compression along any plane and multiple clean surfaces are formed during the compaction process. Thus, the use of a co-processed excipient as a direct compression material may combine the advantages of wet granulation with the lower cost of direct compression (Reimerdes and Aufmuth, 1992). A major limitation of the co-processed excipient mixture is that the ratio of the excipients in the mixture is fixed. When developing a new formulation, a fixed ratio of the excipients may not be optimal for a particular API and for the dose per tablet under development

(Bolhuis and Chowhan, 1996; Saha and Shahiwala, 2009). A co-processed excipient development involves:

• Identifying the two or three excipients to be co-processed by carefully studying material characteristics and functionality requirements.

• Selecting the proportions of the excipients to optimize.

• Assessing a suitable solvent in which to disperse the excipients.

• Selecting an appropriate drying process such as spray or flash drying.

• Optimizing the process to avoid batch-to-batch product variations.

Role of Material Science in Co-processing

Excipient co-processing offers a valuable tool to alter compression and/or flow behavior of a material. A combination of plastic and brittle materials is necessary for optimum tableting performance (Nachaegari and Bansal, 2004). Ideally, a co-processed material exhibits superior properties compared to the simple physical mixture of individual components. Co-processing is generally conducted with one excipient that is plastic deforming with another that is brittle as seen previously in Figure I-1. This combination could minimize storage of elastic energy during compression, which is associated with the compact's tendency for capping and lamination (Jacob et al., 2007). Further, co-processing of these two types of deforming materials produces a synergistic effect, in terms of compressibility, by selectively overcoming individual disadvantages. Such combinations can help improve functional properties, such as compaction performance, flow properties, strain-rate, lubricant and moisture sensitivities, or reduced hornification (ability to form hydrogen bonding). The products so formed are physically modified in a way so that they do not lose their chemical structure and stability. This means that excipients maintain their independent chemical properties, while synergistically increasing their functional performance (Chow et al., 2008).

If the resulting co-processed excipient is porous, segregation is typically diminished since APIs can adhere onto s excipient particles, making process validation and in-process control easy and more reliable. Spray drying, wet granulation, spheronization, and co-crystallization can be used for co-processing. Spray drying is a process in which an aqueous or non-aqueous dispersion of the materials is sprayed through a nozzle at high pressures and the droplets formed are rapidly dried and collected as a powder. Wet granulation involves addition of an aqueous dispersion of a binder to a previously mixed powder blend, followed by wet sieving and drying. In the spheronization process, the wet mixture of excipient(s) is first extruded to produce homogeneous spaghetti-like rods. These rods are, while wet converted to beads by using a spheronizer. In co-crystallization, the two materials are dissolved in a solvent (often with heat) in which both are highly soluble followed by cooling at different rates to produce desired co-crystals. Differences in the cooling rate cause changes in the size and shape of the resulting crystals. These crystals can be then milled or passed through sieves to control their particle size.

Co-Processed Excipients

Table I-2 and Table I-3 list and describe salient features of some commercial and investigational co-processed microcrystalline cellulose excipients, respectively. The following is a brief discussion of the functional properties of some of these co-processed excipients.

Table I-2. Commercial and Investigational Co-processed Cellulosic Excipients.

Type	Brand name	Manufacturer	Ingredients	%	Processing
Cellulose Based	Avicel® HFE	FMC Biopolymers	MCC Mannitol	90 10	Spray drying
	Avicel® RC591	FMC Biopolymers	MCC Na CMC	89 11	Milling, spray drying
	Avicel® RC581	FMC Biopolymers	MCC Na CMC	89 11	Milling, bulk drying
	Avicel® CL611	FMC Biopolymers	MCC Na CMC	85 15	Milling, spray drying
	Avicel® RC591	FMC Biopolymers	MCC Na CMC	89 11	Milling, spray drying
	Avicel® RC581	FMC Biopolymers	MCC Na CMC	89 11	Milling, bulk drying
	Avicel® CL611	FMC Biopolymers	MCC Na CMC	85 15	Milling, spray drying
	Prosolv® SMCC 50 and Prosolv® SMCC 90	JRS Pharma	MCC Colloidal silicon dioxide	98 2	Spray drying
	-	Investigational[a]	MCC Calcium carbonate	80 20	Spray drying
	--	Investigational[a]	Rice starch MCC	70 30	Spray drying
Lactose Based	Cellactose®	Meggle	α-Lactose monohydrate Powder cellulose	75 25	Spray drying
	Microcellac®	Meggle	α-Lactose monohydrate MCC	75 25	Spray drying

[a] Auguello et al., 1998a; Limwong et al., 2004.

Table I-3. Salient Features of Co-processed Cellulosic Excipients.

	Salient features
Lactose-Cellulose (Cellactose®)	• Has good compactibility attributed to the synergic effect of consolidation by fragmentation of lactose and the plastic deformation of cellulose (Arida and Al-Tabakha, 2008). • During spray drying lactose particles coat the cellulose fibers. Lactose renders good flow and solubility whereas cellulose contributes to particle binding (Belda and Mielck, 1996). • Produces stronger compacts than the physical mixture of 75% cellulose and 25% lactose. Compacts made at 150 MPa have a hardness of 140 N (Schwarz et al., 2006). • Disintegration of its particles starts once the outer lactose shell has dissolved allowing access towards the cellulose core (Casalderrey et al., 2004). • At low compression pressures fragmentation predominates, and at higher than 180 MPa plastic deformation is prevalent. It is also more compactable than lactose (Schmidt and Rubensdörfer, 1994). • Compactibility is affected by high compression speeds (Arida and Al-Tabakha, 2008).
Lactose-MCC (MicroceLac® 100)	• It has superior flowability and binding properties compared to the physical mixture of MCC and different lactose grades (Schwarz et al., 2006; Clerch, 2008). • It forms stronger compacts with faster disintegration times than those of Cellactose® (Muzikova and Novakova, 2007).
MCC-Calcium Carbonate (80:20)	• The increased bulk density of the co-processed product (0.41 g/cm^3) compared to MCC (0.29 g/cm^3) allows greater dilution potential, improves flow and lower tablet weight variability (Auguello et al., 1998a). • Calcium carbonate provides a more uniform surface, providing a smooth appearance to the tablets. • This excipient is useful to load drugs with a bulk density ≤ 0.30 g/cm^3 (Auguello et al., 1998b).
MCC-Guar gum (Avicel® CE-15)	• Guar gum decreases the chalkiness taste caused by MCC (Auguello et al., 1998b). • Guar gum makes it suitable to formulate chewable compacts (Auguello et al., 1998b; Gupta et al., 2006; Saigal et al., 2009).

Table I-2. Continued.

MCC-Mannitol (Avicel® HFE)	• MCC imparts greater compressibility and compactibility to the composite particles, but compromises flow. Mannitol, on the other hand, provides good mouth feel, low chalkiness, low plasticity and low sensitivity to humidity and causes a high dissolution rate (Jacob et al., 2007). • The fast compact disintegration is due to the increased porosity and formation of submicron particles of the water wicking mannitol on the surface of MCC (Jacob et al., 2007). • Compacts of this product and acetaminophen are less friable and more compactable than those containing MCC and mannitol, separately (Carlin, 2008). • Compact tensile strength had a 38% decrease with reprocessing (Thoorens et al., 2008).
MCC-NaCMC (Avicel® RC-591/RC-581/Avicel® CL-611)	• These excipients are used as suspending aids to improve the stability and texture of disperse systems, such as suspensions, creams, and lotions. They produce a firm gel structure via steric stabilization due to particle-particle interactions (Battista, 1965; 1966). • Compared to MCC alone, the presence of sodium carboxymethyl cellulose rendered a 2-fold increase of glizipide release within 360 min (Garcia and Ghaly, 2001). • Avicel® RC-591 and RC-581 are used at levels of 1-2% for nasal sprays, topical sprays, lotions and oral suspensions, whereas Avicel® CL-611 is mainly used for reconstitutable suspensions and oral suspensions (Mihranyan et al., 2007).
MCC-Rice Starch	• The cellulose component imparts greater compressibility to the composite particles, but makes particles less spherical, with rougher surfaces, resulting in a decrease in flowability (Limwong et al., 2004). • Gelatinization of starch grains might be responsible for binding rice and cellulose particles together through solid bridge formation to form composite granular particles. The functional properties of this material are better than those of rice starch alone (Limwong et al., 2004).

Table I-2. Continued.

MCC-SiO_2 (Prosolv®)	• It is available in three grades: Prosolv® SMCC 90, Prosolv® SMCC 50 and Prosolv® SMCC HD90 (JRS PHARMA, Patterson, NY) (Bolhuis and Chowhan, 1996). • Compacts of Prosolv® SMCC HD90 had a 60% larger toughness than Prosolv® SMCC 50 and Prosolv® SMCC 90 (Muzikova and Novakova, 2007). • Prosolv® SMCC 90 has better flow and produces stronger compacts than Avicel® PH-200 (Angle of repose of 28° vs. 32°; and crushing strength of 170 N vs. 95 N, respectively) (Lahdenpaa et al., 2001). • Prosolvs® have low sensitivity to magnesium stearate since fumed silica suppresses the negative effect of magnesium stearate on the binding properties of MCC (Edge et al., 2000). • Prosolv® cannot be used at > 50% levels because it leaves an unpleasant gritty sensation in the mouth and it does not dissolve in saliva (Beso and Sirca, 2006). • Prosolvs® possess a high degree of surface roughness, which increases powder shear in the dry blending process and improves low dose API loading (Zeleznik and Renak, 2005). • Prosolvs® have good dilution potential of poorly compressible drugs (Sherwood et al., 2004). • Fumed silica interacts with cellulose possibly through hydrogen bonding and dipole-dipole interactions (Rashid et al., 2008; Van Veen et al., 2005; Kachrimanis et al., 2003). • MCC granulates better than Prosolv® SMCC 50 since the former produced larger granules (Sherwood et al., 2004). Also, both excipients exhibited comparable strain rate sensitivity suggesting that these materials deform by a plastic mechanism (Habib et al., 1999). • The high compactibility of Prosolv® is beneficial in developing direct-fill formulations for automatic capsule-filling machines (Guo et al., 2002; Felton, et al., 2002). • The pore size distribution characteristics are comparable for Prosolv® SMCC 90 and MCC (Emcocel® 90). This suggests that improvement in functionality is due to surface modification caused by SiO_2 (Bolhuis and Armstrong, 2006).

Powder Compaction and Particle Bonding

An optimum excipient should be able to form a successful compact with the intended drug to withstand handling and storage. Usually, the robust indirect measure used to test this property is friability, which should not be larger than 1% (see *compact friability*).

The compaction process is a composite of several events: particle movement into void spaces, particle fracture, elastic deformation, plastic deformation and cohesion between particles surfaces. These processes occur simultaneously, but not necessarily to the same degree at any stage of the compression process (Shlantha and Milosovich, 1964).

During consolidation of a powder bed, a reduction in porosity occurs. This reduction in compact volume brings particles into close proximity to each other. The reduced distance between the particles facilitates creation of bonds and makes the particles adhere together into a coherent compact. Two different types of interactions are normally considered in direct compression of pharmaceutical materials: intermolecular interactions and mechanical interlocking. Van der Waals forces are probably the most important intermolecular forces responsible for holding the particle together in a tablet. Hydrogen bonding is another example of forces that act over a short distance between particles. The nature of these forces depends on the chemical composition of the material. Bonding by hooking or twisting of particles depends on the surface texture and shape of the particles. The dominant bond type depends on various factors, including the degree of compression and the inherent properties of the material. In the high porosity range, the principal attraction between particles has been suggested to be intermolecular forces; whereas in the low porosity range, solid bridges play a major role (Adolfsson and

Nystrom, 1996). Usually solid bridges connect particle by spanning, sintering, melting, and crystallization (Hiestand, 1997).

Powder Consolidation Models

The assessment of powder compressibility can be determined by studying the relationship between compact porosity and compression pressure. If high pressures are applied to a powder bed, low porosities of the resulting compact can be achieved. When the porosity of the tablet is close to zero, the structure of a tablet should be different from the structure at normal porosities (5-25%) (Adolfsson and Nystrom, 1996). The final porosity reduction may eventually represent a transformation to a new physical structure, where the solid constitutes the continuous phase. Thus, the bonding structure of the resulting compact may also be altered. Knowledge of the volume reduction ability of a powder makes it possible to predict the compaction behavior of a pharmaceutical material (Bassam et al., 1990).

Mathematical models have been used to describe the consolidation or volume reduction of powders. Such models were derived from empirical mathematical relationships and were based on the proposal that different mechanisms occur in distinct ranges of applied pressure (Kennedy et al., 1996). These models are used to characterize tableting excipients for compact development. They also identify and describe the predominant powder densification and deformation behavior (plastic, brittle and elastic) (Picker, 2000).

The most widely used equation relating the porosity (ε) of a powder bed during compaction to the applied pressure (P) is the Heckel equation (Eqn. I-1, below). The reciprocal of the slope (m) of the linear portion of the Heckel curve is referred to as the mean yield pressure, P_y.The P_y can be used to indicate the mechanism occurring during compression. From the value of A (the intercept), the total relative density

"D_a" ($D_a = 1 - \exp^{-A}$) or powder solid fraction due to die filling and particle rearrangement can be calculated (Roberts and Rowe, 1986).

$$\mathrm{Ln}\frac{1}{\varepsilon} = m\sigma + A \qquad \text{Eqn. I-1}$$

Heckel curves are constructed by plotting the variation of powder porosity (volume reduction) with compression pressure. Three types (A, B and C) of powder behavior can be obtained from the shape of these curves and are shown in Figure I-3. In Type A, the different sized fractions have different initial packing densities and the plots remain parallel as the applied pressure is increased, owing to plastic deformation. For type B, plots merge at a high pressure; this is attributed to particle fragmentation during rearrangement at low pressures. In type C, i.e., mixtures of lactose and fatty acids, curves are initially steep and then merge into a common plateau close to a solid fraction of 1 at low pressures. For this reason, type C curves have no practical use for this model. Sodium chloride and lactose are examples of types A and B materials, respectively, while C applies to lipid materials (Fassihi, 1988). This latter behavior (type C) is exhibited for materials that do not show particle rearrangement before plastic deformation occurs but possibly, melting of particles.

For plastically deforming materials, such as sodium chloride and potassium chloride, the measured yield pressure varied with particle size. However, for materials which deform by particle fragmentation, such as lactose and calcium carbonate, yield pressure increased with reduced particle size (Roberts and Rowe, 1986). There are two methods used to obtain density-pressure profiles: the in-die and out-die (or ejected tablets) methods. In the out-die method, the compact volume is measured after the tablet is ejected from the die having undergone partial elastic recovery.

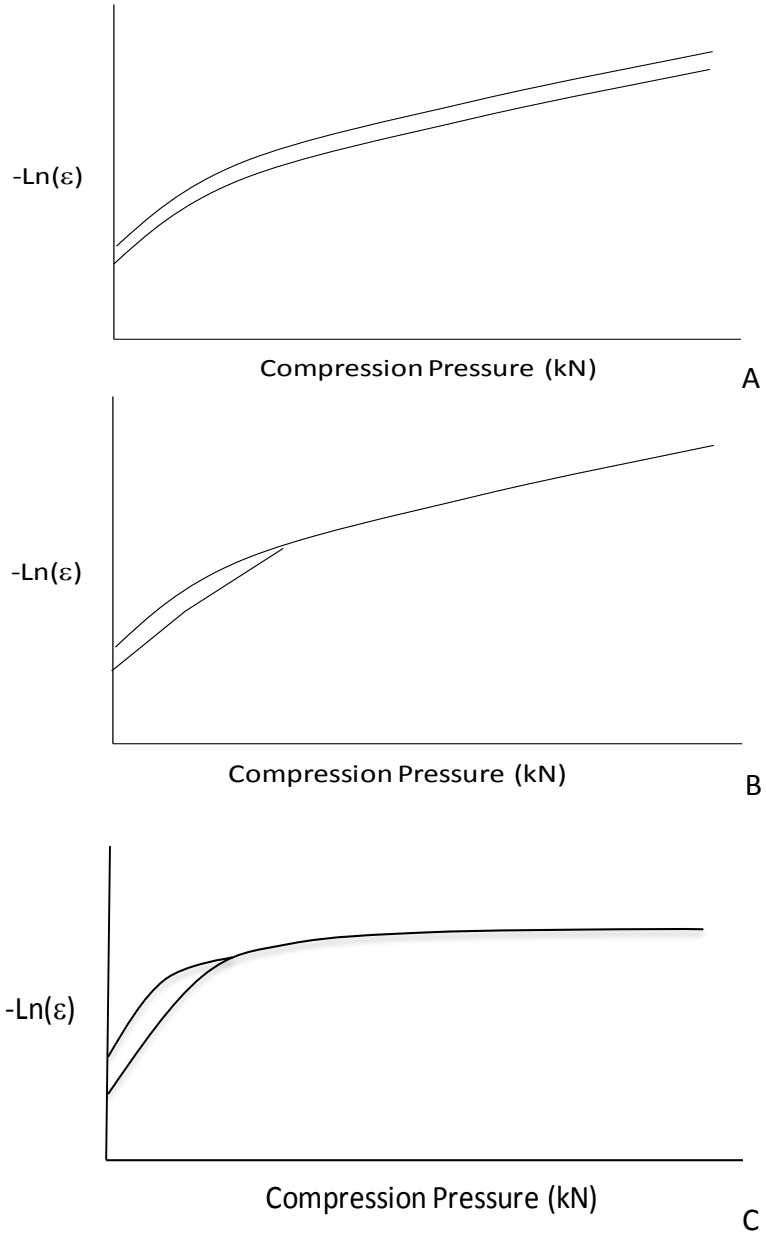

Figure I-3. Various Heckel Plots: (A) Plastic Material at Two Size Fractions; (B) Fragmenting Material; (C) Mixture of Wax and Lactose Reaching Complete Densification at Low Pressures (Adapted from Fassihi, 1988).

In this case, compacts are made for each compression pressure and a linear region of the curve, usually from 50 to 150 MPa, is selected to build the Heckel plots (Gabaude et al., 1999). Conversely, the in-die method measures the compact densification in the die by evaluating punch displacement(s) respect to the increase in compression pressure. This method is faster and consumes less material than the out-die method, which requires a new compact for each compression pressure. However, the in-die density measurement contains an elastic component leading to falsely low mean yield pressures, which is disadvantageous when using the information to prepare a tablet formulation.

The Kawakita linear model is another porosity-pressure function used to characterize powder compressibility. It is expressed as:

$$P/C = P/a + 1/ab \qquad \text{Eqn. I-2}$$

$$C = [1-\rho_0/\rho_a] \qquad \text{Eqn. I-3}$$

Where, P is the applied pressure and C is the degree of volume reduction, ρ_0 is the bulk density, ρ_a is the compact apparent density, "a" is indicative of powder compressibility and "b" determines the likelihood of volume reduction. However, the actual physical meaning of the latter is not well understood. The plot of P/C vs. P gives a straight line. The constants "a" and "b" can be determined from the slope and intercept, respectively.

Another interesting model is the Leuenberger equation, which describes the relationship between compact tensile strength and the product of compression pressure and solid fraction in a modified exponential function (Lanz, 2005):

$$TS = T_{max} * [1 - e^{(-\gamma_c * P * \rho_r)}] \qquad \text{Eqn. I-4}$$

Where, TS is the radial tensile strength, T_{max} is the theoretical tensile strength at infinite compression pressure, γ_c is the compression susceptibility parameter, ρ_r is the relative density, and P is the compression pressure.

Factors That Affect the Mechanical Properties of Powders

Wong and Pilpel (Wong and Pilpel, 1990) investigated the effect of particle shape on the mechanical properties of powders. They concluded that materials that consolidate by plastic deformation, such as Starch 1500® and sodium chloride exhibit a large increase in compressibility and a significant decrease in yield values and elastic recovery in going from regular to irregular particles. This accounts for the increase in tensile strength, which is due to the increased in area of particle contact as they deform. For materials which consolidate by fragmentation such as lactose and dicalcium phosphate, particle shape has no effect on the above properties, but irregular particles fracture more than regular ones (Wong and Pilpel, 1990). The value of parameters related to compact mechanical properties, such as yield pressure, Young's modulus, tensile strength and brittle fracture index depend on the deformation mechanism, compression speed, dwell time, type and amount of lubricant, compression pressure, amount of sample and particle size employed (Narayan and Hancock, 2003).

Cellulose II Allomorph as a Direct Compressive Agent

Cellulose is the most abundant natural linear polymer consisting of 1,4-linked-β-D-glucose repeat units and is known to exist in the following distinct allomorphs: I_α (from algae), I_β (from superior plants), II (the most stable form produced by mercerization), III_I and III_{II} (prepared from ammonia at -30 ºC), and IV_I and IV_{II} (produced at 260 ºC in glycerol). Each allomorph differs in its physicochemical properties (Klemm et al., 1998a; Klemm et al., 1998b). Cellulose III is formed when native cellulose is treated with liquid ammonia at low temperatures, whereas cellulose IV

is obtained by treatment of regenerated cellulose at high temperatures (Figure I-4) (Krassig, 1996). Of these, the cellulose I (CI) allomorph is the most prevalent form and cellulose II is the most stable form (Kroon-Batenburg et al., 1996). CI can be converted to CII, but not vice versa (Blackwell and Kolpak, 1975; Kolpak and Blackwell, 1976). Thus, as shown in Figure I-5, in cellulose I (CI), the chain orientation is exclusively parallel (Krassig, 1996), whereas in cellulose II (CII) the chains are arranged in an anti-parallel manner.

Microcrystalline cellulose (MCC) contains the cellulose I lattice. It is obtained from wood pulp and cotton linter by treatment with a dilute strong mineral acid (HCl) at boiling temperatures until the degree of polymerization levels-off (Battista et al., 1957; Battista and Smith, 1961). Acid hydrolyzes the less ordered regions of the polymer chains, leaving the crystalline regions intact. MCC powder is also called hydrolyzed cellulose or hydrocellulose.

Since the 1970s, microcrystalline cellulose I (MCCI) has been the dominant excipient used for direct compression due to its good diluent and binding properties and low moisture content. The strong binding properties of MCC are due to hydrogen bonding between the plastically deforming cellulose particles. However, it suffers from sensitivity to lubricants and poor flow (Lerk et al., 1974; Moreton, 1996). Because of its strong binding properties, it requires the addition of a disintegrant for effective drug release, making formulations more costly. The compactibility of MCCI is also adversely affected when processed by high shear wet granulation since upon drying part of the water interacts with cellulose through hydrogen bonding and as a result, these hydrogen bonds are not available for further particle bonding (Westermarck et al., 1999).

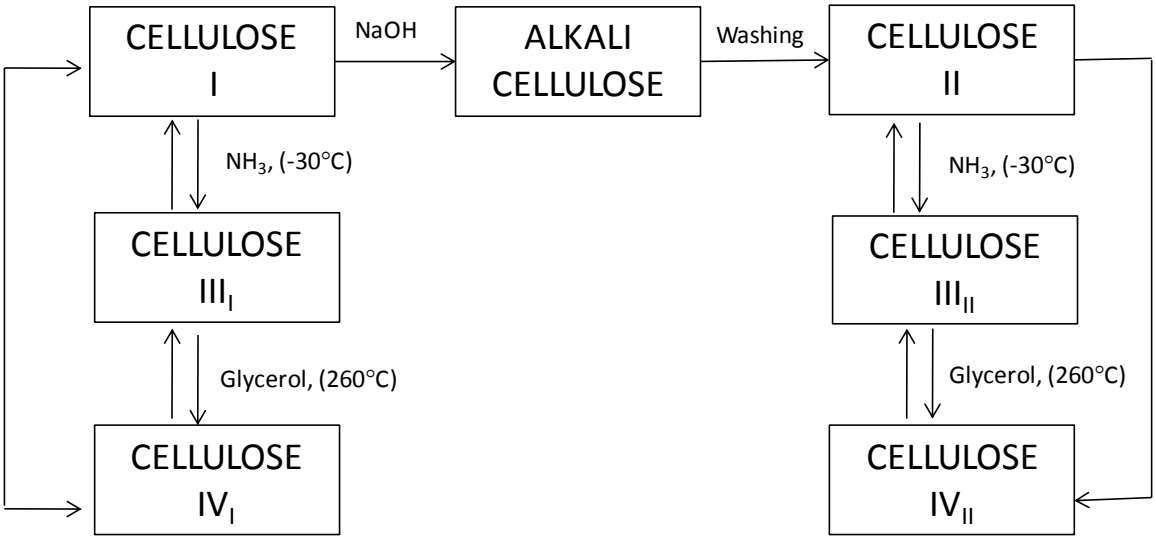

Figure I-4. Scheme for Producing Cellulose Allomorphs.

A. Cellulose I (parallel chain arrangement)

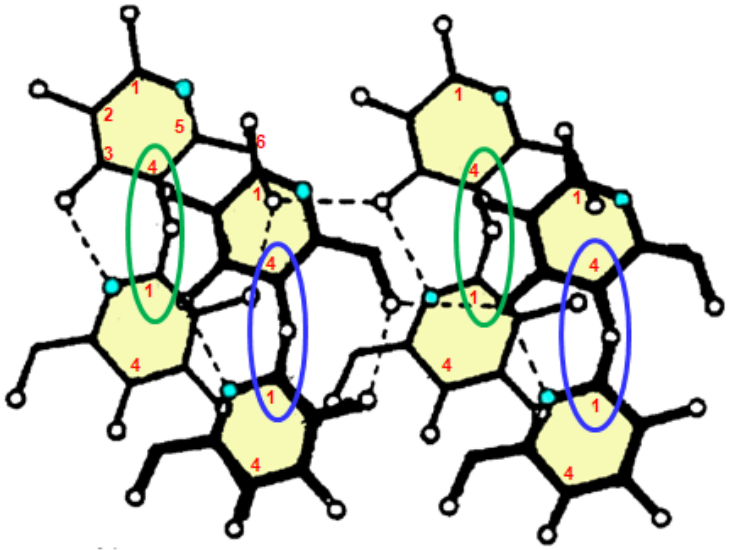

B. Cellulose II (antiparallel chain arrangement)

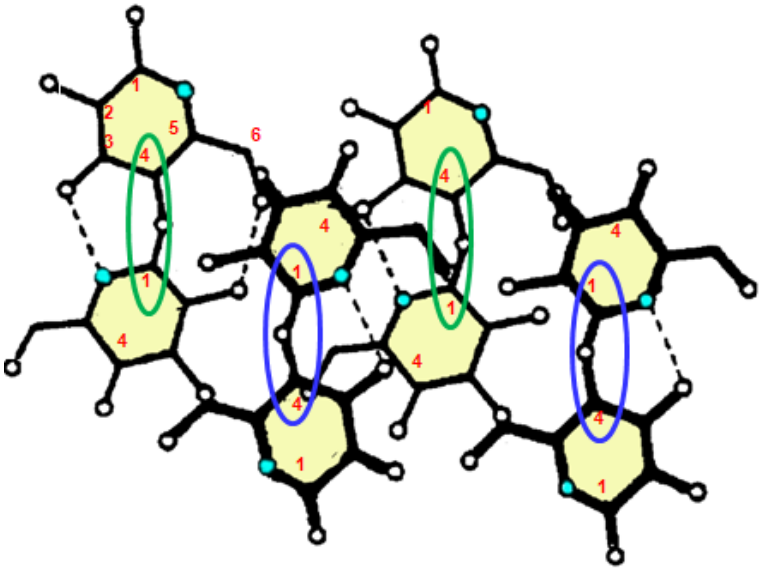

Figure I-5. Conformations of Cellulose I (A) and Cellulose II (B), Adapted from Klemm et al., 1998a.

Recently, cellulose II (CII) was introduced as a new direct compression excipient (Kumar et al., 2002; Leuenberger and Kumar, 2004; Reus and Kumar, 2007). It can be produced by soaking CI (produced from cotton linters) in an aqueous sodium hydroxide solution (> 5 N) at a 1:6 weight-to-volume ratio for 14 h at room temperature, with occasional stirring. The resulting CII gel is then precipitated (regenerated) with a 50-60% aqueous ethanolic solution, filtered, washed with distilled water to neutrality by decantation, filtered again, and dried at 40 °C until reaching a moisture content of less than 6% (Kumar et al., 2002). In general, CII powders show lower crystallinity and higher bulk and tap densities compared to the starting CI counterpart. They are less ductile, and their compacts, irrespective of the compression force used to prepare them, show rapid disintegration (within 30 sec).

Recently, CII was marketed as MCC SANAQ® by Pharmatrans Sanaq AG Pharmaceuticals (Basel, Switzerland). It is available in different grades depending on its particle size and bulk density. Thus, grades 101, 102, 200, 301, 302 and UL-002 corresponds to 50, 100, 180, 50, 100, 50 µm and bulk densities of 0.26 - 0.31, 0.28 - 0.33, 0.29 - 0.36, 0.34 - 0.45, 0.35 -0.46, and 0.13 - 0.23 g/cm^3, respectively (Krueger et al., 2010). This material is used as a diluent, a binder and a rapidly disintegrating material for direct compression, dry and wet granulation and as a diluent for hard gelatin capsules. It could be also used as a pelletization aid. These pellets show faster disintegration and, as a result, have faster release of a poorly water-soluble drug (i.e., chloramphenicol) than pellets made of MCCI (Avicel® PH-102). Differences among MCCI and CII pellets are attributed to water affinity and porosity. Thus, CII requires 15-20% less water to make pellets (Krueger et al., 2010).

Spray Drying to Engineer Functional Properties of Cellulose

Spray drying is a single-step continuous process used to produce dried particles from their dispersions or solutions, preferably, in water. This process is achieved in four stages: atomization of the feed dispersion (or solution) by a pneumatic system, contact of the sprayed droplets with hot air, fast drying of the sprayed droplets and separation of the dried particles from the drying air (Master, 1991). This technique has been extensively applied to prepare free flowing granules, agglomerates, or spherical particles in a narrow particle size range (Billon et al., 1999; Broadhead et al., 1992; Vehring et al., 2007; Vehring, 2008) as well as in the development of new excipients for direct compression (Bolhuis et al., 2004; Limwong et al., 2004; Te Wierik et al., 1996). It has also been used to modify the physicochemical properties of materials. For example, spray-dried lactose shows better flow and compactibility than the unprocessed material (Corrigan and Crean, 2002; Elversson and Millqvist-Fureby, 2005; Sebhatu et al., 1994; Vromans et al., 1986). Other techniques, such as wet granulation do not form spherical particles of small size, but increase particle densification and hence could improve flow and drug uniformity of content. Likewise, extrusion/spheronization is another technique, which is used to produce beads of larger sizes than spray drying. The advantage of beads is that can be used for controlled release of drugs.

Amorphous SiO_2 as a Co-Processing Agent for CII

Fumed silica (SiO_2) is a white, fluffy, odorless and tasteless free-flowing powder of high purity (> 98%) that is widely used as a glidant and antistatic agent in tablet and capsule formulations to promote flow of granulations to avoid caking, clumping or formation of lumps (Hidaka et al., 2009). This latter property has been reported to be superior compared to that of magnesium stearate and talc (Cabot, 2004; Cabot, 2008a; Cabot, 2008b). SiO_2 is light (bulk density of ~0.05 g/cm^3) and is composed of

semispherical nanoparticles (~20 nm in size) with a surface area of ~200 m^2/g. These nanoparticles usually exist as aggregates (Figure I-6). SiO_2 possesses few free hydroxyl groups (silanols), which make the formation of hydrogen bonds with water possible (Figure I-7). These silanols are formed when fumed silica is exposed at high relative humidities for increased periods of time (Wang and Wunder, 2000).

However, fumed silica is poorly soluble in water (0.012 g/100 g). As soon as it is dispersed in water, the aggregates of semispherical particles build up a three dimensional (3D) network, leading to an increase in viscosity and the formation of a stable dispersion. Alternatively, in alkaline aqueous solutions (pH >10), fumed silica is transformed rapidly into silicate anion (SiO_4^{-4}) and becomes water soluble.

Co-Processing of CII with Fumed Silica

One strategy to improve the functional properties (such as flow, compactibility and lubricant sensitivity) of CII as obtained from cotton linter, without compromising its fast disintegration, could be through co-processing with amorphous silicon dioxide using the wet granulation, spray drying and spheronization techniques. The properties of any co-processed product could be beneficial with respect to various tableting properties (Lerk et al., 1974). For example, different co-processing of starch:fumed silica ratios by either co-precipitation or wet granulation rendered different tableting properties to the material. The 1:1, 10:1 and 100:0 (w/w) co-processed products produced compacts of hardness of 20 kN, 40 kN and 250 kN and disintegration times of 10 sec, 30 sec and >10 min, respectively (Badwan et al., 2008). Similarly co-processing of chitin and fumed silica at 50:50 and 80:20 ratios by co-precipitation from an aqueous solution of both components rendered materials with a bulk density of 0.45 g/cm^3 and 0.26 g/cm^3, respectively and Carr indexes of 10% and 28%, respectively (Rashid et al., 2008).

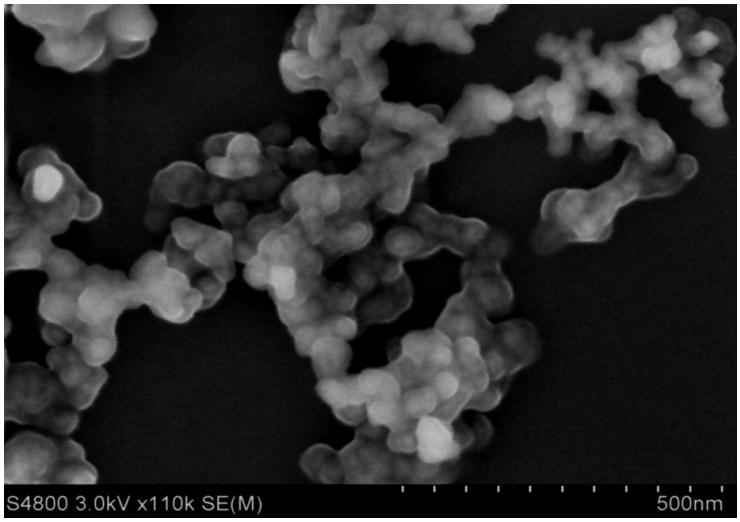

Figure I-6. SEM of Fumed Silica Aggregates at 110,000 Magnification.

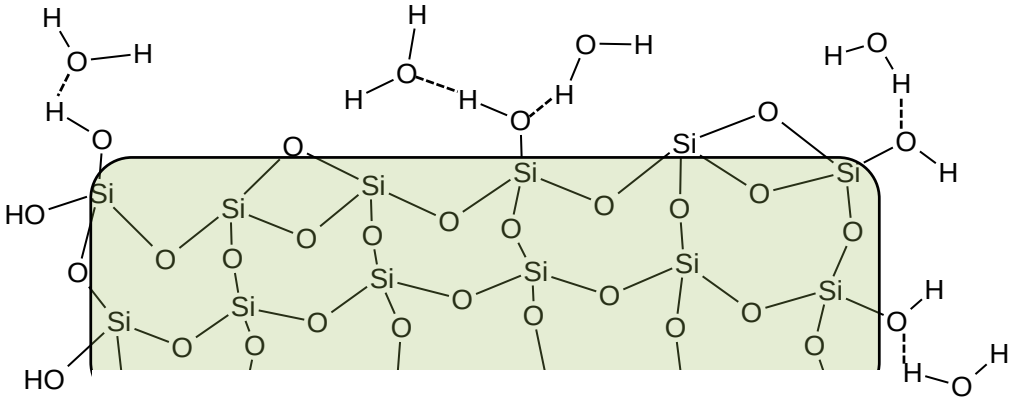

Figure I-7. Hydrogen Bonding between SiO_2 and Water (Adapted from Cabot, 2004)

CHAPTER II

OBJECTIVES

Modifications at the particle level of an excipient could affect tableting behavior and formulation success in a solid dosage form. Usually, particle changes will be reflected at the bulk powder level and on the quality characteristics of the resulting compacts. Further, particles of two different materials could interact synergistically or antagonistically during the compaction process affecting tableting performance. Therefore, the overall goal of this study was to investigate and understand mechanistically the effect of physical changes of cellulose II (CII) on the powder and tableting properties of the treated material. Likewise, the effect of fumed silica incorporation (silicification) on the bulk powder, water sorption, and tableting properties of cellulose II (CII) by co-processing with spray drying, wet granulation and spheronization and the suitability of the resulting materials as direct compression excipients was investigated in comparison to commercial cellulose I. The primary and specific objectives were:

Primary Objective #1

To investigate how particle transformation through spray drying affects powder and tableting performance of CII compared to common direct compression carbohydrate excipients.

Specific Objectives

- To evaluate the effect of spray drying on the dilution potential of CII.
- To compare the functional properties of the spray-dried material (SDCII) with commonly used direct compression carbohydrate excipients.

- To assess the compression and compaction characteristics of SDCII.

Primary Objective #2

To study the suitability of CII and SDCII as disintegrating agents for the development of fast disintegrating compacts.

Specific Objectives

- To investigate the compact disintegration mechanism of these materials.
- To compare the compact disintegration performance of SDCII and CII with that of commercial superdisintegrants.
- To assess the disintegrant effect on the release profile of ibuprofen.

Primary Objective #3

To evaluate how particle modification through silicification and processing affect powder, water sorption, mechanical, drug release and tableting properties of CII powders. The goal is to optimize silicification levels and processing for producing tablets by direct compression.

Specific Objectives

- To characterize the particle properties of CII:SiO_2 composites prepared at different weight ratios by spray drying, wet granulation and spheronization.
- To investigate the effect of silicification on CII water sorption and swelling properties.
- To evaluate the effect of silicification on CII compression behavior and elastic recovery.
- To determine if silicification affects the disintegration properties of CII.
- To assess how CII silicification alters the release profiles of a water-soluble drug (diphenhydramine·HCl) and a poorly water-soluble drug (griseofulvin) compacts.

- To evaluate how CII's mechanical properties (e.g., energy at fracture, compressibility and compactibility) are affected by silicification.
- To assess the influence of silicification on lubricant sensitivity of CII.
- To examine the role of silicification on materials reprocessability after milling.
- To investigate the effect of relative humidity and storage time on compact strength.
- To explore the potential use of CII and CII:SiO_2 composites for spheronization.
- To analyze the effect of silicification on compact surface area.

CHAPTER III

EXPERIMENTAL SECTION

Materials

All materials employed in this study are listed in Table III-1.

Table III-1. List of the Materials Employed.

Material (Brand, lot)	Supplier (City, State)
Acetaminophen (lot GOH0A01)	Sigma-Aldrich (St. Louis, MO)
Acetonitrile (lot 042316)	Fisher Scientific (Fair Lawn, NJ)
Anhydrous dibasic calcium phosphate (A-TAB, lot 024M0118)	Rhodia Inc. (Cranbury, NJ)
Ammonium hydroxide, 29.7% (lot 956272)	Fisher Scientific (Fair Lawn, NJ)
Capsules (Size 0 and 3, lot 9PN734)	Eli Lilly and company (Indianapolis, IN)
Cotton linter (lot R270)	Southern Cellulose Products, Inc. (Chattanooga, TN)
4-Chloroacetic acid (lot 043624)	Fisher Scientific (Fair Lawn, NJ)
Copper (II)-ethylenediamine complex, 1M (lot A0253713)	Acros Organics (Morris Plains, NJ)
Crospovidone (Polyplasdone® XL, lot S10906)	International Specialty Products (Wayne, NJ)
Diphenhydramine HCl (lot 88H1186)	Sigma Aldrich (St. Louis, MO)
Griseofulvin (lot 31K1464)	Sigma Aldrich (St. Louis, MO)
Hydrochloric acid (37%, lot 2612KLHV)	Mallinckrodt Specialty Chemicals Co (St. Louis, MO)

Table III-1. Continued

Material (Brand, lot)	Supplier (City, State)
Ibuprofen (lot QJ0238)	Spectrum Chemicals (New Brunswick, NJ)
Magnesium stearate (Powder Hyqual, lot 2256KXDS)	Mallinckrodt Baker (St. Louis, MO)
Mannitol (lot 26821)	Research Products International Corp. (Mt. Prospect, IL)
Methanol (lot A4412)	Research Products International Corp. (Mt. Prospect, IL)
Microcrystalline cellulose powder (Avicel® PH-102, lot 2339)	FMC Biopolymers (Newark, DE)
Microcrystalline cellulose powder (Avicel® PH-101, lot 1430)	FMC Biopolymers (Newark, DE)
Microcrystalline cellulose I, Celphere® beads (CP-203®, lot 26J10)	Asahi Kasei Chemical Corp (Tokyo, JP)
Pregelatinized Starch (Starch 1500®, lot IN504089)	Colorcon (West Point, PA)
Silicified microcrystalline cellulose (Prosolv® 50, lot XCSD9D661X)	JRS Pharma (Patterson, NY)
Silicified microcrystalline cellulose (Prosolv® 90, lot XCSD5B61X)	JRS Pharma (Patterson, NY)
Sodium carboxymethyl cellulose (Ac-Di-Sol®, lot T353NDR63)	FMC Biopolymers (Philadelphia, PA)
SiO_2 (Cab-o-Sil M5, lot I107)	Cabot Corp (Billerica, MA)
Sodium hydroxide 97.5%, (lot 51758)	Fisher Scientific (Fair Lawn, NJ)
Sodium lauryl sulfate (lot 984881)	Fisher Scientific (Fair Lawn, NJ)
Sodium starch glycolate (Primojel®, lot 953813624)	DMV-Fonterra Excipients LLC (Princeton, NJ)
Spray-dried lactose (Fast Flo® 316, lot 8596021361)	Foremost Farms (Baraboo, WI)
Triethylamine (lot 8974943)	Fisher Scientific (Fair Lawn, NJ)

Methods

Preparation of Unprocessed Cellulose II Powders (CII)

The method reported by Kumar and collaborators (Kumar et al., 2002) was employed, with minor modifications, to prepare CII. Approximately 5 kg of cotton linter sheet was cut into strips (size: 5 cm x 0.5 cm) and soaked in 30 L of 7.5 N NaOH for 72 h (cellulose:NaOH solution 1:6, w/v) at room temperature. The mixture was manually stirred every 12 h with a stainless steel stirrer. The NaOH-treated cotton linter strips were collected by filtration and washed with deionized water until the washing showed the same pH range as distilled water (pH of 5-7). An appropriate amount of the washed cotton linter strips, equivalent to 280 g of cellulose, on a dry weight basis, was transferred to a five-liter round-bottom flask equipped with a condenser and a mechanical stirrer along with two liters of 1 N HCl. The mixture was allowed to stand at room temperature for 1 h and then heated at 105°C. When the strips were reduced to small pieces, the reaction mixture was stirred at 600 rpm. Heating was continued for an additional 1.5 h. The reaction mixture was then cooled to room temperature and filtered. The white powder thus obtained was washed with deionized water until the pH of the filtrate was between 5 and 7 and then dried at room temperature to a moisture content of less than 7% (w/w). The yield of this powder in dry basis was ~90%.

Preparation of Spray-Dried Cellulose II (SDCII)

The Spray Drying Process

Figure III-1 shows a schematic of the laboratory scale Yamato Pulvis spray-drier (Model GB22, Yamato Scientific America, Inc., Santa Clara, CA) used in this research.

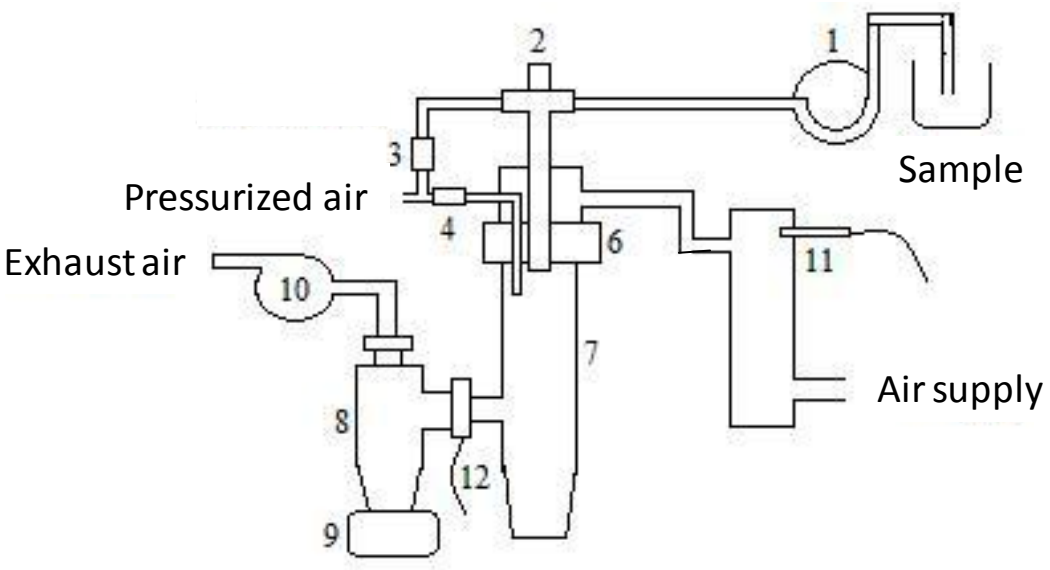

1. Fluid pump	2. Spray nozzle	3. Needle valve	4. Electromagnetic valve
5. Heater	6. Distributor	7. Drying chamber	8. Cyclone
9. Product vessel	10. Aspirator	11. Inlet temperature sensor	12. Outlet temperature sensor

Figure III-1. Yamato Spray-Drier.

The feed dispersion is pumped (1) through an atomization gun equipped with a two fluid nozzle tip (also called air-atomizing nozzle) (2), which generates fine droplets (usually from 20 to 180 µm) in the upper part of the drying chamber (Portmann et al., 2007)(7). The hot drying air (5) is passed through the distributor (6) and meets the droplets drying them into particles and also enables the dried particles to have short residence times in the drying chamber (7) and in the cyclone (8). The dried particles trapped in the cyclone are then collected in the product vessel (9). Inlet temperatures were always above 100º C with water as the solvent. Organic liquids with low flash points, such as ethanol, were not used.

The air-atomizing nozzle (a two fluid nozzle) was used to provide the energy required to break up the liquid into fine droplets (Figure III-2). These devices atomize liquid by a simple shearing action provided by a high velocity air stream impacting on a circulating liquid. A spray set-up consists of a seal, liquid cap, air cap and a locknut. The spray mechanism is formed by internal mix of the liquid and air jets. Usually, the central feed line conducts the liquid, whereas the six surrounding ducts conduct air. The resulting mix will form a cone shape spraying with a rosette type cross-sectional pattern.

Statistical Experimental Protocol

Preliminary runs were conducted to determine the spray-drying processing. A 3% aqueous dispersion of CII was employed and the material was pumped through the 411 µm nozzle using when the inlet temperature reached 100 ºC. The atomization air and the drying air speed were kept at 0.5 kg-f/cm^2 and 0.36 m^3/min, respectively. Since condensation on the drying wall was observed, the temperature was increased until no appreciable condensation was observed (140 ºC). Further, the flow rate was increased from 1 to 5 mL/min, but frequent clogging was observed. Thus, by using a 711 µm nozzle clogging was reduced.

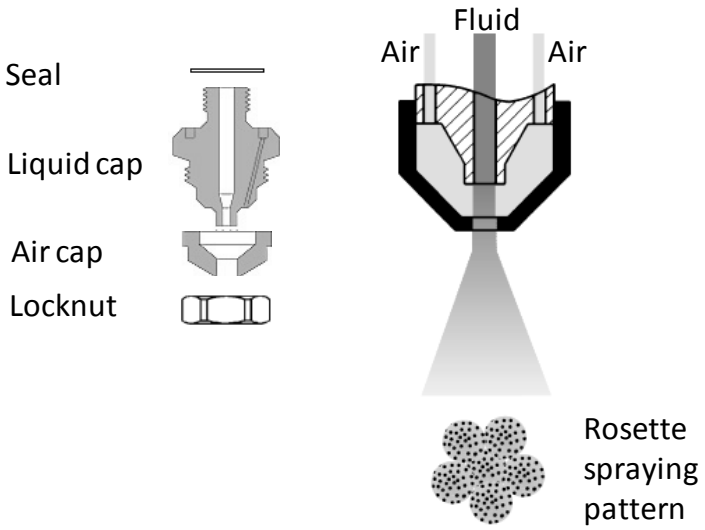

Figure III-2. Schematic of an Air-Atomizing Nozzle.

From these preliminary testing conditions, was decided to conduct a Fractional Factorial Design, using a low and a high level of some of these preliminary testing conditions. The independent spray drying variables employed were: feed concentrations (C) = 3 and 6% w/v; inlet air temperatures (IT) = 140 and 200 °C; drying air speeds (DA) = 0.36 and 0.46 m^3/min; atomization air pressures (AA) = 0.5 and 1.5 kg-f/cm^2; feed spraying rates (FR) = 1.0 and 5.0 mL/min; and sprayer nozzle diameters (ND) = 411 and 711 µm. The main response factors were yield (Y) and particle size (PS).

A randomized two factor factorial design (FFD), 2_{IV}^{k-p} [where, 2 represents the two levels design, k = 6 (the number of factors), p = 2 (the number of generators), and IV is the resolution of the factorial design], without center points, was employed to determine the main operational parameters that significantly affected the response factors. Confounding or mixing of effects of the main factors with higher order interactions, was assumed negligible. A Box Behnken design with the three significant factors (concentration, inlet temperature and flow rate) was employed for optimization of spray drying conditions.

Aqueous dispersions of cellulose II, containing 3, 4.5 and 6% w/v cellulose content, were prepared by suspending the wet cake or dry cellulose powder, produced according to the method described under *Preparation of Unprocessed CII Powders (CII)*, in water by first vigorous stirring using a mechanical stirrer, and then by passing the mixture through a colloid mill, (Gifford-Wood Co., Hudson, NY) for 10 min.

The resulting homogeneous aqueous dispersion was divided into 100 mL volumes, constantly stirred on a magnetic stirrer (Model 14-505-21, Yamato Scientific, Co. Tokyo, Japan) and spray-dried using a Yamato Pulvis spray-drier (Model GA-22, Yamato Scientific, Co. Tokyo, Japan), employing the operating parameters listed in Tables IV-3 and IV-5, respectively). The dispersion was continuously stirred while being

spray-dried. Spray-dried powders were collected and kept in a desiccator over Drierite® at 15 to 30% RH at room temperature until characterization. The percent yield of the spray-dried powder was calculated by dividing the weight of the spray-dried product obtained by the weight of cellulose employed in the feed and multiplying by 100.

The geometric mean diameter (d_g) of the spray-dried particles was determined microscopically using a Hitachi S-4800 scanning electron microscope (Hitachi High Technologies America, Inc., Schaumburg, Illinois), operated at an acceleration voltage of 10 kV. The powder was fixed on an aluminum stub using a double-sided adhesive and a vacuum was applied (7 mm Hg. The stub and sample was coated with a thin layer of gold/palladium sputter (3-5 nm) under an argon atmosphere for four minutes at 30W. SEMs were taken at 30X magnification. Six hundred particles were randomly selected in each SEM and their projected diameter (d_p) was calculated using ImageJ (v. 1.37, National Institutes of Health, Bethesda, MD), according to the relationship: $d_p = 2*(\text{projected area}/\pi)^{0.5}$. Log-normal distribution plots were then constructed of d_p versus cumulative percent frequency to calculate the geometric mean diameter, d_g, using Minitab (v.16, Minitab®, Inc., State College, PA). Percentile sizes (25%, 50% and 75%) were found using the same software by sorting the diameters from the lowest to the highest value and finding by interpolation of the log-normal plots the lowest diameter which is greater than or equal to 25, 50 and 75% of the observations. In the log-normal plots the 50th percentile will approximate to the geometric mean diameter if data follow a log-normal distribution.

Pilot Scale Preparation of SDCII Powder

Approximately five liters of an aqueous CII dispersion (cellulose content 3% w/v) was prepared following the procedure described in *Preparation of Spray-Dried Cellulose II* (SDCII) employing the optimized spray drying conditions as obtained from the Box

Behnken design discussed under *Box Behnken Design for Spray Drying Optimization* of the discussion section (inlet air temperature 195 ºC, feed flow rate 2 mL/min, drying air speed 0.44 m^3/min, atomization air pressure 1.0 kg-f/cm^2, and nozzle diameter 711 µm).

Particle Size and Particle Size Distribution Analyses of SDCII

The geometric mean diameter (d_g) of the disintegrants was determined microscopically using a Hitachi S-4800 scanning electron microscope (Hitachi High Technologies America, Inc., Schaumburg, Illinois), operated at an acceleration voltage of 3 kV. The powder was fixed on an aluminum stub using a double-sided adhesive stub, applied vacuum of $7x10^{-2}$ bars and thin coated with gold/palladium (3-5 nm) by sputtering under an argon atmosphere for four minutes at 30 W. The photographs were taken at 35X magnification. Six hundred particles were randomly selected in each picture and their projected diameter (d_p) was calculated using the ImageJ software (v. 1.37, National Institutes of Health, Bethesda, MD) according to the relationship: $d_p = 2*(\text{projected area}/\pi)^{0.5}$. The log-normal distribution plot was then constructed between d_g and cumulative percent frequency to calculate the geometric mean diameter, d_g, using Minitab® (v.16, Minitab, State College, PA).

The particle size of the 3% aqueous cellulose II dispersion before and after homogenization was measured by optical microscopy (Sixty Spencer Microscope, American Optical Co., Southbridge, MA) at 10X magnification. The geometric mean diameter, d_g, was determined as described above using between 200-600 particles for the samples prior to milling and between 100 to 200 particles for the homogenized samples. The 25th, 50th and 75th percentiles were also obtained from Minitab® software. They indicate that 25, 50 and 75% of the data fall below the interpolated d_g value in the graph. The 50th percentile also approximates to the median diameter if the data follow a log-normal distribution.

Moisture Content (MC)

The gravimetric method described in the United States Pharmacopoeia 28 /National Formulary 23 was employed (US Pharmacopoeia, 2005, pages: 3024, 3088, 2982, 2994, 1345 and 2993). Lactose (Fast Flo® 316) was heated at 80 °C for 2 h, pregelatinized starch (Starch 1500®) at 120°C for 4 h and cellulose and composite samples at 105 °C for 3 h in a mechanical convection oven (Model STM 80, Precision Scientific, Inc., Chicago, IL). Crospovidone (Polyplasdone® XL) was dried at 105 ºC for 3 h, sodium starch glycolate (Primojel®) at 130 ºC for 90 min, and sodium carboxymethyl cellulose (Ac-Di-Sol®) at 105 ºC for 6 h using the same mechanical convection oven (Model STM 80, Precision Scientific, Chicago, IL). After the drying period samples were kept in a in a desiccator over dried silica before weighing the dry sample. The moisture content was determined by:

$$\mathrm{MC} = \left[\frac{W_w - W_d}{W_W}\right] * 100\% \qquad \text{Eqn. I-1}$$

Where, W_w and W_d correspond to the weights of the wet and dry samples, respectively.

Fumed Silica Content

A gravimetric method was employed. Approximately, 0.2 g of sample was placed in a crucible and dried in an oven (Lindberg/BlueM, Thermo Scientific, Waltham, MA) at 105 °C for 2 h. Heating was then continued at a heating rate of 20 °C/min until reaching a temperature of 900 °C. Heating was then continued for 2 h, and the samples allowed to cool completely. Once samples were cooled, they were then taken out from the oven and placed in a desiccator over dried silica gel before weighing. The percentage of fumed silica was found by:

$$\text{Fumed silica} = \left[\frac{W_i - W_f}{W_i}\right] * 100\% \qquad \text{Eqn. I-2}$$

Where, W_i and W_f correspond to the initial and final sample weights, respectively. The analysis was conducted in triplicate.

Fourier Transform-Infrared Spectroscopy (FT-IR)

Approximately 1.5 mg of carbohydrate excipients (CII, SDCII, Avicel® PH-102, Starch 1500® and Fast Flo® 316) were mixed with about 300 mg of dry potassium bromide (dried at 110 °C for 4 h before use) with an agate mortar and pestle. The powdered samples were compressed into a pellet using a 1.3 cm flat-faced punch and die set on a hydraulic press (Pasadena Press, Pasadena Hydraulics, Inc., El Monte, CA) at ~15,000 lbs. The dwell time was five minutes. A Nicolet 210 FT-IR spectrophotometer (Nicolet Corp, Madison, WI), equipped with Omnic® software (Nicolet Corp, Madison, WI) was used to obtain the spectra between 650 to 4000 cm^{-1}.

Swelling Studies (Swelling Value)

The swelling value is expressed as the ratio of the expanded volume of the disintegrants and cellulosic powders after being placed in water compared to the initial sample weight. It was determined following the procedure reported by Edge and collaborators (Edge et al., 2002a; Edge et al., 2002b). Approximately 500 mg of the powder was manually dispersed in a 10 mL graduate cylinder filled with 10 mL of distilled water at room temperature. The cylinder was placed on a flat surface and the increase in volume of the powder was measured with time (~5 days). The swelling value at each time point was calculated by dividing the sediment volume by the sample weight and was expressed as mL/g. The analysis was conducted in triplicate.

Water Uptake of SDCII and CII

The water uptake ability of SDCII, CII and disintegrants (crospovidone, sodium carboxymethyl cellulose and sodium starch glycolate) was determined according to the reported procedure (Zhao and Augsburger, 2005) with minor modifications. One difference was that 10 mL of water and 500 mg of sample was used, instead of a continuous water flow for 120 sec and 200 mg of sample. This procedure measures the rate of water sorption by a material when it comes in contact with water. Briefly, a funnel (diameter 6 cm), attached to Tygon tubing at the stem was placed on an analytical balance (Model R200D, Sartorius, Bohemia, NY) with a tripod stand (Figure III-3). The Tygon tubing was long enough to deliver water into a collecting vessel placed next to the balance without affecting water flow, and measurements of the weight were obtained at different time points during the test. Whatman qualitative filter paper # 1(dia. 90 mm) was wetted with distilled water and placed in the funnel. An accurately weighed sample of test material (~ 500 mg) was then added and the weight of the stand, funnel, wetted filter paper, powder, and Tygon tube, all together, was measured. Ten milliliters (10 mL) of distilled water was poured into the funnel through the filter paper, ensuring that the test sample was completely immersed in water. The change in water uptake weight as a function of time was recorded. The measurement was stopped when a stable weight was obtained. The experiment was repeated without powder. The weight differences with and without the powder, as a function of time, was taken as the water uptake ability of the powder. All materials were analyzed in triplicate.

CII-SiO_2 Composites Prepared by Spray Drying

A slurry of CII (conc. ~15-35 % w/v) was produced as described under *Preparation of Unprocessed CII Powders (CII)*.

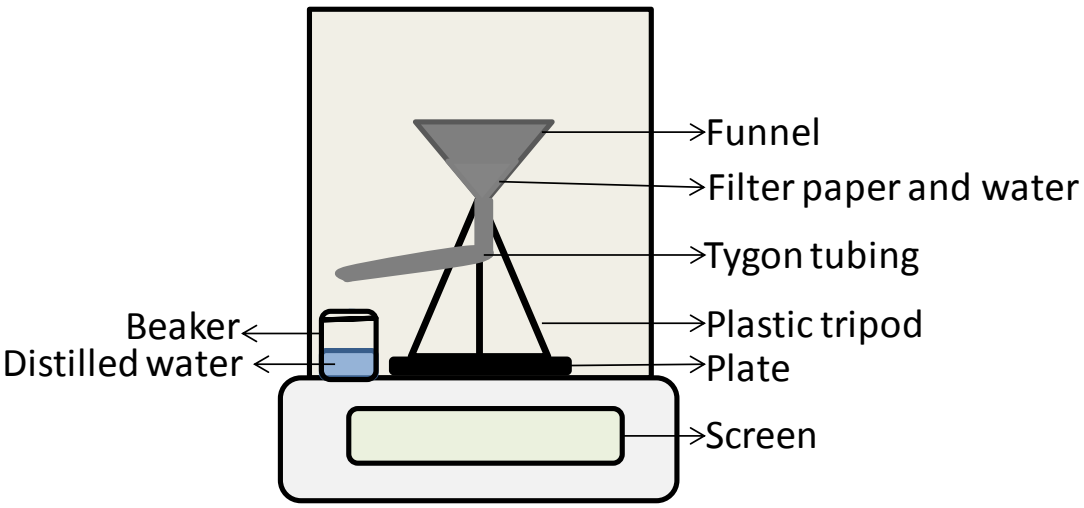

Figure III-3. Schematic of the Water Uptake Set-up.

Appropriate amounts of the cellulose slurry and SiO_2, equivalent to 98:2, 95:5, 90:10, and 80:20 weight-by-weight ratios were mixed and diluted with distilled water to obtain a 3% dispersion of the CII:SiO_2 composite using either a homogenizer (Biospec Products, Bartlesville, OK) for 10 min at 10,000 rpm or a colloid mill at a graduation of 60 (Model 2001B, Eppenbach colloid mill, Gifford-Wood Co., Hudson, NY) for 10 min at room temperature. A Yamato Pulvis spray-drier (Model GB-22, Yamato Scientific, Co., Santa Clara, CA) was employed. The dispersion was continuously stirred while being sprayed at the previously optimized spraying conditions: inlet air temperature (IT) 195 °C; atomizing air pressure (AA) 1.0 kg-f/cm^2; drying air speed (DA) 0.44 m^3/min; feed flow rate (FR) 2.0 mL/min and nozzle diameter (ND) 0.711 mm. Lot sizes ranged from 30 to 100 g.

CII-SiO_2 Composites Prepared by Wet Granulation

The method of preparation of the slurry of CII (conc. ~15-35% w/v) and a 5% dispersion of CII and SiO_2 (98:2, 95:5, 90:10, and 80:20 w:w ratios) were prepared as described in *CII-SiO_2 Composites Prepared by Spray Drying*. The resulting homogeneous mixture of CII:SiO_2 was collected by vacuum filtration and then air-dried to 45% moisture content (see *Moisture Content*) and then granulated using an Erweka oscillating granulator (Model AR400, Chemical and Pharmaceutical Industry, Inc., New York, NY), equipped with 710 µm screen. The granulation step was repeated at 30% and 20% moisture contents using screens having an aperture of 250 µm and 100 µm, respectively. These moisture contents and screen sizes were chosen by trial and error since the original material having a high moisture content was not possible to pass it through a 150 µm directly, without progressive drying. The granules obtained were dried either in air or in a convection oven at 35 ºC until the moisture content was less than 5% (see *Moisture Content*). Batch sizes ranged from 100 to 300 g.

CII-SiO_2 Composites Prepared by Spheronization

A slurry of CII (conc. ~15-35% w/v) and a 5% dispersion of CII and SiO_2 (98:2, 95:5, 90:10 and 80:20 w:w ratios) were prepared as described in *CII-SiO_2 Composites Prepared by Spray Drying*. The resulting homogeneous mixtures of CII:SiO_2 were collected by vacuum filtration and tray-dried at room temperature until the moisture content was 40-50% (see *Moisture Content*) and then granulated using an Erweka oscillating granulator (Model AR400, Chemical and Pharmaceutical Industry, Inc., New York, NY), equipped with a 710 µm screen size. The extrudate (spaghetti-like rods) was further dried to a moisture content (MC) of ~30% and then extruded using the same granulator at a 250 µm screen size. The same procedure was repeated at moisture content level of ~20% using a 150 µm screen size. These MC and screen sizes were chosen by trial and error of the appropriate MC in which the wet pass could pass through. The extrudate obtained was put in the spheronizer chamber (Marumerizer, Model QJ-230T, Fuji Paudal Co., Ltd., Charlotte, NC) and spheronized at 1000 rpm for 10 to 15 min. The resulting beads were collected and air-dried for 24 h at room temperature until the moisture content was less than 5% (see *Moisture Content*).

Preparation of Excipient-Griseofulvin and Excipient-Diphenhydramine HCl Beads by Spheronization

Approximately 13 g of CII, microcrystalline cellulose I (Avicel® PH-101), or silicified microcrystalline cellulose I (Prosolv® SMCC 50) and 6.5 g griseofulvin were mixed using a V-blender (Model LB429, Patterson Kelley Co., East Stroudsburg, PA) for 30 min. An appropriate amount of distilled water was sprayed and mixed manually to prepare a wet mass containing ~45% moisture content (see *Moisture Content*). The wet mass was passed through an Erweka oscillating granulator (Model AR400, Chemical and Pharmaceutical Industry, Inc., New York, NY), equipped with a 425 µm screen. The granules obtained were put in the spheronizer chamber (G.B. Caleva LTD, Model

SPH120, Dorset, England) and spheronized at 2000 rpm for 5 to 10 min. The beads so obtained were dried at room temperature until the moisture content was less than 5%. Gelatin capsules (size Ø) were filled manually with ~380 mg of beads (125 mg of griseofulvin).

The above procedure was repeated to prepare excipient-diphenhydramine·HCl beads except that the ratio of excipient:drug was 1:5 (5 g drug and 25 g excipient) and the gelatin capsules (size 3) were filled manually with ~150 mg of powder, equivalent to 25 mg of diphenhydramine HCl.

Particle Size and Particle Size Distribution of Composite Materials

The CII:SiO_2 composites were fractionated on a Ro-Tap sieve shaker (Model, RX29, W.S. Tyler, Mentor, OH) using stainless steel 600, 420, 250, 177,150, 125, 105, 75, 53, 45, and 38 µm sieves (Fisher Scientific Co., Pittsburgh, PA). Approximately 100 g of the sample was shaken for 30 min. For composites of spheronized CII:SiO_2, the fraction of 150-420 µm similar to the fraction of Celphere-203® (silicified microcrystalline cellulose I) beads (Asahi Kasei Chemical Corp, Tokyo, JP), was collected and used for comparison purposes.

The spheronized products containing diphenhydramine HCl or griseofulvin were fractionated using a set of sieve screens corresponding to 2380, 2000, 1400, 841, 600, 425, 250, 180 and 90 µm. The geometric mean diameter, d_g, and particle size distribution were determined from a log-normal distribution plot constructed between the sieve mean diameter and cumulative percent frequency using the Minitab® software (v.16, Minitab, Inc., State College, PA).

True Density Determination

The helium displacement micropycnometer (Model MPY-2, Quantachrome Corp., Boynton Beach, FL) was employed. Samples were dried in a vacuum desiccator (Model 68351, Precision Scientific Co., Chicago, IL) at 60 °C and at a reduced pressure of 40 mm Hg for 24 h before testing. Approximately one gram of the sample was used for analysis. The sample was out-gassed with helium for at least 40 minutes before each measurement. The control switch was turned to "cell out (P1)," followed by pressurizing the system between 15 and 17 psi with helium, holding this pressure for one minute, and then the pressure was recorded. The control switch was then turned to the "cell in (P2)" position and the pressure value reading was recorded after one minute. The true density was calculated by dividing the mass of the material by its volume, obtained from the equation:

$$V_p = \mathrm{V_c} - \mathrm{V_r} * \left[\frac{P_1}{P_2} - 1\right] \qquad \text{Eqn. III-3}$$

Where, V_p is the volume of the powder, V_c is the cell volume and $V_{r.}$ is the volume of the two reference balls. The test was carried out in triplicate on independent samples.

Bulk/Tap Densities, Powder Porosity and Hausner Ratio

Bulk density (ρ_{bulk}) was determined using a 100 mL graduated cylinder filled with 20 g of sample. The cylinder was tapped twice to remove the powder adhering to the walls, prior to recording the volume. Bulk density was calculated as: ρ_{bulk} = mass/volume. For tap density, the same graduated cylinder used to measure ρ_{bulk} was tapped 1,200 times using a VanKel tap density analyzer (Model 50-1000, VanKel Industries, Cary, NC). No further reduction in the tap volume was noted after 1,200 taps. The volume of the sample was then read and tap density calculated as ρ_{tap} =

mass/volume. The density determination was carried out in triplicate. Porosity (ε) of the powder was determined from the equation:

$$\varepsilon = \left[1 - \frac{\rho_{bulk}}{\rho_{true}}\right] * 100\% \qquad \text{Eqn. III-4}$$

Where ε, ρ_{bulk}, and ρ_{true} are the powder porosity, bulk density and true density, respectively. The Carr index (CI), which is a measure of the powder compressibility and an indirect measurement of powder flow, was obtained from:

$$CI = \left[\frac{\rho_{tap} - \rho_{bulk}}{\rho_{tap}}\right] * 100\% \qquad \text{Eqn. III-5}$$

Where, ρ_{tap} and ρ_{bulk} corresponded to the tap and bulk densities, respectively. If the resulting percentage ranges as: < 10, 11-15, 16-20, 21-25, 26-31, 32-37 and >38, powder flow is classified as excellent, good, fair, passable, poor, very poor, and very, very poor, respectively. Likewise, Hausner ratio of silicified materials, which is a measure of friction forces to overcome when a powder is tapped, was determined from the ratio of tap and bulk densities according to the relationship (Hausner, 1967):

$$HR = \left[\frac{\rho_{tap}}{\rho_{bulk}}\right] \qquad \text{Eqn. III-6}$$

Where, ρ_{tap} and ρ_{bulk} are the tap and bulk densities, respectively. Further, this ratio can be used as an indirect measurement of flow. For instance, if the resulting ratio ranges as: 1.0-1.11, 1.12-1.18, 1.19-1.25, 1.26-1.34, 1.35-1.45, 1.46-1.59 and > 1.60, powder flow is classified as excellent, good, fair, passable, poor, very poor and very, very poor, respectively.

Powder Flow Measurements

The powder flow was determined by the "flow-through-an-orifice method." The test was executed on a custom-made flowmeter, which consisted of a stainless steel cylinder (2.5 x 20.0 cm), mounted on a metal block, and a replaceable set of steel plates with a hole in the center supported by a lower plate without a hole. Approximately 20 g of the sample was filled in the cylinder by using a glass funnel and the supporting plate was then pulled out, so that the powder could freely flow through the upper plate orifices (14.3, 17.5 and 19.1 mm in dia.) and the time to flow was taken. The flow rate was expressed as g/sec. The test was done in triplicate.

Degree of Crystallinity (DC)

Powder X-ray diffraction (PXRD) measurements were conducted over a 5 to 45º 2θ range using a Siemens diffractometer (Model D5000, Siemens Energy and Automation, Inc., Madison, WI), with monochromatic CuKα (α_1= 1.5460 Å, α_2= 1.5444 Å) X-ray radiation. The step width was 0.020º 2θ/min with a time constant of 0.5 sec. The Difrac® Plus Eva software, version 2.0 (Siemens Energy and Automatization, Inc., Madison, WI) was used for calculation of the peak areas. The DC was calculated by separating the crystalline and amorphous scattering using the baseline selection menu from the software toolbox according to the relationship (Rabek, 1980):

$$DC = \frac{I_C}{(I_C + I_a)} * 100\% \qquad \text{Eqn. III-7}$$

Where, I_c is the sum of the areas of all X-rays diffraction peaks and I_a is the area of the diffuse halo due to the amorphous region (Figure III-4).

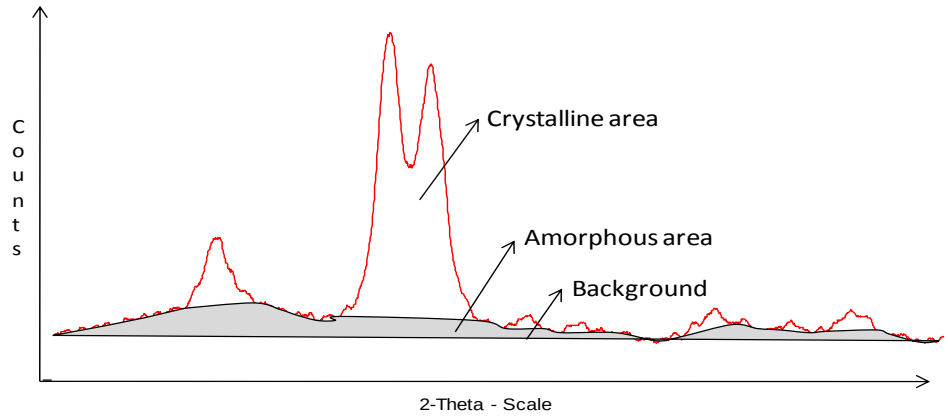

Figure III-4. Typical Powder X-ray Diffractogram of Cellulose II Showing Crystalline and Amorphous Regions.

The amorphous area comprises the region between the background and the base of the crystalline peaks. The crystalline area was obtained by setting the curvature base of the crystalline peaks and calculating their area (Figure III-4).

Degree of Polymerization

The viscosity-average molecular weight or $\bar{M}_v$ for cellulose samples was determined by capillary viscometry following the procedure adapted from the American Standard for Testing Materials (ASTM # D1795-96). Cupriethylendiamine hydroxide (CUEN) was used as a solvent for cellulose in which a Prussian blue cellulose-copper complex is formed. Cellulose solutions were prepared by dissolving 250 mg of cellulose, on a dry weight basis, in 50 mL of a 1:1 (v/v) mixture of 0.5M CUEN. The final cellulose concentration was 0.5 g/dL. Samples were constantly stirred on a magnetic stirrer and flushed with nitrogen for 30 min to prevent oxidation of the cellulose complex in the alkaline medium. A Cannon-Fenske capillary viscometer (No. 50) (Cannon Instrument Company, State College, PA) was used to measure the efflux times of the solvent and cellulose solutions. The viscometer has a capillary tube diameter of 0.44 mm, which provided efflux times of ≥ 80 seconds for CUEN and cellulose solutions, which were long enough to be measured precisely to reduce variability associated with the possible kinetic energy effects (i.e., shear rate). The capillary viscometer was immersed in a water bath, equipped with a temperature controller set at 25 ºC. Approximately, 10 mL of the cellulose or CUEN solution was withdrawn with help of a pipettor and placed in the lower bulb of the viscometer. The solution was drawn up into the upper neck of the bulb by vacuum such that the level of the liquid was above the upper mark of the bulb. Once the vacuum was released, the efflux time of the solution from the upper mark to the lower mark was recorded. The relative viscosity η_{rel} was obtained from:

$$\eta_{rel} = t/t_o \qquad \text{Eqn. III-8}$$

Where, t and t_o are the efflux times of the cellulose solution and the solvent, respectively. The ASTM # D1795-96 (Meyer, 2006) table lists the predetermined values of the product of intrinsic viscosity and concentration, [η]C of cellulose solutions exhibiting η_{rel} values between 1.1 and 19. This table is used as the one point viscosity method. From interpolation of this table, the [η]C values were obtained. The [η] values were obtained from the Martin equation (Meyer, 2006):

$$\log[\eta] = log\left[\frac{\left(\frac{t}{to}\right)-1}{0.5g/dL}\right] - 0.13 * [\eta]C \qquad \text{Eqn. III-9 or}$$

$$\log[\eta] = logN_{red} - 0.13 * [\eta]C \qquad \text{Eqn. III-10}$$

Where, [η] is the intrinsic viscosity, and η_{red} is the reduced viscosity and 0.13 is a constant.

The degree of polymerization (DP) was calculated by multiplying [η] by 190, which is a constant previously determined from correlations between intrinsic viscosity and degree of polymerization of cellulose (Vidal et al., 1991). The viscosity average molecular weight $\bar{M}_V$ was obtained by multiplying DP by 162 g/mol (molecular weight of the anhydroglucose repeat unit). All samples were analyzed in triplicate.

Water Sorption Analysis

The water sorption analysis was performed on a VTI Symmetric Gravimetric Analyzer (Model SGA-100, VTI Corporation, Hialeah, FL), equipped with a chilled mirror dew point analyzer (Model DewPrime IF, Edgetech, Milford, MA). The sample pan assembly was cleaned with ethanol and dried before each run. The left pan was tared and calibrated using a 100 mg calibration weight. The weight was then removed and the

pan tared before loading the sample. Sample sizes between 5 to 15 mg were tested. Before each run, the water reservoir was filled with distilled water and the system was continuously purged for 90 min with nitrogen gas to avoid impurity deposition in the sample.

Even though dried samples were employed, an initial drying phase at 60 ºC and at a heating rate of 5ºC/min, with continuous nitrogen gas purging at a relative humidity of less than 1%, was executed. Once a stable reading (weight change of no more than 0.01%) was obtained for 10 min, the sample was considered dry. Runs were conducted at 25 ºC at the desired relative humidity step (from 10 to 90% RH). Moisture uptake in the sample was considered at equilibrium when a stable reading (a weight change of no more than 0.01% or maximum drying time of 240 min) was reached.

The resulting sorption curves were fitted to the GAB (Guggenheim, Andersen and de-Boer) sorption model. The advantages of the GAB (Van den Berg, 1984) model are that it has the same assumptions as the BET theory and it has a simple mathematical form with only three fitted parameters (C, k and m_m). Its parameters have a physical meaning in terms of the sorption process and it has a fitting range at all water activities (0-1).

The assumptions of the GAB model are: The energy of the multilayer is different from that of liquid water; the sites are equivalent, distinguishable and independent; on each site, there are certain numbers of molecules which can be sorbed in a vertical stack without horizontal interactions; and the positions of the molecules in the sorption stack are distinguishable. In this model, the first layer of water evenly covers the sorbent surface and is very tightly bound in a monolayer. Subsequent layers of water have less interaction with the material surface (Qui Rijns et al., 2005).

The GAB equation is:

$$m = \frac{k*\frac{P}{P_0}*m_m*C}{\left(1-k*\frac{P}{P_0}\right)*\left(1-k*\frac{P}{P_0}+C*k*\frac{P}{P_0}\right)} \quad \text{Eqn. III-11}$$

$$C = D * e^{(H_1-H_m)/RT} \quad \text{Eqn. III-12}$$

$$k = B * e^{(H_L-H_m)/RT} \quad \text{Eqn. III-13}$$

Where, m is the weight of the adsorbate (water) per gram of adsorbent (cellulose), m_m is the monolayer capacity or weight of the adsorbate when the surface of one gram of adsorbent is covered by a monolayer (g/g). P/P_0 is the equilibrium partial pressure of the adsorbate (water activity), P is the partial vapor pressure, P_0 is the vapor pressure at saturation. C and k are energy constants of monolayer and multilayer, respectively. B and D are fitted constants, usually taken as 1 (Zografi et al., 1984). H_1 is the heat of sorption of adsorbate in the first layer (kJ/mol). H_m is the heat of sorption of the adsorbate in the intermediate state (kJ/mol). H_L is the heat of liquefaction (kJ/mol). R is the universal gas constant (8.3145 J/mol-K) and T is absolute temperature.

The fitting procedure of equation III-11 was performed using the Statgraphic® software, version 5 (Warrenton, VA). A non-linear regression was conducted with the least square analysis. The test was conducted on three independent samples.

Surface Area Measurements

These measurements were performed using a Quantasorb sorption system (Quantachrome Corp., Boynton Beach, FL). Helium was used as the carrier and diluent gas, while nitrogen gas was used as the adsorbate. Liquid nitrogen was used as a coolant during the adsorption step so that the adsorbate gas (N_2) condenses on the surface of the samples. For powder samples, a capillary cell (Part #74002, Quantachrome Corp.,

Boynton Beach, FL) was used for minimizing thermal diffusion because most of the samples had low surface areas. Before performing the surface area measurements, samples were dried in a vacuum oven (Model 68351, Precision Scientific Co., Chicago, IL) at 60 °C and at a reduced pressure of 40 mm Hg for 24 h. Samples were then degassed for 24 h under continuous nitrogen flow. A five point BET analysis was conducted on all samples, by performing the N_2 adsorption and desorption at relative pressures (P/P_0) ranging from 0.05 to 0.25, using proportional amounts of carrier gas and adsorbate gas flowing through the sample cell. The attenuator was adjusted from 32 to 256, depending on the sample being analyzed since the surface areas of all samples were significantly different and a fixed single attenuation value was not possible to use for all. Adsorption occurred when the sample cell was immersed in liquid nitrogen and the adsorbate (N_2) condensed on the sample surface. Typically, the adsorption peaks were broad and thus, for quantitative purposes, the counts from desorption peaks were used. In order to calibrate the N_2 detector counts, fixed volumes of nitrogen were injected into the sample port, with a glass syringe, and the amount of N_2 was calculated from the equations:

$$X_c = \frac{P_a * M_a * V_c}{\mathrm{R} * T} \qquad \text{Eqn. III-14}$$

$$X = \frac{\mathrm{A} * X_C}{A_{cal}} \qquad \text{Eqn. III-15}$$

Where, X_c is the weight of nitrogen gas injected for calibration, P_a is the ambient pressure (mmHg), M_a is the molecular weight of nitrogen (28 g/mol), V_c is the volume of nitrogen gas injected for calibration (L), R is the gas constant (62.35 L*mmHg/mol*K), T is the temperature (K) at which the adsorption experiment was conducted, X is the weight of the nitrogen gas adsorbed, A is the detector signal area from the sample desorption step

and A_{cal} is the detector signal area from the desorption of nitrogen gas used for calibration. The sorption data were fitted according to the linear Brunauer, Emmet and Teller (BET) equation:

$$\frac{1}{X*\left[\left(\frac{P_0}{P}\right)-1\right]} = \frac{C-1}{X_m*C} * \left(\frac{P}{P_0}\right) + \frac{1}{X_m*C} \qquad \text{Eqn. III-16}$$

Where, P is the partial pressure of the adsorbate, P_0 is the saturated vapor pressure of the adsorbate, X is the mass of adsorbate sorbed at the specific relative P/P_0, X_m is the mass of the adsorbate sorbed at monolayer coverage, and C is a constant related to the heat of adsorption.

The weight of the gas adsorbed at the monolayer coverage was obtained from the slope (s) and the intercept (I) of the BET plot using the equation:

$$X_m = \frac{1}{S+I} \qquad \text{Eqn. III-17}$$

The total surface area of powders was obtained using the equation:

$$S_t = \frac{X_m*N_A*A_{CS}}{M_a} \qquad \text{Eqn. III-18}$$

Where, S_t is the total surface area of the sample, A_{cs} is the cross sectional area of the nitrogen molecule ($16.2x10^{-20}$ m^2), N_A is the Avogadro's number ($6.023\ x10^{23}$ molecules/mol) and M_a and X_m are as described above. The specific surface area (S) was given by:

$$S = \frac{S_t}{W} \qquad \text{Eqn. III-19}$$

Where, S_t is as described above and W is the sample weight. The test was conducted on three independent samples.

Scanning Electron Microscopy (SEM)

The SEM photographs were obtained using a scanning electron microscope (Model S-4800, Hitachi High Technologies America, Inc., Pleasanton, CA), which consisted of a cold cathode field emission electron gun and a two stage electromagnetic lens. The powder was fixed on an aluminum stub using a double-sided adhesive tape and coated using a sputter coater (Model K550, EmiTech, Ashford, UK). Samples were sputtered with a thin layer (3–5 nm) of gold/palladium (60:40) under an argon atmosphere for four minutes at 30W. The acceleration voltage and depth of field were 5 kV and between 4 and 8 mm, respectively. Images were obtained using the SEM software at magnifications of 400X and 10K for the disintegrants (Ac-Di-Sol®, Polyplasdone® XL and Primojel®) and at 50X, and 10K for the CII:SiO_2 composites.

Energy Dispersive X-ray Spectroscopy (EDS)

A variable pressure scanning electron microscope (VP-SEM, Model 3400, Hitachi High Technologies America, Inc., Pleasanton, CA), coupled with a back-scatter electron detector, was used to determine the distribution of SiO_2 in the CII-SiO_2 composites. The X-rays were detected by a line scan mode using a Bruker AXS Microanalyzer (Model GmbH, Bruker AXS, Germany) for 90 sec, employing an accelerating voltage of 15 kV and 10 mm depth of field. These conditions allowed the detection of at least 1,000 X-ray counts.

Tableting Properties

Cylindrical Compacts and Determination of Compact Porosity

Approximately 500 mg of powdered sample was accurately weighed on a Sartorius analytical balance (Model R200D, Sartorius Corp., Bohemia, NY). The powder was poured into a 1.3 cm diameter die cavity with a flat-faced lower punch in place. The

flat-faced upper punch was then placed on top of the powder bed, the punch-die set was placed on the lower platen of a Carver Press (Model C, Fred S. Carver, Inc. Wabash, IN). An industrial load cell (Model LCGD-10K, Range: 0-10,000 lbs., Omega Engineering, Inc., Stamford, CT) was placed on top of the upper punch. Force was manually applied so that the lower platen of the press ascended until contact was established between the load cell and the upper platen. Pumping the pressure lever was performed until the desired force was achieved. This force was kept constant for a period of 30 sec (dwell time). Pressures ranged from ~10 to ~260 MPa and were normalized to a one inch diameter compact. Forces were read on a strain gauge from a panel meter (Model DP25B-S, Omega Engineering, Inc., Stamford, CT) connected to the load cell. The applied force pressure was then released on the hydraulic press, allowing the lower platen to descend.

The tooling was removed from the press and the compact ejection was facilitated with the help of the upper punch, which was longer than the lower punch. Once the tablet was ejected it was stored in a desiccator containing Drierite® (RH= 15-30%) for 48 h. After 48 h, the tablet thickness and diameter were measured with an electronic digital caliper (Ted Pella, Inc., Redding, CA; measuring range 0-150 mm and readability of 0.01 mm). The tablet thickness was measured at five different points around the compact and the average was taken. The volume of the compact at a given pressure was calculated from:

$$V = \pi r^2 h \qquad \text{Eqn. III-20}$$

Where, V, r and h are the volume, radius, and thickness of the compact, respectively. The apparent density of the compact was calculated by dividing the tablet mass by its volume. Compact porosity (ε) was calculated from:

$$\varepsilon = \left[1 - \frac{\rho_{app}}{\rho_{true}}\right] \qquad \text{Eqn. III-21}$$

Where, ρ_{app} is the apparent density of the compact and ρ_{true} is the true density of the material. The ratio of ρ_{app}/ρ_{true} is a measure of the relative density or solid fraction of the compact.

Compact Water Sorption Ratio

The method of Bi et al., was employed to measure the water sorption ratio (Bi et al., 1999). This method evaluates the water uptake ability of a compact when comes in contact with water. Briefly, on a petri dish that contained a KimWipe tissue and 6 mL of water, a tablet was placed in the center. Once the tablet was completely wetted, the water sorption ratio (WSR) was calculated according to the relationship: $WSR = (W_a - W_b)/W_b$, where W_b and W_a are the weights before and after water sorption, respectively. The volume increase was determined by replacing the compact weights in the equation above by the compact volumes. Round tablets (1.3 cm dia.) used in the analysis were prepared on a hydraulic Carver press (Model C, Carver Press, Wabash, IN) using 120 MPa of compression pressure and a dwell time of 30 sec. Tests were conducted on three separate samples.

Compressibility Analysis

Compacts were prepared as described under *Preparation of Cylindrical Compacts and Determination of Compact Porosity*. Each compact was accurately weighed and its dimensions (diameter and thickness) were measured with an electronic digital slide caliper (Ted Pella, Inc., Redding, CA). The natural logarithm of the inverse of a compact porosity, $\ln(1/\varepsilon)$, was plotted against the compression pressure to construct a Heckel plot (Heckel, 1961a; Heckel, 1961b). The slope (m) of the linear region of this curve is inversely related to the yield pressure (P_y), which is a measure of the plasticity of the

material (Alderborn and Nyström, 1996):

$$\ln\frac{1}{\varepsilon} = m\sigma + A \qquad \text{Eqn. III-22}$$

Where, A is the intercept obtained by extrapolating the linear region to zero pressure. Other parameters useful in assessing the compressibility are D_o, D_a, and D_b, which are related to initial powder packing/densification, total compact densification, and particle rearrangement/fragmentation at an initial compaction stage, respectively (York, 1992). D_o was calculated by dividing the bulk density by the true density (Chowhan and Chow, 1980). D_a was obtained from the intercept (A) with the expression: D_a : 1- $\exp^{-A}$, and D_b was calculated with the expression: $D_b = D_a - D_0$.

Kawakita Analysis

The Kawakita model describes the relationship between the degree of volume reduction of the powder and the applied pressure (Kawakita and Ludde, 1971). The Kawakita equation is given by:

$$P/(1- \rho_0/\rho_a) = P/a + 1/ab \qquad \text{Eqn. III-23}$$

Where, P is the applied compression pressure, "a" is related to the total volume reduction for the powder bed (compressibility index), "1/b" is related to the resistant interparticle forces to compression, ρ_0 is the bulk density and ρ_a is the compact apparent density (Patel et al., 2007).

Compact Elastic Relaxation

Compacts were prepared as described under *Preparation of Cylindrical Compacts and Determination of Compact Porosity.* Immediately after compact ejection from the die took place, compact height was measured with an electronic digital caliper (Ted Pella,

Inc., Redding, CA) and stored in a desiccator over Drierite®. After five days, compact height was measured again and elastic relaxation was expressed as percentage as follows:

$$ER = 100*(H_b-H_a)/H_a \qquad \text{Eqn. III-24}$$

Where, H_b and H_a are the compact height after five days of storage and immediately after ejection, respectively.

Tablets for Disintegration Studies

Powder blends of about 25 g each, comprised of components listed in Table III-2, were prepared by mixing in a V-blender (Model LB429, Patterson Kelley Co. East Stroudsburg, PA) for 30 min. Tablets, each weighing 500 mg, were prepared on a hydraulic Carver Press as described in *Preparation of Cylindrical Compacts and Determination of Compact Porosity*. Tablets were stored in a desiccator (RH < 30%) for 48 h before analysis. Relative humidity was monitored employing a digital hygrometer (Extech Instruments, Waltham, MA). Further, compacts of ~500 mg of disintegrants were made at 120 MPa as described above and their disintegration time was measured in distilled water and 0.1N HCl.

Ibuprofen Dissolution Studies

Compacts of blends of Avicel® PH-102, ibuprofen, disintegrant and magnesium stearate were prepared as described under *Tablets for Disintegration Studies* and their composition is given in Table III-3. Dissolution studies of these compacts were performed employing a PharmaTest dissolution apparatus with paddles (Scientific Instruments and Technology Corp., Piscataway, NJ) in pH 7.2 phosphate buffer at 37 ^{o}C with a stirring speed of 50 rpm.

Table III-2. Tablet Compositions.

	Tablet composition (%w/w)					
	I	II	II	III	IV	V
Filler/binder[a]	0	97	94.5	89.5	79.5	0
Disintegrant[b]	99.5	2.5	5	10	20	59.5
Ibuprofen	0	0	0	0	0	40
Magnesium stearate	0.5	0.5	0.5	0.5	0.5	0.5

[a] Avicel® PH-102, Lactose (Fast Flo® 316), Dicalcium phosphate (A-TAB®), Starch 1500®, or mannitol.

[b] CII, SDCII, Polyplasdone® XL, Ac-Di-Sol®, or Primojel®.

Table III-3. Composition of Compacts Made with Ibuprofen and Disintegrants.

Component	Lot 1(%)[a]	Lot 2(%)[a]	Lot 3(%)[a]	Lot 4(%)[a]
Avicel® PH-102	59.5	54.5	49.5	39.5
Ibuprofen	40.0	40.0	40.0	40.0
Disintegrant[b]	0.0	5.0	10.0	20.0
Magnesium stearate	0.5	0.5	0.5	0.5

[a] 25 g size.

[b] CII, SDCII, Polyplasdone® XL, Ac-Di-Sol®, or Primojel®.

At 5, 10, 20, 30, 45 and 60 min, aliquots (1 mL each) of the dissolution medium were withdrawn, passed through a 0.22 µm membrane filter (Millipore Filter Corp., Bedford, Mass., USA), and analyzed for ibuprofen content. The removed dissolution medium was replaced with an equal volume of fresh buffer solution. A high performance liquid chromatography (HPLC) method using a Shimadzu HPLC system, equipped with a pump (Model LC-10AT), an autoinjector (Model SIL-10A), a system controller (Model SCL-10A), an UV-VIS detector (Model SPD-10A) and a Chromatopac integrator (Model C-R6A) was employed. A C_{18} reverse phase analytical column (25 cm x 4.6 mm, 5µm, Waters, Milford, MA) was also used for the analysis. The mobile phase was a mixture of 60% acetonitrile and 40% water containing 4-chloroacetic acid (4 g), adjusted to pH 3.0 using aqueous ammonium hydroxide (30% v/v). The drug retention time was 1.4 minutes and drug was eluted at a flow rate of 2.0 mL/min. The detection was made at 221 nm. The test was conducted on five independent samples.

Compact Crushing Strength

Compact strength was determined using a Schleuniger Pharmatron tablet hardness tester (Model 8M, Dr. Schleuniger Pharmatron Inc., Manchester, NH). Cylindrical compacts were prepared as described under *Preparation of Cylindrical Compacts and Determination of Compact Porosity*. Compacts were placed between the horizontally moving platens and the diametric crushing (breaking) strength (kP), required to break the compacts was recorded. The crosshead speed of the left moving platen was 3.5 mm/sec.

Dilution Potential of SDCII and CII

Acetaminophen and the test excipient (25:75, 50:50, 75:25. 85:15 and 95:5) were mixed in a V-Blender (Model LB429, The Patterson Kelley Co. East Stroudsburg, PA) for 30 min and then compressed on a Carver Press at 120 MPa and a dwell time of 30 sec. Crushing strength of the compacts was determined and these values were divided by the crushing strength of the pure excipient. The plot of crushing strength ratio versus composition was then constructed. The dilution potential was found by interpolation of the resulting straight line to the x-axis. Samples were analyzed in eight replicate.

Lubricant Sensitivity of CII and SDCII

The lubricant sensitivity of SDCII and other excipients was assessed by mixing them (separately) with magnesium stearate in 99.5:0.5, 99:1, and 98:2 weight ratios in a V-blender (Model LB429, Patterson Kelley Co. East Stroudsburg, PA) for 30 min. Tablets were prepared using a Carver Press at 120 MPa and at a dwell time of 30 sec. The lubricant sensitivity was expressed as the lubricant sensitivity ratio (LSR):

$$\mathrm{LSR} = \left[\frac{H_0 - H_{lub}}{H_0}\right] \qquad \text{Eqn. III-25}$$

Where, H_{lub} and H_o are the crushing strengths of tablets prepared with and without lubricant, respectively. Samples were analyzed in triplicate.

Lubricant Sensitivity of CII-SiO_2 Composites

Magnesium stearate was used as a model lubricant. The composite powder and the lubricant were mixed at a 99:1 weight ratio using a V-blender for 30 min. Tablets were prepared as described under *Preparation of Cylindrical Compacts and Determination of Compact Porosity* at a compression pressure of approximately 60 MPa. Compacts were stored in a desiccator over Drierite® for 48 h before testing. A Schleuniger Pharmatron tablet hardness tester (Model 8M, Dr. Schleuniger Pharmaton

Inc., Manchester, NH) was employed. Crushing strength measurements were then performed as described under *Compact Crushing Strength*. Calculations were done as established under *Lubricant Sensitivity of CII and SDCII*.

Load-deformation Curves and Diametrical Compression Test of Cellulose II:SiO_2 Composites

A Q-test I universal tester (Model, QT-1, MTS, System Corp., Eden Prairie, MN), was employed. Cylindrical compacts of ~500 mg weight were prepared as described under *Preparation of Cylindrical Compacts and Determination of Compact Porosity*. The force-deformation curves were obtained using the Testworks QT software v. 2.03 (MTS, System Corp., Eden Prairie, MN). The crosshead speed of the upper platen was kept constant at 0.01 mm/sec and the lower platen was kept stationary, holding the compact in the center resting on its axial side perpendicularly. Before each measurement, a zero calibration was performed with no compact between the platens. The test was stopped once the compact was broken in two symmetrical halves. The upper platen was then unlocked (released) so the compact fragments could be cleaned up.

The trapezoidal method was used to find the area under the load-deformation curves, which gives an indication of toughness, energy at break or energy at fracture (EF) of the compacts according to the equation:

$$EF = \sum_{n=1}^{\infty} \left(\frac{(\mathrm{F1} + \mathrm{F2})}{2} * (\mathrm{d2} - \mathrm{d1}) \right) \qquad \text{Eqn. III-26}$$

Where, F1 and F2 are the forces applied to the compact when the compact has deformed from a distance d1 to a distance d2.

The radial tensile strength (TS) values were obtained according to the Fell and Newton equation (Fell and Newton, 1968):

$$TS = \left[\frac{2F}{\pi * D * t}\right] \qquad \text{Eqn. III-25}$$

Where, F is the breaking force (in Newton) needed to fracture the compact into two halves, D is the diameter of the compact (mm), and t is the compact thickness (mm). The data of the radial tensile strength were fitted to the Leuenberger model (Lanz, 2005) which relates the radial tensile strength versus the product of solid fraction and the compression pressure. The Leuenberger equation is:

$$TS = T_{max} * [1 - e^{(-\gamma_c * P * \rho_r)}] \qquad \text{Eqn. III-27}$$

Where, TS is the radial tensile strength (MPa), T_{max} is the theoretical tensile strength at infinite compression pressure, γ_c is the compression susceptibility parameter (MPa^{-1}), ρ_r is the relative density and P is the compression pressure (MPa). Compacts were prepared as described under *Preparation of Cylindrical Compacts and Determination of Compact Porosity*. The equation fitting was performed employing Statgraphic® software (StatPoint Technologies, Warrenton, VA) using the principle of least squares.

The area under the tensile strength curve (AUTSC) obtained from the Leuenberger model was used to determine the material compactibility. In this study, the AUTSC was calculated using the trapezoidal rule:

$$AUTSC = \sum_{n=1}^{\infty} \left(\frac{(TS1 + TS2)}{2} * [P * SF2 - P * SF1]\right) \qquad \text{Eqn. III-28}$$

Where, TS1 and TS2 are the tensile strength of the compacts made at the product of compression pressures and solid fraction P*SF1 and P*SF2, respectively.

Compact Friability

A VanKel friabilator apparatus was employed (Model 45-1000, Erweka, Cary, NC) at 25 rpm. Compact friability was tested according to USP28/NF23 specifications

(US Pharmacopoeia, 2005, page 2745). Thirteen compacts, each weighing ~500 mg, were placed in the rotating drum at 25 rpm for 100 cycles. Compacts were then de-dusted and reweighed. Compacts used in this study were compressed at a 15% porosity. The percentage friability was calculated using:

$$\% = \frac{W_i - W_f}{(W_i)} * 100\% \qquad \text{Eqn. III-30}$$

Where, W_i and W_f are the initial and final compact weights, respectively. Compacts are considered non-friable if friability is < 1%. Samples were analyzed in triplicate.

Bead Friability

A VanKel friabilator apparatus was employed (Model 45-1000, Erweka, Cary, NC) at 25 rpm. The friability test was performed according to the method of Agrawal et al. (Agrawal et al., 2004). Approximately, 1 g of the beads collected on a # 20 mesh (840 µm) screen were placed in the friabilator along with 25 glass beads (dia. 3 mm), which was then operated at 25 rpm for 4 min. The beads were collected on a 20 mesh screen and reweighed after de-dusting. The percentage friability was calculated as described above. Each sample was evaluated in triplicate.

Disintegration Studies

The disintegration test of CII, SDCII, and commercial excipients was determined with five replicates in distilled water at 37 ºC according to the USP28/NF23 specifications (US Pharmacopoeia, 2005, page 262) employing an Erweka GmbH disintegration apparatus (Model 712, Erweka, Offenbach, Germany) at 30 strokes/min. Compacts were prepared as described under *Preparation of Cylindrical Compacts and Determination of Compact Porosity*. Compacts were prepared on a Carver press at 0.05-

0.45 porosities and a dwell time of 30 sec. Tests were conducted on three independent samples.

Bead disintegration studies were performed in triplicate in distilled water at 37ºC according to the modified method of Tho et al., (Tho, Sande, Kleinebudde, 2002) employing an Eureka GmbH disintegration apparatus (Model 712, Erweka, Offenbach, Germany) operated at 30 strokes/min. The basket was equipped with a 250 µm screen. Approximately 100 mg of sample was used in the test.

Griseofulvin Release Studies

Griseofulvin, due to its poor water solubility (0.0346 mM) was used for the dissolution studies of compacts and capsules. Mixtures of 125 mg of drug and 375 mg of cellulosic excipients were prepared in a mortar and pestle by mixing for five minutes followed by compaction at 120 MPa and 30 seconds of dwell time as described under *preparation of cylindrical compacts and determination of compact porosity*. The release from the compacts of cellulosic materials was determined employing the USP28/NF23 UV method (US Pharmacopoeia, 2005, page 921). The dissolution study was performed using USP Apparatus 2 with paddles (Pharma Test, Scientific Instruments and Technology Corp., Piscataway, NJ) at 75 rpm in distilled water (1000 mL) containing sodium lauryl sulfate (40 mg/mL). Aliquots (1 mL) taken every 5, 10, 20, 30, 45, 60 and 90 min were diluted in a methanol:water mixture (4:1 ratio) solvent and analyzed by UV-VIS spectrophotometry (Aligent 8453, Hewlett-Packard Company, Palo Alto, CA) 291 nm. A calibration curve was prepared with griseofulvin at 2, 4, 8 and 12 µg/mL. The test was conducted on three separate tablets.

For the capsules containing beads prepared with griseofulvin and a cellulosic, a USP/NF (28/23) UV method was used (US Pharmacopoeia, 2005, page 920). The, USP Apparatus 2 with paddles (Pharma Test, Scientific Instruments and Technology Corp.,

Piscataway, NJ) at a speed of 50 rpm in distilled water (1000 mL) containing sodium lauryl sulfate (5.4 mg/mL) was used. Since drug release was quite slow, aliquots (1 mL) were withdrawn at 0.08 to 104 h and analyzed by UV-VIS spectrophotometry (Aligent 8453, Hewlett-Packard Company, Palo Alto, CA) at 291 nm. A calibration curve was constructed with griseofulvin at 2, 4, 8 and 12 µg/mL. The test was conducted on three separate capsules.

Diphenhydramine HCl Release Studies

The method reported in the USP/NF (28/23) for capsules was employed (US Pharmacopoeia, 2005, page 2175). Diphenhydramine HCl is a water soluble drug (100 mg/mL). Mixtures of 25 mg of drug and 475 mg of cellulosic excipients were prepared in a mortar and pestle for five minutes followed by compaction at 120 MPa and 30 seconds of dwell time as described under *preparation of cylindrical compacts and determination of compact porosity*. For the release studies from the beads, the apparatus 1 with baskets (Pharma Test, Scientific Instruments and Technology Corp., Piscataway, NJ) was employed at 100 rpm. The medium used was distilled water (500 mL). The test was run for 60 min. Aliquots of 1 mL were withdrawn at 5, 10, 20, 30, 45, and 60 min and immediately replaced with an equal volume (1 mL) of distilled water. A Shimadzu HPLC system was used for the analysis. It had a pump (Model LC-10AT), an autoinjector (Model SIL -10A), a system controller (Model SCL-10A), a UV-VIS detector (Model SDP-10A) and a Chromatopac integrator (Model C-R6A). A C_{18} DB reverse phase analytical column (Serial # 58978, 3.3 cm x 4.6 mm, 3 µm, SUPELCO, Bellefonte, PA) was employed for the analysis. The mobile phase was a solution of acetonitrile, water and triethylamine (50:50:0.5 v/v). The pH was adjusted to 6.5 with glacial acetic acid and then degassed. The flow rate, injection volume and detector wavelength employed were 1 mL/min, 50 µL and 254 nm, respectively. The standard calibration curve was prepared

using 0.02, 0.05, 0.25, and 0.5 mg/mL of the drug in distilled water. The peak retention time was 1 min. Three separate capsules were tested. For tablets of silicified materials and diphenhydramine HCl mixtures, the same procedure as described above was employed except that a C_{18} reverse phase analytical column (25 cm x 4.6 mm, 5 µm, Waters, Milford, MA) was employed.

Preparation of Square Compacts

Load-deformation curves were determined on square compacts, each weighing ~3 g, and measuring 3.84 cm^2 in area. They were prepared using a stainless steel split die, die yoke and a hydraulic press (Frame: Model 341-20, Loomis Engineering & Mfg. Co., Caldwell, NJ) coupled with a cylinder (Hydraulic Specialty Company, Fridley, MN), a motor (Model C6117DB7C, Leeson, Grafton, WI), and a pump (Model F051, Brand Hydraulic, Omaha, NE). Upon loading 3 g of powder into the square tooling set, the hydraulic pump motor was started. A lower platen velocity of 2 mm/sec, a compression dwell time of 30 sec and decompression time of 1 sec was employed. The maximum applied load was controlled with an adjustable pressure relief valve so compacts reach a solid fraction between 0.6 and 0.7. Further, square compacts were made with an upper punch equipped with a 1 mm diameter, spring-loaded retractable pin. This pin enables the preparation of compacts with an axially-oriented hole in the center. This hole constitutes a reproducible stress concentration in the compact. During compression, the side piston drives the platen, which secures the split die and allows uniaxial compression. Upon decompression, the side piston retracts simultaneously with the punches, allowing triaxial decompression. The triaxial decompression minimizes compact lamination during decompression since the elastic recovery occurs axially and perpendicular to the die. Compacts were stored in a desiccator at 15-30 % RH for 48 h and their tensile strength evaluated.

Load-Deformation Curves and Brittle Fracture Index

Load-deformation curves and tensile strength of the square compacts were determined on a universal stress-strain analyzer (Model Q-Test I, Material Testing Systems, Cary, NC). The crosshead speed was adjusted to compensate for any contribution of the viscoelasticity of the materials so that any time-dependent contribution remains constant. However, this rate was not critical for square compacts. Since the rate force approximates an exponential curve, the selected rate was such that the time between 1/e of the maximum force was ~15 sec (Hiestand et al., 2006). Brittle Fracture Index (BFI) of the square compacts was calculated by:

$$BFI = 0.5\left[\left|\frac{\sigma}{\sigma_0}\right| - 1\right] \qquad \text{Eqn. III-31}$$

Where, σ and σ_0 correspond to the tensile strength of normal compacts (no hole) and the tensile strength of the compromised compact (with a hole). The center hole is a defect, which simulates the actual voids formed in the tablets (due to air entrapment) during manufacture. The voids or low density regions in the tablet are weak points from which cracks emanate when stress (due to die wall) is applied to the tablet (Esezobo and Pilpel, 1987).

Stress-Strain Curves of Compacts

The load-deformation curves produced from the compression data of the square compacts were normalized to cross-sectional area and the percentage deformation. The normalized load-deformation curves are stress-strain graphs (Figure III-5). The first portion of these graphs is linear and corresponds to the elastic region. In this region, the stress applied is proportional to its strain.

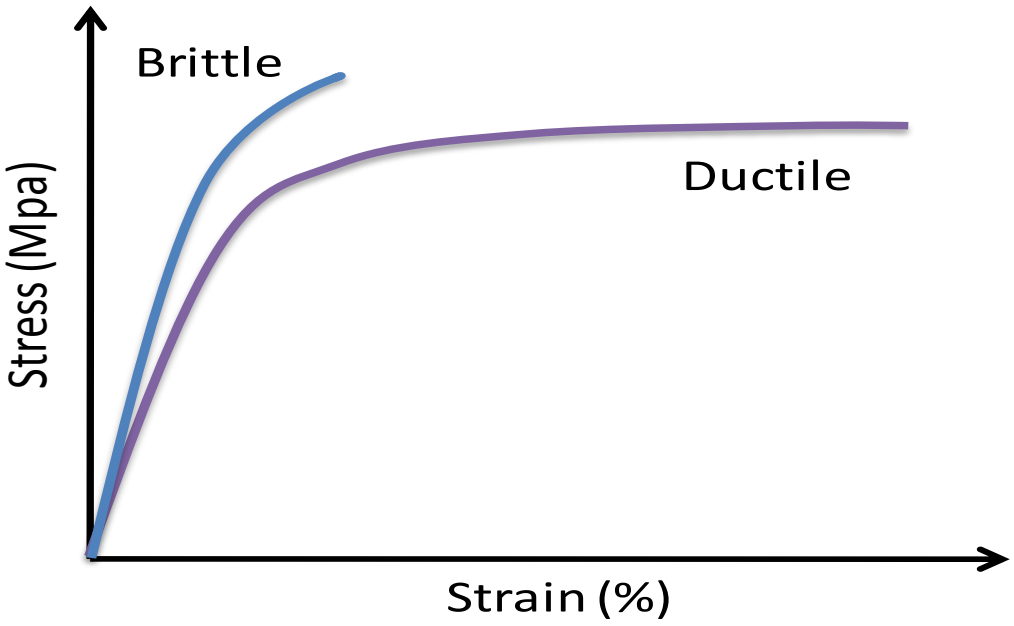

Figure III-5. Typical Stress-Strain Curves for Brittle (blue line) and Plastic Materials (purple line).

The ratio of stress to strain (slope of the linear region) is a constant called elastic or Young's modulus:

$$E = \frac{\sigma}{\varepsilon} \qquad \text{Eqn. III-32}$$

Where, σ and ε correspond to the stress and strain, respectively. This modulus is a measure of the stiffness (resistance of an elastic body to withstand changes in length when a force is applied). For compacts the Young's modulus is obtained from a compression test used to generate stress-strain curves. In the elastic region, if the load is removed the material then returns to its original shape. As strain is increased, most materials deviate from this linear proportionality, which is usually associated with stress-induced "plastic" flow. In this plastic region, the material undergoes a rearrangement of its microscopic structure, in which planes of the crystals slide over each other to new positions (Boyer, 1987). Typically, ductile materials suffer from dislocation motions, whereas brittle materials have internal microstructures that block possible dislocations. The stress-strain curves for brittle materials are typically linear over their full range of strain, eventually terminating in fracture near the end of the linear elastic portion of their curve without appreciable plastic flow. Thus, for brittle materials, the tensile strength will be at the end of the elastic portion of the stress-strain curve or close to the elastic limit.

In ductile materials, the tensile strength is the highest point of the plastic region of the stress-strain curve. Moreover, in most materials, there is a gradual transition from the elastic to plastic behavior and the exact point (yield stress) at which plastic deformation begins is difficult to determine (Davis, 2004).

The elastic modulus applies to when the material is deformed by the applied stress in the elastic region (i.e., low stresses) and upon unloading will return to its original

shape. When the strain exceeds the yield point, the material is deformed irreversibly (Hengel, 2001). The modulus of elasticity is then the quantity of energy the material stores without undergoing permanent change in length (i.e., compression). Similarly, the modulus of toughness is the energy needed to completely fracture the material.

In theory, a compression test is the opposite of the tension test with respect to the direction of loading. In compression testing, the compact is compressed, while the load and deformation are recorded simultaneously (i.e., diametric compression test). Compression tests result in mechanical properties that include the compressive yield stress, compressive tensile strength, and compressive modulus of elasticity.

Mechanical Properties of the Compacts Stored as a Function of Humidity

Preparation of the Relative Humidity Chambers

Glass desiccators were thoroughly cleaned and removed from all gaseous contaminants by suction with the in-house vacuum line. Saturated salt solutions were prepared by adding an excess of the salt to 500 mL of distilled water and continuously stirring the suspension for seven hours (Table III-4).

The saturated solutions were placed in separate desiccators, sealed with vacuum grease applied to the lids, and allowed to equilibrate for seven days. The relative humidity was measured using a digital hygrometer (Model EC, National Marine Products, Inc., Preston, WA).

Cylindrical Compacts for Moisture Sorption Studies

Round compacts were prepared as described under *Preparation of Cylindrical Compacts and Determination of Compact Porosity*. Pressures varied for each material so the solid fraction remained constant at 0.9 for all compacts.

Table III-4. Salt Solutions for Relative Humidity Chambers.

Substance	Solubility (g/mL)[a]	Concentration used (g/mL)	Relative humidity at 25°C (%)[b]
Sulfuric acid (96% w/v)	[c]	[c]	0
Lithium chloride	0.8	0.85	11.3± 0.3
Potassium acetate	2.81	2.85	21.6±0.5
Magnesium chloride	0.56	0.6	32.8 ±0.2
Sodium bromide	1.16	1.18	56.0±0.4
Sodium chloride	0.37	0.45	75.3±0.1
Distilled water	[c]	[c]	100

[a] CRC Handbook of Chemistry and Physics (Lide, 2003).

[b] Greenspan, 1977.

[c] These substances were added without dilution (Greenspan, 1977).

Once the tablet was ejected it was stored in a desiccator at a relative humidity as described in *Preparation of the Relative Humidity Chambers*. After 5, 10, 20 and 30 days of storage, the tablet tensile strength (*measured as described under Load-deformation Curves and Diametrical Compression Test of Cellulose II:SiO_2 Composites*), thickness and diameter were measured with an electronic digital caliper (Ted Pella, Inc., Redding, CA; measuring range 0-150 mm and readability of 0.01 mm).

Compact Reprocessability

About 25 g of an acetaminophen:excipient (1:1) mixture was passed freely through a 250 µm sieve to remove aggregates and blended in a V-blender for 30 min. Round compacts, each weighing about 1 g and measuring 1.3 cm in diameter were made using a Loomis hydraulic press as described previously (Model 341 20, Loomis Engineering & Mfg. Co., Caldwell, N.J.) set at a lower platen speed of 2 mm/sec, a dwell time of 30 sec and a decompression time of 1 sec. Following measurements of load-deformation were made on a Q-Test (Model Q-Test I, Material Testing Systems, Cary, NC). Tablet pieces were milled using a roller mill (Model KU1, Erweka G.m.b.H, Chemical and Pharmaceutical Industry, New York, NY), passed through a 105 µm sieve, and then compressed into a tablet as described above. Tablets were then tested as previously with the Q-Test.

Compacts Specific Surface Areas

For tablets, the sample cell (part # 74005-10) having a wide diameter (14.97 x 12.4 mm outer/inner diameter) body was used, which facilitated compact loading directly for evaluation of surface area. Before performing the analysis, samples were dried in a vacuum oven (Model 68351, Precision Scientific Co., Chicago, IL) heated at 60 °C and at a reduced pressure of 40 mm Hg for 24 h. Samples were then degassed for 24 h under continuous nitrogen flow.

For each sample, one round intact tablet, measuring 1.1 cm in diameter and weighing ~500 mg, was employed. These compacts were prepared as described under *preparation of cylindrical compacts and determination of compact porosity* at porosities from 0.05 to 0.6. The surface area measurements were performed using a Quantasorb Sorption System (Quantachrome Corp., Boynton Beach, FL). Helium gas was used as the carrier and diluent gas, while nitrogen gas was used as the adsorbate. A three point BET analysis was conducted on all samples by performing the N_2 adsorption and desorption at relative pressures (P/P_0) ranging from 0.05 to 0.15. The attenuation was maintained from 32 to 256, depending on the sample being analyzed since the surface areas of all samples were significantly different and a fixed single attenuation value could not be used for all samples. Adsorption occurred when the sample cell was immersed in liquid nitrogen and the adsorbate (N_2) condensed on the sample surface. Typically, the adsorption peaks were broad and thus, for quantitative purposes, the counts from the desorption peaks were used. In order to calibrate the N_2 detector counts, fixed volumes of nitrogen were injected into the sample port with a glass syringe and the amount of N_2 was calculated from:

$$X_C = \frac{P_a * M_a * V_c}{R * T} \qquad \text{Eqn. III-33}$$

$$X = \frac{A * X_C}{A_{cal}} \qquad \text{Eqn. III-34}$$

Where, X_c is the weight of nitrogen gas injected for calibration, P_a is the ambient pressure (mmHg), M_a is the molecular weight of nitrogen (28 g/mol), V_c is the volume of nitrogen gas injected for calibration (L), T is absolute temperature at which the adsorption experiment was conducted (K), R is the gas constant (62.35 L*mmHg/mol*K), X is the weight of the nitrogen gas adsorbed, A is the detector signal area from the desorption step, and A_{cal} is the detector signal area from the desorption of nitrogen gas used for

calibration. The N_2 sorption data were analyzed by fitting the data to the linear BET equation:

$$\frac{1}{X*\left[\left(\frac{P_0}{P}\right)-1\right]} = \frac{C-1}{X_m*C} * \left(\frac{P}{P_0}\right) + \frac{1}{X_m*C} \qquad \text{Eqn. III-35}$$

Where, P is the partial pressure of the adsorbate, P_0 is the saturated vapor pressure of the adsorbate, X is the mass of adsorbate at the specific relative pressure P/P_0, X_m is the mass of the adsorbate (N_2) at the monolayer coverage, and C is a constant related to the heat of adsorption. The specific surface area (S) was obtained by:

$$S = \frac{N_A*A_{CS}}{(S+I)*W*M_a} \qquad \text{Eqn. III-36}$$

Where, S and I are the slope and intercept of the BET plot, respectively. N_A is the Avogadro's number (6.023 $X10^{23}$ molecules/mol), A_{cs} is the cross sectional area of the nitrogen molecule ($16.2x10^{-20}$ m^2), W is the sample weight and M_a is the nitrogen molecular weight.

CHAPTER IV

RESULTS AND DISCUSSION

Spray drying was employed as a technique to modify the functional properties of CII. These properties were compared to those of common carbohydrate excipients. Further, the disintegration properties of CII and its spray-dried powder (SDCII) were evaluated along with commonly used disintegrants. In addition, the effect of processing (wet granulation, spray drying and spheronization) and silicification on CII particles was studied and the resulting particle and tableting properties were evaluated in comparison with those of commercial CI powders such as Prosolv® SMCC 50, Prosolv® SMCC 90 and Celphere®203. Finally, the effect of relative humidity and reprocessing on compact tensile strength of selected cellulose II materials, silicified (Prosolv® SMCC 50 and Prosolv® SMCC 90) and unsilicified (Avicel® PH-101 and Avicel® PH-102) CI materials was evaluated.

Preparation and Tableting Properties of SDCII for Direct Compression

Spray drying was used as a process to improve flow and compaction properties of CII, without compromising its rapid disintegration properties. The preparation of spray-dried cellulose II (SDCII) was optimized using a statistical fractional factorial design and Box-Behnken experimental approaches. A factorial design studies the effect of a variation of independent variables (factors) and their combination on a dependent variable. Each factor has different possible values or levels. It also facilitates the study of factor interactions. A Box-Behnken design specifically studies the effect of three variables with three levels on a response. It is used to optimize a response using a second degree polynomial equation.

Powder and mechanical compact properties of CII and SDCII were evaluated and compared with those of commercial carbohydrate excipients: Avicel® PH-102 (spray-dried cellulose I; FMC Biopolymers, Newark, DE), Starch 1500® (pregelatinized starch; Colorcon, West Point Pike, PA) and Fast Flo® 316 (spray-dried lactose; DMV International Pharma and Foremost Farms, Baraboo, WI).

Cellulose II Preparation (CII)

The process of soaking cotton linter in 7.5 N NaOH for 72 h at room temperature converts cellulose I into cellulose II. To ensure complete saturation of the cotton linter, (i) the size of the cotton linter pieces was kept to no more than 0.5 x 5 cm; (ii) The weight-to-volume ratio of cellulose I cotton linter strips to 7.5N NaOH solution was maintained at 1:6. This ratio was previously determined to completely cover the cellulose pieces and convert cellulose I to cellulose II (Kumar et al., 2002); (iii) The cotton linter-NaOH mixture was periodically stirred (every 12 h). The final product, before washing, had a yellowish color and a soapy odor. The swollen material was either first washed with tap water until a pH between 5 and 7, followed by final washes with deionized water to reduce traces of ions, or was washed completely with deionized water.

The NaOH treatment causes cellulose to swell, making the cellulose fibril interstices more accessible. This results in disruption of inter-molecular and intra-molecular hydrogen bonds, and consequently, a change in the crystal lattice dimension and chain conformations, transforming the highly ordered regions into alkali cellulose I and then into the cellulose II lattice (Krassig, 1996). It has been reported that other types of cellulose, such as cellulose III, are only obtained when cellulose is treated with liquid ammonia at -80 °C. Further, cellulose IV can be obtained from cellulose III by treatment with glycerol at 260 °C (Krassig, 1996). Thus, only CII and no other polymorphic forms were found after the alkali treatment (mercerization).

The powder X-ray diffractograms of cellulose II materials showed characteristic peaks at 12, 20 and 22° 2θ due to 1 $\bar{1}$ 0, 110 and 200 reflections, respectively, confirming the presence of the CII lattice (Figure IV-1) (Kumar et al., 2002). In contrast, the corresponding diffraction peaks in cotton linter have been identified at 14.8, 16.3 and 22.4^{o} 2θ. Powder X-ray diffractograms show clearly that CII products contained the cellulose II lattice, while cotton linter and commercial cellulose contained only the cellulose I lattice form (Klemm et al., 1998a)

The transformation of cellulose I into cellulose II is irreversible. Cellulose II exhibits an antiparallel arrangement of its chains while cellulose I exhibits a parallel chain arrangement. It is believed that the transition from cellulose I to cellulose II takes place without complete loss of the crystalline order. The backfolding of the amorphous regions of the glucan chains produces an antiparallel direction of the chains. It has been reported that in 3.8 to 7 N NaOH an ionic cellulose-sodium compound is formed, containing one mole of NaOH per anhydroglucose unit and a firmly bound molecular water (Krassig, 1996). A complete transformation of cellulose I to cellulose II in cotton linter requires a minimum concentration of 7.5N of NaOH at room temperature (Krassig, 1996). Extensive washing of the NaOH treated cotton linter with water produces the cellulose II (Isogai and Atalla, 1998). Conversely, if washing and neutralization is incomplete, traces of sodium cellulose could be obtained rendering an alkaline pH.

The wet cellulose II pieces, thus obtained, can be either dried in a convection oven or treated directly with 1N HCl solution. A hydrolysis step is required since up to this point in the process the small strips of CII cannot be compressed directly into a compact. In order to achieve a direct compressible powder, either exhaustive milling (to obtain powdered cellulose) or hydrolysis (to obtained microcrystalline cellulose) need to be conducted to reduce the particle size and the degree of polymerization.

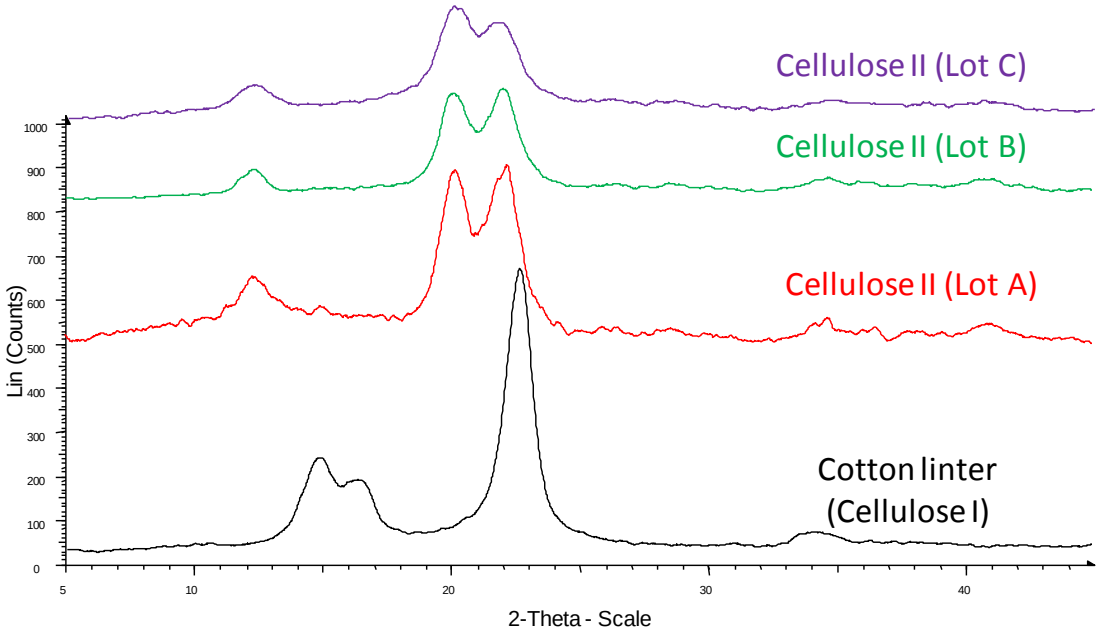

Figure IV-1. Powder XRD of CII Lots and Cotton Linter.

It has been reported that dilute (< 2 N) mineral acids such as HCl or H_2SO_4 are able to dissolve the amorphous regions of cellulose after boiling for 2 h. Acid concentrations > 2N rapidly hydrolyze cellulose to sugars and soluble oligosaccharides (Battista et al., 1957; Battista and Smith, 1964).

Thus, dried CII samples were hydrated in water for ~1 h before hydrolysis. This causes cellulose to swell, rendering more anhydroglucose ether linkages to become accessible for hydrolysis. The acid-catalyzed hydrolysis of cellulose (cleavage of β-1,4-glycosidic bond) is shown in Figure IV-2. Acid hydrolysis proceeds in three steps: (i) A proton from HCl protonates the glycosidic oxygen linking two glucose units (dominant pathway), or the cyclic oxygen forming a conjugate acid; (ii) The cleavage of the ether linkage leads to the formation of a carbocation; (iii) Water is then added and the free glucose and a proton (acid) are liberated. The formation of the intermediate carbocation takes place more favorably at the chain end than in the middle of the cellulose chain (Xiang et al., 2003).

The degree of polymerization, viscosity-average molecular weight, and degree of crystallinity for CII lots are presented in Table IV-1. The acid mediated degradation of high molecular weight cellulose from cotton linter with a DP of ~1,450 and a MW of 235,554 leads to a reduction of the DP to ~80-150 and a MW of 12,960-24,300. Lin et al. reported values of DP for cotton linter of 1,565 (Lin et al., 2009). During hydrolysis, the acid mainly attacks the glycosidic bonds located on the less ordered surface (i.e. non-crystalline) of the microfibrils since they are more accessible than the glycosidic bonds located in the ordered regions of cellulose microfibrils (Figure IV-3). For this reason, the acid hydrolysis kinetics are initially fast and then slow as the microcrystalline regions break down. The degree of polymerization at this point is referred to as leveled-off degree of polymerization (leveled-off DP)(Krassig, 1996).

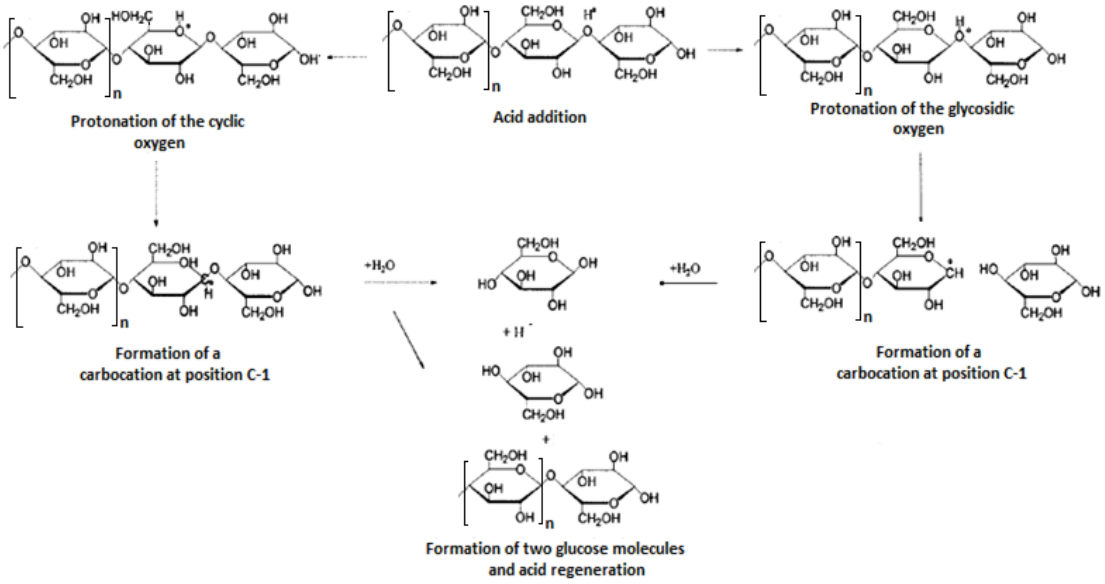

Figure IV-2. Cellulose Hydrolysis Mechanism (Adapted from Xiang et al., 2003).

Table IV-1. Crystallinity and Degree of Polymerization of CII and Cotton Linter.

Lot	Batch Size	Degree of crystallinity[a] (%) (n=1)	Degree of polymerization[b] (DP) (n=1)	Viscosity-average molecular weight[c]($\bar{M}_v$)
A	50 g	69.6	122.3	19,813
B	50 g	64.9	108.5	17,577
C	3.5 kg	68.0	146.1	23,668
Cotton linter	NA[d]	90.3	1454	235,548

[a] Determined by the ratio of the powder X-ray crystalline peaks.

[b] Determined by capillary viscometry.

[c] Determined by the product of 190 and intrinsic viscosity.

[d] NA: Not applicable.

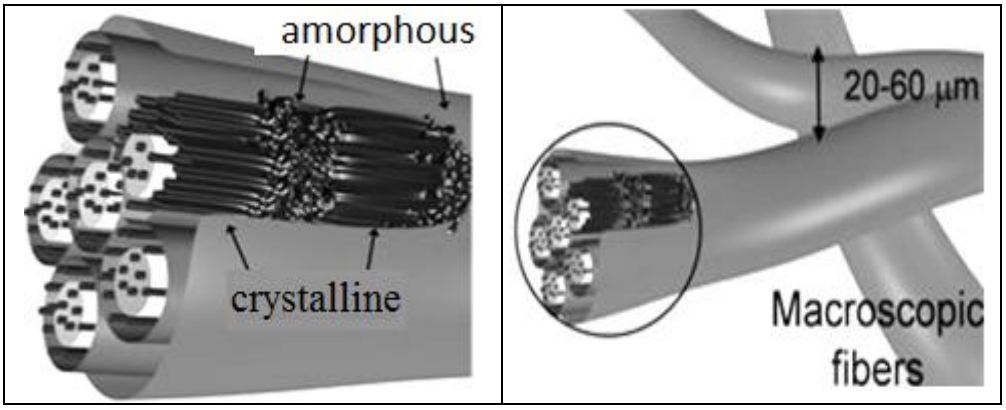

Figure IV-3. Microstructure and Accessibility of Cellulose Microfibrils (Adapted from Pääkkö, 2010).

The degree of crystallinity of cellulose II produced ranged from 64 to 70%. Cellulose I materials, including cotton linter in contrast, showed a degree of crystallinity of ~90% (Table IV-1). Reported crystallinity values for cotton linter range from 78 to 92% (Nada et al., 2009; Parikh et al., 2007).

Spray-Dried Cellulose II Preparation (SDCII)

Cellulose II powder (CII) prepared as described above, was converted into aqueous dispersions by homogenization in water using a hand-held laboratory homogenizer or by passing a slurry through a colloid mill. Table IV-2 lists the processing and time conditions employed and the resulting particle size distribution of the dispersions. Stirring the aqueous suspensions of CII using a laboratory mixer did not produce a stable dispersion. When a hand-held homogenizer (Model M10000, Biospec Products, Inc., Bartlesville, OK) was used, a good dispersion was formed in as little as 1 min. No significant change in particle size occurred (geometric mean diameter "d_g" of ~74.2 -83.7 µm) even after homogenization for 20 min. However, after 40 min of homogenization, the particle size decreased from an initial d_g of ~74.2-83.7 µm to ~50 µm (49 % decrease).

When a colloid mill was used for homogenization, the formation of a stable dispersion and particle size was observed to be dependent on the distance/gap (aperture) between the rotor and the stator. When this distance was set at 6 (small), stable dispersions were obtained after homogenization for 1 min and the d_g significantly decreased by a 75%. At a setting of 60 (large), no significant change of d_g was noticed after homogenization for 10 min. A further increase in the homogenization time to 20 min, however, lead to a 75% decrease in d_g and was comparable to that achieved at a lower gap setting of 6. So, for larger aperture settings a longer time was needed to reach the same particle size attained at a smaller aperture in less time (Table IV-2).

Table IV-2. Effect of Homogenization and Colloid Mill on Particle Size.

Process[a]	Time (Min.)	Geometric[b] mean±SE	Particle size percentiles 25	50	75
Stirring	240	83.7 ± 3.4	61.2	78.3	100.1
Homogenization	1	74.2 ± 3.4	51.5	68.1	90.0
Homogenization	5	82.5 ± 4.2	53.5	73.7	101.6
Homogenization	10	76.4 ± 3.9	49.9	68.5	93.9
Homogenization	20	71.9 ± 2.8	52.5	67.2	86.1
Homogenization	40	49.9 ± 3.1	31.2	43.9	61.8
Colloid milling, (aperture 6)	1	21.6 ± 0.8	16.3	20.4	25.5
Colloid milling (aperture 6)	5	22.5 ± 0.9	16.1	20.9	27.2
Colloid milling (aperture 6)	10	19 ± 0.7	15.3	19.0	23.6
Colloid milling (aperture 6)	20	26.3 ± 2.4	11.7	19.6	32.9
Colloid milling (aperture 6)	40	17.6 ± 0.5	14.3	17	20.2
Colloid milling (aperture 60)	1	74.8 ± 2.3	48.2	66.6	92.2
Colloid milling (aperture 60)	5	73.1 ± 5.9	40.4	60.8	91.4
Colloid milling (aperture 60)	10	82.2 ± 4.3	53.7	73.7	101.1
Colloid milling (aperture 60)	20	21 ± 0.6	16.7	20.2	24.3

[a] The ANOVA table showing variation of geometric means is shown in the appendix B section.
[b] This mean corresponds to the theoretical 50 cumulative frequency of the data assuming a log-normal distribution.

D_g resulted from homogenization and colloid milling at a 60 gap set were comparable, whereas d_g from colloid milling at a 6 gap set was significantly smaller. Further, independent of the homogenization process employed, d_g resulted from homogenization times from 1-10 min were comparable.

Fractional Factorial Study of Spray Drying Conditions

A Fractional Factorial Design is a widely used tool in product development to compare each factor level and to determine which factors are important for describing a product quality as a function of multiple process variables (Montgomery, 2004). The statistical analysis was conducted with Minitab® software (v.16, State College, PA). The high and low values of the factors were selected based on the allowable equipment operational parameters. The controllable factors used in this study were feed concentration (C), inlet air temperature (IT), drying air speed (DA), atomization air pressure (AA), feed flow rate (FR) and sprayer nozzle diameter (ND). The responses employed were yield (Y) and particle size (PS) as listed in the experimental matrix (Table IV-3). For yield quantification, no scraping of the powder coating the drying chamber was employed.

Table IV-4 shows the *t*-test results from the fractional factorial design. Since little or no condensation of the feed droplets on the drying chamber wall occurred with an increase in inlet air temperature, the increase in yield with increasing inlet air temperature probably occurred due to more effective drying of the droplets when contacting the incoming hot air in the drying chamber. Conversely, at high levels of feed flow rate and feed concentration, a decrease in yield was observed that could be attributed to the enhanced condensation of the feed droplets on the drying chamber wall. Similar observations have been reported for spray drying of sugars (Maury et al., 2005).

Table IV-3. CII Spray Drying Conditions and Results from the Fractional Factorial Design for Yield and Particle Size.[a]

Run order	C[b] (% w/w)	IT[b] (ºC)	DA[b] (m^3/min)	AA[b] (kg-f/cm^2)	FR[b] (mL/min)	ND[b] (µm)	Y[c] (%)	PS[c] ±SE[d] (dg, µm)
1	(-) 3	(+) 200	(-) 0.36	(-) 0.5	(+) 5	(+) 711	14.3	26.1 ± 0.8
2	(-) 3	(+) 200	(-) 0.36	(+) 1.5	(+) 5	(-) 411	39.7	27.5 ± 1.4
3	(-) 3	(-) 140	(+) 0.46	(+) 1.5	(+) 5	(-) 411	26.6	84.0 ± 2.3
4	(-) 3	(+) 200	(+) 0.46	(-) 0.5	(-) 1	(-) 411	78.3	103.0 ± 5
5	(+) 6	(-) 140	(+) 0.46	(-) 0.5	(-) 1	(+) 711	31.5	160.4 ± 2.3
6	(+) 6	(+) 200	(-) 0.36	(-) 0.5	(-) 1	(+) 711	31.0	109.5 ± 4.7
7	(+) 6	(-) 140	(-) 0.36	(-) 0.5	(+) 5	(-) 411	11.5	115.1 ± 2.6
8	(+) 6	(-) 140	(+) 0.46	(+) 1.5	(-) 1	(-) 411	36.2	16.6 ± 0.6
9	(+) 6	(+) 200	(+) 0.46	(+) 1.5	(+) 5	(+) 711	6.5	105.5 ± 3.8
10	(-) 3	(-) 140	(+) 0.46	(-) 0.5	(+) 5	(+) 711	17.3	17.6 ± 4.2
11	(-) 3	(-) 140	(-) 0.36	(+) 1.5	(-) 1	(+) 711	32.3	95.1 ± 4.8
12	(+) 6	(+) 200	(+) 0.46	(-) 0.5	(+) 5	(-) 411	12.2	97.3 ± 2.6
13	(+) 6	(-) 140	(-) 0.36	(+) 1.5	(+) 5	(+) 711	13.2	18.7 ± 0.8
14	(-) 3	(+) 200	(+) 0.46	(+) 1.5	(-) 1	(+) 711	66.7	126.5 ± 4
15	(+) 6	(+) 200	(-) 0.36	(+) 1.5	(-) 1	(-) 411	36.5	114.0 ± 3.4
16	(-) 3	(-) 140	(-) 0.36	(-) 0.5	(-) 1	(-) 411	33.6	97.8 ± 3.8

[a] High and low values are coded as (+) and (-), respectively.

[b] Factors: C, Feed concentration; IT, inlet air temperature; DA, drying air speed; AA, Atomization air pressure; FR, feed flow rate; NR, sprayer nozzle diameter.

[c] Responses: Y, yield; PS, particle size expressed as the geometric mean (d_g).

[d] Standard error (SE).

Table IV-4. Coefficients Estimates and *t*-test Results from the Fractional Factorial Design for Yield and Particle Size.

	Yield			
Term	Model Coeff.[a]	SE[b]	t-value	*p-value*
Intercept	30.46	1.50	20.58	0.000
Feed concentration (C)	-8.14	1.50	-5.50	0.012
Inlet air temperature (IT)	5.19	1.50	3.51	0.039
Drying air speed (DA)	3.95	1.50	2.67	0.076
Atomization air speed (AA)	1.75	1.50	1.18	0.322
Feed flow rate (FR)	-12.80	1.50	-8.65	0.003
Nozzle diameter (ND)	-3.86	1.50	-2.61	0.080
C*IT (or FR*ND)	-5.96	1.50	-4.03	0.028
C*DA (or AA*ND)	-4.68	1.50	-3.16	0.051
C*AA (or DA*ND)	-0.98	1.50	-0.66	0.557
C*FR (or IT*ND)	1.33	1.50	0.90	0.437
C*ND (or IT*FR or DA*AA)	2.09	1.50	1.41	0.253
IT*DA(or AA*FR)	0	0	-	-
IT*AA (or DA*FR)	-0.05	1.48	-0.03	0.980
Root mean square error = 5.92		r^2 = 98.18%		
	Particle size			
	Model Coeff.[a]	SE[b]	t-value	*p-value*
Intercept	82.17	11.72	7.01	0.010
Feed concentration (C)	9.97	11.72	0.85	0.458
Inlet air temperature (IT)	6.51	11.72	0.56	0.618
Drying air speed (DA)	6.70	11.72	0.57	0.608
Atomization air speed (AA)	-8.68	11.72	-0.74	0.513
Feed flow rate (FR)	-20.69	11.72	-1.77	0.176
Nozzle diameter (ND)	0.26	11.72	0.02	0.984
C*IT (or FR*ND)	7.93	11.72	0.68	0.547
C*DA (or AA*ND)	-3.88	11.72	-0.33	0.762
C*AA (or DA*ND)	-19.76	11.72	-1.69	0.191
C*FR (or IT*ND)	12.71	11.72	1.08	0.357
C*ND (or IT*FR or DA*AA)	6.13	11.72	0.52	0.637
IT*DA (or AA*FR)	0	0	-	-
IT*A (or DA*FR)	13.38	11.72	1.14	0.340
Root mean square error =46.89		r^2 = 78.84%		

[a] Coefficient of the linear model.

[b] Standard error of the coefficient.

On the other hand, it has been reported that spray drying of water soluble and low molecular weight substances, such as mannitol, sucrose and lactose, results in high yields (Portmann et al., 2007). The yield of SDCII, in comparison, was low because cellulose II is a water-insoluble and high molecular weight substance (~20,000) and hence, needs to be spray-dried at low concentrations and at low feed flow rates in a small scale spray-drier. At an industrial scale, the yield of spray-dried cellulose is typically much higher because of the taller drying chambers with larger diameters that minimize deposition of the sprayed droplets on the walls (Portmann et al., 2007).

The calculated *p-values* showed that none of the main factors had any significant effect on particle size. Thus, when *p-values* were > 0.05, H_0 (no effect) cannot be rejected. On the other hand, the factors: feed concentration (C, p= 0.012), inlet air temperature (IT, p= 0.039) and feed flow rate (FR, p= 0.003) varied significantly with a change in yield, and thus, H_0 was rejected for these factors. Likewise, among the two-way interaction factors, only C*IT revealed a significant negative effect on yield (Y, p= 0.028).

The coefficient sign showed that concentration and flow rate adversely affected yield, while inlet temperature had a positive effect. The negative effect of flow rate on yield was more pronounced than that of concentration. On the contrary, particle size increased with increasing feed concentration (C), inlet air temperature (IT) and drying air speed (DA); however, powder yield was reduced with atomization air pressure (AA) and feed flow rate and none of these factors were significant. Summarizing, increase in yield occurred with increasing IT, DA, and AA, and a decrease in yield happened with increasing feed concentration, feed flow rate and nozzle diameter.

Drying air speed and atomization air pressure had a positive, but a minor effect on yield. In general, the effect of two-way interaction factors was minor, except for C*DA

and C*IT. These results indicate that all factors that rendered fast drying of the spray droplets in the drying chamber have a positive effect on yield. For example, higher inlet air temperatures will accelerate droplet drying. Similarly, the increase in drying air speed will remove water vapor more efficiently from the droplets and the drying chamber, resulting in reduced condensation of water vapor on the walls of the drying chamber. Further, an increase in atomization air pressure also creates smaller droplet sizes, which are exposed to the concurrent incoming inlet temperature and as a result, dry faster.

The smaller diameter and length of the drying chamber, however, limit the amount of feed material that can be fed efficiently. This means that factors which increase the amount of droplets in the drying chamber might have a negative effect on drying and hence on yield. Thus, an increase in feed concentration, feed flow rate or nozzle diameters were found to increase deposition of material on the walls of the drying chamber, rather than in the cyclone, resulting in a lower yield.

An increase in concentration probably rendered larger droplets resulting in a large particle size. This effect was also favored if high temperatures and high drying air speeds are employed since a rapid drying is achieved, allowing the large feed droplets to convert into particles. However, when large particles are produced, the yield is highly reduced due to a saturation of the drying chamber wall.

An increase in atomization air pressure increases the formation of smaller size droplets (and consequently particles), which are easily carried by the drying air to the cyclone. On the contrary, increasing the nozzle diameter from 411 to 711 µm showed no effect on the particle size. This indicates that only the contact of fluid and the atomizing air controls droplet size and not the aperture of the nozzle.

A high feed flow rate decreased the particle size since most of the large particles are probably slammed into wall and got adhered because they did not dry completely and

only the small ones would be able to reach the cyclone and product vessel. The powder adhered on the drying chamber was not scraped out and used for the analysis. The two-way interaction factors concentration and atomization air pressure increased the negative effect of feed flow rate on particle size. A high feed concentration on the other hand, favors larger particle size. This effect is decreased by increasing atomization air pressure since in the nozzle when it contact the feed it breaks down the feed into smaller droplets, decreasing the chance of clogging and as a result, counteracting the positive effect of concentration on particle size.

The goodness of fit statistic was examined by the coefficient of determination (r^2), which indicates how much variation in the response is explained by the linear model composed by the terms shown in Table IV-4. The higher the r^2, the better the model fits to the data and the better the model describes the relationship between the factors and the responses. Thus, about 98.18% and 78.84% of the experimental variances for yield and particle size, respectively, are explained by the linear model. The random error was larger for particle size compared to yield, suggesting more variability in the particle size data.

Box Behnken Design for Spray Drying Optimization

The Box-Behnken design was employed for the spray drying optimization. This is a quadratic design which requires 3 levels of each factor including a center point in the space design. The statistical analysis was made employing the Minitab® software v.16 (Minitab® Inc., State College, PA). In this design, the significant three main factors, concentration, inlet temperature, and flow rate, determined from the factorial experiments were employed for yield since for particle size none of the factors were significant. The atomization air pressure (AA, 1.0 kg-f/cm^2), sprayer nozzle diameter (ND, 711 µm) and drying air rate (DA, 0.44 m^3/min) were kept constant. The smaller size sprayer nozzle diameter (411 µm) had clogging problems and therefore was not used. The experimental

matrix and the *t*-test results obtained from the Minitab® software (State College, PA) for the coefficients are presented in Tables IV-5 and IV-6, respectively. The *t-test* results established that IT (p = 0.001), FR (p = 0.000), C*IT (p = 0.017), IT*FR (p = 0.021), and the quadratic term FR*FR (p = 0.021) significantly affected yield. Different from the factorial analysis, concentration was not significant. Further, as seen for the factorial analysis, concentration and feed flow rate had a negative impact on yield. Conversely, all the square terms had a positive effect on yield. Based on the results from the *t-test* the fitted quadratic model for yield was:

$$Y = 19.47 - 2.00C + 15.62\,IT - 26.85FR + 4.34C^2 + 5.94IT^2 + 9.04FR^2 - 9.15C*IT + 5.20C*FR - 8.65IT*FR \quad \text{Eqn. IV-1}$$

Even though only three factors were taken into account in this design, a low yield was also obtained at low inlet air temperature and high feed flow rate. The loss in yield at lower inlet temperature was due to the observed condensation of the feed droplets on the drying chamber wall, which is a common problem observed in pilot scale spray-dryers, in comparison to production scale spray-driers, due to the short residence time and short radial distances from the atomizer to the drying chamber wall (Pisecky, 1997).

The multiple regression coefficients (Table IV-6) indicate that 98.52% of the experimental variance for yield is explained by the fitted quadratic model (the remaining 1.48 % experimental variation is attributed to random error, such as run #, type of drying chamber or collector vessel used; all of them are considered negligible).

Table IV-5. Spray Drying Conditions and Results for Box Behnken Design (BBD).

Run order	Feed concentration (% w/v)	Inlet air temperature (°C)	Feed flow rate (mL/min)	Yield (%)
1	4.5	200	1	82.4
2	6.0	140	3	17.5
3	4.5	170	3	21.8
4	3.0	170	1	66.3
5	3.0	170	5	3.6
6	4.5	170	3	19.3
7	3.0	140	3	3.0
8	6.0	170	1	51.7
9	3.0	200	3	60.3
10	4.5	140	1	41.6
11	4.5	200	5	10.0
12	6.0	200	3	38.2
13	4.5	170	3	17.3
14	6.0	170	5	9.8
15	4.5	140	5	3.8

Table IV-6. Coefficients Estimates and *t-test* Results from Box Behnken Analysis for Yield.

Term	Yield		
	Model Coeff.[a]	SE[b]	*p*-value
Intercept	19.47	2.99	0.001
Feed concentration (C)	-2.00	1.83	0.325
Inlet air temperature (IT)	15.62	1.83	0.001
Feed flow rate (FR)	-26.80	1.83	0.000
C*IT	-9.15	2.59	0.017
C*FR	5.20	2.59	0.101
IT*FR	-8.65	2.59	0.021
C*C	4.34	2.70	0.168
IT*IT	5.94	2.70	0.079
FR*FR	9.04	2.70	0.021
RMSE [c] = 5.18			r^2 = 98.52%

[a] Model Coefficient.

[b] Standard error of the coefficient.

[c] Root mean square error (estimates standard deviation of the random error).

This high r^2 value indicates that the quadratic model is a good predictor for yield and that the model describes very well the relationship between the three factors (concentration, inlet temperature, and flow rate).

The model was validated by the lack of fit test (Table IV-7). The goodness of fit statistical test evaluates whether the variation due to lack of fit of the model is small enough to be accepted as a negligible portion of the pure error. In this case, the null hypothesis (H_0) is that the lack of fit error is zero. The *p*-value for the lack of fit was > 0.05, indicating that H_0 cannot be rejected and the reduced model with three factors is sufficient to accurately describe the observed variation in yield and that experimental variations observed for yield could be attributed to random errors ($p = 0.111$).

The optimized contour response plot is shown in Figure IV-4. It highlights the region with process combinations where a desired range of the response occurred. In this case, it was used to identify the factor settings that maximize response (yield > 70%). Thus, a high yield is expected if inlet temperature is kept at high levels and concentration and flow rate are set at low levels. The upper left region of the plot offers the best factor combinations that rendered a high product yield. Thus, a feed flow rate of 2 mL/min, a feed concentration of 3% and inlet air temperature of 195 ºC were selected as the optimal operational parameters, keeping drying air speed (0.44 m^3/min); atomization air pressure (1.0 kg-f/cm^2); and nozzle diameter (711 µm) constant. Even though the optimal concentration ranged from 3-3.8%, the lower value was selected to avoid possible clogging problems. The predicted response (mean ± SE) at those conditions was: yield = 72.5 ± 4.2 %. This result was confirmed by conducting five runs at the optimized factor settings. The average yield value obtained was 70.7 ± 7.6% (Table IV-8).

Table IV-7. Analysis of Variance from Box Behnken Design.

Yield					
Source	Degrees of freedom	Sum of Squares	Mean Square	*F*- ratio	*p*-value
Model	9	8938.9	993.2	37.0	0.001
Error	5	134.3	26.9	-	-
Lack of Fit*	3	124.1	41.4	8.1	0.111
Pure Error*	2	10.2	5.1	-	-
Total Error	5	134.3	-	-	-

* The lack of fit compares the local group mean with the fitted value, whereas the pure error compares the observed value with the local group mean.

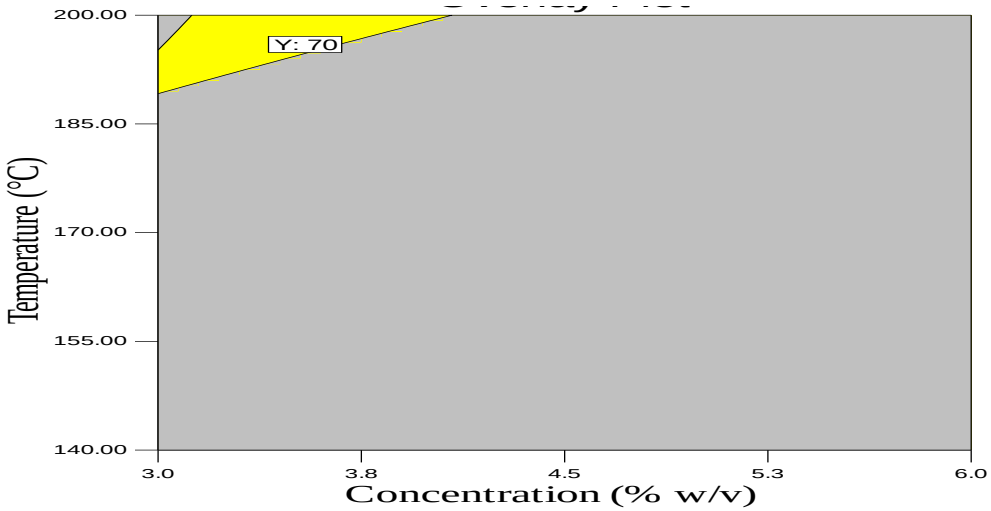

Figure IV-4. Plot for Yield Obtained from the Box Behnken Design. Constant Factors: 0.44 m^3/min Drying Air Speed; 1.0 kg-f/cm^2 Atomization Air Pressure; 2.0 mL/min Feed Flow Rate; 711 µm Sprayer Nozzle Diameter. The Yellow Region of the Plot Represents the Optimal Temperature and Feed Concentration Ranges to Produce SDCII > 70% Yields.

Table IV-8. Validation of the Box Behnken Model for Yield under Optimal Operating Conditions.[a]

Replicate	Moisture Content (%)	Yield (%)	PS[b]± SE[c] (µm)	Geometric mean (percentile, µm) 25	50	75
1	1.20	71.7	34.7 ± 1.6	34.3	45.1	56.0
2	0.59	83.3	40.9 ± 2.7	41.8	58.3	74.6
3	0.38	66.8	35.2 ± 2.4	37.5	53.1	68.7
4	0.89	63.7	47.8 ± 2.7	42.4	58.8	75.2
5	0.71	68.0	54.0 ± 2.7	45.0	61.7	78.5
Avg±SD	0.75±0.31	70.7±7.6	42.5 ± 8.3	40.2±4.3	55.4±6.5	70.6±8.9

[a] 3.0 % w/v feed concentration; 195 °C inlet air temperature; 0.44 m^3/min drying air speed; 1.0 kg-f/cm^2atomization air pressure; 2.0 mL/min feed flow rate; 711 µm sprayer nozzle diameter.

[b] Particle size expressed as a geometric mean diameter.

[c] Standard error.

Carbohydrate Excipient Powder Properties

The chemical structures and FT-IR spectra of SDCII, along with those of CII and commercial excipients (Avicel® PH-102, Starch 1500® and Fast Flo® 316) employed for comparative purposes are shown in Figures IV-5 and IV-6 and Table IV-9, respectively. The characteristic vibrational peaks of cellulose are present at ~3446 cm^{-1}, 2899 cm^{-1}, 1379 cm^{-1} and 893 cm^{-1}, attributable to intramolecular OH stretching, CH stretching, hydrogen bonding between C6 and its OH group, and antisymmetric C-1 out-of-plane stretching vibrations, respectively. The 893 cm^{-1} band has also been reported to be associated with the cellulose II lattice and crystallinity of cellulose (Carrillo et al., 2004). Starch 1500® had four peaks at 3300, 1610, 1350 and 1000 cm^{-1}. The absorption bands at 3300 and 1610 cm^{-1} are due to bound water, while that at 1350 cm^{-1} is due to the bending vibrational modes of O–C–H, C–C–H, and C–O–H. In the region between 1200 and 900 cm^{-1}, several strong absorption peaks are assigned to C–C and C–O stretching modes (Lizuka and Aishima, 1999; Zhbankov, 1964).

Spray-dried lactose (Fast Flo® 316) shows a broad band from 3600 to 3200 cm^{-1} due to the stretching vibrations of the C-O-H bonds. Two bands at 3000-2800 $cm^{-1}$are due to the stretching vibrations of C-H bonds inside the rings and C-H bonds of the hydroxymethyl moiety (-CH_2OH) outside the rings. The band from 1600 to 1700 cm^{-1} is ascribed to the stretching vibrations of adsorbed water. The bands between 1500 and 1200 cm^{-1} are due to the bending of C-H bonds. The bands from 1040 to1160 cm^{-1} are due to the asymmetrical stretching of C-O-C ether linkage (glucose and galactose). Bands from 730 to 960 cm^{-1} corresponds to the typical vibrations of the entire molecule (Drapier-Beche et al., 1999).

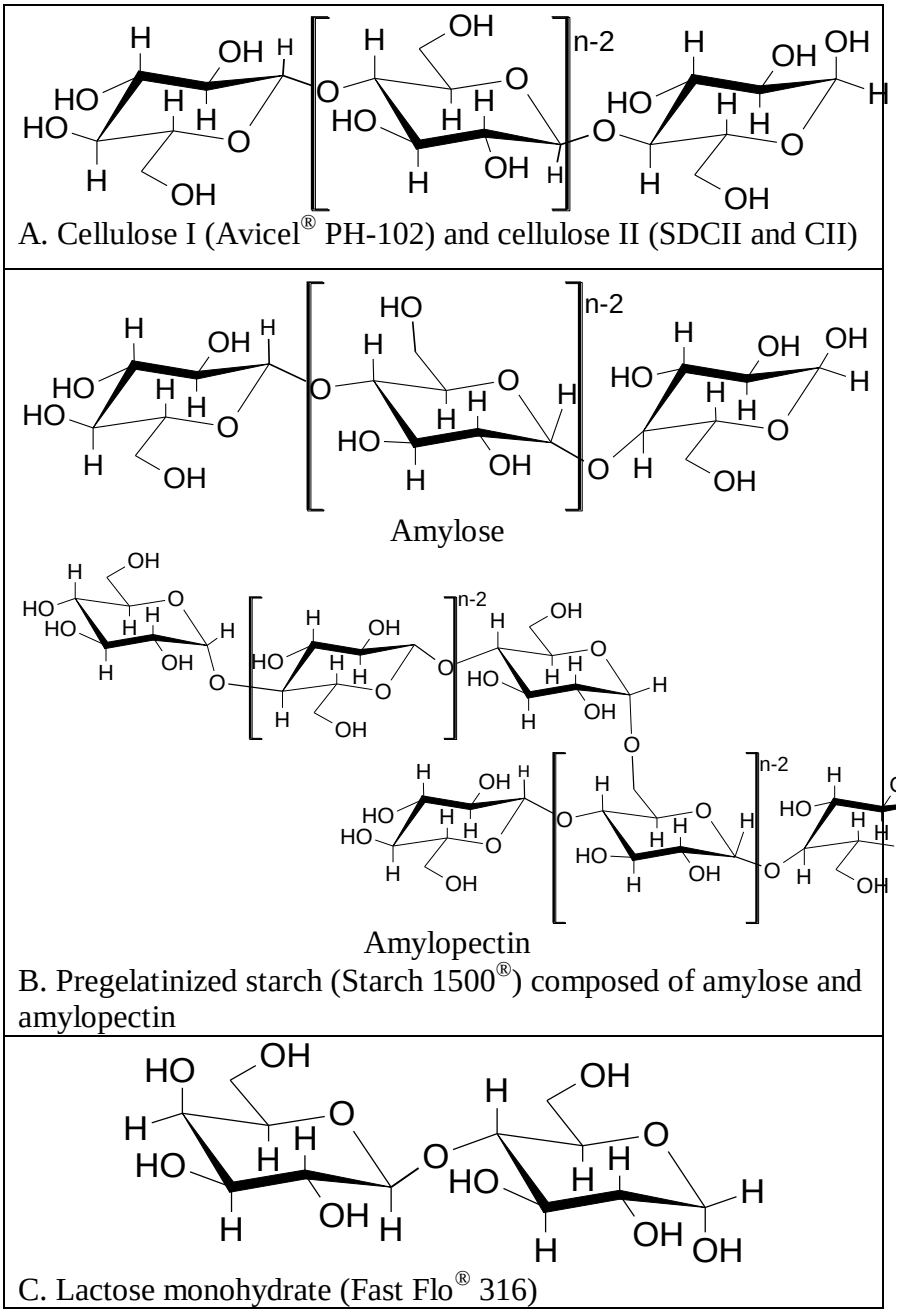

A. Cellulose I (Avicel® PH-102) and cellulose II (SDCII and CII)

B. Pregelatinized starch (Starch 1500®) composed of amylose and amylopectin

C. Lactose monohydrate (Fast Flo® 316)

Figure IV-5. Chemical Structure of: (A) CII, SDCII and Avicel® PH-102; (B) Starch 1500®; (C) Fast Flo® 316 Made with ChemSketch v. 11.01 (Advanced Chemistry Development, Inc., Toronto, Canada).

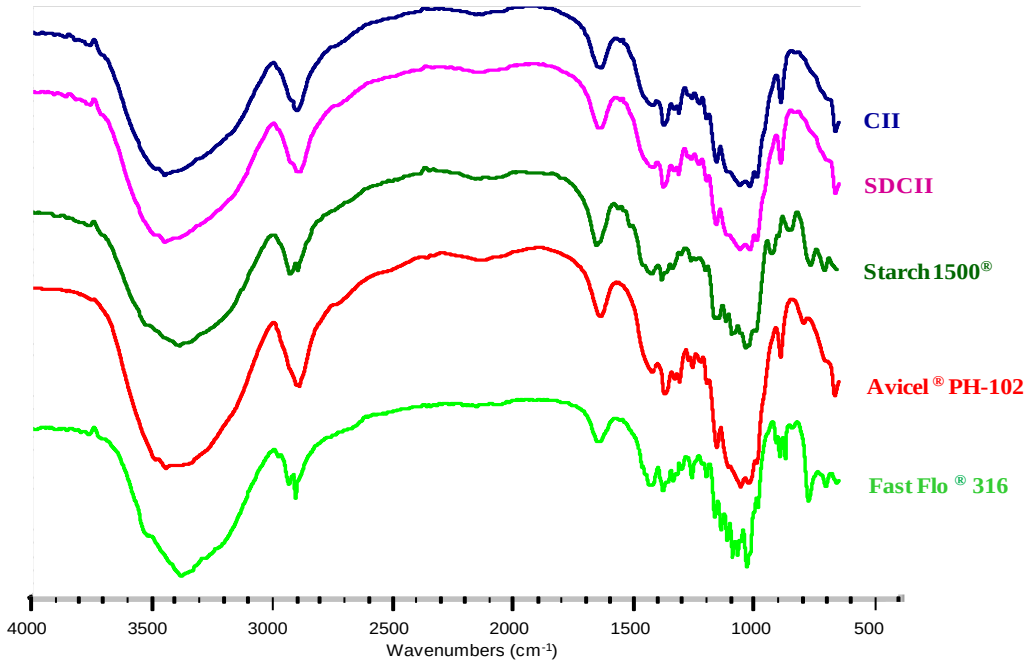

Figure IV-6. FT-IR Spectra of Carbohydrate Excipients: CII, SDCII, Fast Flow® 316 (lactose monohydrate), Starch 1500® (pregelatinized starch) and Avicel® PH-102 (microcrystalline cellulose I).

Table IV-9. FT-IR Bands Obtained for Cellulosics and their Assignments.

SDCII (cm^{-1})	CII (cm^{-1})	Avicel® PH-102 (Microcrystalline Cellulose I) (cm^{-1})	Assignments
3445	3444	3424	Intramolecular OH stretching
2894	2892	2898	CH and CH_2 stretching
1638	1642	1638	OH from absorbed water
1422	1419	1430	CH_2 symmetric bending
1380	1383	1382	CH bending
1316	1317	1317	OH in plane bending
1162	1161	1162	C-O-C asymmetric stretching
1062	1062	1060	C-O/C-C stretching
1021	1023	1028	C-O stretching or bending of C-OH
993	994	994	C-O stretching
895	895	898	Asymmetric rocking of C-1
	3388		Free, inter/intramolecular OH stretching (Pushpadars et al., 2008)
Starch 1500® (Pregela-tinized starch)	2932 and 2901		CH_2 symmetrical stretching
	1653		Scissoring of O-H bonds of absorbed water (Li et al., 2010)
	1423 and 1383		C-H bending
	1163, 1118 and 1091		C-C and C-O stretching modes
	986		O-C Stretching (Pushpadars et al., 2008)
	795 and 708		Skeletal and ring modes (Singh, et al, 2009)
	3379		Stretching vibration of C-O-H bonds
Fast Flo® 316 (Lactose mono-hydrate)	2934 and 2900		Stretching of C-H vibrations
	1652		Stretching of OH bond of water
	(1428, 1383, 1342, 1304, 1262 and 1202)		Bending of C-H bonds
	(1168, 1142, 1094, 1072 and 1033),		Asymmetric stretching of C-O-C
	915, 899 and 877		Vibrations characteristic of α-lactose monohydrate (Crisp et al., 2010)

Figure IV-7 shows the powder X-ray diffractograms of SDCII, CII, Fast Flo® 316, Avicel® PH-102 and Starch 1500®. The diffraction peaks appearing at 12, 20, and 22° 2θ for SDCII confirmed the cellulose II lattice attributable to 1 $\bar{1}$ 0, 110 and 200 reflections, respectively. Avicel® PH-102, in contrast, displayed characteristic diffraction peaks at 14.8, 16.3 and 22.4° 2θ, corresponding to the 1 $\bar{1}$ 0, 110 and 200 reflections of cellulose I, respectively. No difference in the diffractograms of SDCII and CII suggests that spray drying had no effect on the cellulose II crystalline structure. However, the degree of crystallinity of the samples (from~ 68 to ~ 63%) slightly decreased, indicating partial amorphization of the chains. In the case of Starch 1500®, a diffuse amorphous halo typical of pregelatinized starch obtained from corn starch was observed (Laovachirasuwana et al., 2010). In fact, the degree of crystallinity of this material was very low (< 7.5%). The characteristic peaks for Fast Flo® 316 (α-lactose monohydrate) were observed at 12.5°, 16.4° and 20° 2θ (Miao and Ross, 2005). The peak at 12.5° is characteristic of α-lactose monohydrate, which is the most common form of crystalline lactose (Szepes et al., 2007). It also showed the highest degree of crystallinity among all the materials evaluated (87%).

The selected powder properties of carbohydrate excipients, as produced or received, are presented in Table IV-10. Figures IV-8 and IV-9 show scanning electron micrographs (SEM) depicting particle morphologies of unprocessed and spray-dried cellulose II materials (CII and SDCII) and commercial carbohydrate excipients, respectively. CII consisted of fibers (d_g., 89.9 ± 5.0 μm), while SDCII was a mixture of round to oblong shaped particles (d_g., 52.5 ± 3.0 μm) with smooth surfaces. This indicates that spray drying due to the rapid droplet drying, causes the CII fibers to coalesce and form oblong smooth particles.

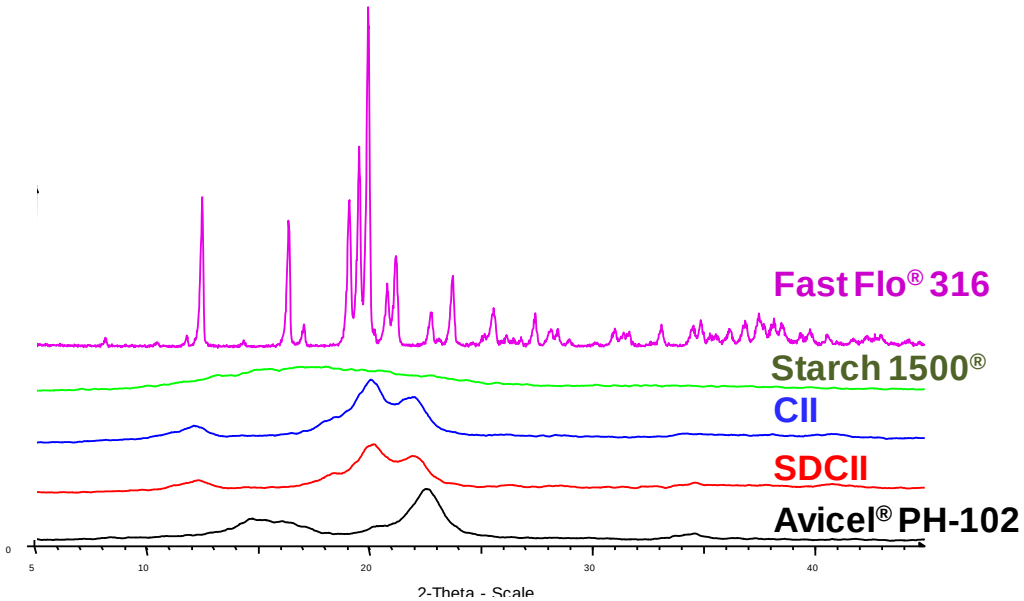

Figure IV-7. Powder X-ray Diffractograms of Carbohydrate Excipients: CII, SDCII, Fast Flow® 316 (lactose monohydrate), Starch 1500® (pregelatinized starch) and Avicel® PH-102 (microcrystalline cellulose I).

Table IV-10. Carbohydrate Excipient Powder Properties.

Property	n	Sample				
		CII	SDCII[d]	Avicel® PH-102[e]	Starch 1500®[e]	Fast Flo®316[e]
Geometric mean diameter[a] (µm±SE[b])	N.A.	89.9 ± 5.0	52.5 ± 3.0	70.9 ± 7.0	47.2 ± 2.9	83.2 ± 7.2
Moisture content (%)[c]	3	3.6 ± 0.4	2.8 ± 0.7	3.7 ± 0.3	9.2 ± 0.0	1.0 ± 0.2
Degree of crystallinity (%)[c]	3	68.0 ± 1.4	61.5 ± 1.2	72.1 ± 2.6	7.5 ± 1.2	87.0 ± 1.5
True density (g/cm^3)[c]	3	1.538 ± 0.025	1.554 ± 0.006	1.551 ± 0.003	1.50 ± 0.003	1.554 ± 0.003
Bulk density (g/cm^3)[c]	5	0.38 ± 0.03	0.55 ± 0.00	0.37 ± 0.00	0.61 ± 0.02	0.59 ± 0.01
Tap density (g/cm^3)[c]	5	0.54 ± 0.06	0.81 ± 0.00	0.48 ± 0.00	0.78 ± 0.01	0.71 ± 0.00
Powder porosity (%)	1	75.5	64.4	76.2	59.1	62.3
Flow rate (g/min)						
14.3 mm orifice[c]	3	1.3 ± 0.2	5.2 ± 0.6	4.5 ± 0.2	2.4 ± 0.1	1.9 ± 0.3
17.5 mm orifice[c]	3	2.6 ± 0.1	13.4 ± 0.5	8.0 ± 0.5	5.7 ± 0.6	4.7 ± 0.4
19.1 mm orifice[c]	3	3.4 ± 0.1	15.6 ± 0.4	9.6 ± 1.7	11.0 ± 1.6	11.2 ± 1.6

[a] Determined from the cumulative frequency versus particle size plot constructed using log-normal scales.

[b] Standard error determined as $\frac{\sigma}{\sqrt{n}}$

[c] Mean±Standard deviation.

[d] 1 kg batch.

[e] Commercial samples: microcrystalline cellulose I (Avicel® PH-102), pregelatinized starch (Starch 1500®), lactose monohydrate (Fast Flo®316).

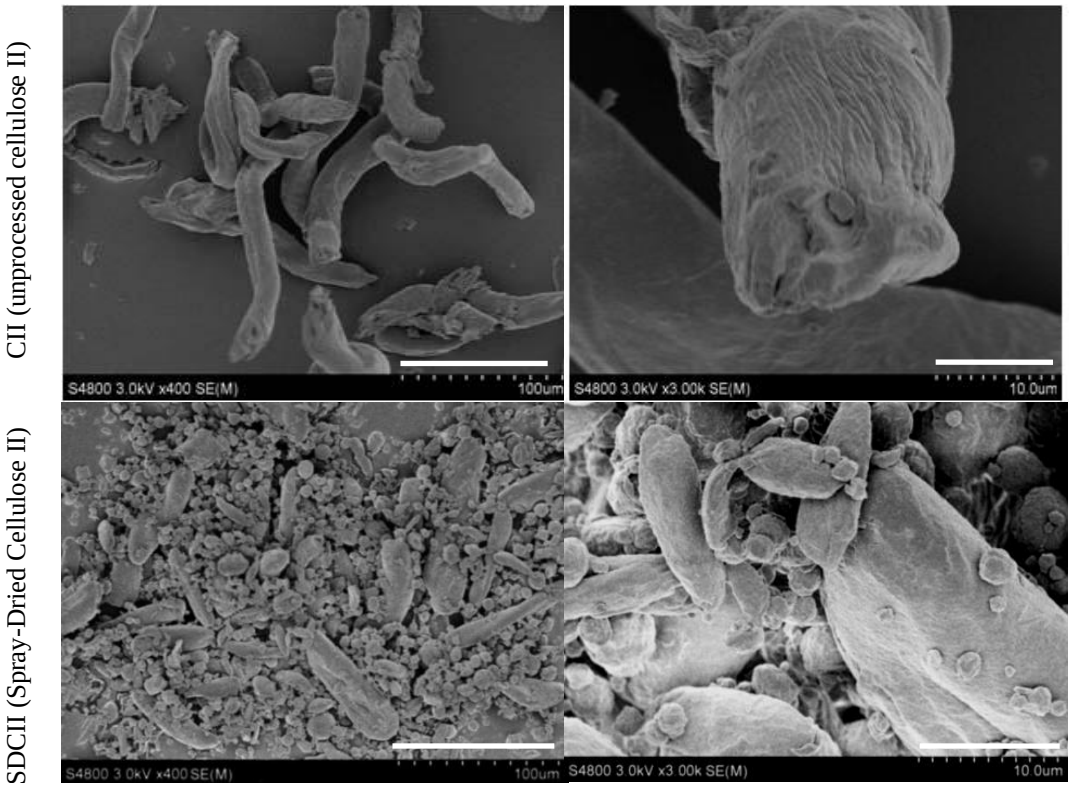

(400X, Scale 100 µm) (3,000X, Scale 10 µm)

Figure IV-8. SEMs of SDCII and CII at 400X and 3,000X.

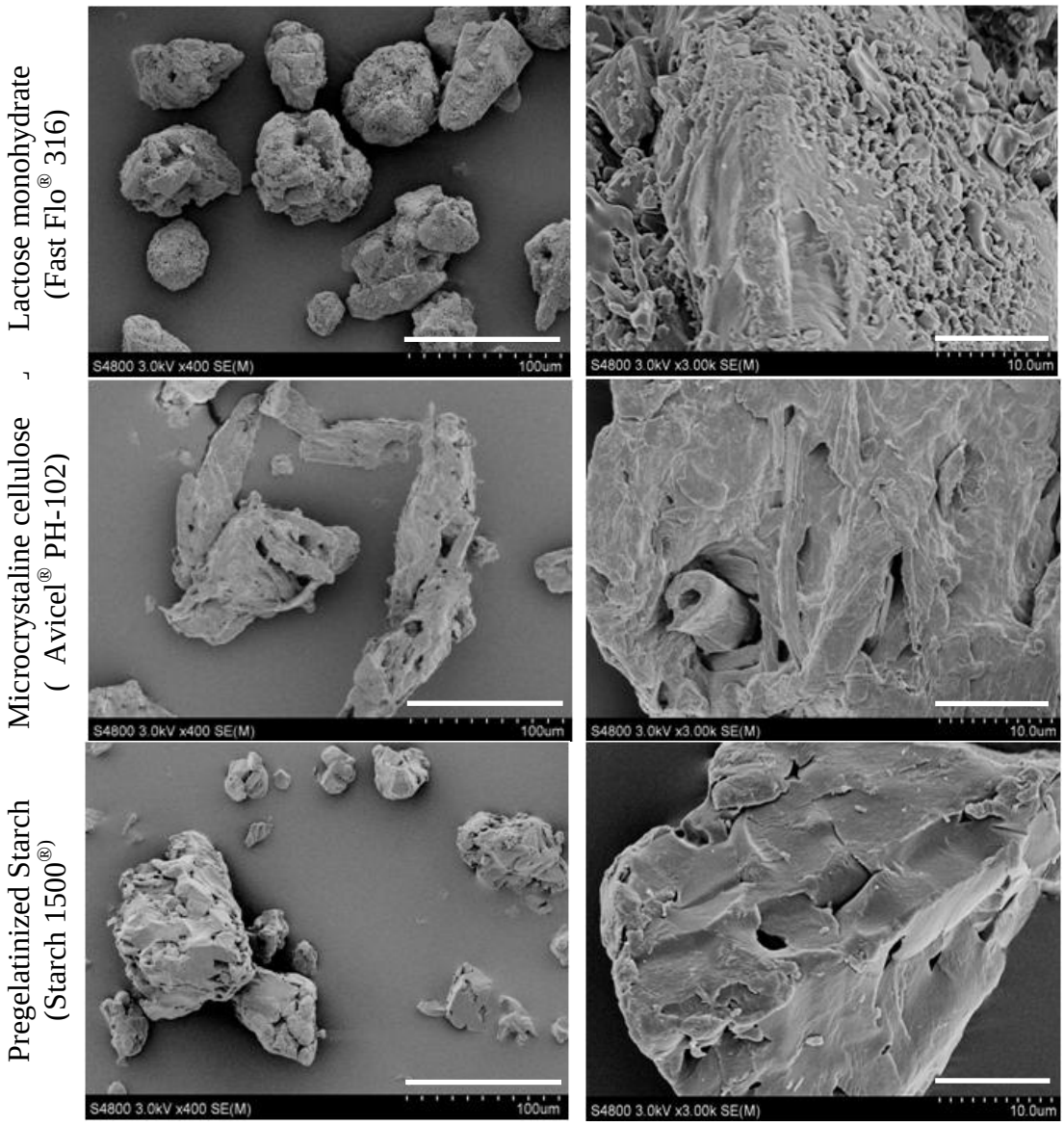

Figure IV-9. SEMs of Fast Flo® 316, Avicel® PH-102 and Starch 1500® at 400X and 3,000X.

Likewise, Fast Flo® 316 was composed of aggregates of crystalline lactose particles linked by amorphous particles as reported previously by Vromans et al. (Vromans et al, 1986). Other spray-dried excipients such as Avicel® PH-102 and Starch 1500®, in contrast, had irregularly-shaped particles with rough surfaces and sharp edges. The differences among the particle sizes obtained for the commercial products might be caused by the spray drying conditions used and the physicochemical properties of the starting materials.

The bulk and tap densities of SDCII, Starch 1500® and Fast Flo® 316 were higher than those for CII and Avicel® PH-102 (Table IV-10). Since the spray drying process modified the morphology of CII, SDCII showed more regular particles which were able to pack more efficiently and hence their powder was denser. The flowability of all materials was assessed by the flow-through-an-orifice test. SDCII showed the fastest flow, whereas CII the slowest flow due to its fibrous shape which causes a steric hindrance hampering flow due to entanglement of the fibers. The flow property of commercial materials was between those of SDCII and CII. Despite the small particle size of SDCII, it showed the fastest flow which could be attributed to its dense, round-to-oblong shaped particles with smooth surfaces. Further, the low moisture content (< 10%) for all materials is expected to have no contribution on their flow properties.

Spray drying had no effect on the true density of CII. In fact, this property was comparable among all materials except for Starch 1500® which has a less condensed polymer packing. It must be noticed that starch is formed by a combination of two polymers, amylose (minor component) and amylopectin (major component). The latter is responsible of the branching arrangement of the polymer, and the reduced packing of the chains resulting in a very low degree of crystallinity and low true density. It must be pointed out that this loose packing of the chains has no relationship with particle

properties such as bulk and tap densities which were very high due to the regularity in the particle morphology.

Compression and Compaction Characteristics of Carbohydrate Excipients

Although initially developed for metals, the Heckel analysis is widely used to assess the compressibility of pharmaceutical powders (Alderborn and Nyström, 1996). For this reason, a lot of caution must be taken when using this equation to characterize the compaction of powders with several deformation mechanisms. In this study, the out-of-die Heckel plots were constructed for tablets prepared at 10-260 MPa compression pressures and a dwell time of 30 sec. The Heckel plots are shown in Figure IV-10 and Table IV-11 lists the Heckel analysis results. The yield pressure value, P_y, which has been associated with the inverse of the slope of the linear portion of the Heckel curve, is a measure of the pressure at which the material begins to form a coherent compact by apparent plastic deformation. Heckel demonstrated that for plastic deforming metals such as copper, iron and nickel the plots are initially curve and then form a straight line. However, for brittle materials such as alumina which does not have high particle bonding, the Heckel plot is not linear during the pressure range used ($0\text{-}14x10^4$ psi) (Heckel, 1961b). Further, this equation does not account for the elastic recovery upon decompression which can happen for pharmaceutical powders. For this reason, interpretation of this equation should be made cautiously because pharmaceutical powders can be either plastic or brittle which cannot be determined only from the P_y values.

In the present study, SDCII and CII had intermediate and comparable P_y values (~116 and 122 MPa, respectively). It is not surprising that spray drying did not affect the deformation characteristics of CII.

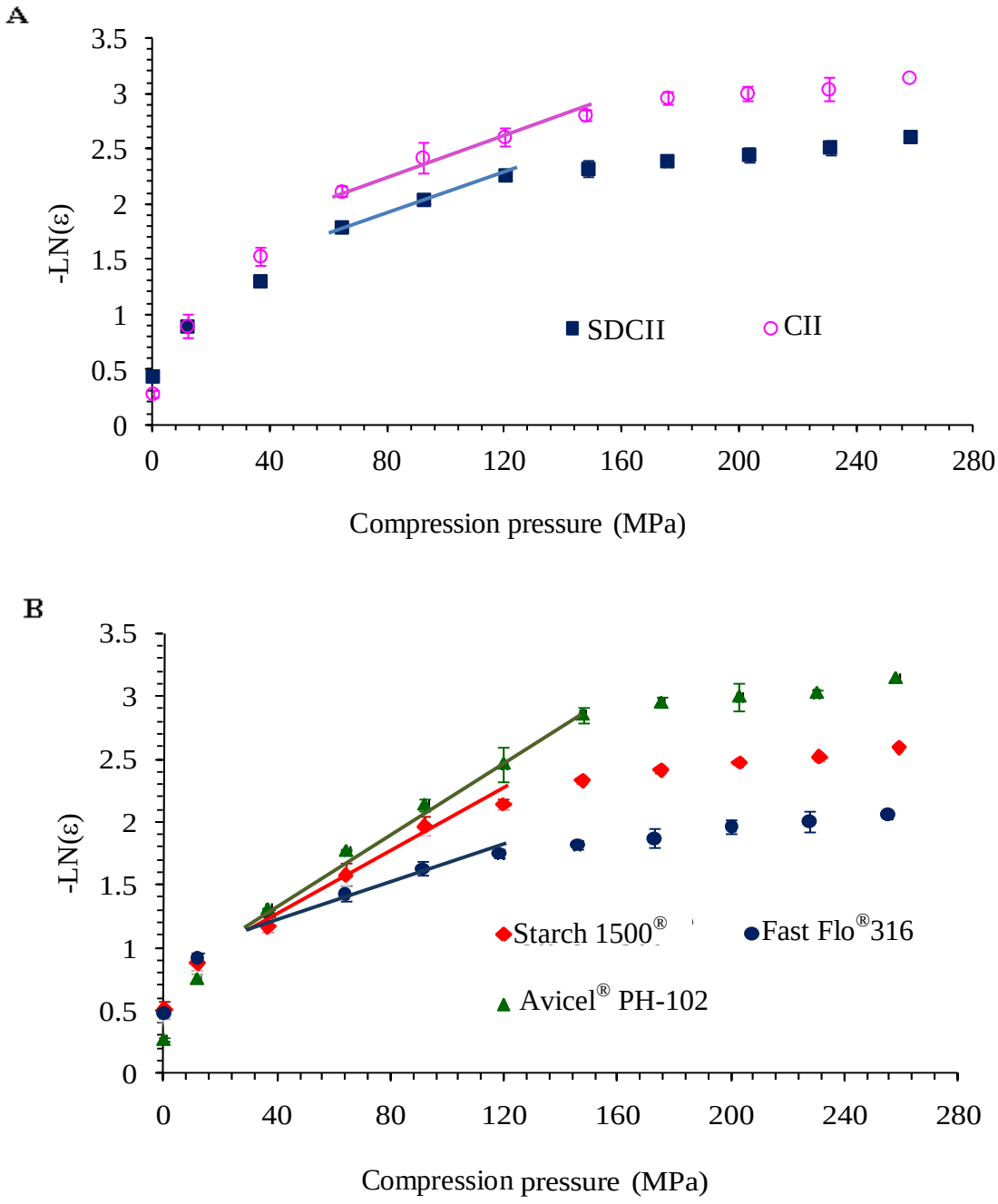

Figure IV-10. Heckel Plots (out-of-die) for: (A) SDCII (spray-dried cellulose II) and Unprocessed Cellulose II (CII); (B) Fast Flo® 316 (lactose monohydrate), Starch 1500® (pregelatinized starch) and Avicel® PH-102 (microcrystalline cellulose I). Y-Axis Corresponds to the Inverse Logarithm of Porosity.

Table IV-11. Out-of-die Heckel Results.

	Pressure range	P_y (MPa)[a]	D_0[b*]	D_a[c*]	D_b[d*]	AUHC[e] (MPa)	r^2
CII	65-150	122.0	0.24	0.80	0.56	625.1	0.9850
Avicel® PH-102[f]	35-150	73.5	0.24	0.57	0.34	596.5	0.9963
SDCII[h]	65-120	116.3	0.36	0.71	0.36	526.3	0.9990
Starch 1500®[f]	35-120	73.0	0.41	0.51	0.10	514.1	0.9979
Fast Flo®316[f]	35-120	166.7	0.38	0.65	0.27	420.9	0.9922

[a] Yield pressure found by P_y= 1/slope.

[b] Initial rearrangement as a result of die filling, found by $D_0 = \rho_{bulk}/\rho_{tap}$.

[c] Total powder packing at low pressures found from $D_a = 1-e^{-intercept}$

[d] Particle rearrangement/fragmentation at early compression stages found by $D_b = D_a - D_0$.

[e] Area under the Heckel curve.

[f] Commercial materials: microcrystalline cellulose I (Avicel® PH-102), pregelatinized starch (Starch 1500®), lactose monohydrate (Fast Flo®316).

*Dimensionless.

The fast drying of the wet material during this process probably is not a sufficient to cause a significant rearrangement of the cellulose chains. For this reason, it is expected the same degree of ability for crystal planes to slide when particles are subjected to compression.

Avicel® PH-102 and Starch 1500® had the lowest P_y values (~73 MPa); whereas, Fast Flo® 316 had the highest P_y value (~167 MPa). These results are in good agreement with the values reported in the literature [Avicel® PH-102, 77.3 MPa (Mitrevej et al., 1996) and 70.8 MPa (Reus, 2005); Starch 1500®, 72 MPa (Martinez-Pacheco et al., 1987); Fast Flo® 316, 152 MPa (Martinez-Pacheco et al., 1987); CII prepared from Avicel® PH-102, 125.6 MPa (Reus, 2005)]. Although Starch 1500® had the largest moisture content (9.2%) compared to other carbohydrate excipients; it still was within the USP maximum limit of 14%. It is interesting that this material gave a low P_y which agreed with the reported value cited above. It is possible that water favored plastic deformation even at high moisture contents. Results demonstrate that both Avicel® PH-102 and Starch 1500® were apparently highly plastic deforming materials, whereas Fast Flo® 316 was identified as an apparent brittle deforming material. These finding have been also reported previously (David and Augsburger, 1977; Rees and Rue, 1978; Van der Voort Maarschalk et al., 1997; Vromans et al., 1987).

The above results indicate that SDCII appears to be less ductile than Avicel® PH-102 and Starch 1500®, but is comparable in ductility to CII. Based on the area under the Heckel curve (AUHC), the overall compressibility of the materials followed the order: CII ≅ Avicel® PH-102 > SDCII ≥ Starch 1500® > Fast Flo® 316. In this case, the volume reduction ability of CII decreased due to the conversion of fibrous particles into a more densified and regularly-shaped particles with a reduced ability for compression. For this

reason, it is not surprising that the granular and dense particles of Fast Flo® 316 had the lowest compressibility.

The D_o, D_a and D_b parameters obtained from the Heckel plots as listed in Table IV-11 represent initial packing of the material upon die filling, total packing at low pressures, and the degree of powder bed arrangement or fragmentation at low pressures, respectively.

The D_o values followed the same trend as the bulk density values reported in Table IV-10 showing that regularly-shaped and dense particles such as Starch 1500® and Fast Flo® 316 had the highest densification at zero pressure, whereas CII and Avicel® PH-102 had the lowest D_0 values due to the fibrous and aggregate morphology along with low particle density. Since spray drying produced a more densified material, this powder had a lower tendency for volume reduction (densification) than CII. The D_b values indicate the degree of particle rearrangement/fragmentation at low pressures. In this case, fibrous materials such as CII showed the highest value, while the most regularly-shaped materials such as Starch 1500® and Fast Flo 316®, showed the lowest particle rearrangement. The combined effect of densification by particle rearrangement and densification by die filling is given in the rank order according to the D_a value: CII > SDCII > Fast Flo® 316 > Avicel® PH-102 > Starch 1500®, suggesting a decreasing tendency towards densification at lower pressures was especially driven by particle rearrangement than densification by die filling for CII and Avicel® PH102. Spray drying decreased the particle rearrangement ability of CII, but increased the densification capability by die filling due to the conversion of this highly fibrous material to more regularly-shaped particles.

The cross-sectional views of tablets prepared with cellulosic II materials (SDCII and CII) and commercial excipients made at 10, 120 and 260 MPa compression pressures

are shown in Figure IV-11 and Figure IV-12, respectively. At 10 MPa (~0.4 porosity), particle fragmentation was more evident for CII, SDCII and Fast Flo® 316 compacts, causing them to have a reduced void volume whereas for Starch 1500® and Avicel® PH-102 showed a tight packing due to particle rearrangement. At higher applied pressures (120 and 260 MPa) all compacts showed increased powder bed densification.

At 120 MPa of compression pressure, particle morphology for SDCII and CII tablets appear similar indicating no major differences in the powder consolidation mechanism under pressure. Further, the surface of the most fragmenting material (Fast Flo® 316) appears smooth due to particle fragmentation generating smaller particles that filled up the spaces and pores between larger particles. Even though its compact surface seems smooth, it had the largest porosity (~0.18) compared to other materials (~0.1). This suggests a larger number of compact micropores which are not visible at the 350X magnification. This could be a consequence of extensive fragmentation taking place in this material.

At 260 MPa, the core and outer surfaces of Avicel® PH-102 and Starch 1500® compacts appear similar. Thus, the compact surface of these most plastic deforming materials was more packed and the edges of the original particles were not distinguishable. The coalescence of particle boundaries observed for Starch 1500® and Avicel® PH-102 has been reported previously (Nicklasson et al.,1999). Further, the edge of the compact transverse cut of these plastic deforming materials was very sharp. Conversely, the compact's edges of less plastic deforming materials such as CII and SDCII, was rougher.

The large volume reduction ability of CII and Avicel PH-102 was observed at 260 MPa since at this pressure they showed the lowest porosity (~0.05). CII also showed mainly a plastic deformation along with partial fragmentation to produce fibers of sizes comparable to that of SDCII.

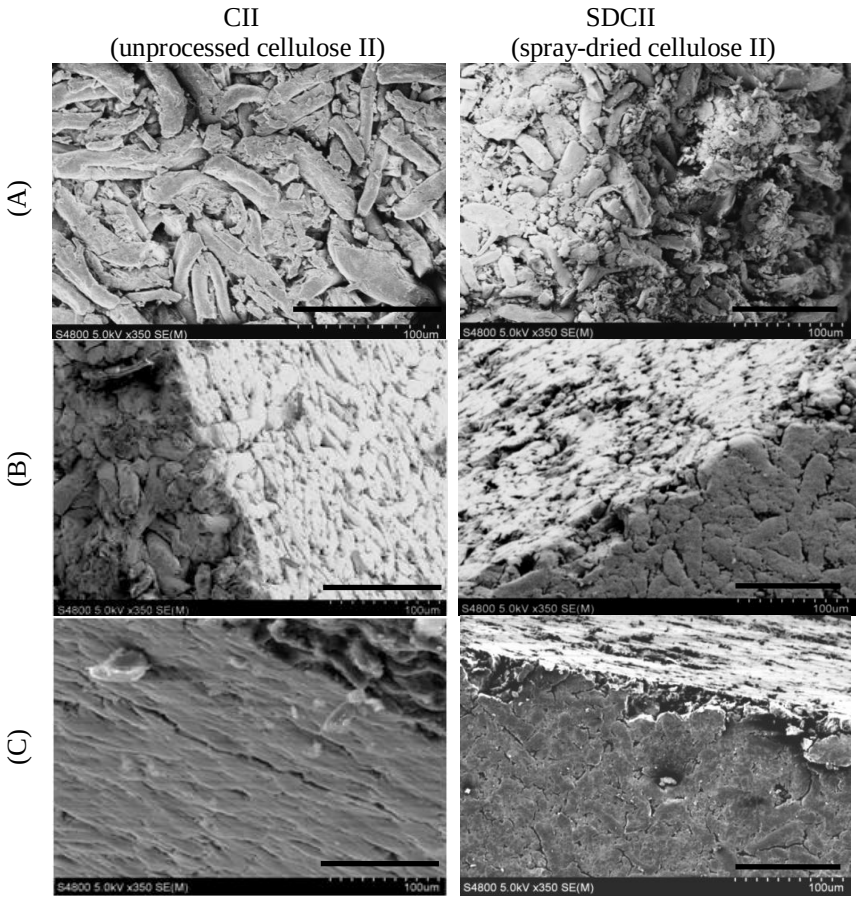

Figure IV-11. Cross-sectional Images of CII and SDCII Compacts at: (A) 10 MPa; (B) 120 MPa; (C) 260 MPa Compression Pressures at 350X (scale bar, 100 µm).

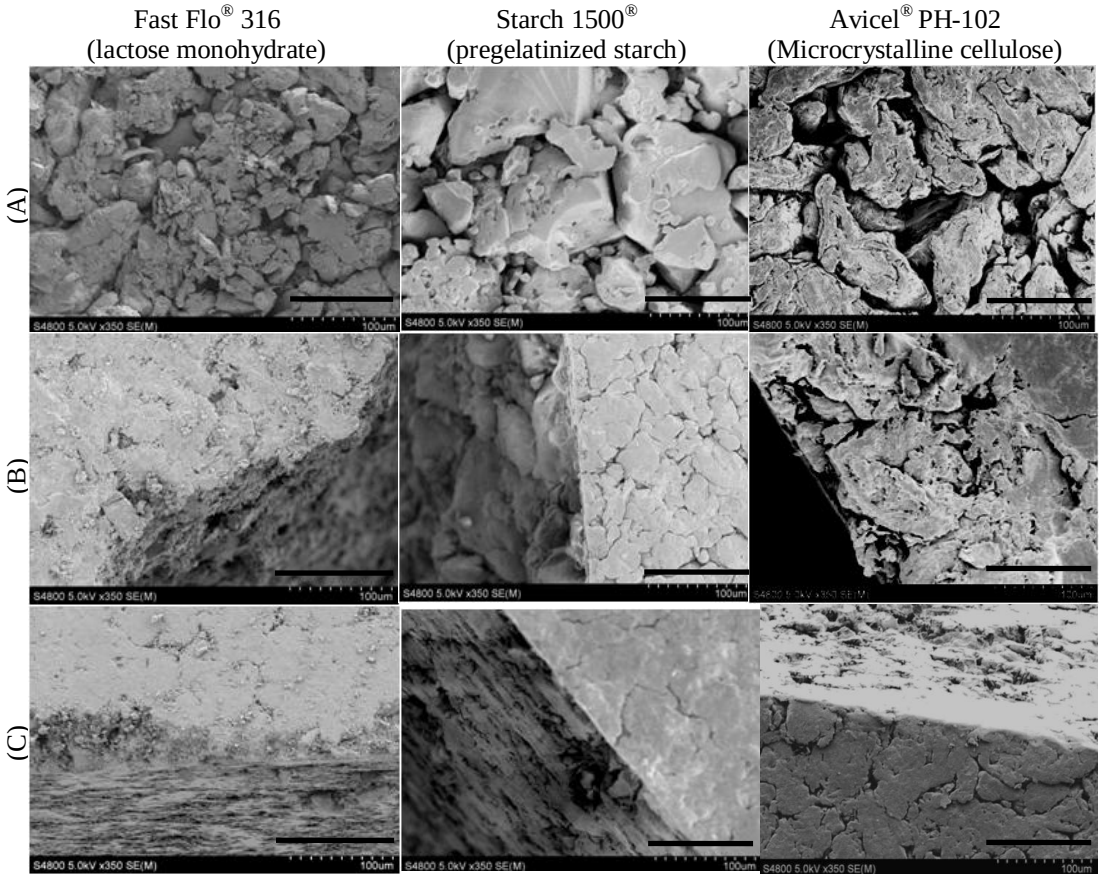

Figure IV-12. Cross-sectional Images of Commercial Carbohydrate Compacts at: (A) 10 MPa; (B) 120 MPa; (C) 260 MPa Compression Pressures at 350X (scale bar, 100 µm).

For Fast Flo® 316 compacts, the surface showed the presence of fine particles and the interior of the tablet appeared stratified, conforming to reports about materials which undergo fragmentation during consolidation (Vromans et al., 1987).

Figure IV-13 shows the variation of compact crushing strength with compact porosity. SDCII formed stronger compacts than those made from Starch 1500® and Fast Flo® 316. The latter showed the least reduction in porosity at high compression forces since the fragmenting ability at the compression pressure used did not contribute much to volume reduction and formation of more binding sites which is necessary to form strong compacts. Further, at 350X the cross-sectional views of their compacts showed a non-porous surface with some stratified particles in the interior of the compacts, indicating extensive fragmentation forming very tiny particles and hence, very small interparticle voids.

As seen previously, Fast Flo® 316 had the lowest volume reduction with applied pressure. This was reflected in the data for porosity since even at 260 MPa of compression pressure the porosity remained above ~0.13 while the porosities obtained for all other materials were ~0.05-0.07. Moreover, it is clear that materials having completely different consolidation mechanisms such as Starch 1500® and Fast Flo® 316 showed comparable compactibility profiles. However, the advantage of Starch 1500® over Fast Flo ® 316 is outstanding because Fast Flow® 316 requires higher compressive pressures to form compacts of comparable porosity to those of Starch 1500®.

The comparable compactibility of SDCII and CII compacts at porosities > 0.3 suggest that at low pressures particle consolidation is similar for both materials, possibly due to partial fragmentation of CII fibers.

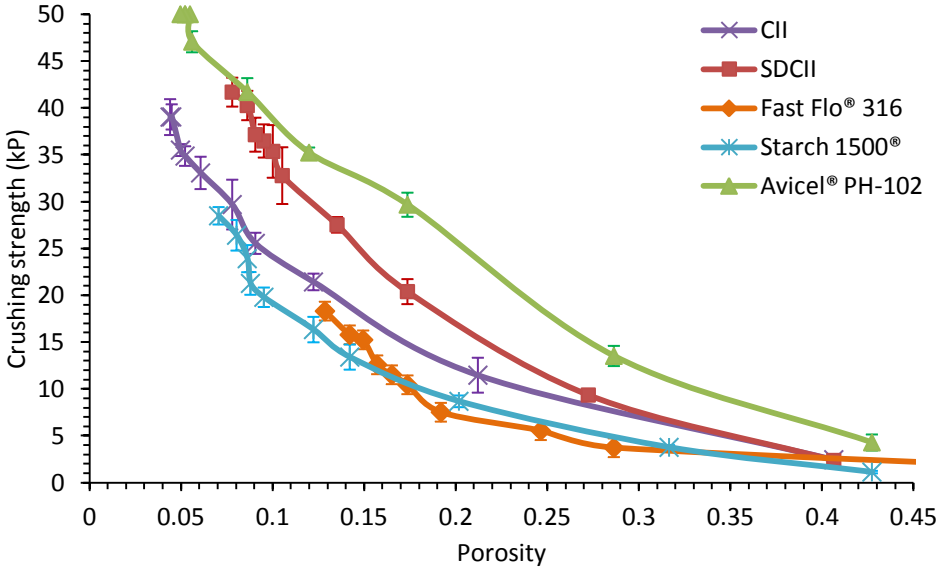

Figure IV-13. Crushing Strength of Carbohydrate Excipient Compacts: CII, SDCII, Fast Flow® 316 (lactose monohydrate), Starch 1500® (pregelatinized starch) and Avicel® PH-102 (microcrystalline cellulose I).

However, at < 0.3 porosity, SDCII compactibility differed from that of CII and increased steadily to form compacts of improved strength likely due to the formation of more binding sites. It should be pointed out that a high volume reduction ability of a material is not always associated to a high compactibility. For example, Avicel® PH-102 and CII had the largest densification with applied compression pressure. However, the compactibility of Avicel® PH-102 was much larger than that of CII due to the tight parallel arrangement of the chains. Overall, compactibility varied in the order: Avicel® PH-102 >> SDCII ≥ CII > Starch 1500® ≅ Fast Flo® 316.

Compacts prepared at 0.15 porosity were tested for friability. According to the USP (US Pharmacopoeia, 2005, page 2745), tablets should show no more than 1% loss in weight. This test is more rigorous than the crushing strength test since in the friability test compacts are submitted to mechanical stresses simulating wearing due to handling and mechanical shock. As seen in Figure IV-14, except for Fast Flo® 316, all materials met the USP requirement. Although CII is less compactable than Avicel® PH-102, both materials showed comparable friability results. Even though Starch 1500® and Fast Flo® 316 had comparable crushing strength results, friability values of the latter were higher due to its brittleness which makes particles detach from the compacts every time the compacts fall into the bottom of the drum. Conversely, the plastic deforming Starch 1500® does not suffer from much wear since particles deform in each cycle of the drum absorbing any mechanical shock.

The dilution potential of the materials was determined on compacts made at different weight ratios of the excipient and acetaminophen (a very poorly compactable drug) and their crushing strength was then measured (Figure IV-15).

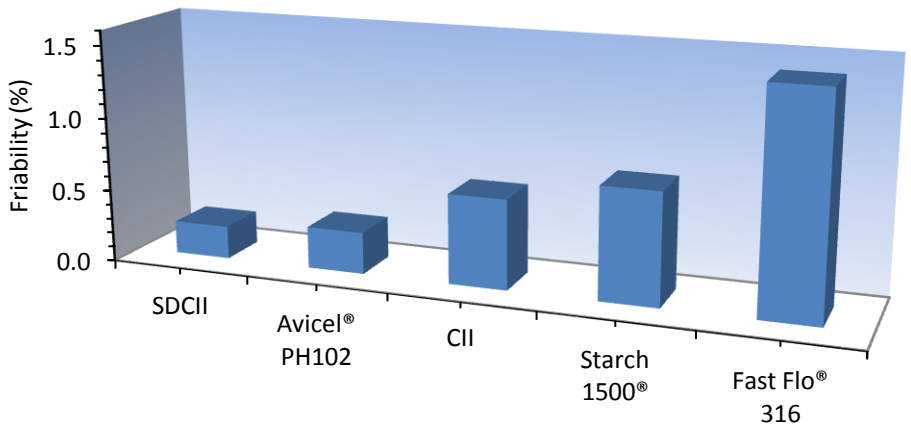

Figure IV-14. Friability of Carbohydrate Excipient Compacts: CII, SDCII, Fast Flow® 316 (lactose monohydrate), Starch 1500® (pregelatinized starch) and Avicel® PH-102 (microcrystalline cellulose I).

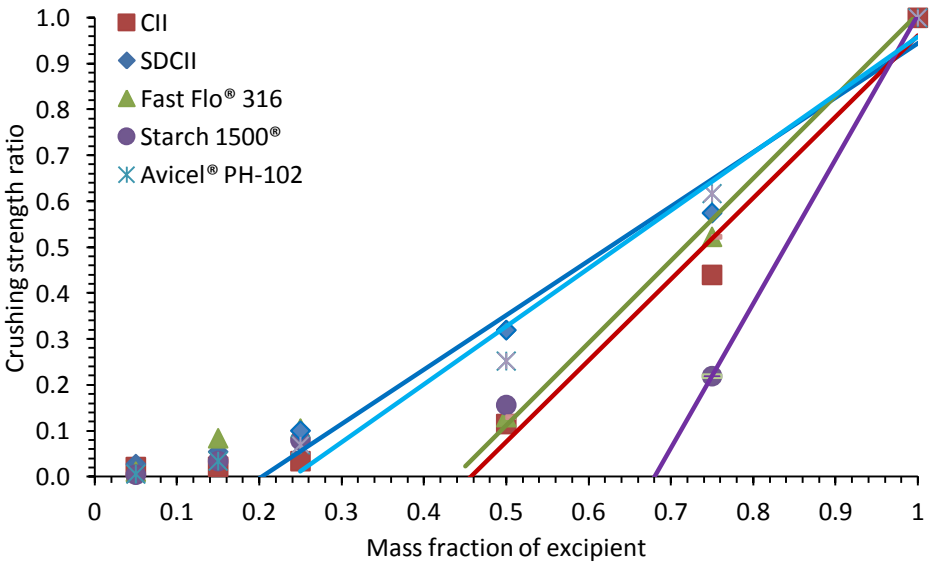

Figure IV-15. Dilution Potential of Carbohydrate Excipient Compacts: CII, SDCII, Fast Flow® 316 (lactose monohydrate), Starch 1500® (pregelatinized starch) and Avicel® PH-102 (microcrystalline cellulose I).

The normalized crushing strength ratio, which is the ratio of the crushing strength of the mixture to the crushing strength of the pure excipient was then plotted versus the mass fraction of the excipient. Lines were fit in the region where non-defective compacts were formed. The intercept of the lines with the x-axis represents the experimental dilution potential of these materials (Habib et al., 1996). This number represents the minimum amount of excipient which is needed to form non-friable compacts. The dilution potential of SDCII was comparable to that of Avicel® PH-102 (0.2 and 0.24, respectively). For CII and Fast Flo® 316, the dilution potential was also comparable (0.46 and 0.44, respectively).

These results suggest that SDCII and Avicel® PH-102 serve as the most effective binders to produce tablets by direct compression formulated with poorly compressible drugs. For this reason, the formations of densified and oblong particles by spray drying eased flow and probably, enabled the formation of more contact points with the elongated and needle-shaped acetaminophen particles. As a result, it formed compacts of comparable strength to those of Avicel® PH-102. Although CII showed the highest compressibility among the carbohydrate excipients (Table IV-11), it presented a low dilution potential. For this reason, the fibrous character of CII and the needle-shaped and the brittle deforming acetaminophen (Billon et al., 1999) particles might have prevented the formation of sufficient contact points needed for the formation of strong compacts.

Lubricant Sensitivity

The lubricant sensitivity of the excipients was tested with magnesium stearate at 0.5, 1.0 and 2.0% w/w concentrations. Lubricant sensitivity was measured by taking the ratio of compact crushing strength decrease due to lubricant with respect to that of unlubricated compact. Magnesium stearate is commonly used in tablet formulations to reduce friction between materials and machine tooling. The results presented in

Figure IV-16 show the following rank order in terms of an excipient's sensitivity towards magnesium stearate: Starch 1500® > Avicel® PH-102 > CII > SDCII > Fast Flo® 316.

These results suggest that more regularly-shaped and plastically deforming materials are more sensitive to magnesium stearate than the apparent less ductile materials. Starch 1500® was more sensitive than Avicel® PH-102 possibly due to more complete lubricant coating on Starch 1500®'s regularly-shaped particle surface. It is possible that for highly irregular and poorly flowing powders such as Avicel® PH-102, the lubricant is trapped inside the cavities of the particles and thus, had less effect on strength. Other authors have also found Starch 1500® as more sensitive to magnesium stearate than Avicel PH-102 and lactose (Fast Flo® 316) (Bos et al., 1992). The effect of water in Starch 1500® is considered small since these lubricant sensitivity measurements were conducted on the same material containing a fix amount of water, and thus the level of water of the lubricated and unlubricated material was constant. Fast Flo® 316 was apparently the least ductile material, and thus, the negative effect of magnesium stearate on crushing strength is negligible since new surfaces, free of magnesium stearate, are formed constantly during compaction as reported previously for lactose (Vromans and Lerk, 1988; Bolhuis and Zuurman, 1995). On the other hand, in highly ductile materials, is possible that magnesium stearate coated the particle surfaces and thereby, restricted contact between particles resulting in compacts of lower strength. Since CII and SDCII showed comparable P_y values, but SDCII presented a lower lubricant sensitivity, its higher specific surface area (1.6 vs. 0.5 m^2/g; for SDCII and CII, respectively) might be responsible for this finding.

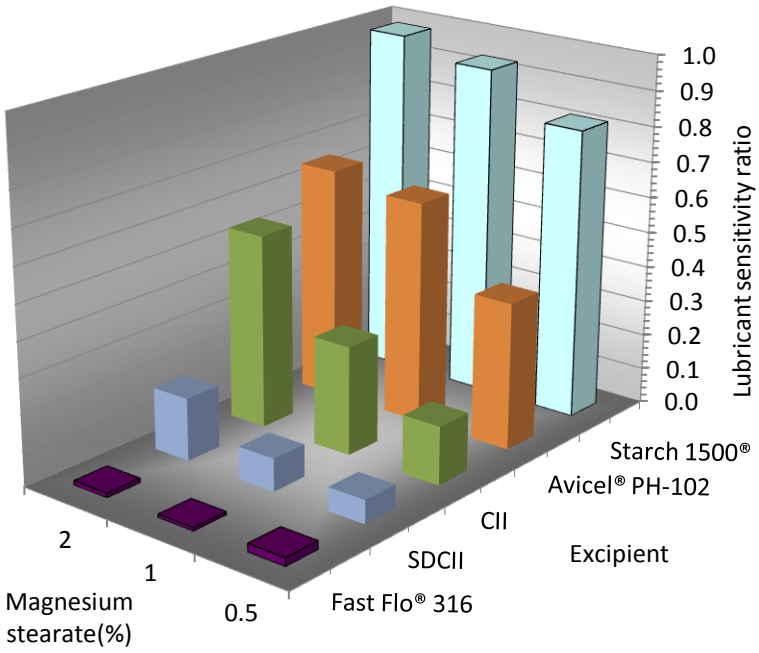

Figure IV-16. Sensitivity of Carbohydrate Excipient Compacts to Magnesium Stearate: CII, SDCII, Fast Flow® 316 (lactose monohydrate), Starch 1500® (pregelatinized starch) and Avicel® PH-102 (microcrystalline cellulose I).

Compact Disintegration

The relationship between compact porosity and disintegration time is illustrated in Figure IV-17. The disintegration time of SDCII and CII was comparable and fast (<11 sec) at >0.1 porosities. At < 0.1 porosity, SDCII showed longer disintegration times due to the formation of stronger compacts. These materials also had the lowest critical compact porosity indicating that disintegration time was virtually independent of compression pressure. Therefore, spray drying did not vary the fast disintegration properties of CII.

Starch 1500® compacts took ~1,000 sec to disintegrate due to the slow swelling and compact gelification which hindered dissolution of the polymer into the medium. The slow compact disintegration of Fast Flo® 316 was due to its slow dissolution, which was more evident at < 0.25 porosity. For cellulose I (Avicel® PH-102), the disintegration time of compacts increased sharply with decreasing porosities (< 0.12 porosity or up to 90 MPa); beyond 90 MPa compacts remained intact for the duration of the test (~5 h). In this case, its high binding properties counteract the disintegration ability. Summarizing, disintegration times for CII and SDCII were characterized by a steady change followed by a sharp increase (up to 100 sec) at a compact porosity below 0.1. Disintegration times of starch compacts were virtually independent of compact porosity, whereas for Avicel® PH-102 and Fast Flo® 316 increased especially at porosity < 0.25. Disintegration times were dependent on material compactibility, especially for Avicel® PH-102.

In conclusion, results indicate that physical modifications of CII particles through spray drying produced a material (SDCII) with transformed functional properties that can be summarized as follows:

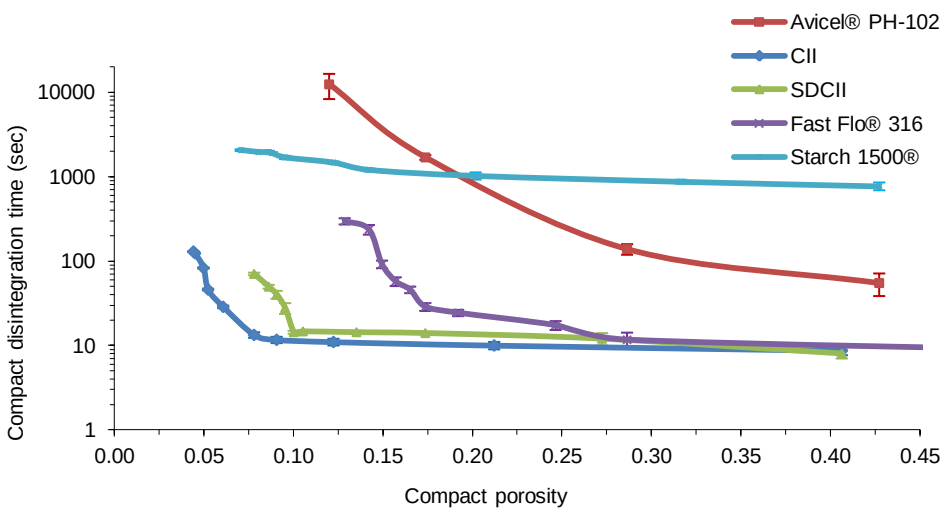

Figure IV-17. Disintegration Profiles of Carbohydrate Excipient Compacts: CII, SDCII, Fast Flow® 316 (lactose monohydrate), Starch 1500® (pregelatinized starch) and Avicel® PH-102 (microcrystalline cellulose I).

- Small particle size (~52 µm) and slightly low crystallinity (~62%);
- Increased flow (~16 g/sec) and powder densification due to a more regularly-shaped particles;
- No change in consolidation mechanism as indicated by its comparable P_y values (~116 MPa) with the parent material (CII);
- A low powder densification ability (D_a of 0.71);
- A better ability to form strong compacts than CII;
- Better mechanical properties as shown by the dilution potential (~20%), low friability (~0.3) and low lubricant sensitivity (~0.15);
- Comparable disintegration times (~10 sec).

All the above properties show that a physical processing such as spray drying was able to improve powder and tableting properties of CII, resulting in material (SDCII) with better functionality as a direct compression excipient. The following section will deal with the evaluation of disintegration properties of SDCII and the assessment of other processes such as wet granulation and spheronization through silicification and their impact on the powder and tableting properties of CII.

Evaluation of Disintegration Properties of CII, SDCII and Commercial Disintegrants

Disintegrants are agents that promote disintegration of tablets into primary particles when placed in an aqueous environment. The proper choice and amount of a disintegrant in a formulation is important, especially for poorly soluble drugs, as the tablet disintegration could be a limiting factor determining drug availability for dissolution and, subsequently, absorption, following peroral administration (Kottke and Rhudic, 2002; Shangraw et al., 1979).

Traditionally, sodium carboxymethyl cellulose and starch have been used as disintegrants. In the 1980s, new disintegrants, based on cross-linked sodium carboxymethyl cellulose (Ac-Di-Sol®), sodium starch glycolate (Primojel®) and poly(vinyl pyrrolidone) (Polyplasdone® XL), became commercially available. These agents, commonly called, "superdisintegrants," trigger compact disintegration within few seconds of coming in contact with an aqueous environment and, hence, are ideally suited to develop compressed dosage forms intended to deliver and rapidly release drug in the mouth or upper gastrointestinal (GI) tract (Mishra et al., 2006). A chemical modification has been the most efficient way to change disintegration properties of the materials. For example, crosslinking by carboxymethylating potato starch produced a sodium starch glycolate with better disintegrant/swelling properties due to the incorporation of the carboxyl moiety, especially in the amylase fraction which is responsible for the disintegration properties of starch. For starch alone, rapid disintegration is achieved at concentrations between 10 to 15% in a formulation (Banker and Rhodes, 2002). Likewise, the incorporation of the carboxyl moiety in sodium carboxymethyl cellulose (Ac-Di-Sol®) resulted in a faster disintegration than its parent material.

The mechanisms by which these superdisintegrants infuse water uptake are through wicking, heat of wetting, shape deformation, swelling, and/or particle repulsion (Bhargava et al., 1991; Massimo et al., 2000; Zhao and Augsburger, 2005). Repulsion results from the weakening of interaction forces between particles due to the building up of hydrostatic pressure as result of water uptake (Gordon et al., 1984). Of the above mechanisms, water penetration through wicking and swelling is the main disintegration mechanism for disintegrants (Chen et al., 1998).

Several factors have been reported that affect the performance of these super-disintegrants. For example, the use of lubricants, such as magnesium stearate, adds hydrophobicity, and as a result delays disintegration of tablets (Fukami et al., 2006; Plaizier-vercammen and Van den Bossche, 1992). Studies show that the same superdisintegrant from different vendors causes a different disintegration performance (Bolhuis et al., 1994; Ferrari et al., 1996; Zhao and Augsburger, 2005; Zhao and Augsburger, 2006).

In this section, the disintegration property of cellulose II excipients, such as SDCII and unprocessed cellulose II (CII) was investigated in comparison to commercial disintegrants, namely, sodium croscarmellose (Ac-Di-Sol®), sodium starch glycolate (Primojel®) and Crospovidone, NF (Polyplasdone® XL).

Powder Properties

Figures IV- 18 shows the chemical structures of cellulose II powders and the commercial disintegrants, whereas Figure IV-19 depicts the corresponding powder X-ray diffractograms. As reported in the previous section, SDCII and CII display peaks at 12, 20, and 22^{o} 2θ due to the cellulose-II lattice (1 $\bar{1}$ 0, 110 and 200 reflections, respectively). Ac-Di-Sol® and Polyplasdone® XL show no sharp peaks indicating a low crystallinity in these materials.

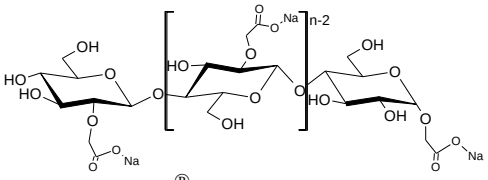

Ac-Di-Sol® (sodium carboxymethyl cellulose)

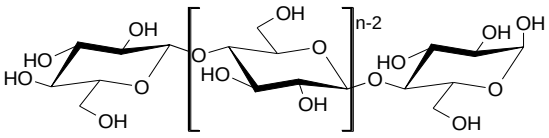

Cellulose II (SDCII and CII)

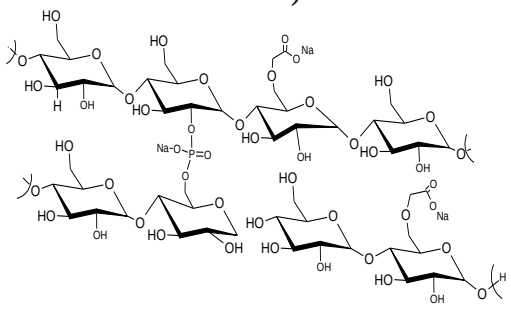

Primojel® (sodium starch glycolate)

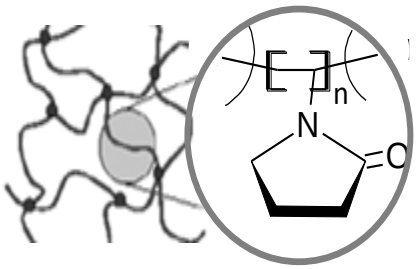

Polyplasdone® XL (crospovidone)

Figure IV-18. Chemical Structures of Disintegrants Made with ChemSketch v. 11.01 (Advanced Chemistry Development, Inc., Toronto, Canada).

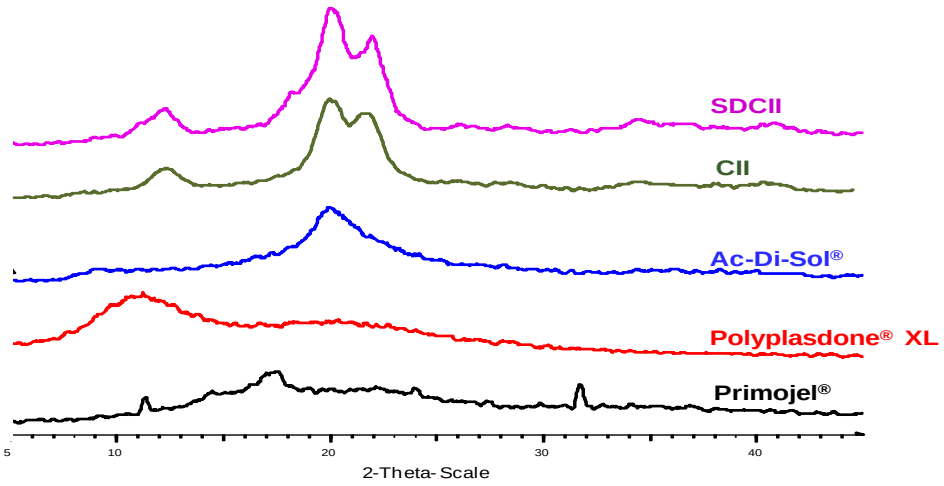

Figure IV-19. PXRD Characterization of Disintegrants: Ac-Di-Sol® (sodium carboxymethyl cellulose), Polyplasdone® XL (crospovidone), Primojel® (sodium starch glycolate).

Primojel®, on the other hand, shows a diffuse halo with small peaks at 11.5, 14, 17.5, 24 and 31.8° 2θ due to the crystalline sodium salt in its structure (Chowdary and Srinivasa, 2000; Edge et al., 2002a; Sindhu et al., 2006). The major amorphous content, as in the case of Primojel® partially accounts for their high affinity for water and swelling (Young et al., 2005). For this reason, it has been reported a degree of crystallinity of only 24% for Primojel® due to its high amorphous content (Young et al., 2005). Except for SDCII and CII, superdisintegrants such as Ac-Di-Sol®, Primojel® and Polyplasdone® XL presented a degree of crystallinity less than 45%, indicating that for these commercial materials, a high amorphous content is associated to a good water affinity (Table IV-12).

Figure IV-20 and Figure IV-21 depict particle morphology by SEM and Table IV-12 lists the selected powder properties. CII, SDCII and commercial disintegrants exhibited various shapes and particle sizes indicating that their disintegrant ability cannot be ascribed only to these two factors. Polyplasdone® XL contained porous and irregularly-shaped particles. Primojel® consisted of spherical and semi-spherical particles. Conversely, Ac-Di-Sol® is fibrous in shape with highly irregular (rough) surfaces containing protrusions and cavities. Polyplasdone® XL, Primojel® and Ac-Di-Sol® had particle sizes of ~94 µm, 30 µm and 31 µm, which are close to the reported values (110-140 µm, 40 µm, 34.5 µm, respectively) (Faroongsarng and Peck, 1991; ISP Corp., 2009; Bi et al., 1999). The true density of cellulose II materials and Ac-Di-Sol® was comparable, indicating that the packing arrangement of the cellulose chains was not affected by spray drying or crosslinking of carboxymethyl cellulose. Materials with a low true density such as Polyplasdone® XL and Primojel® also had a low degree of crystallinity indicating that the crystalline component of these polymers is responsible for the molecular packing of the chains.

Table IV-12. Powder Properties of CII, SDCII and Commercial Disintegrants.

	SDCII	CII	Polyplasdone® XL	Ac-Di-Sol®	Primojel®
$Dg_{\pm}$ SE[a] (µm)	52.5 ± 3.0	89.1 ± 5.0	93.9 ± 8.9	30.9 ± 3.0	29.9 ± 2.8
Moisture content (%)[b]	4.1 ± 0.4	3.6 ± 0.4	4.9 0.1	6.4 ±	7.4 ± 0.6
Bulk density (g/cm^3)[b]	0.56 ± 0.01	0.38 ± 0.03	0.21 ± 0.00	0.46 ± 0.00	0.8 ± 0.01
Tap density (g/cm^3)[b]	0.80 ± 0.01	0.54 ± 0.06	0.28 ± 0.00	0.66 ± 0.01	1.03 ± 00
True density (g/cm^3)[c]	1.55	1.54	1.16	1.57	1.50
Degree of crystallinity (%)[c]	62	68	25	45	12
Porosity (%)[c]	64.0	75.5	81.8	70.6	47.0
Water sorption ratio[a]	2.3 ± 0.5	1.6 ± 0.1	4.8 ± 0.1	6.6 ± 0.5	10.4 ± 0.3
Compact volume Increase[c]	2.9 ± 0.5	2.6 ± 0.1	8.1 ± 1.8	8.8 ± 0.5	13.5 ± 2.9

[a] SE= Standard error determined as $\frac{\sigma}{\sqrt{n}}$

[b] n= 3.

[c] n= 1.

[d] Crospovidone.

[e] Sodium carboxymethyl cellulose.

[f] Sodium starch glycolate.

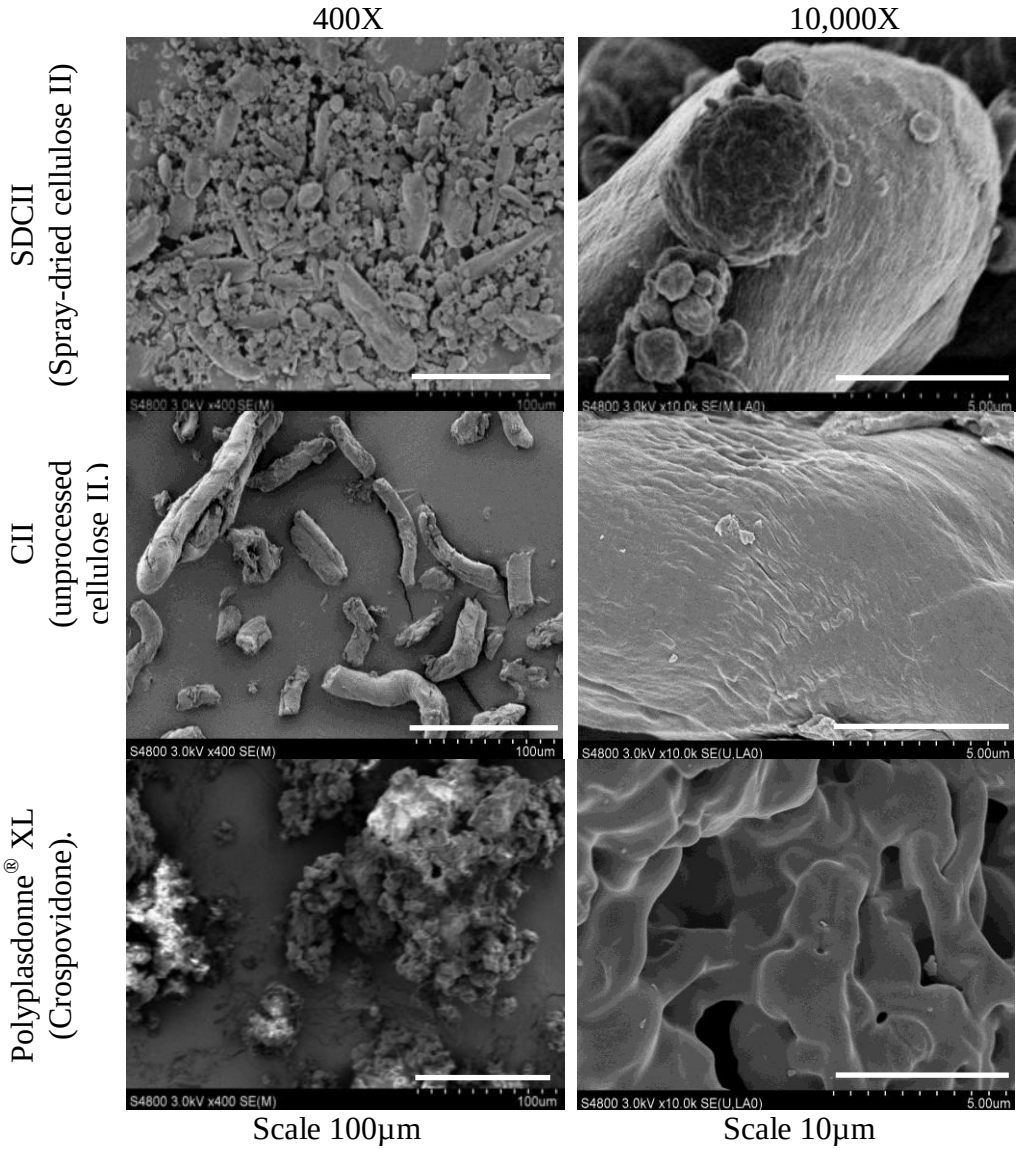

Figure IV-20.SEM Images of Water Wicking Disintegrants: at 400X and 10,000X Magnifications.

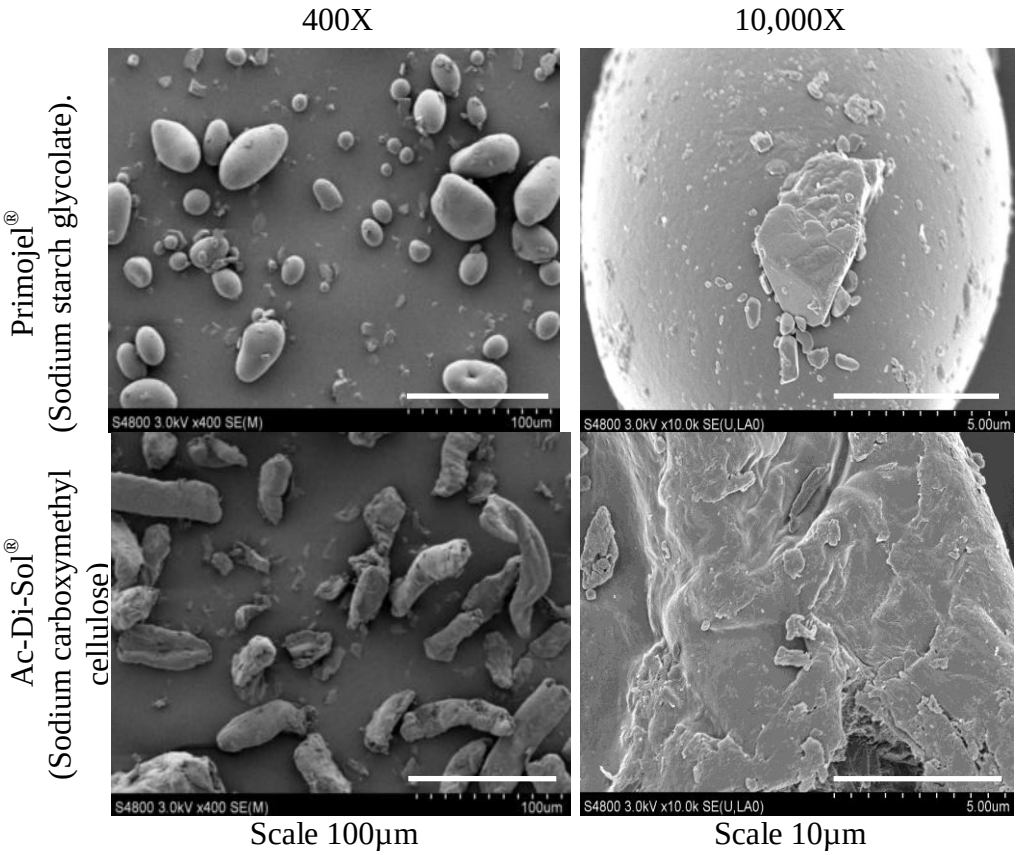

Figure IV-21 SEM Images of Swelling Disintegrants at 400X and 10,000X Magnifications.

Bulk and tap densities depended mainly on particle shape and surface smoothness. In this case, Primojel®, composed of the smoothest and the most spherical material and Polyplasdone® XL, with the most irregular and rough surface, resulted in the largest and smallest values, respectively. Reported bulk densities for Primojel®, Ac-Di-Sol® and Polyplasdone® XL are: 0.76 g/cm^3, 0.46 g/cm^3 and 0.28 g/cm^3, respectively (Quadir and Kolter, 2006). Since the moisture content of these materials was low, its contribution in particle density is assumed to be negligible compared to its ability to take up water.

The swelling values determined as a function of time for each disintegrant are shown in Figure IV-22. The swelling value describes the ability of the powder to increase in size/volume due to water uptake by their particles. Primojel® showed the highest swelling with Ac-Di-Sol® being next (swelling values: 16.7 mL/g and 12.8 mL/g, respectively). In comparison, CII, SDCII and Polyplasdone® XL showed substantially less swelling (0.3 mL/g, 1.0 mL/g and 1.7 mL/g, respectively). The time to peak is interpreted as the time needed to reach a maximum water saturation of the particles pores while absorbing water. In this case, the largest values were observed for highly swelling materials, especially Primojel® (10.5 min), and the lowest values were observed for capillary-driven materials (~5 min). In the first case, water is absorbed in the particle pores to the interior and in this process water migration causes the polymer chains to expand creating more space among them. As water is migrating between the chains, a three dimensional network is created in which water is retained. The time to peak is reached once there are sufficient number of polymer chains with inter-and intramolecular hydrogen bonding available for binding liquid water.

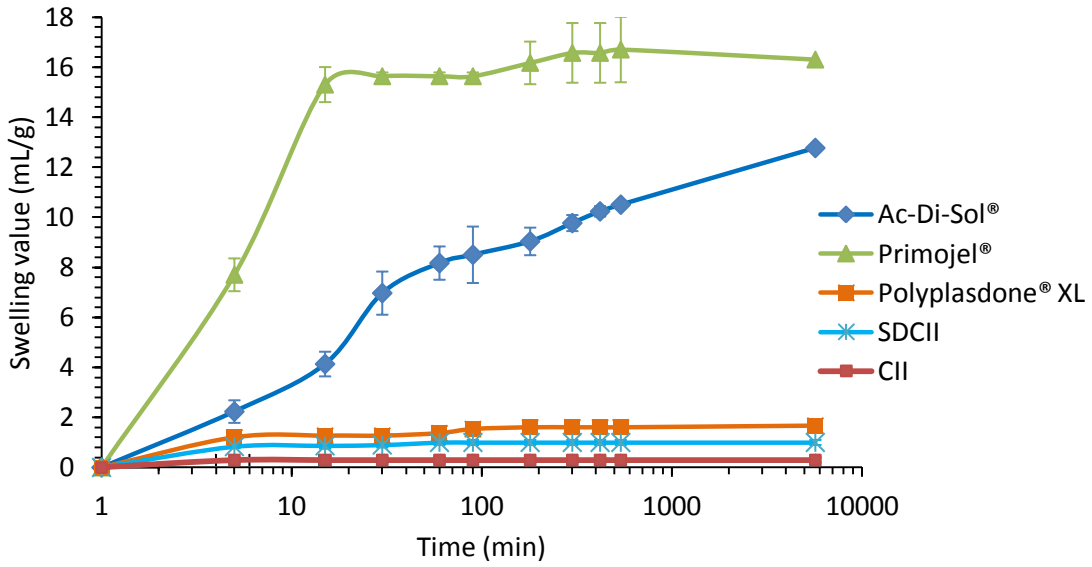

Figure IV-22. Swelling values of SDCII, CII and Commercial Disintegrants: Ac-Di-Sol® (sodium carboxymethyl cellulose), Primojel® (sodium starch glycolate), and Polyplasdone® XL (crospovidone).

On the contrary, for capillary-driven materials, water uptake begins through the particle pores followed by migration into the interior of the capillaries. In this case, particle expansion is negligible since capillaries and particles experienced a minor disruption attributable to particle swelling. The time to peak (~5 min) in these materials was shorter than that showed by swelling materials since they did not form a viscous halo upon water uptake. Ac-Di-Sol® which was a highly swelling material did not show a clear time to peak for the test period (~7 days), but rather showed an initial fast swelling followed by a slow increase. The higher crystallinity and the linear rather than branching conformation of the chains might be responsible for the biphasic swelling. This could be explained by a fast swelling of the amorphous regions followed by a slow swelling due to the slow penetration into the less accessible crystalline regions. It has been reported that the larger Primojel® swelling compared to Ac-Di-Sol is due to its ability to carry out a 3-dimentional swelling, whereas, Ac-Di-Sol® is only able to swell in two dimensions causing almost no change in the fiber length (Troy and Hauber, 2005).

Figure IV-23 shows the water uptake values of the particles upon the addition of 10 mL of water. Primojel®, Ac-Di-Sol®, CII and SDCII took about 60-70 sec to attain maximum uptake, while Polyplasdone® XL required only 40 sec. Beyond these times, unretained excess water by the powder drained off. Alternately, most swelling materials retained a larger amount of water. The amount of water uptake was more prominent for highly swelling materials, whereas capillary-driven materials exhibited lower values.

In order to measure the water uptake rate, the slope of the linear region of the curve during the first 30 seconds was measured. The rate was faster in swelling materials (~0.30 mL/sec) and slower for essentially water wicking materials such as SDCII (0.20 mL/sec) and CII (0.18 mL/sec).

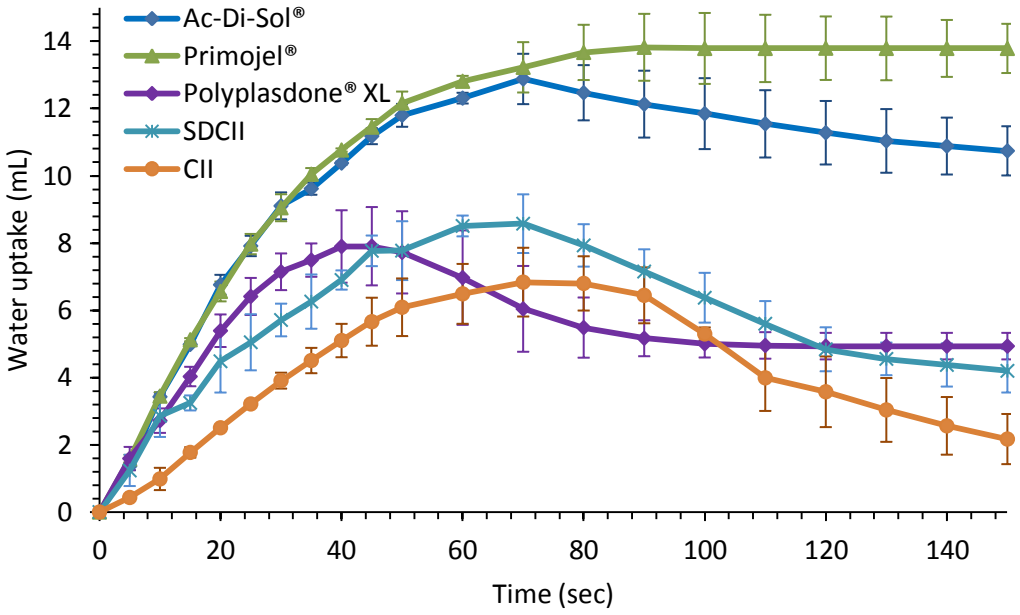

Figure IV-23. Water Uptake of SDCII, CII and Commercial Disintegrants: Ac-Di-Sol® (sodium carboxymethyl cellulose), Primojel® (sodium starch glycolate), and Polyplasdone® XL (crospovidone).

The fast water uptake and high swelling of Primojel® and Ac-Di-Sol® is attributed to the presence of carboxylic moiety and their ability to quickly hydrate and produce gels upon water uptake. The slightly higher water uptake rate of SDCII compared to MCCII could be ascribed to the smaller particle size and higher amorphous content which eased water accessibility.

Polyplasdone® XL showed a moderate water uptake rate, probably due to its own cross-linked nature causing entanglement of the polymer chains making it water insoluble with the ability to take up water quickly without considerable swelling (Quadir and Kolter, 2006).

High powder porosity or low crystallinity were not the only requirements for a rapid water uptake since Primojel® and Ac-Di-Sol® had low and high porosity and crystallinity, respectively and exhibited approximately the same uptake rates (~0.3 mL/sec). Further, CII and SDCII had high porosity values (~76% and 64%, respectively), but had about the same low water uptake rate (~0.2 mL/sec). For this reason, the difference observed in water uptake was mainly attributed to the disintegrant's chemical natures, rather than to their physical properties such as particle size, porosity, crystallinity and packing ability.

Although CII and SDCII had different particle sizes and morphology (fibrous vs. oblong, respectively), crystallinity and porosity, they appear to have the same water uptake mechanism. This behavior is characterized by very low swelling but high water wicking, indicating that the fast intrinsic disintegration property of cellulose II is almost independent of the particle size, crystallinity, shape and packing tendency of the powder.

Table IV-12 shows the water sorption ratio and compact volume expansion after soaking in 10 mL of water. In this case, CII and SDCII showed the lowest values, whereas Ac-Di-Sol® and Primojel® showed the highest volume expansion and weight

increase. The rank order in compact volume increase and water sorption ratio was: Primojel® (13.5 and 10.4) >Ac-Di-Sol® (8.8 and 6.6) ≅ Polyplasdone® XL (8.1 and 4.8) > CII (2.6 and 1.6) ≅ SDCII (2.9 and 2.3). Since this test was conducted on a compact resting on a wet surface, compact water migration occurred from its base to the top causing axial expansion due to water disruption of the particles and a minor radial growth. Highly swelling materials formed the largest water sorption ratios and volume increase. Polyplasdone® XL expanded significantly in the compact forming a highly porous sponge-like structure as a result of water interaction and disruption of its polymeric chains. Further, this material also showed the highest porosity (~82%) providing void space for a substantial water penetration inside the compact matrix. Conversely, compacts of SDCII and CII cracked when put in contact with water and showed minimal volume expansion.

In order to compare the functional property of these materials, the ratio of compact disintegration time to its crushing strength (DT/CS) was used. In theory, if the ratio is low, the material works very well as disintegrant and vice versa. An arbitrary maximum ratio of 5 sec/kP was selected for a material having a fast disintegration property. The change in DT/CS ratio as a function of compact porosity is depicted in Figure IV-24. Independent of the compact porosity, capillary driven materials showed the lowest ratio, indicating that a rapid water uptake through the pores and capillaries is essential for a rapid particle deaggregation followed by a complete compact disintegration.

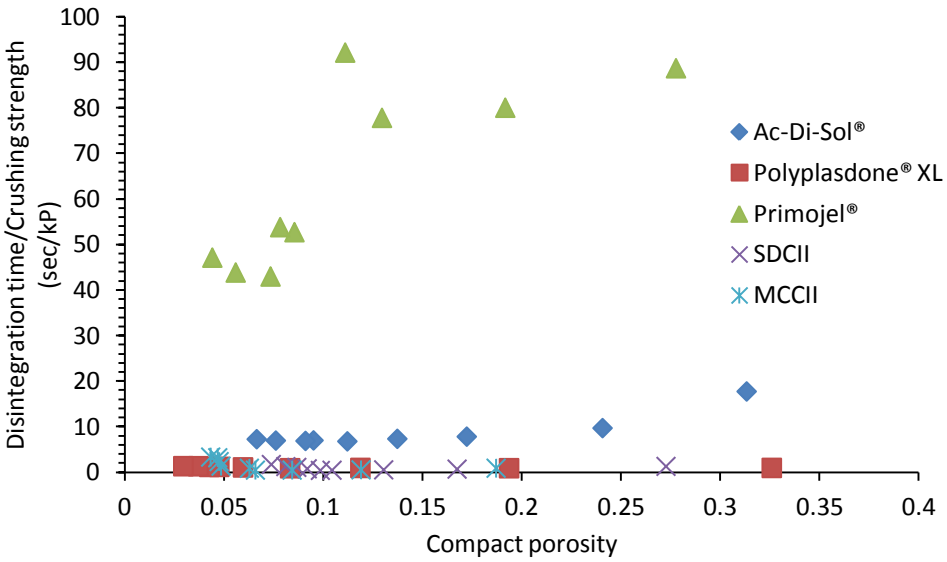

Figure IV-24. Disintegration Time/Crushing Strength Ratio as a Function of Compact Porosity of: CII, SDCII, Ac-Di-Sol® (sodium carboxyethyl cellulose), Primojel® (sodium starch glycolate), and Polyplasdone® XL (crospovidone).

Particle disintegration in capillary-driven materials occurs due to the rapid replacement of intermolecular hydrogen bonding and disruption of Van der Waals forces of the compacts with incoming water molecules. On the contrary, highly swelling materials such as Primojel® showed a DT/CS ratio > 40 sec/kP due to the very low compact strength. The high compact swelling produced upon contact with water causes a delay in disintegration time since the 3-dimentional gel produced is eroded and dissolved slowly in the aqueous medium. Ac-Di-Sol® had moderate DT/CS ratios due to its high disintegration time and crushing strength.

For water wicking materials, there was no correlation between interparticle bonding strength and disintegration time. For instance, a material can form compacts of high strength showing a low disintegration time as demonstrated by Polyplasdone® XL. However, for Primojel®, which was the largest swelling material, disintegration time was always large due to the formation of weak compacts independent of compact porosity. In Ac-Di-Sol®, a combination of high swelling (reflected by a slow disintegration time) and high compact strength rendered moderate DT/CS ratios.

Disintegration time and crushing strength varied among the disintegrants. Thus, SDCII (~15 sec), CII (~15 sec) and Polyplasdone® XL (36 sec) formed the fastest disintegrating compacts, whereas, Primojel® (~67 sec) and Ac-Di-Sol® (265 sec) were the slowest disintegrating compacts made at 0.2 porosity. Polyplasdone® XL and Ac-Di-Sol® formed the strongest compacts (41.4 kP and 35.4 kP, respectively), followed by SDCII and CII (14.8 kP, 11.5 kP, respectively). Primojel®, on the other hand, formed the weakest compacts (0.5 kP).

Crushing strength essentially measures the weakest bonds which break to form a compact crack. On the other hand, compact disintegration has to overcome all interparticle bonds (especially hydrogen bonding) resulting in individual powder particles deaggregation, especially for compacts made of water wicking materials (CII, SDCII and Polyplasdone® XL) by direct compression. Thus, it is likely that for these materials water penetration and bond breaking occur simultaneously.

Considering the water uptake rate, water sorption ratio and compact volume expansion for Primojel® and Ac-Di-Sol®, it appears that the faster disintegration observed for Primojel® can be attributed to its higher swelling propensity and the formation of weaker compacts. Ac-Di-Sol® and Primojel® compacts disintegrate via swelling and dissolution mechanisms. SDCII and CII showed fast water wicking and compact bursting. In the case of Polyplasdone® XL, it has been reported that fast disintegration is due to the combined effect of high powder porosity and irregular particle morphology which leads to a quick water wicking action and compact disintegration (Gonnissen, Remon, Vervaet, 2008).

Figure IV-25 shows the compact disintegration time in 0.1N HCl and distilled water. Acid media in 0.1N HCl was selected to simulate gastric pH conditions. Primojel® was the only disintegrant that showed a significant difference in both media (~92% decrease in acid medium). This difference could be ascribed to different swelling abilities in the two media. It has been reported that the strong decrease in swelling capacity of Primojel® is attributed to the conversion of the carboxymethyl sodium salt moiety to its free acid form in acidic media. This acid form is less hydrating and swelling than its salt form, and hence, the water holding capacity is reduced in acid medium (Zhao and Augsburger, 2005).

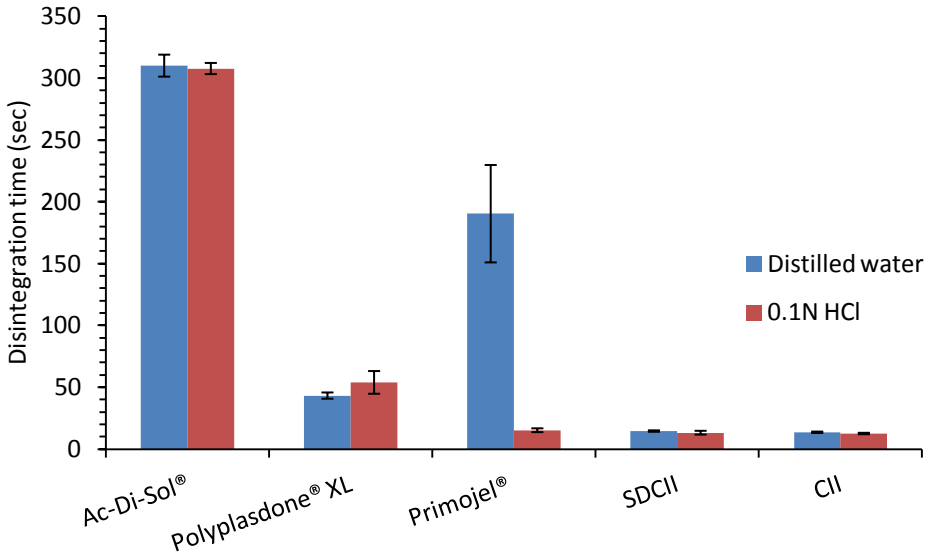

Figure IV-25. Disintegration Time of Compacts in Distilled Water and 0.1N HCl of: Ac-Di-Sol® (sodium carboxymethyl cellulose), Primojel® (sodium starch glycolate), and Polyplasdone® XL (crospovidone).

On the contrary, this effect was not observed for Ac-Di-Sol® which also has a carboxymethyl sodium moiety. This might be due to the linear nature of cellulose polymer chains and high crystallinity which limits water accessibility to these moieties.

For Primojel®, the highly swelling ability is also due to the amylopectin component of starch which is also responsible for water retention (Herman et al., 1989). It has been reported this material does not affect the medium viscosity in a pH range from 3 to 7. However, at pH >7, viscosity increases due to the reorientation or random coiling of the amylopectin component forming a viscous layer in contact with water delaying further water penetration (Mitrevej et al., 1996). On the contrary, no change in disintegration time was found for Polyplasdone® XL, SDCII and CII due to the absence of the carboxylic moiety.

In order to compare the performance of SDCII against commercial disintegrants, tablets of A-TAB®, mannitol, Fast Flo® 316, Avicel® PH-102 and Starch 1500® containing 0, 2.5, 5, 10 and 20% of the test disintegrant and 0.5% magnesium stearate were evaluated. The change in compact disintegration time as a function of disintegrant level is shown in Figure IV-26 and Figure IV-27 for cellulosic II materials and commercial disintegrants, respectively. In the absence of the disintegrant, compact disintegration varied as: Avicel® PH-102 (1902 sec) > Starch 1500® (510 sec) > mannitol (346 sec) > A-TAB® (344 sec) > Fast Flo® 316 (36 sec), respectively. Mannitol and Fast Flo® 316 compacts disintegrate by slow dissolution (Cheng et al., 1998), Avicel® PH-102 by fragmentation, A-TAB® mainly by erosion and Starch 1500® by swelling and erosion.

Except when Starch 1500® (a gel forming material) and Fast Flo® 316 (Fast dissolving material) are used as diluents, the addition from 2.5-5% of disintegrant caused a major decrease in disintegration time.

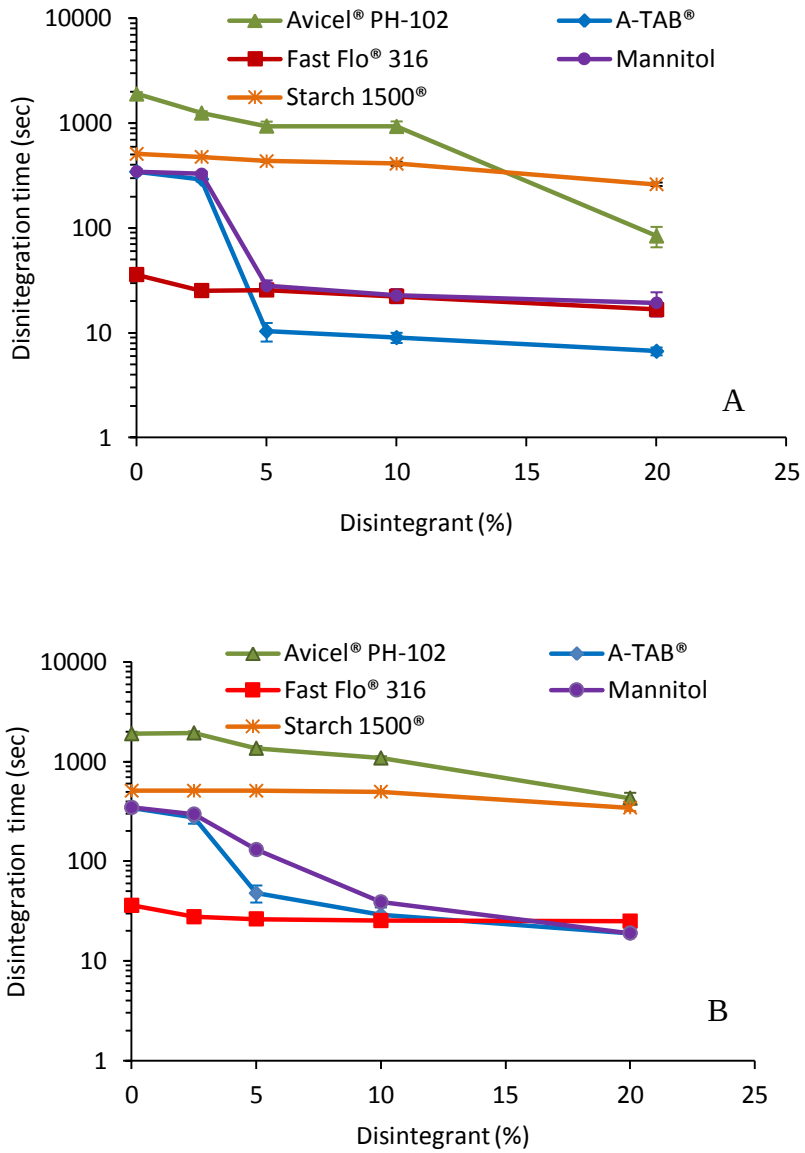

Figure IV-26. Disintegrant Level Effects on Disintegration Time of Direct Compression Excipients: (A) SDCII (spray-dried cellulose II) and (B) CII (unprocessed cellulose II).

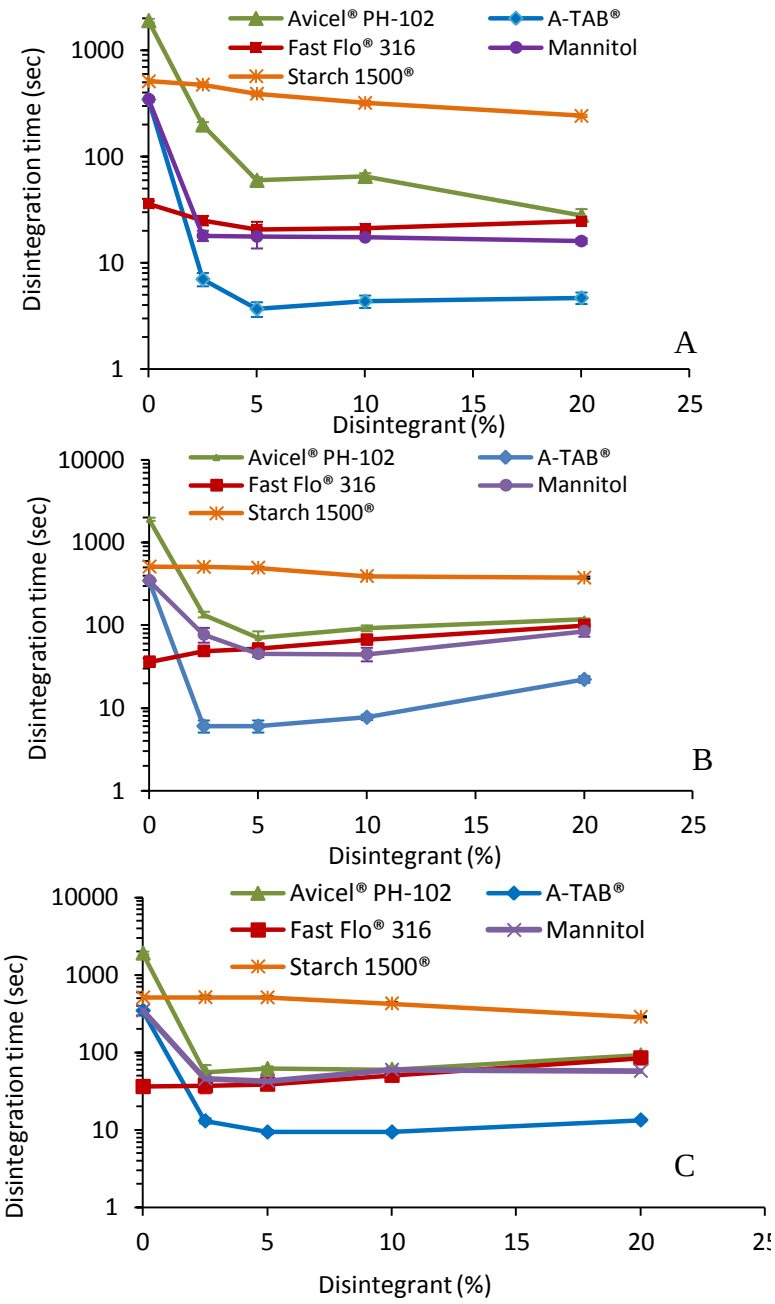

Figure IV-27. Disintegrant Level Effects on Disintegration Time of Direct Compression Excipients: (A) Polyplasdone® XL (crospovidone); (B) Ac-Di-Sol® (sodium carboxymethyl cellulose); and (C) Primojel® (sodium starch glycolate).

Further increase in the disintegrant level did not reduce disintegration times. On the contrary, for highly swelling materials such as Ac-Di-Sol® and Primojel®, levels higher than 5% delayed disintegration times, irrespective of the diluent employed. Similar findings have been reported previously (El-Barghouthi et al., 2008; Mattson, Bredenberg, Nystronm, 2001). This is explained by the formation of a viscous gel around the compacts due to water uptake retained in its tridimensional network hindering compact erosion/dissolution, as discussed previously.

Fast Flo® 316 *per se* showed fast disintegration, and a formulator might be inclined to not add a disintegrant. However, it is possible that combined with a drug and storage at a low relative humidity compacts harden causing a delay in disintegration.

Starch 1500® showed virtually no improvement when formulated with swelling disintegrants since these materials delayed compact disintegration. Disintegration time for this material is only reduced by half when formulated with ~20% of water wicking disintegrants.

The combination of an eroding/dissolving binder and a swelling disintegrant at levels from 2.5-5% caused sufficient swelling for an effective disintegration. However, capillary driven materials such as SDCII and CII were appropriate only for moderate binding materials, but not sufficient for highly binding diluents such as Avicel PH-102, since partial swelling is needed to possibly cause a hydrostatic pressure and hence, fast disintegration.

CII and SDCII were very effective as disintegrants at levels from 2.5 to 5% when formulated with slow eroding/dissolving diluents such as A-TAB® and mannitol, respectively.

Conversely, Polyplasdone® XL and swelling materials such as Primojel® and Ac-Di-Sol® were very effective when formulated with the above mentioned materials (A-TAB®, mannitol) and highly binding diluents such as Avicel® PH-102 at levels from 2.5 to 5%. In terms of the minimal disintegrant level required to reduce disintegration time, the best disintegrant that worked for strong non-soluble binders such as Avicel® PH-102 was Primojel®. In this case, only a 2.5% level was needed to cause a disintegration time of ~60 sec. For slowly eroding and fragmenting materials such as A-TAB®, either, Ac-Di-Sol®, Primojel® or Polyplasdone® XL worked fine at the 2.5% level.

As mentioned previously, for fast dissolving diluents such as Fast Flow® 316, a disintegrant might be needed if compacts upon storage harden. On the contrary, if highly swelling materials are employed, disintegration times are lengthened. For slow dissolving diluents such as mannitol, Polyplasdone® XL was the best disintegrant at the 2.5% level since it had a high water wicking action combined with a moderate swelling, easing dissolution. For highly swelling diluents such as Starch 1500®, water wicking agents such as SDCII and Polyplasdone® XL, and no swelling disintegrants are recommended at levels > 2.5%.

Water wicking materials which show low swelling abilities such as Polyplasdone® XL at levels < 5% are efficient in combination with the highly binding Avicel® PH-102. However, CII and SDCII, which are virtually non-swelling, require levels from 5-20%. This indicates that a partial swelling is also needed for bond disruption of highly binding diluents. Conversely, for highly swelling disintegrants such as Ac-Di-Sol® and Primojel®, increasing disintegrant levels from 5-20% led to a delay in disintegration times since the rapid water penetration and expansion is accompanied by compact gelling.

To further investigate the practical use of SDCII and CII as disintegrants, tablets containing Avicel® PH-102, ibuprofen, disintegrant and magnesium stearate at a 54.5:4 0.0:5.0:0.5, 49.5:40.0:10.0:0.5, 39.5:4 0.0:20.0:0.5, and 59.5:40.0: 0.0:0.5 weight ratios were made and their friability, crushing strength and disintegration time were determined (Table IV-13). All compacts showed a decrease in disintegration time with increasing levels of disintegrant except for Primojel® at a 20% level. As explained before, the gel formation caused a delay in compact disintegration. Since all compacts contained a good binder as diluent (Avicel® PH-102), their friability was below the maximum 1% limit set by the USP. Further, the SDCII and Polyplasdone® XL increase level from 10% to 20% caused a decrease in friability due to the contribution of the good binding properties of these materials on the overall compact strength. Friability values of SDCII were better than those of CII since the former performed as a better binder in mixtures with drugs, probably due to formation of better contact points in the particles. On the contrary, poorly compactable disintegrants such as Primojel® caused an increase in friability.

Figure IV-28 compares the release profiles of ibuprofen tablets. It is important to guarantee a fast drug release, especially for low-water soluble drugs such as ibuprofen since this step could predict a rapid drug load in the stomach or duodenum available for absorption. All tablets containing disintegrant met the USP requirement of releasing at least 80% of the drug within 60 min and some disintegrants showed a faster ibuprofen release than Advil® compacts. The amount of drug released after 5 min can be used to compare the disintegrant efficacy. Thus, at the 5% disintegrant level, Ac-Di-Sol® provided the fastest release, followed by Primojel® and Polyplasdone® XL and SDCII in equal magnitude

Table IV-13. Disintegrant Effects on Properties of Ibuprofen Compacts.

Compact Composition	Disintegrant	Friability (%)	Crushing strength (kP)	Disintegration Time (sec)
Avicel® PH-102 Ibuprofen Magnesium stearate (59.5:40.0:0.5)	None	0.49	20.9 ± 1.3	520.5 ± 33.6
Avicel® PH-102	SDCII	0.39	20.2 ± 0.7	519.8 ± 15.8
Ibuprofen	CII	0.42	16.0 ± 0.3	456.3 ± 3.2
Disintegrant	Ac-Di-Sol®*	0.40	21.0 ± 0.8	135.5 ± 8.3
Magnesium stearate	Polyplasdone® XL*	0.46	19.9 ± 1.1	342.3 ± 11.8
(54.5:40.0:5.0:0.5)	Primojel®*	0.39	19.6 ± 0.9	105.8 ± 23.2
Avicel® PH-102	SDCII	0.29	19.3 ± 0.9	450.3 ± 134.1
Ibuprofen	CII	0.45	16.6 ± 0.2	396.8 ± 25.1
Disintegrant	Ac-Di-Sol®*	0.32	21.2 ± 1.0	106.3 ± 12.5
Magnesium stearate	Polyplasdone® XL*	0.45	19.2 ± 0.6	275.3 ± 54.2
(49.5:40.0:10.0:0.5)	Primojel®*	0.36	17.5 ± 0.8	59.3 ± 3.4
Avicel® PH-102	SDCII	0.19	19.4 ± 1.1	8.0 ± 0.8
Ibuprofen	CII	0.55	16.7 ± 0.2	166.0 ± 17.1
Disintegrant	Ac-Di-Sol®*	0.33	20.9 ± 1.0	89 ± 3.4
Magnesium stearate	Polyplasdone® XL*	0.22	18.9 ± 1.1	8.3 ± 1.0
(39.5:40.0:20.0:0.5)	Primojel®*	0.50	15.9 ± 0.5	90.8 ± 4.6

[a] SDCII (spray-dried cellulose II).

[b] CII (unprocessed cellulose II).

* Commercial disintegrants: Polyplasdone®XL (crospovidone), Ac-Di-Sol® (sodium carboxymethyl cellulose), Primojel® (sodium starch glycolate).

In the release profiles containing a 10% disintegrant level, Polyplasdone® XL and Ac-Di-Sol® showed the fastest release followed closely by Primojel®. Further, at the 20% disintegrant level, Polyplasdone® XL and Primojel® were comparable and the fastest, followed by SDCII. Further, compacts without disintegrant released the drug slowly, but still met the USP criteria of releasing at least 80% of the drug within 60 minutes. Since water solubility of ibuprofen is very low (<1mg/mL) and was formulated with a strong binder, it is important to select at least a low level of a swelling disintegrant for a rapid compact disintegration and hence, compact release.

These results indicate that at < 5% levels, swelling disintegrants caused the fastest disintegration and hence ibuprofen release. However at > 10% disintegrant the capillary-driven Polyplasdone® XL material was the fastest; whereas at a 20% level highly swelling and capillary materials had comparable contribution releasing ~80% drug within 5 min.

Disintegration times cannot always be used to predict which disintegrant will work effectively for drug release due to differences with the physicochemical properties of such drugs. The above results indicate that SDCII and CII work better as disintegrant at levels ≥ than 10%. This is comparable to that of traditional disintegrants, such as starches, when used in wet granulation (Pourkavoos and Peck, 1994).

In contrast, superdisintegrants worked more effectively at low concentrations (2.5-5%). Such a low concentration was sufficient for an effective ibuprofen release. In some studies, superdisintegrants have been used at concentrations as high as 10%, although it is not advisable due to the high cost involved during the production process (Bhargava et al., 1991; Sekar and Chellan, 2008).

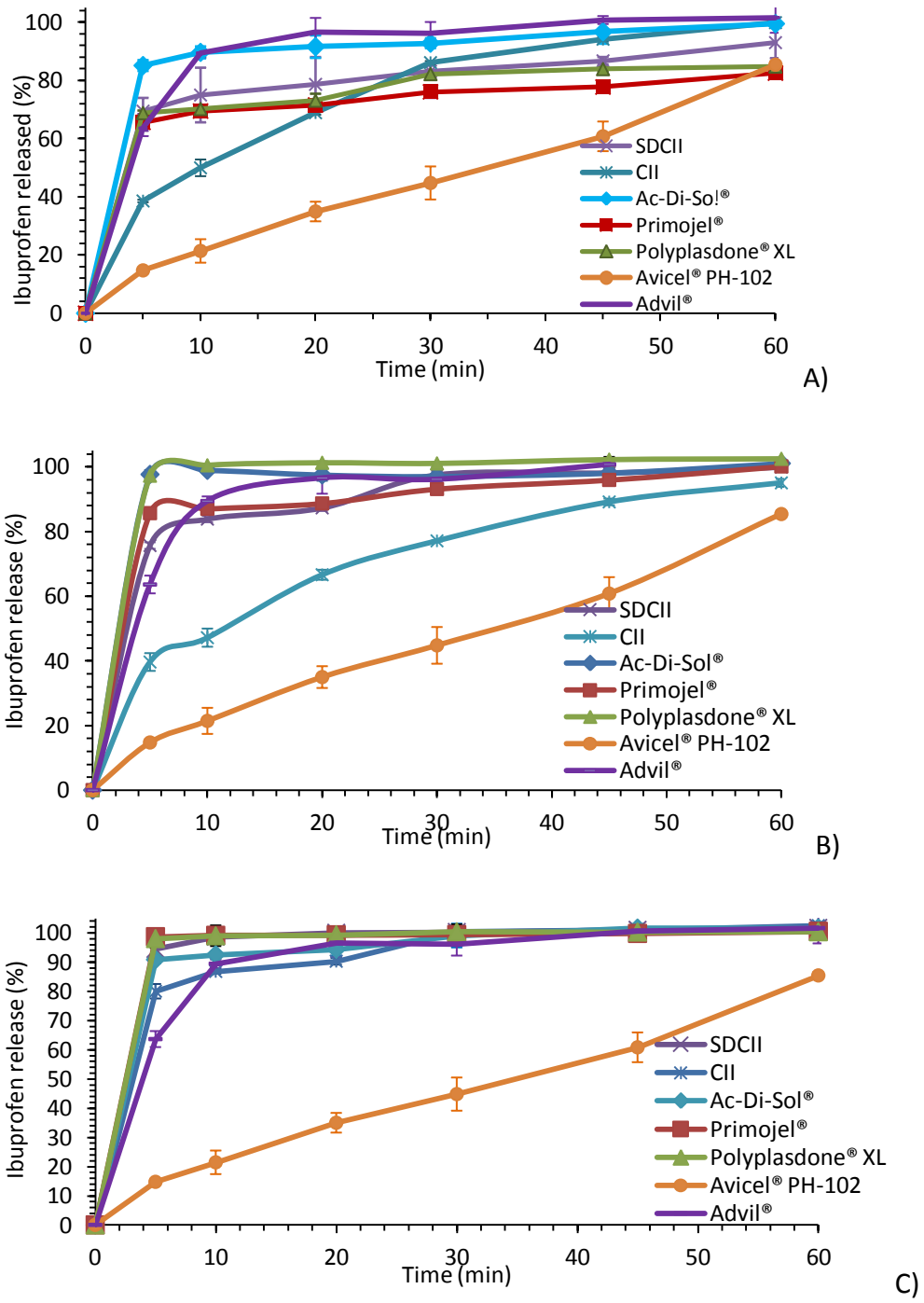

Figure IV-28. Effect of Disintegrant Levels on Ibuprofen Release Profiles: (A) 5%; (B) 10%; (C) 20% of: Ac-Di-Sol® (sodium carboxymethyl cellulose), Primojel® (sodium starch glycolate), Polyplasdone® XL (crospovidone).

In conclusion, the most important aspects of the disintegrants studied can be summarized as follows:

- Primojel® and Ac-Di-Sol® had very high swelling values, which were responsible for their large compact volume increase and water sorption ratios. A high swelling also led to a rapid water uptake;
- SDCII and CII were the best capillary driven materials, whereas Polyplasdone® XL showed a moderate capillary and low swelling mechanism;
- The ideal disintegrants showed a disintegration time/crushing strength ratio <5 sec/kP and corresponded to mainly capillary-driven materials such as SDCII, CII and Polyplasdone® XL;
- Highly soluble (i.e., lactose and mannitol) or swelling (i.e., starch) diluents are not advisable to use in a formulation with highly swelling disintegrants. Further, very good binding diluents such as Avicel® PH-102 are suitable to formulate with moderate swelling disintegrants at levels ≤ 5%.

CII-SiO_2 Composites

Preparation and Characterization

This section discusses the effects of silicification and processing on the particle and tableting properties of CII. Aqueous CII-SiO_2 dispersions, made by suspending CII and SiO_2, in different weight ratios in water and passing through a colloid mill or by subjecting to homogenization using a hand-held homogenizer, were processed by spray drying, wet granulation and spheronization.

Physical blending of CII and SiO_2 were first attempted to produce the co-processed materials. Initially, when the two materials are blended together at the 98:2 CII:SiO_2 ratio, segregation was not evident. However, as the amount of SiO_2 increased in the powder blend the cohesive nature of SiO_2 caused their particles to aggregate, resulting in segregation of the blend. For this reason, physical blends of SiO_2 and CII failed to produce a homogeneous product. Large differences in particle size (~100 µm vs. 30 nm) and density (0.38 g/cm^3 vs. 0.05 g/cm^3) between CII and SiO_2 contributed to segregation.

In comparison, homogenization of aqueous suspensions of SiO_2 and CII led to stable dispersions. Vacuum filtration of the dispersions followed by sequential granulation at ~20, 30 and 45% moisture contents using 150 µm, 250 µm and 710 µm sieves, respectively, successfully produced granules of CII:SiO_2. The sequential granulation at decreasing moisture contents was efficient and important to the preparation of the granules since high moisture contents (>20%) of the wet mass did not favor granulation using a 150 µm screen directly.

Likewise, the oscillating granulator was successfully employed as an extruder to obtain the granules or extrudate needed to feed the spheronizer. Further, there was no need to increase the moisture content of the granules for the spheronization process. Spheronization times from 10 to 15 min were sufficient to produce spherical particles.

Longer times produced agglomeration of the beads into undesirably larger particles. If the spheronization time is lower than 10 min, the spheronization process is incomplete rendering beads of irregular shape which break easily.

Since CII always was the major component in the co-processed product, spray drying of the silicified materials was conducted at the previously selected conditions determined for CII: 3% w/v feed concentration, 195ºC inlet air temperature, 2 mL/min feed spraying rate, 0.44 m^3/min drying air speed, 1.0 kg-f/cm^2 atomization air pressure and 711 µm nozzle diameter. As seen for the spray dried CII, preliminary runs at 3 mL/min and 5 mL/min keeping all other parameters constant led to a high deposition of droplets in the drying chamber as seen in the CII dispersions.

Table IV-14 shows the fumed silica content for each silicified material. Spray-dried silicified materials presented the most approximate values to the theoretical SiO_2 percentage in each material. Thus, the rapid drying in this process allowed for a minimum powder loss in the cyclone. In contrast, wet granulation and spheronization which initially had to go through a filtration process of the wet slurry had some loss of fumed silica which possibly passed through the filter making the filtrate solution partially cloudy. Further, SiO_2 loss could be more pronounced when more processing is involved as in the case of extrusion/spheronization due to sample clogging in the screen meshes and partial sample stickiness in the rotating axis of the granulator and in the walls of the spheronizer chamber.

Powder X-ray diffractograms of CII, SiO_2, Prosolv® and silicified materials prepared by spray drying, wet granulation and spheronization methods are shown in Figures IV-29-31. CII and silicified materials all showed peaks at 12°, 20° and 22° 2θ due to the $1\bar{1}0$, 110 and 200 reflections, respectively, confirming the presence of the cellulose II lattice as discussed previously. In this case, the amorphous fumed silica had

no effect on the position of the crystalline peaks of CII. As seen in Figures IV-29, IV-30 and IV-31, Prosolv® SMCC 50, Prosolv® SMCC 90 and CP-203®, in contrast, displayed characteristic diffraction peaks due to the cellulose I lattice at 14.8°, 16.3° and 22.4° 2θ, corresponding to the $1\bar{1}0$, 110 and 200 reflections, respectively (Klemm et al., 1998b). Fumed silica showed a diffuse halo indicating its amorphous nature. Tobyn and coworkers previously reported that silicification in Prosolv® does not change the position of the crystalline peaks of cellulose I (Edge et al., 1999). As seen in Table IV-14, the degree of crystallinity (DC) of all silicified CII samples and SDCII was lower compared to that of CII (~68%, vs. 57-62%). Since SiO_2 is completely amorphous, its presence led to a major decrease in crystallinity since the crystalline component of the samples will be reduced. Further, the rapid drying process during spray drying might be responsible for the decrease in crystallinity of SDCII. On the contrary, other processes such as wet granulation and spheronization alone did not change the crystallinity of CII indicating that partial amorphization of CII did not occur when these processes are used. The degree of crystallinity of commercial cellulose I excipients has been reported to be between 65-80% (Reus, 2005). Conversely, Celphere-203® (CP-203®) presented the lowest degree of crystallinity among the CI materials (Prosolv® SMCC 50, Prosolv® SMCC 90). It is evident that silicification decreased the degree of crystallinity of CII independent of the process employed. The reported degree of crystallinity for CII (as obtained from hydrocellulose), Prosolv® SMCC 50 and Prosolv® SMCC 90 are 59% (Reus, 2005), 71.8% (Jumaa et al., 2000) and 70.7% (Soh Lay Peng, 2006). The above results confirmed that the crystal structure of cellulose does not change by either silicification or processing.

Table IV-14. Geometric Mean Diameter of Cellulosic Composites and Commercial Cellulose I Materials.

Sample	Geometric mean diameter ±SE (µm)[a] n=1	Degree of Crystallinity (%) n=3	SiO_2 (%) n=3
CII	158 ±42	68.0 ± 1.4	0.00 ± 0.00
SDCII	66 ± 6	62.6 ± 2.3	0.00 ± 0.00
SD-CII:SiO_2(98:2)	61 ± 9	62.4 ± 1.3	1.96 ± 0.03
SD-CII:SiO_2(95:5)	64 ± 9	62.3 ± 3.8	4.92 ± 0.02
SD-CII:SiO_2(90:10)	75 ± 9	63.3 ± 1.0	9.65 ± 0.33
SD-CII: SiO_2(80:20)	51 ± 5	56.8 ± 0.6	19.77 ± 0.11
Prosolv® SMCC 50[b]	58 ± 5	67.6 ± 1.8	1.94 ± 0.02
WGCII	107 ± 6	67.5 ± 1.3	0.00 ± 0.00
WG-CII:SiO_2(98:2)	129 ± 7	63.1 ± 2.4	1.79 ± 0.07
WG-CII:SiO_2(95:5)	110 ± 7	57.1 ± 1.1	4.82 ± 0.06
WG-CII:SiO_2(90:10)	128 ± 6	56.5 ± 2.9	9.10 ± 0.24
WG-CII: SiO_2(80:20)	105 ± 6	53.6 ± 1.1	17.94 ± 0.27
Prosolv® SMCC 90[b]	110 ± 9	67.1 ± 1.8	1.93 ± 0.04
SPCII	207 ± 39	68.0 ± 1.4	0.00 ± 0.00
SP-CII:SiO_2(98:2)	148 ± 4	64.6 ± 0.7	1.67 ± 0.04
SP-CII:SiO_2(95:5)	339 ± 18	61.1 ± 0.4	4.09 ± 0.11
SP-CII:SiO_2(90:10)	558 ± 21	56.1 ± 1.6	8.10 ± 0.10
SP-CII: SiO_2(80:20)	450 ± 33	52.9 ± 2.5	16.6 ± 0.53
CP-203®[c]	303 ± 7	52.1 ± 1.2	0.00 ± 0.00

[a] Standard error determined as $\frac{\sigma}{\sqrt{n}}$

[b] Silicified microcrystalline cellulose I.

[c] Spheronized microcrystalline cellulose I.

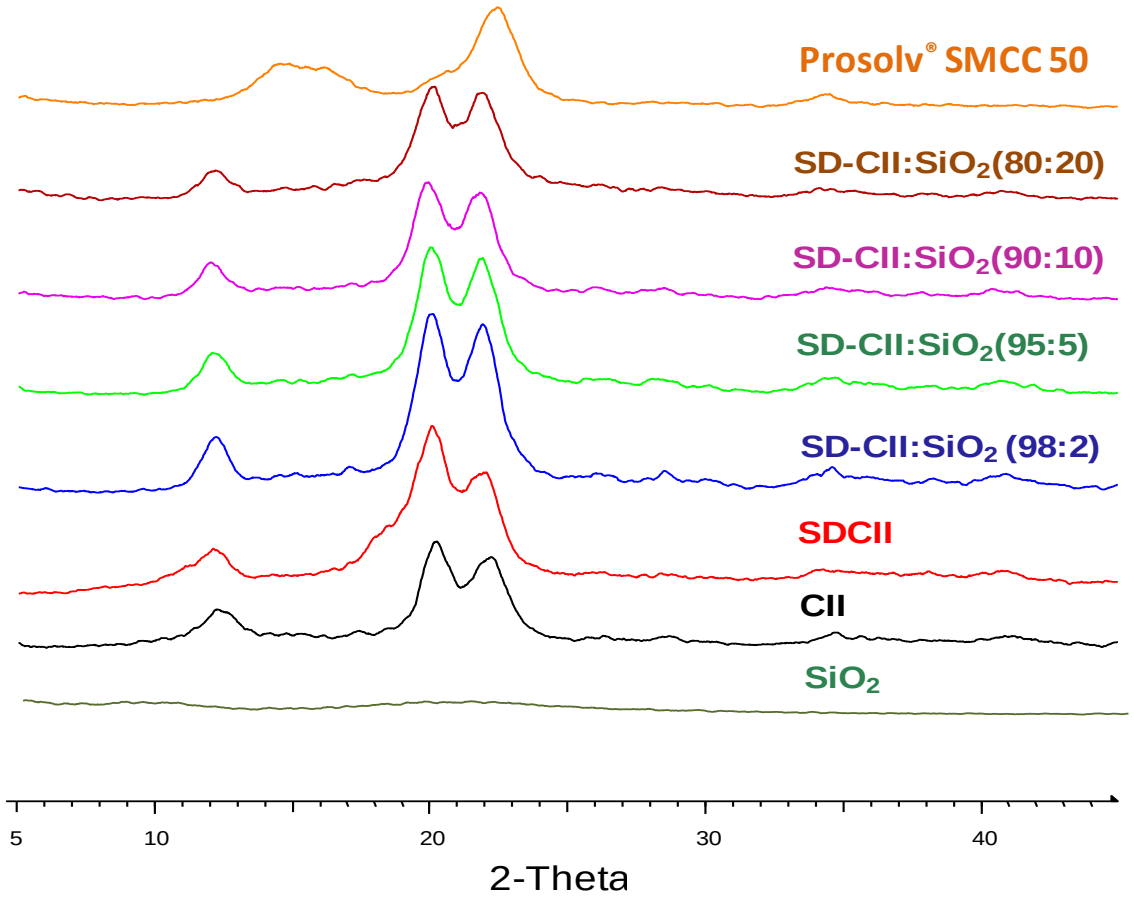

Figure IV-29. Powder X-ray Diffractograms of CII, Prosolv® SMCC 50 (silicified microcrystalline cellulose I) and Spray-Dried Materials.

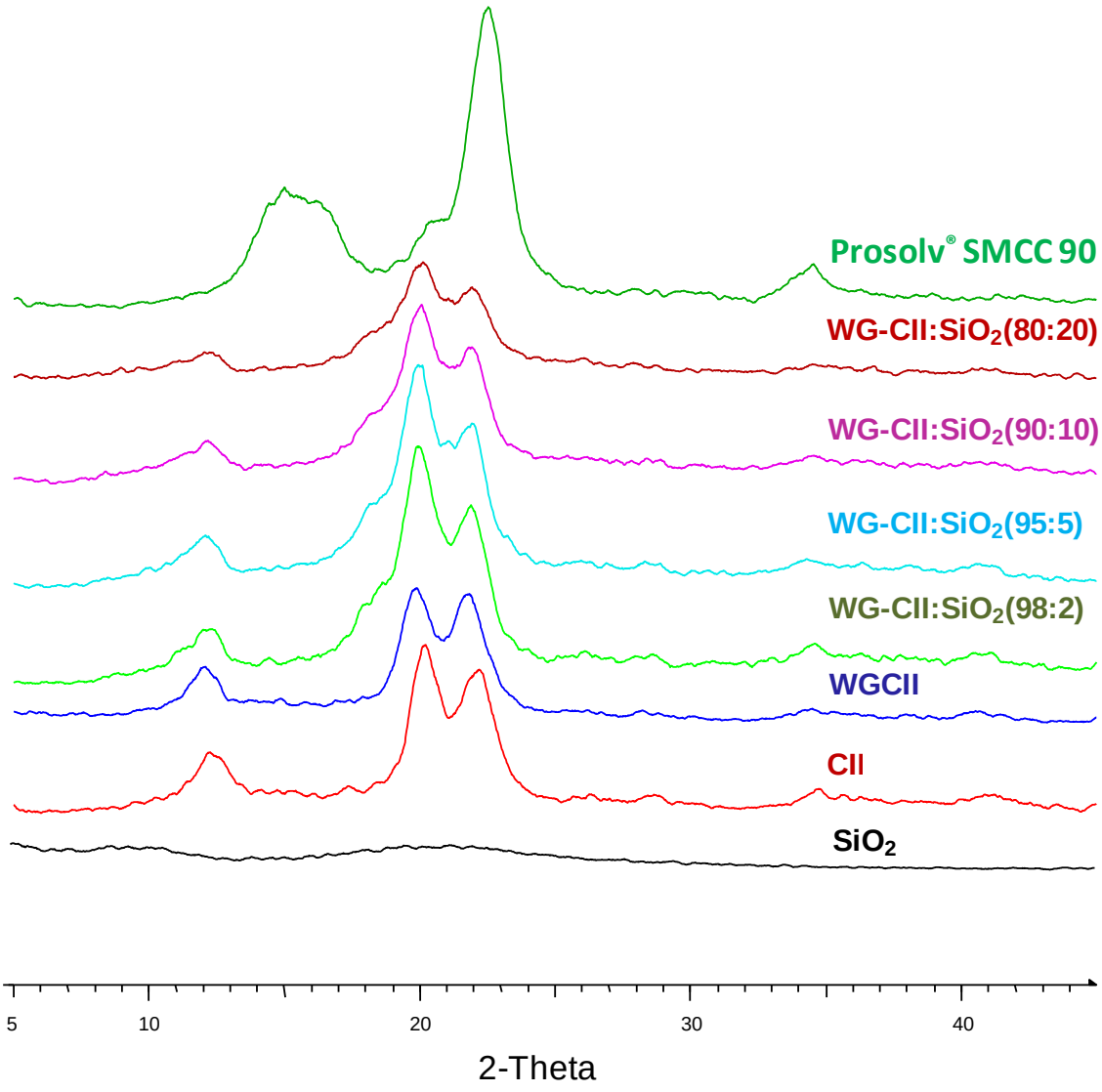

Figure IV-30. Powder X-ray Diffractograms of CII, Prosolv® SMCC 90 (silicified microcrystalline cellulose I) and Wet Granulated Materials.

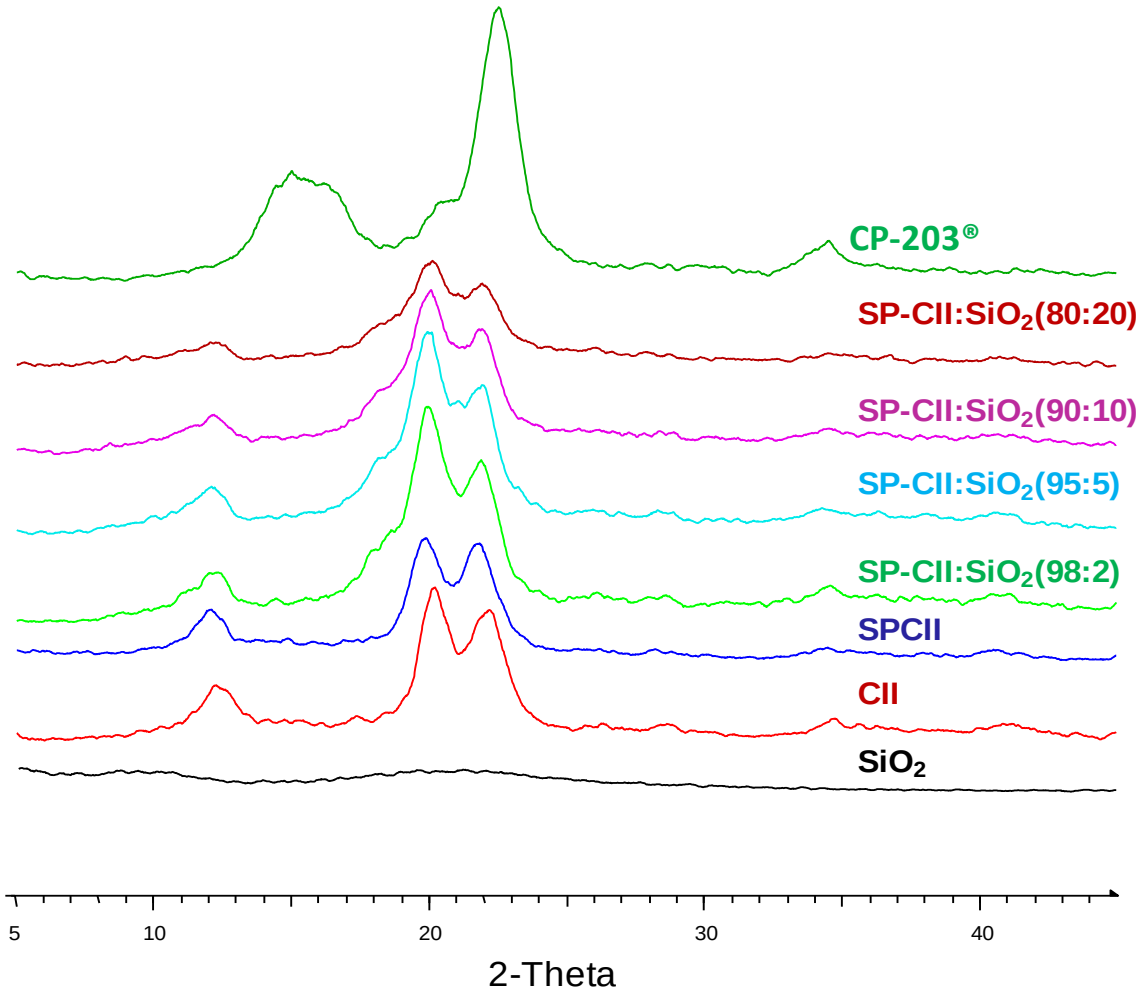

Figure IV-31. Powder X-ray Diffractograms of CII, CP-203® (spheronized microcrystalline cellulose I) and Spheronized Materials.

Powder Properties

Particle Size Distribution

Figure IV-32 shows the particle size distributions obtained by the sieve method, with a log transformation of the size axis. It is apparent by looking at these plots that a log-normal distribution describes all the size distribution results. Processing was important for modifying the particle size and particle size distribution of CII (broad distribution) to a narrower distribution (i.e., less skewed) as seen in Figure IV-32.

Spray-dried products had the narrowest particle size distribution, followed by the wet granulated and spheronized materials. Usually, the spray droplets from the laboratory scale spray-drier produce the smallest particle size (Portmann et al., 2007). The distributions of particle size of commercial materials, such as Prosolv® SMCC 50, Prosolv® SMCC 90 and CP-203® are close to those materials obtained by spray drying, wet granulation and spheronization, respectively. Geometric mean diameters for all materials are listed in Table IV-14 and Figure IV-33 shows the log-normal plots of size data.

The logarithms of the mean size were taken and plotted against their cumulative frequency on a normal scale assuming the data of particle size follow a log-normal distribution, which is characteristic of most pharmaceutical powders as reported previously (Ahuja and Scypinski, 2011). Spray-dried materials showed a geometric mean diameter ranging of 51-71 µm, matching the particle size of Prosolv® SMCC 50 (~58 µm). Likewise, particle size range (105-130 µm) of the wet granulated products approaches the particle size of Prosolv® SMCC 90 (~110 µm). Spheronized materials had a geometric diameter range of 148-558 µm, matching the particle size of CP-203® (~303 µm).

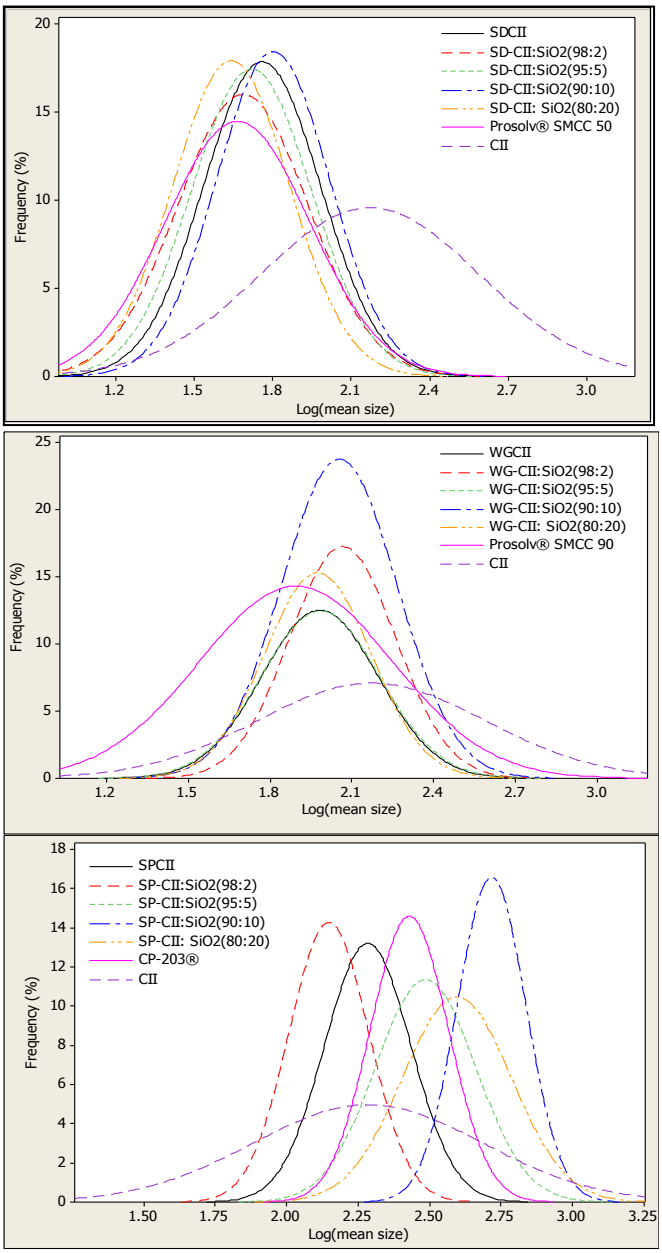

Figure IV-32. Particle Size Distribution of CII, CII-SiO_2 Composites, Prosolv® (silicified cellulose I) and CP-203® (spheronized cellulose I) Determined by Sieve Analysis.

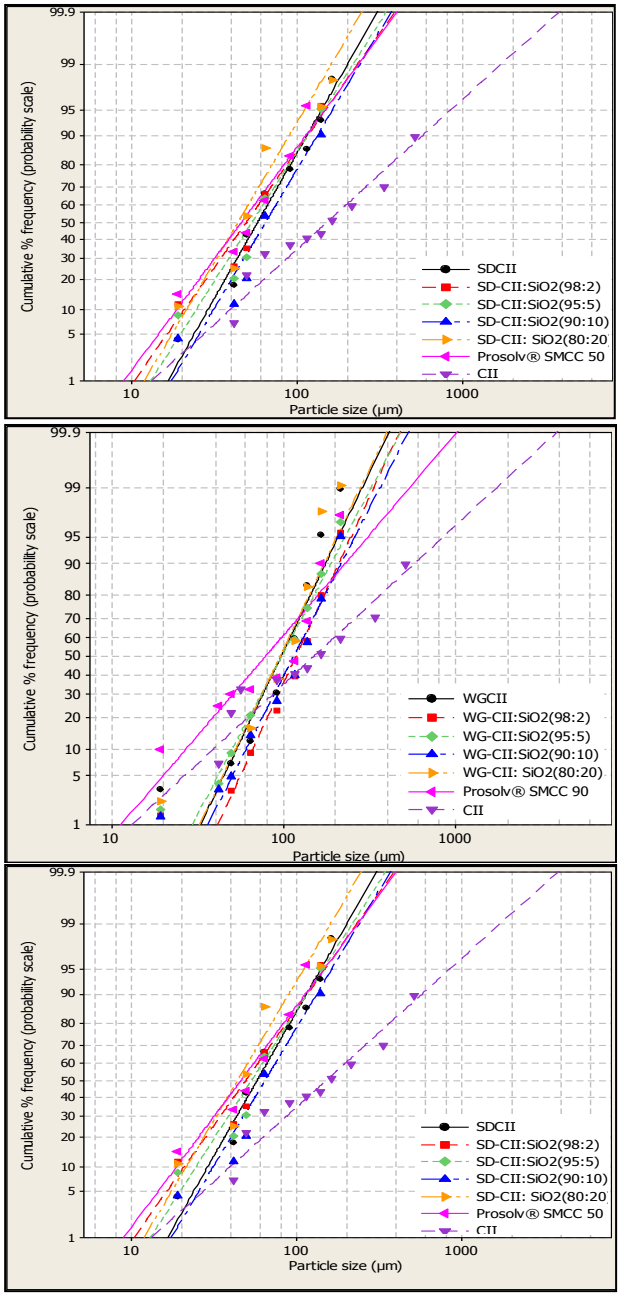

Figure IV-33. Log-Probability Plots of CII-SiO_2 Materials and Commercial Cellulosic Materials (produced by the Minitab® software).

The reported mean particle size for Prosolv® SMCC 50, Prosolv® SMCC 90 and CP-203® are 52.0, 104.4 and 262.8 µm, respectively (Hou and Changquan, 2008). In the spheronization process, bead size depends primarily on the mesh size used during the extrusion process and in most equipment this is ~1,000 µm.

In this study, the extrusion process was by-passed by using the same screens used for the wet granulated materials and as a result, the spheres formed were smaller. For this reason, by controlling the screen size in the manufacturing process the resulting bead size could be controlled. Since spheronized materials had broad distributions, the fraction of beads retained between 150-420 µm sieve sizes was selected and characterized further.

Morphological Characterization

Figure IV-34 shows SEM of CII, Prosolv® SMCC 50, Prosolv® SMCC 90 and CP-203®. CII has a fibrous nature as obtained from cotton linters without any further processing. Prosolv® SMCC 50 and Prosolv® SMCC 90 are spray-dried CI:SiO_2 composites at a ratio 98:2 and appear as aggregates. The SEMs show tiny SiO_2 aggregates homogeneously distributed on the surface of cellulose I and possibly in the core of Prosolv® making its surface rougher and showing an irregular shape. On the contrary, CP-203® presented a smooth and non-porous surface and a regular spherical shape. These characteristics show that processing and silicification of cellulose I have a major effect on particle morphology and surface characteristics, respectively.

Energy dispersive spectroscopy (EDS) was employed for determining the SiO_2 distribution in the cellulosic materials. Figure IV-35 shows the EDS micrographs of Prosolv® SMCC 50 and Prosolv® SMCC 90. The image on the left column has a composite backscatter and SiO_2 X-ray signal, whereas on the right only the X-ray signal is shown. Prosolv® SMCC 90 particles were composed of a conglomerate of tiny chunks of elongated particles.

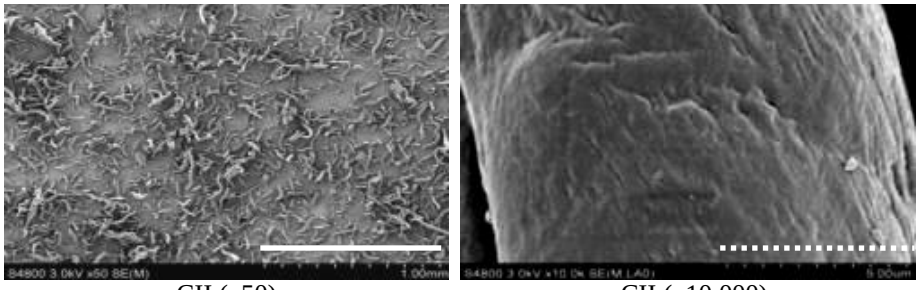
CII (x50)

CII (x10,000)

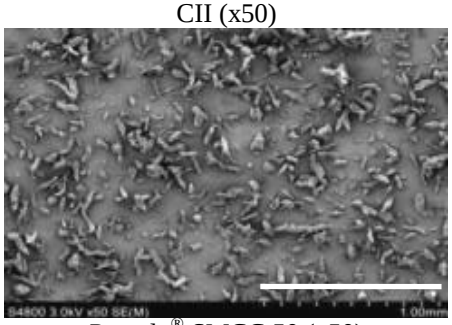
Prosolv® SMCC 50 (x50)

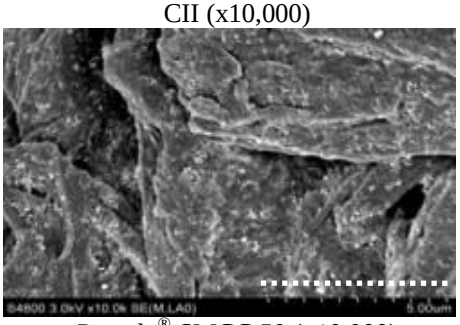
Prosolv® SMCC 50 (x10,000)

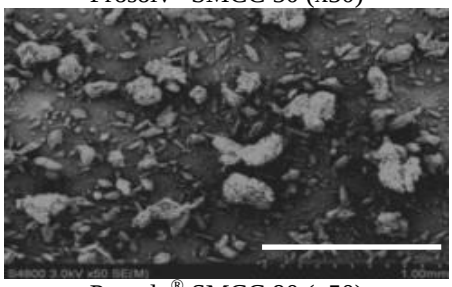
Prosolv® SMCC 90 (x50)

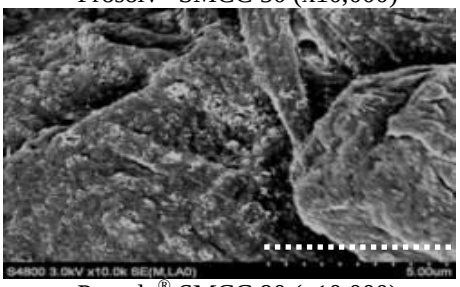
Prosolv® SMCC 90 (x10,000)

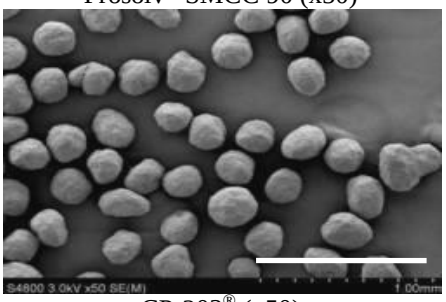
CP-203® (x50)
Scale bar (1 mm)

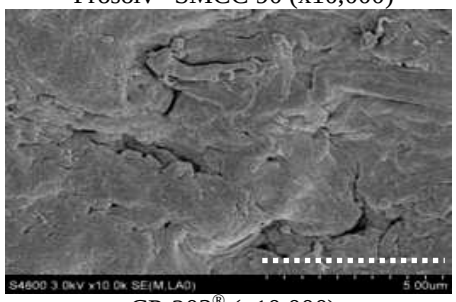
CP-203® (x10,000)
Scale bar (5 µm)

Figure IV-34. SEMs of CII and Commercial Products: Prosolv® (silicified microcrystalline cellulose I) and CP-203® (spheronized microcrystalline cellulose I) at 50X and 10,000X.

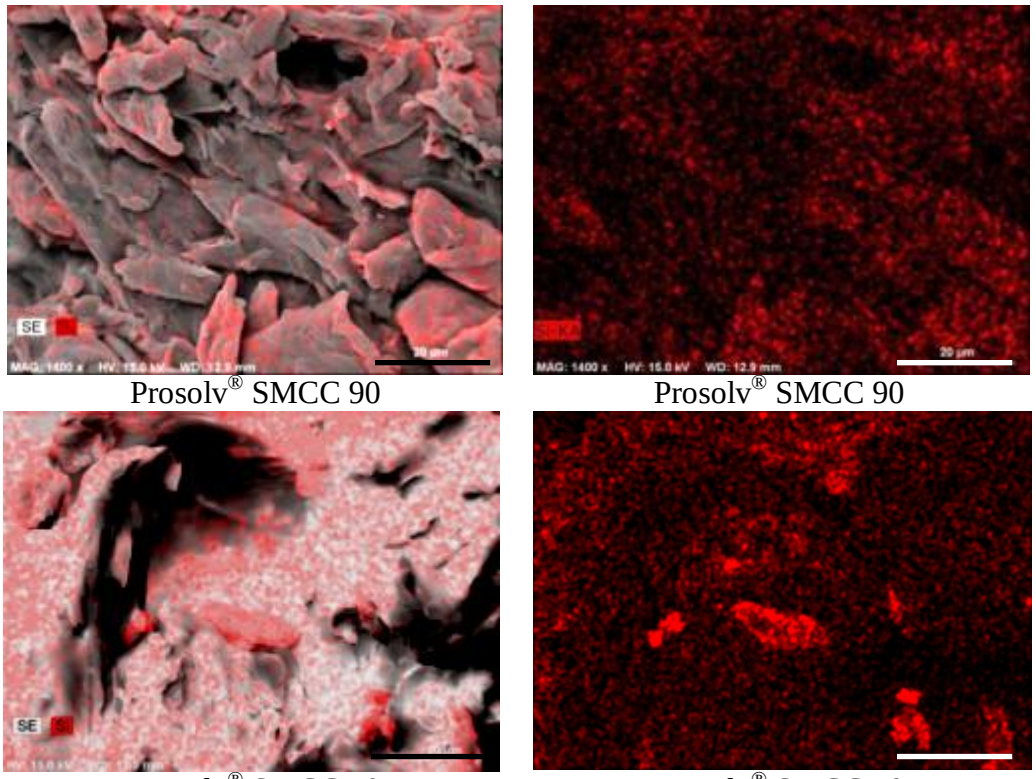

Figure IV-35. EDSs Showing SiO_2 Distribution on the Surface of Prosolv® (silicified microcrystalline cellulose I) at 1,400X.

Although SiO_2 is found all over the particles, there are some regions in which the SiO_2 signal is more intense and other regions such as cavities where its signal is absent. In contrast, Prosolv® SMCC 50 shows a more uniform coverage of SiO_2 which is seen even in the holes and cavities of the particles. This might be due to the fact that particles are small and more accessible and thus, silica particles will be able to penetrate cavities more deeply. Further, a few tiny isolated chunks of SiO_2 are present.

Figure IV-36 and Figure IV-37 show that the original fibrous shape of CII was modified by the spray drying process. This process, due to the rapid drying of droplets transformed the fibers into smaller particles with a more rounded to elongated shape. However, the deposition of SiO_2 on the surface of the particles generates some rougher features on the surface. This effect was more pronounced at SiO_2 levels higher than 10% since the surface of those particles was very rough and cracked due to overlapping and high deposition levels of SiO_2 aggregates. However, the rough effect caused by silicification with more regularly-shaped particles can be more beneficial than the fibrous shape of CII since fibers could oppose to flow and hence could prevent a good die filling during the tableting process and hence could lead to poor uniformity of content of drugs.

Figure IV-38 shows the energy dispersive spectroscopy (EDS) images for the spray-dried materials. The backscatter image is shown on the left column (white color), while the right side shows the intensity of the SiO_2 X-ray signal (blue color) for the same image, which increased as the amount of SiO_2 increased. Silicification levels of 2% and 5% produced a homogeneous surface coverage of the CII particles and it was absent in the spaces between particles with few individual round particles having an intense coverage. At 10 % and 20% silicification, a denser surface particle coating was observed. This indicates that SiO_2 particles piled up on top of each other on the cellulose particles increasing the SiO_2 signal.

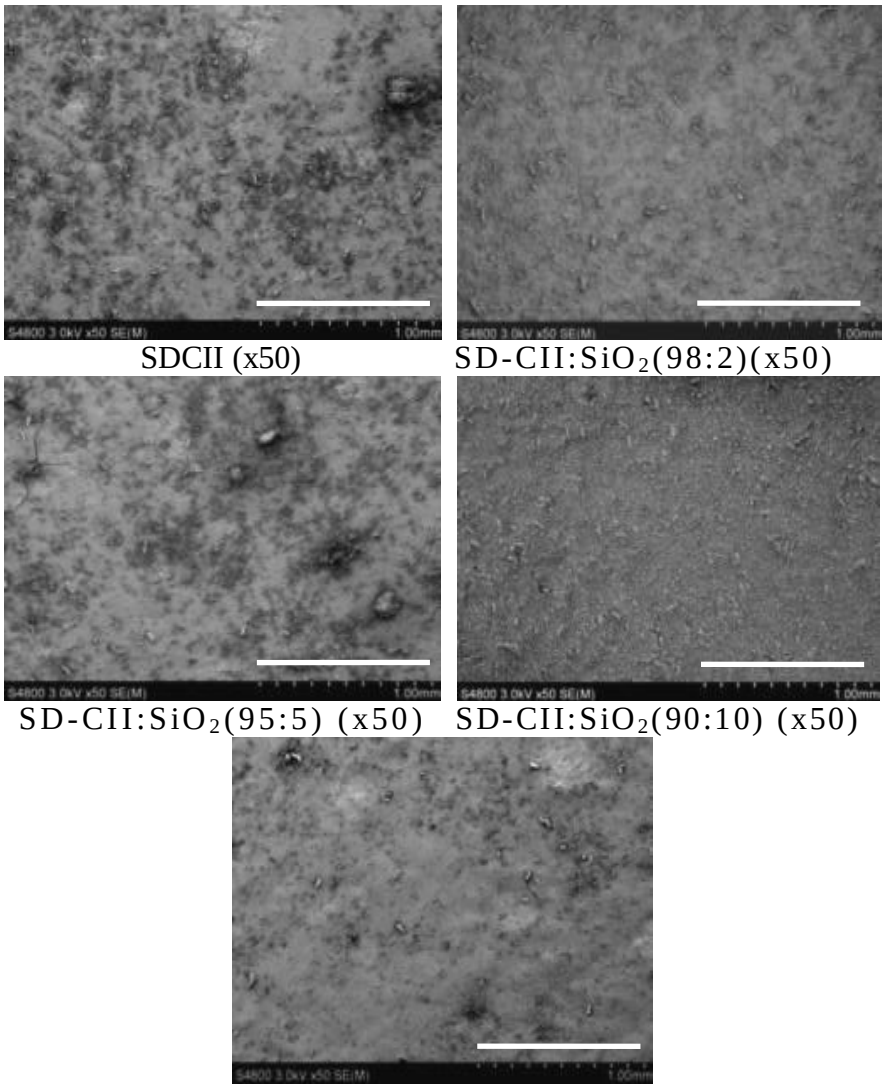

Figure IV-36. SEMs of Spray-Dried CII with Various Ratios of SiO_2 at 50X.

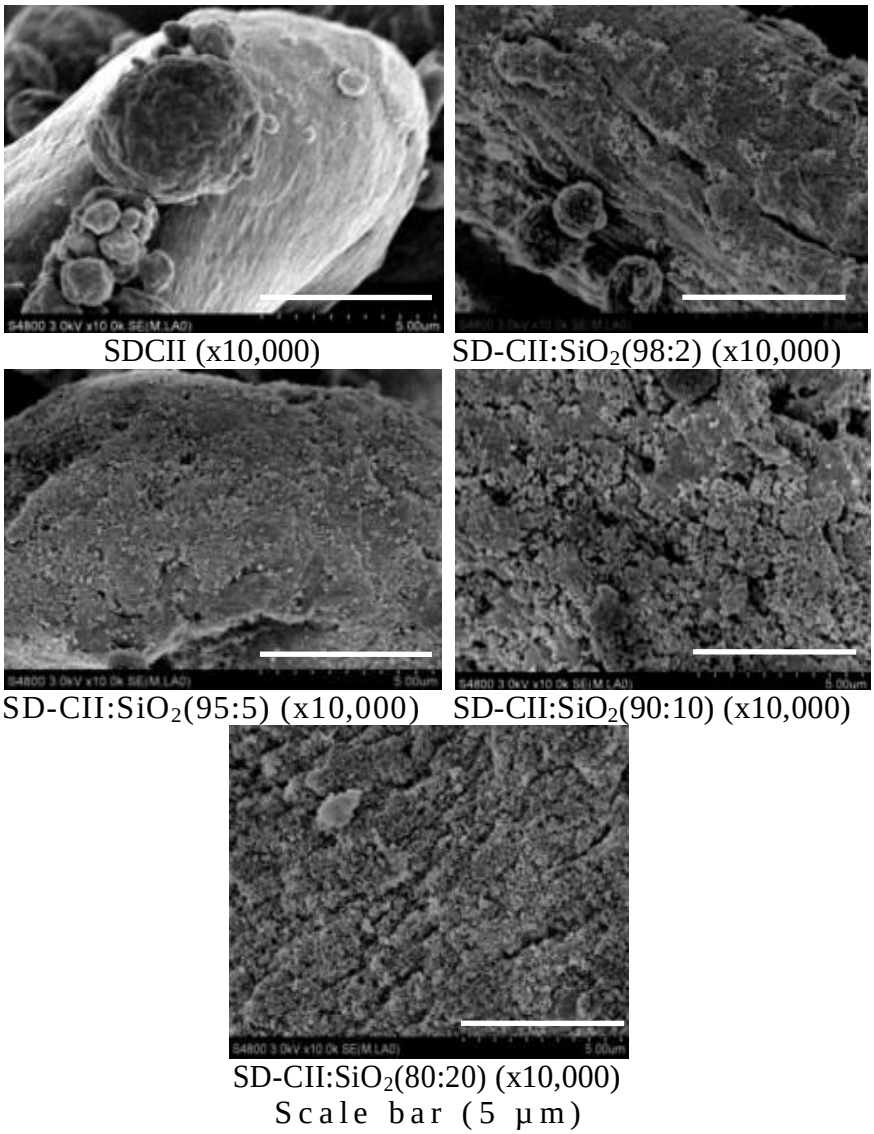

Figure IV-37. SEMs of Spray-Dried CII with Various Ratios of SiO_2 at 10,000X.

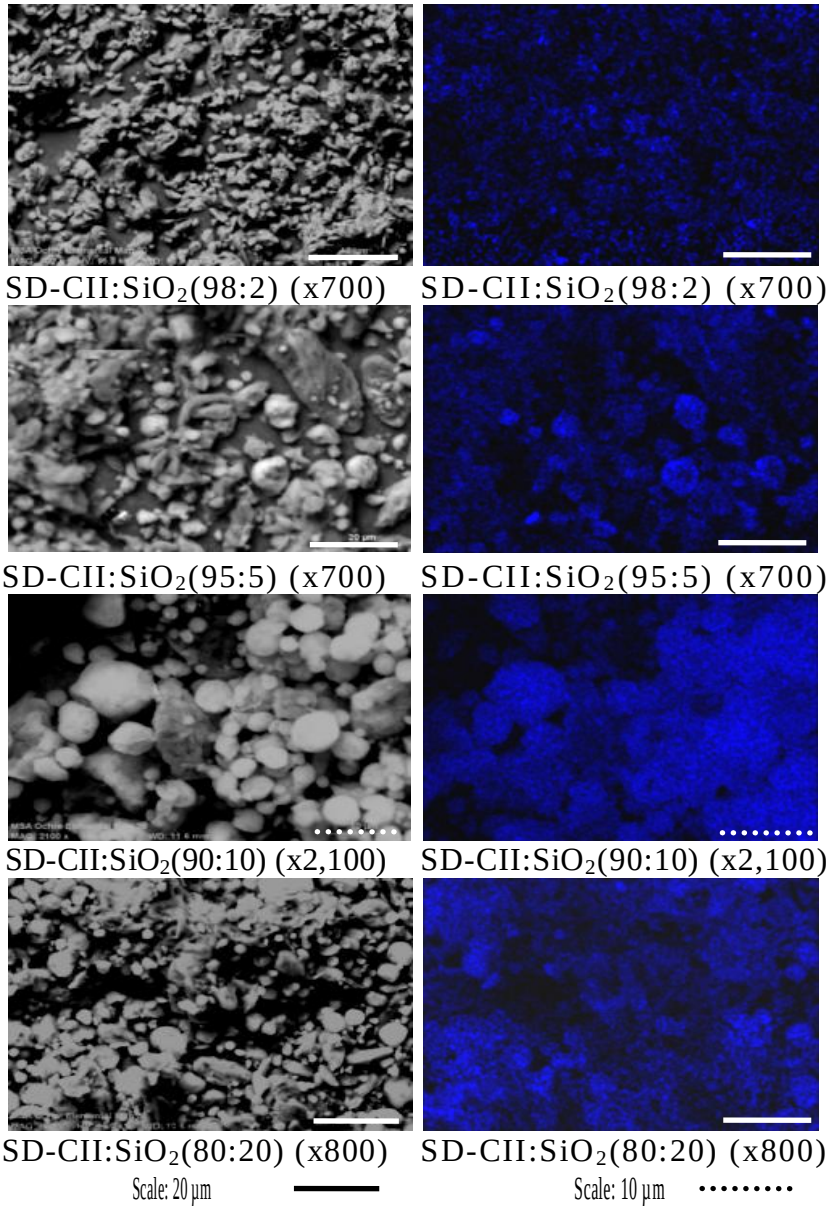

Figure IV-38. EDSs Images Showing SiO_2 Distribution on the Surface of SD-CII:SiO_2 Composites.

It is possible that during the spray drying process a rapid droplet drying of the homogeneous dispersion of cellulose II and SiO_2 leads to a more uniform distribution of SiO_2 particles.

Figure IV-39 and Figure IV-40 show the SEMs of the CII:SiO_2 composites prepared by wet granulation. The granules consist of aggregates with rough surfaces and presented an irregular shape. A high silicification (20%) caused the deposition of aggregates clusters of SiO_2 on the surface. It is also possible that some of the SiO_2 particles penetrated into the core of the granules.

Figure IV-41 shows the distribution of SiO_2 on the granules produced by wet granulation. The composite backscatter and X-ray image is seen on the left and only the X-ray image is shown in the right column. At 2% silicification level there is insufficient SiO_2 for a homogeneous coverage of the surface. At 5% and 10% silicification better coverage is achieved although some patches in the surface are uncovered including some surface holes and cracks. It has been reported that this technique is surface specific, indicating that only elements in the surface or near the surface are detected with approximately 10 µm in depth in the material if ~40 keV of the electron beam is employed (Garratt-Reed and Bell, 2003). This might explain why at the 15 keV employed in this study no SiO_2 signal was detected inside the cracks and holes of the materials. A 20% silicification had a more efficient CII surface coating. Compared to the spray-dried composites, tiny clusters of SiO_2 are also visible at all SiO_2 levels (shown as dark red color spots), indicating that the coating using this process is not homogeneous. Thus, when the homogenous dispersion of CII and SiO_2 is vacuum-filtered and wet granulated, SiO_2 particles move around the wet mass as aggregates/deaggregates around CII particles.

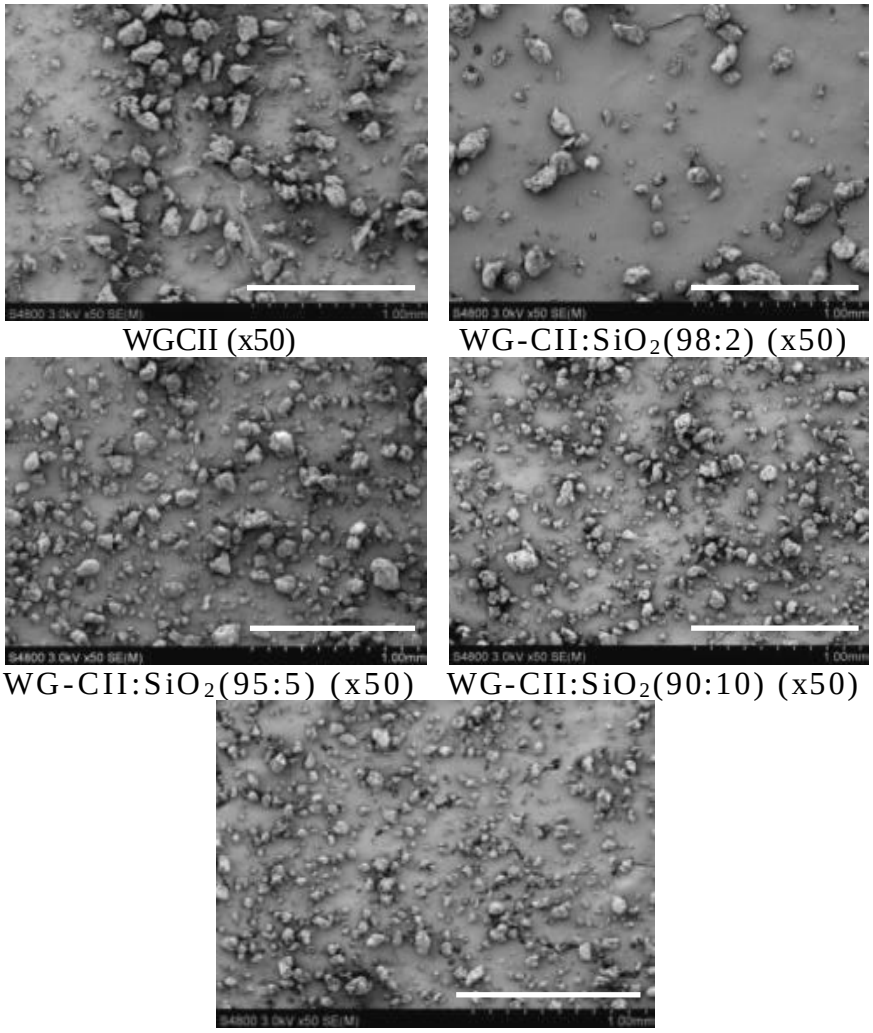

Figure IV-39. SEMs of Wet Granulated CII:SiO_2 Composites at 50X.

.

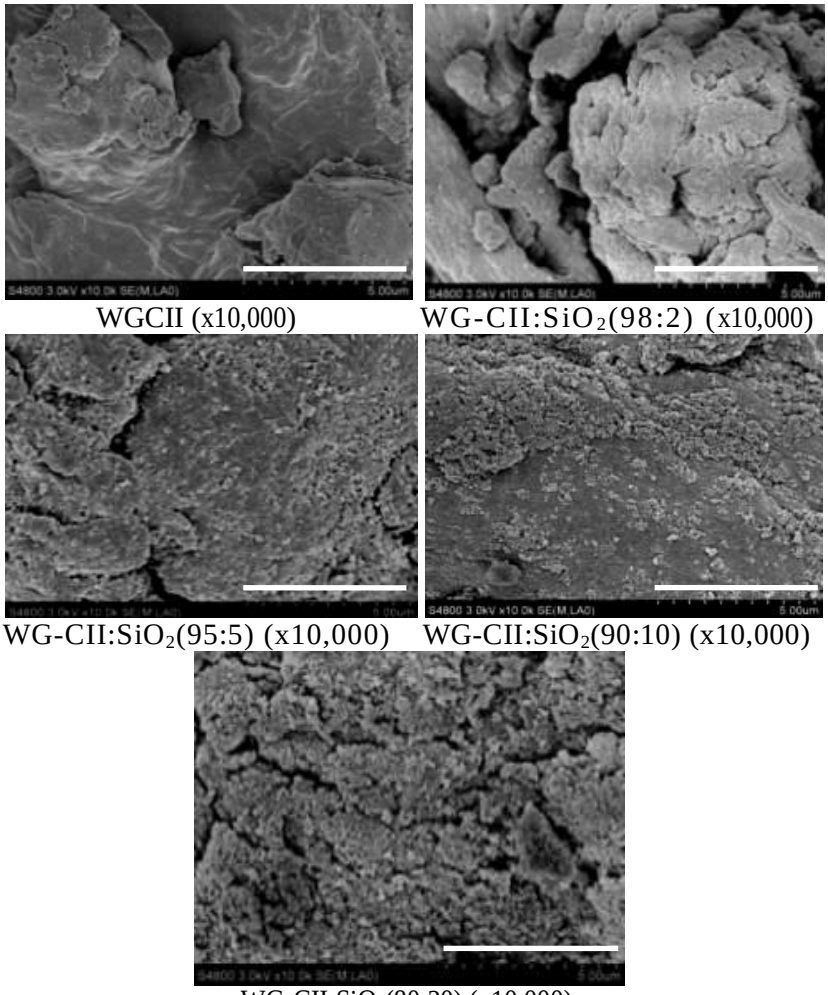

Figure IV-40. SEMs of Wet Granulated CII:SiO_2 Composites at 10,000X.

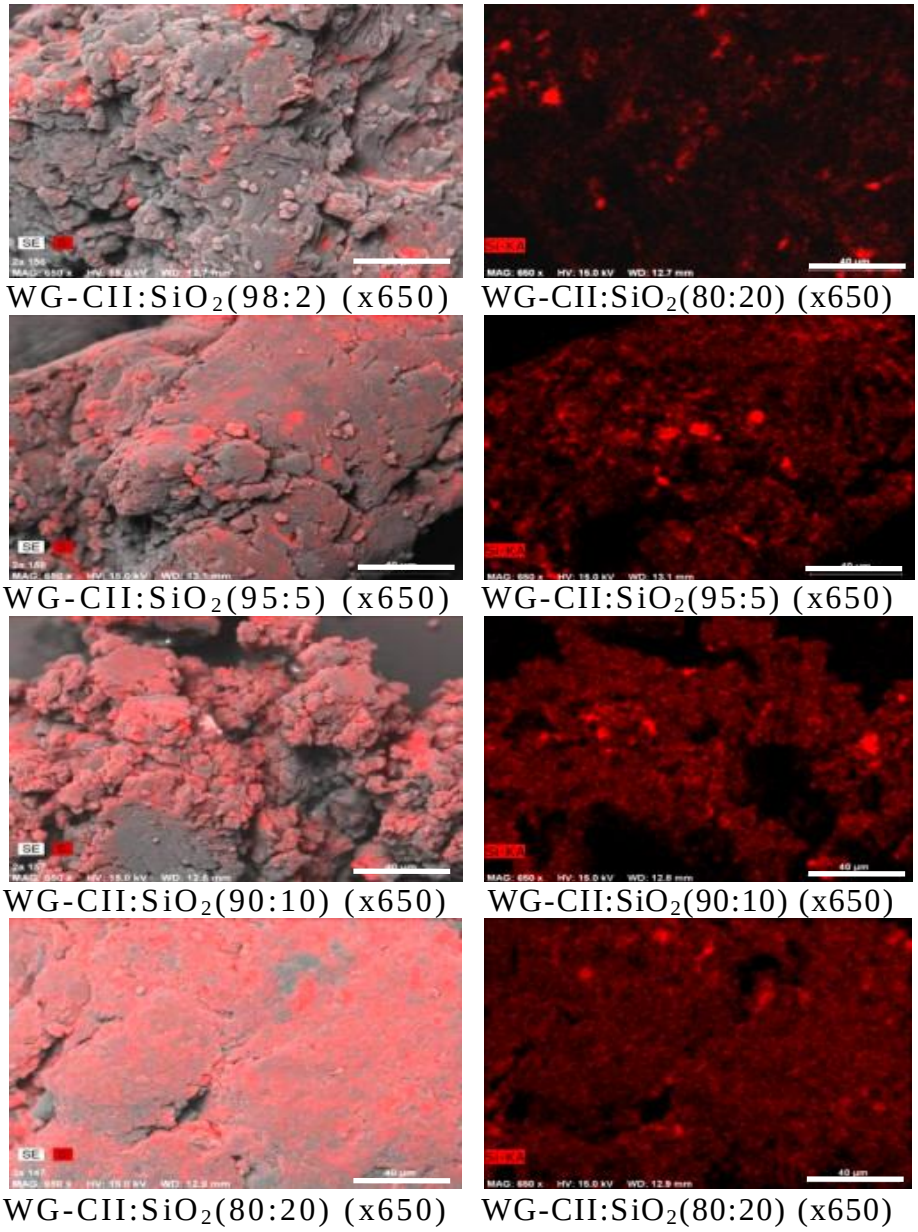

Figure IV-41. EDSs Showing SiO_2 Distribution on the Surface of Wet Granulated CII:SiO_2 Composites.

As a result, some SiO_2 particles are attached to the CII surface, whereas, others get entrapped inside the granule cores (although not visible due to the large size of the granules preventing full penetration of the X-rays). A cross-sectional view of SiO_2 was not determined for the wet granulated materials due to technological limitations to cut in half granules of a mean size of ~100 µm.

Figure IV-42 and Figure IV-43 show the SEMs for spheronized materials. Since spheronization is an extension of wet granulation, the individual fibers in the wet state coalesce forming cylindrical rods when passed through a 711µm sieve. These tiny rods are then passed through 250 µm and 150 µm sieves and broken down into small particles having an irregular granular shape. The resulting granules are then converted in the spheronizer to smoother and nearly spherical beads. Silicification levels up to 10% did not cause any change in morphology or surface of the composite particles. Only at 20% SiO_2 did granules with rough surfaces appear. The morphology and surface appearance of SPCII was very similar to CP-203®. This indicates that mainly the spheronization process was responsible for the smooth surface characteristics of those materials, except when a 20% silicification is used rendering a rougher surface.

Figure IV-44 shows the SiO_2 distribution on the CII beads surface. In general, no large features were visible on the surface. In contrast to the results observed for wet granulated granules, these granules showed a more uniform SiO_2 distribution on the surface although some denser surface patches were observed at 2% silicification. The cross-sectional area of the beads showed that at all silicification levels SiO_2 was also present in the bead core. Clusters of SiO_2 are less distinguishable on the surface except for the core at 2% and 5% silicification levels, in which isolated or random clusters of SiO_2 were predominant.

.

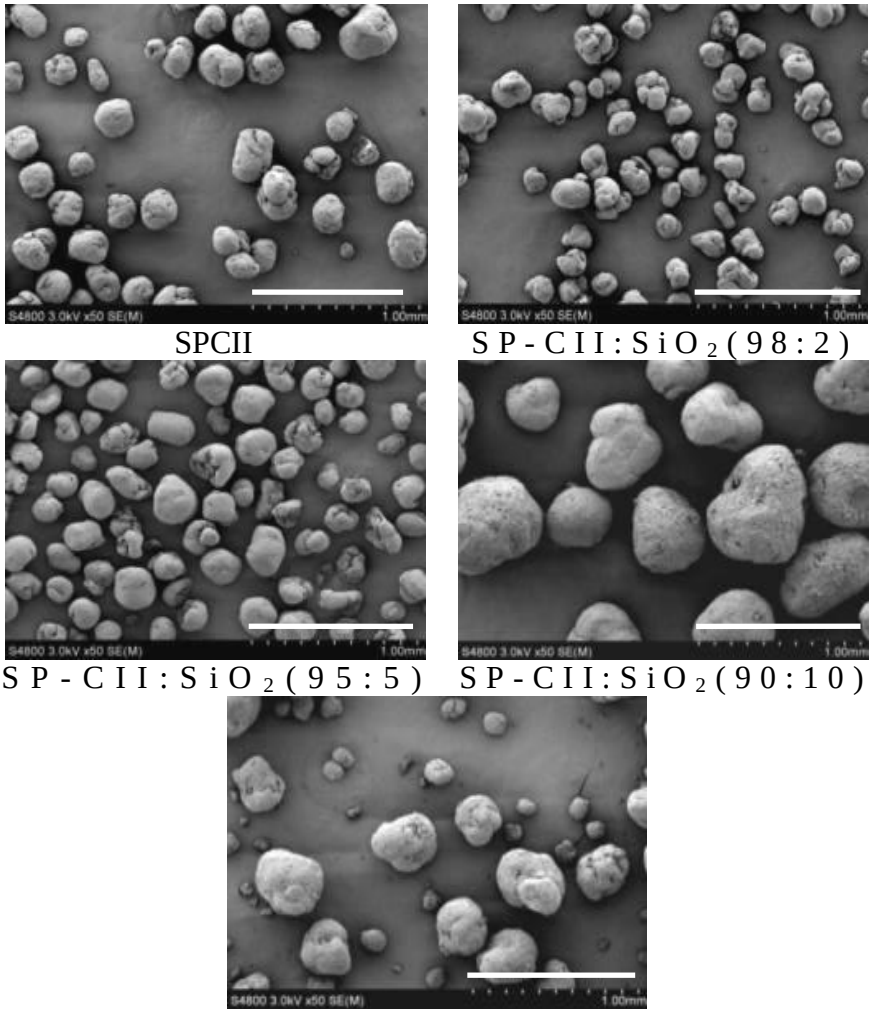

Figure IV-42. SEM Microphotographs of Spheronized Products at 50X

.

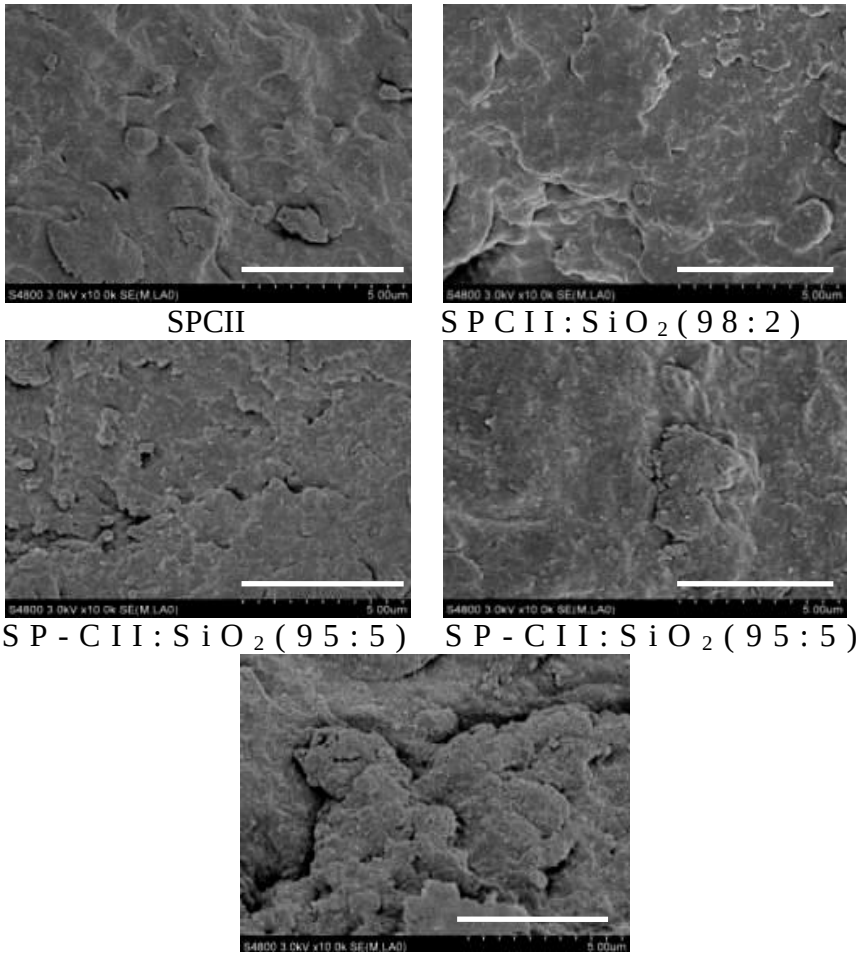

Figure IV-43. SEM Microphotographs of Spheronized Products at 10,000X .

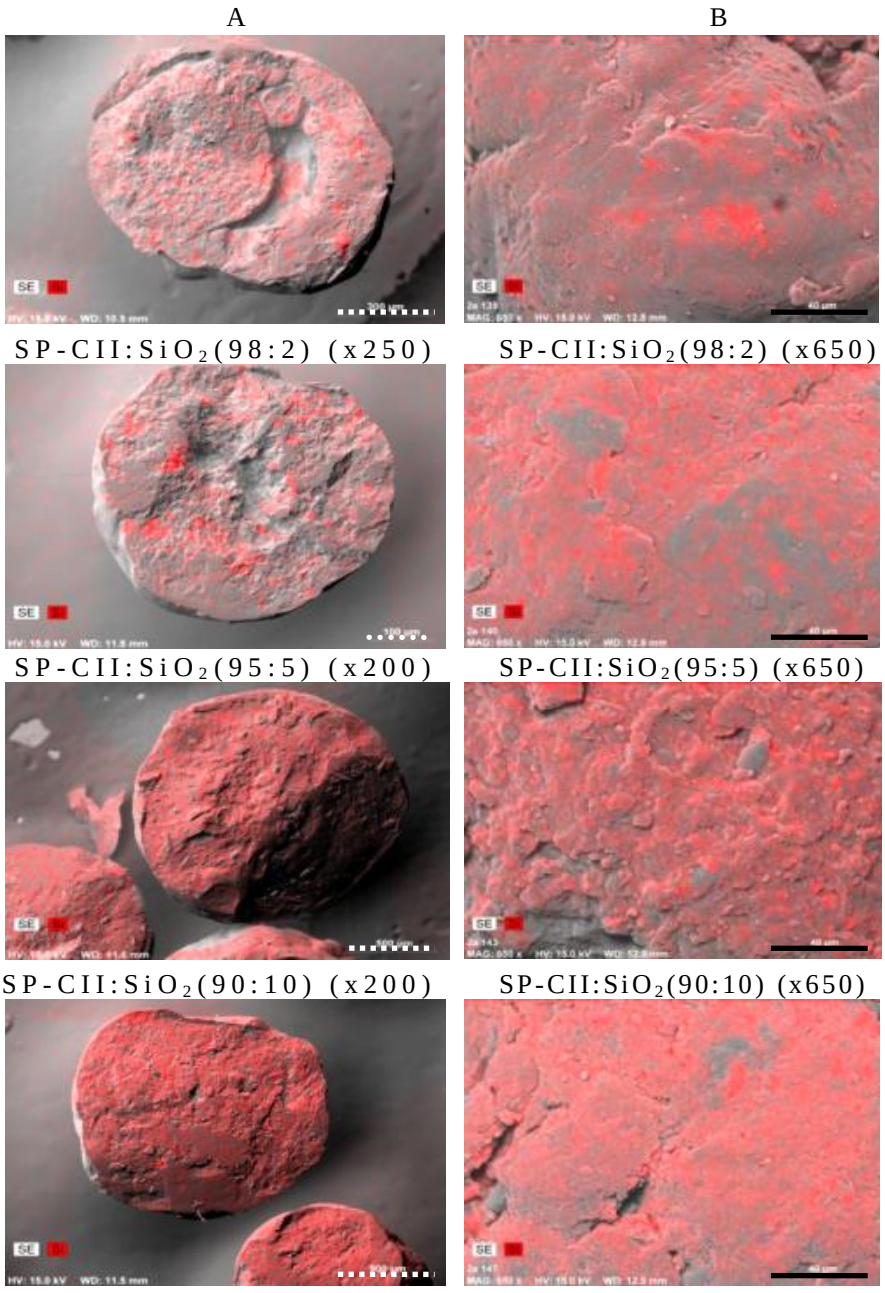

Scale bar: 300µm(.....), 200µm(------), 40µm (━).

Figure IV-44. SiO_2 Distribution (red spots) in: (A) Spheronized Bead Core (B) Bead Surface.

Nevertheless, silicification levels higher than 10% produced beads with a homogeneous and more intense coverage inside the core compared to that on the surface. This indicates that at these levels most of the SiO_2 was present inside the beads rather than on the surface. The high amount of SiO_2 during the granulation process is taken by the plastic deforming CII particles, which entrap or wrap SiO_2 when particles are forced through the sieves holes while they are in a wet state and growing in size, thus fewer SiO_2 particles are attached to the surface.

Powder properties of the composite materials are summarized in Tables IV-15-17. The true density of the composite materials increased, especially at silicification > 10%. This observation was common for all silicified materials independent of the process employed. Since fumed silica possesses a higher true density (2.27 g/cm^3) than CII (~1.54 g/cm^3), the resulting physical mixture of both materials at SiO_2 levels > 10% had a small increase in true density of the composites compared to the unprocessed CII. Reported densities for Prosolv® SMCC 50 and Prosolv® SMCC 90 are 1.62 g/cm^3 and 1.60 g/cm^3, respectively (Michrafy et al., 2007). CP-203®, on the contrary, had the lowest true density, which is correlated with its low value of crystallinity, indicating a low contribution of the amorphous component on the chain packing. The effect of moisture on the powder properties is assumed to be negligible since in all cases it was < 4.0 % w/w in compliance with the USP requirement of a maximum level of 7%.

Compared to SDCII and WGCII, silicification caused a decrease in the bulk and tap densities when spray drying and wet granulation are employed. On the contrary, silicification in the spheronized materials had no effect on the bulk and tap densities of SPCII. Further, processing alone by modifying CII morphology was able to increase these densities for CII.

Table IV-15. Powder Properties of CII, Spray-Dried Materials and Prosolv® SMCC 50 (silicified microcrystalline cellulose I).

Material	True density (g/cm^3)[a]	Moisture content (%)	Bulk density (g/cm^3)[a]	Tap density (g/cm^3)[a]	Hausner ratio[a]	Powder Porosity
	n=3	n=1	n=3	n=3	n=3	n=1
CII	1.54 ± 0.02	3.1	0.38 ± 0.03	0.54 ± 0.06	1.44 ± 0.05	0.76
SDCII	1.55 ± 0.01	2.8	0.55 ± 0.00	0.81 ± 0.01	1.46 ± 0.03	0.64
SD-CII:SiO_2(98:2)	1.55 ± 0.01	2.7	0.48 ± 0.01	0.73 ± 0.05	1.52 ± 0.08	0.69
SD-CII:SiO_2(95:5)	1.57 ± 0.00	3.1	0.45 ± 0.00	0.69 ± 0.03	1.53 ± 0.07	0.70
SD-CII:SiO_2(90:10)	1.60 ± 0.00	2.4	0.42 ± 0.01	0.66 ± 0.04	1.57 ± 0.13	0.73
SD-CII: SiO_2(80:20)	1.67 ± 0.00	2.8	0.36 ± 0.00	0.65 ± 0.02	1.79 ± 0.06	0.78
Prosolv® SMCC 50	1.56 ± 0.01	3.0	0.32 ± 0.00	0.44 ± 0.01	1.35 ± 0.02	0.79

Material	Degree Polymeriza-tion[a]	Molecular weight (g/mol)[a]	Specific surface area (m^2/g)	Flow rate (g/sec)[a]		
	n=5	n=5	n=3	(14.3 mm) n=3	(17.5 mm) n=3	(19.1mm) n=3
CII	78.6 ± 5.1	12731 ± 828	0.52 ± 0.06	1.2 ± 0.1	2.6 ± 0.1	3.3 ± 0.1
SDCII	79.1 ± 5.5	12820 ± 886	1.59 ± 0.04	1.4 ± 0.2	2.3 ± 0.5	4.0 ± 0.3
SD-CII:SiO_2(98:2)	85.5 ± 7.4	13844 ± 1199	3.94 ± 0.05	4.7 ± 0.1	5.5 ± 0.5	6.9 ± 0.7
SD-CII:SiO_2(95:5)	95.1 ± 4.9	15413 ± 797	10.46 ± 0.14	3.2 ± 0.0	5.8 ± 1.0	6.7 ± 1.0
SD-CII:SiO_2(90:10)	94.2 ± 8.2	15257 ± 1320	20.91 ± 0.36	2.4 ± 0.2	4.3 ± 0.1	4.7 ± 4.7
SD-CII: SiO_2(80:20)	85.1 ± 1.3	13790 ± 211	41.36 ± 1.43	1.1 ± 1.1	1.8 ± 0.1	2.2 ± 0.7
Prosolv® SMCC 50	191.7 ± 6.1	31061 ± 986	6.32 ± 0.05	2.4 ± 0.1	4.1 ± 0.2	5.5 ± 0.6

[a] Mean ± standard deviation.

Table IV-16. Powder Properties of CII, Wet granulated Materials and Prosolv® SMCC 90 (silicified microcrystalline cellulose I).

Material	True density (g/cm^3)[a]	Moisture content (%)	Bulk density (g/cm^3)[a]	Tap density (g/cm^3)[a]	Hausner ratio[a]	Powder Porosity
	n=3	n=1	n=3	n=3	n=3	n=1
CII	1.54 ± 0.02	3.1	0.38 ± 0.03	0.54 ± 0.06	1.44 ±.05	0.76
WGCII	1.56 ± 0.00	3.6	0.64 ± 0.01	0.79 ± 0.00	1.23 ± 00	0.59
WG-CII:SiO_2(98:2)	1.55 ± 0.01	3.0	0.61 ± 0.00	0.77 ± 0.00	1.27 ± 00	0.61
WG-CII:SiO_2(95:5)	1.57 ± 0.01	2.9	0.58 ± 0.00	0.72 ± 0.02	1.23 ± 00	0.63
WG-CII:SiO_2(90:10)	1.60 ± 0.00	3.0	0.55 ± 0.01	0.68 ± 0.02	1.24 ± 0.1	0.66
WG-CII: SiO_2(80:20)	1.66 ± 0.00	2.4	0.28 ± 0.00	0.36 ± 0.00	1.29 ± 00	0.83
Prosolv® SMCC 90	1.55 ± 0.00	3.3	0.28 ± 0.00	0.36 ± 0.00	1.29 ± 00	0.82

Material	Degree Polymeriza-tion[a]	Molecular weight (g/mol)[a]	Specific surface area (m^2/g)[a]	Flow rate (g/sec)[a]		
	n=5	n=5	n=3	(14.3 mm) n=3	(17.5 mm) n=3	(19.1 mm) n=3
CII	78.6 ± 5.1	12731 ± 828	0.52 ± 0.06	1.2 ± 0.1	2.6 ± 0.1	3.3 ± 0.1
WGCII	97.2 ± 1.4	15747.3 ± 229	0.39 ± 0.01	11 ± 1.1	16.7 ± 2.2	19.3 ± 0.1
WG-CII:SiO_2(98:2)	87.4 ± 4.7	14156 ± 754	1.12 ± 0.14	12.8 ± 1.5	17.7 ± 0.0	19.9 ± 0.1
WG-CII:SiO_2(95:5)	87.8 ± 2.6	14230 ± 419	6.63 ± 0.07	12.7 ± 1.1	15.2 ± 1.7	18.5 ± 0.0
WG-CII:SiO_2(90:10)	88.6 ± 6.6	14360 ± 1061	16.23 ± 0.10	9.5 ± 0.3	12.0 ± 1.1	15.7 ± 1.1
WG-CII: SiO_2(80:20)	76.9 ± 5.6	12455 ± 903	28.34 ± 1.29	9.4 ± 0.1	12.4 ± 0.1	15.9 ± 0.6
Prosolv® SMCC 90	206.4 ± 4.7	33441 ± 679	5.46 ± 0.01	5.9 ± 0.2	6.4 ± 0.4	8.2 ± 0.1

[a] Mean ± standard deviation.

Table IV-17. Powder Properties of CII, Spheronized Materials and CP-203® (spheronized microcrystalline cellulose I).

Material	True density (g/cm^3)[a]	Moisture content (%)	Bulk density (g/cm^3)[a]	Tap density (g/cm^3)[a]	Hausner ratio[a]	Powder Porosity
	n=3	n=1	n=3	n=3	n=3	n=1
CII	1.54 ± 0.02	3.1 ± 0.3	0.38 ± 0.03	0.54 ± 0.06	1.44 ± 0.05	0.76
SPCII	1.55 ± 0.01	2.1 ± 0.1	0.78 ± 0.01	0.90 ± 0.01	1.2 ± 00	0.50
SP-CII:SiO_2(98:2)	1.56 ± 0.01	2.6 ± 0.1	0.77 ± 0.00	0.91 ± 0.04	1.2 ± 0.1	0.50
SP-CII:SiO_2(95:5)	1.57 ± 0.00	1.4 ± 0.1	0.78 ± 0.02	0.88 ± 0.02	1.1 ± 0.0	0.51
SP-CII:SiO_2(90:10)	1.60 ± 0.00	2.2 ± 0.1	0.78 ± 0.01	0.89 ± 0.02	1.1 ± 0.0	0.51
SP-CII: SiO_2(80:20)	1.67 ± 0.01	2.3 ± 0.5	0.78 ± 0.01	0.87 ± 0.01	1.1 ± 0.0	0.53
CP-203®	1.50 ± 0.01	5.3 ± 0.0	0.86 ± 0.01	0.99 ± 0.03	1.1 ± 0.0	0.43

Material	Degree Polymeriza-tion[a]	Molecular weight (g/mol)[a]	Specific surface area (m^2/g)[a]	Flow rate (g/sec)[a]		
	n=5	n=5	n=3	(14.3 mm) n=3	(17.5mm) n=3	(19.1 mm) n=3
CII	78.6 ± 5.1	12731 ± 828	0.52 ± 0.06	1.2 ± 0.1	2.6 ± 0.1	3.3 ± 0.1
SPCII	74.4 ± 5.4	12045 ± 880	0.33 ± 0.02	13.6 ± 1.0	23.5 ± 0.6	31.7 ± 0.9
SP-CII:SiO_2(98:2)	80.2 ± 3.5	12996 ± 562	0.26 ± 0.03	17.4 ± 1.0	27.6 ± 1.3	32.4 ± 1.7
SP-CII:SiO_2(95:5)	71.7 ± 3.2	11613 ± 516	0.43 ± 0.03	19.7 ± 0.1	28.6 ± 0.1	40.5 ± 0.2
SP-CII:SiO_2(90:10)	79.7 ± 2.6	12913 ± 419	1.12 ± 0.43	15.4 ± 0.2	26.2 ± 0.4	39.8 ± 0.4
SP-CII: SiO_2(80:20)	70.8 ± 3.0	11466 ± 493	1.67 ± 0.02	8.0 ± 0.0	14.5 ± 0.0	22.7 ± 2.3
CP-203®	230.3 ± 5.3	37317 ± 865	0.16 ± 0.05	18.9 ± 1.0	30.3 ± 0.2	41.0 ± 0.2

[a] Mean ± standard deviation.

The spheronization process had a greater effect on these densities than silicification. Therefore, the rounded geometry and the large particle size played a major role on the bulk and tap densities making the CII particles denser. CP-203® had high bulk and tap densities suggesting that these two variables depend on the shape and size rather than the cellulose type. Conversely, CII and SD/WG:SiO_2(80:20) had the lowest bulk and tap densities due to the fibrous and high silicification degree, respectively. Since fumed silica has a reported ρ_{bulk} =0.03 g/cm^3 and ρ_{tap} =0.05 g/cm^3 (Jonat, 2005), the lowering effect of densities is not unexpected.

Densities of commercial products also depended on their morphology, with Prosolv® having the lowest and CP-203® the highest values, respectively. Reported values of bulk and tap densities are 0.35 g/cm^3 and 0.49 g/cm^3; and 0.36 g/cm^3 and 0.47 g/cm^3; and 0.87 g/cm^3 and 0.99 g/cm^3 for Prosolv® SMCC 50, Prosolv® SMCC 90, and CP-203®, respectively (Hou and Changquan, 2008).

The degree of frictional forces of powders is given by the Hausner ratio. This value was obtained from the ratio of the tap to bulk densities. High values indicate higher frictional forces in the powder to overcome and achieve powder densification (Hausner, 1967). The Hausner ratio increased as the level of silicification increased for spray-dried materials. This trend was not observed for the wet granulated and spheronized materials. Overall, particles produced by spray drying had higher Hausner ratios than those produced by wet granulation or spheronization. Since spray-dried particles and CII had Hausner ratios >1.4, they are considered cohesive with high interparticle forces. On the contrary, Prosolv® SMCC 50 was less cohesive. Commercial products had the same cohesiveness trend in the order: Prosolv® SMCC 50 > Prosolv® SMCC 90 > CP-203®. This suggests that cohesiveness depended mainly on particle size and density, rather than silicification. Furthermore, bulk and tap densities and particle size followed the trend

spheronized > wet granulated > spray-dried particles. As particle size increased, particles became less cohesive. Reported Hausner ratios for Prosolv® SMCC 50, Prosolv® SMCC 90 and CP-203®are 1.40, 1.31 and 1.14, respectively (Hou and Changquan, 2008).

The spray drying and wet granulation processes decreased the powder porosity of CII. This means that the fibrous nature of CII was transformed into particles with less voids spaces as discussed previously. Compared to SDCII and WGCII, which are unsilicified materials, the total powder porosity of the composites increased as the amount of SiO_2 increased, due to an increased coating on the surface of SDCII and also in the core of the WGCII granules. Prosolv® SMCC 50 and Prosolv® SMCC 90 had high powder porosity (0.79 and 0.82, respectively). Compared to SPCII, silicification had no effect on the porosity of the beads (~0.5). In this case, the spheronized process *per se* produced smooth beads preventing or correcting any roughness due to silicification.

Neither silicification nor processing produced a major change on the degree of polymerization (DP) of CII. Thus, DPs of 79- 95, 77-97 and 71-80 for the spray-dried, wet granulated and spheronized particles, respectively, were attained. This indicates that the relative viscosity measured for the CII dispersions for the DP tests was not affected by SiO_2. Hence, the resulting intrinsic viscosities and degree of polymerization remained virtually unchanged. Nonetheless, Prosolv® SMCC 50, Prosolv® SMCC 90 and CP-203® exhibited higher degrees of polymerizations than silicified materials, and as a result, their average molecular weights were higher too. It has been reported that cellulose I has a higher DP and molecular weight than CII (Klemm et al., 1998b) and a reported value of DP for Prosolv® SMCC is ~230 (Jumaa et al., 2000).

The specific surface area obtained by the linear BET analysis using N_2 as the adsorbate suggested that silicification increased the specific surface area (SSA) of CII. This is expected since fumed silica has a high surface area (200 m^2/g) (Jonat, 2005).

Spray drying was the most effective process to disperse SiO_2 onto the CII particles since it produced the largest values of SSAs. Spheronization produced the lowest SSAs probably due to the fact that the beads had low porosity, large sizes and a smooth surface. Wet granulated materials had SSAs intermediate between SDCII-SiO_2 and SPCII-SiO_2 particles. SSAs for Prosolv® SMCC 50 (4.92 m^2/g) and Prosolv® SMCC 90 (5.49 m^2/g) have also been reported (Steele et al., 2003).

The anisotropy of the pharmaceutical powders leads to differences in flow rates because flow depends on how cohesive forces and the interlocking structure of the powder affect flow. This characteristic is evidenced in measurements of powder flow rates. Tables IV-15 and 16 show the flow rates of spray-dried and wet granulated materials, respectively. The powder flow of silicified materials was measured at 14.3 mm, 17.5 mm and 19.1 mm orifice diameters. At 2% and 5% SiO_2 the best flow rate was observed when both processes are employed. In fact, these values were ~2-fold higher than that for CII. This indicates that partial surface coating is needed to ease flow. In this case, a low level of fumed silica is beneficial to avoid friction forces, or other particle interactions among CII particles. However, at high SiO_2 levels, particle interactions of fumed silica aggregates might be considerably high hampering flow. For instance, SD-CII:SiO_2(80:20) had very low flow rates due mainly to high porosity, low bulk and tap densities and more interparticle frictions. Likewise, the low flow rates of CII are explained by its fibrous nature producing particle interlocking, high porosity and low powder densities.

Thus, it is plausible that silicification levels >10% rendered low flow rates possibly due to detachment of SiO_2 clusters from the granule surfaces causing friction and cohesiveness and less densification preventing free particle flow. The small particle size plus the irregular aggregate structure and rough surface of Prosolv® SMCC 50 might

contribute to its poor flow. Further, Prosolv® SMCC 90 also had low flow rates respect to granules produced with or without silicification. Silicification and wet granulation of CII produced larger granules which had also larger bulk and tap densities than spray-dried materials favoring good powder flow.

The flow rates of the spheronized materials are presented in Table IV-17. These materials had the highest flow rates independent of orifice size. Flow rates were comparable to that of CP-203® and from one to 15-fold larger than CII. These results are not surprising since these particles had the largest bulk and tap densities which promote better flow. Other factors which contributed to flow were the smooth surface, larger size and low porosity. CP-203® exhibited similar flow rate values to silicified CII materials. Compared to the original CII (unprocessed), it is clear that both silicification and the particle processing methods improved flow rate. As seen for powder densities, the general trend for flow rates was: spheronization > wet granulation > spray drying.

Principal Component Analysis

There are several ways of reducing the dimensionality of a large set of data by means of linear projections and choosing projections, which preserves the structure of the data. The best way to do it is by using Principal Component Analysis (PCA), where the variance of the data is preserved. PCA identifies patterns in data and expresses the data in such a way as to highlight their similarities and differences. Patterns in data can be hard to find in graphs of high dimensions, but, PCA is able to summarize them by reducing the number of dimensions (usually to 2), without losing valuable information. Thus, PCA transforms the original data into two main axes (PC1 and PC2), which are perpendicular to each other. As a result, the data show patterns between them, where the patterns are the lines that most closely describe the relationships between the data. The PC1 vector is the direction on the abscissa along which projections that have the largest

variance. The second principal component (PC2) is the direction, which maximizes variance among all directions orthogonal to the first. The horizontal axis shows projections onto the first principal component, the vertical axis the second component. Every axis has a value associated with the magnitude of the vector. Minitab® software (v.16, Minitab®, State College, PA) was used for the PCA data analysis.

In this study, the PC1 had a variance of 6.5 and accounted for 50.3% of the total variance. The PC2 has a variance of 3.7 and accounts for 28.5% of the data variability. Thus, the first two principal components represent ~79% of the total data variability indicating that the most data structure can be captured into the two underlying dimensions studied.

The loading plot of measured properties is shown in Figure IV-45. The lines show projections of the original powder properties onto the PC1 and PC2 using the coordinate scales on the abscissa and ordinate axes, respectively. The loadings can be understood as the weights for each original property when calculating the principal component. The x-axis explains the maximum amount of variation in the data set. This plot is the result of the linear combination of original data that maximizes data variance. For this reason, the numbers on the axis are arbitrary units. Further, each point (property) in the graph indicates the contribution of this property in defining these components. Properties contributing very little to the components have small loading values and are plotted near the center of the plot. On the other hand, properties which contribute most are plotted around the borders of the plot. The loading plot shows that all of the original variables have comparable importance for the description of the first two principal components (no loading vector has a near-zero element for both principal components).

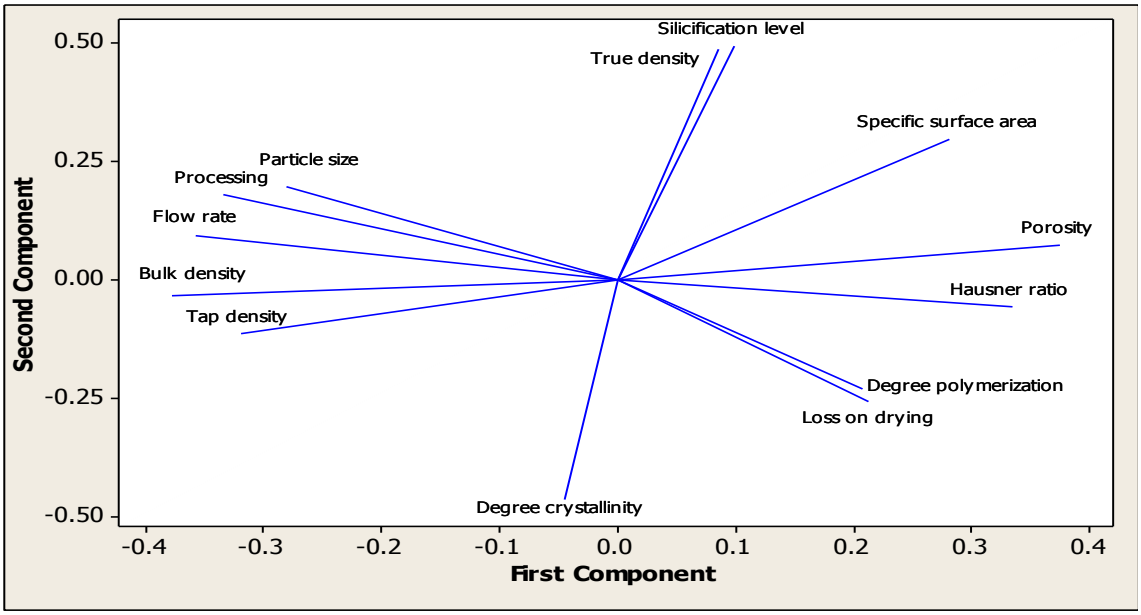

Figure IV-45. Loading Plot of Measured Properties of CII and CII-SiO_2 Composites.

By looking at the plot, it can be seen that the processing formed a data set cluster with particle size, flow rate and bulk and tap densities vectors indicating they are highly correlated. In other words, these properties mainly depended on the type of processing employed for manufacturing (spray drying, wet granulation, or spheronization). On the other hand, flow rate, bulk and tap densities vectors were almost directly opposite to the porosity and Hausner ratio vectors indicating an inverse correlation. This means that if the powder porosity or Hausner ratio are increased, powder densities will be expected to decrease accordingly. Therefore, one can look at this plot and quickly conclude which variables are correlated with each other and which are not. For instance, silicification was correlated with true density and in a lower degree with the specific surface area of the materials indicating that increments of SiO_2 will be reflected in increases of these powder properties. On the contrary, silicification had a negative influence on the degree of crystallinity of the samples.

Figure IV-46 shows the PCA score plot of the materials. The scores plot of the two principal components contains the original data in a rotated coordinate system. This plot was able to classify the variability of the data set according to the processes depicted by three colored lines: red, blue and green, corresponding to the spheronization, wet granulation and spray drying process, respectively. The first component separates the spheronized from the spray-dried and wet granulated materials. The PC2 shows a decreasing trend of the powder properties with increasing silicification levels, since SiO_2 increased from the top to bottom in the graph.

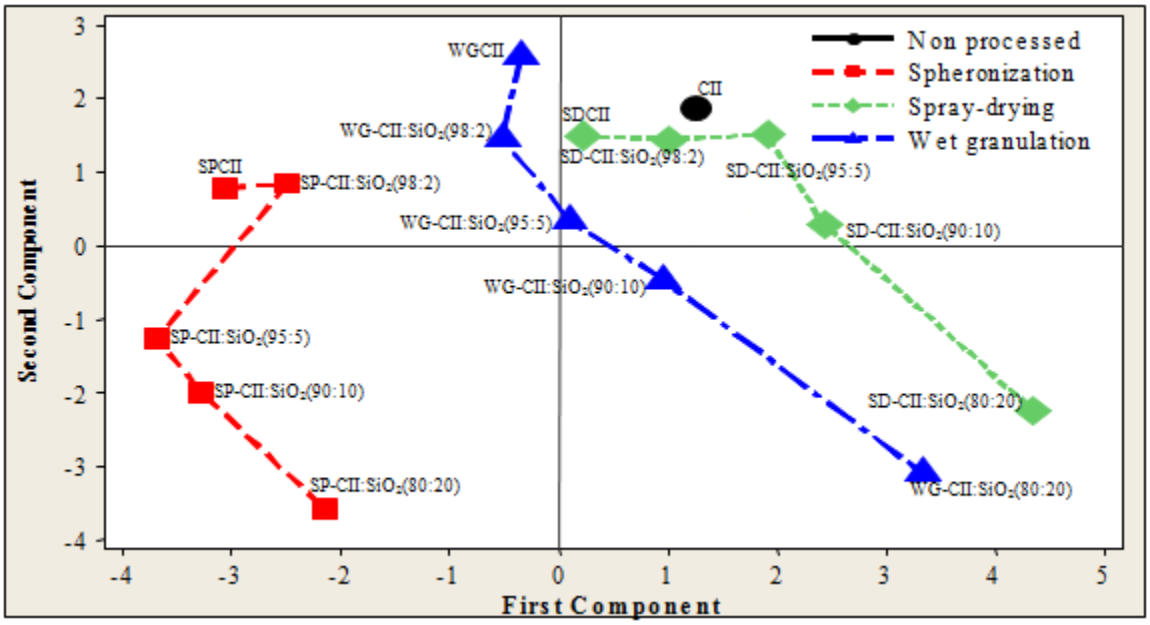

Figure IV-46. PCA Score Plot of Measured Properties of CII and CII-SiO_2 Composites.

This plot also shows that most of the powder properties of CII, SDCII (spray-dried cellulose II), WGCII (wet granulated cellulose II) and their silicified materials up to 5% levels were comparable independent of the process employed. Likewise, SPCII (spheronized cellulose II) and SP-CII:SiO_2(98:2) showed comparable powder properties. Since the last three points in each curve showed a linear decrease, the degree of change in magnitude of the powder properties is constant to levels higher than 5%, being especially high for the spray-dried and wet granulated materials.

Water Sorption Characteristics

Water activity is related to the equilibrium moisture content of a material in a non-linear relationship known as a moisture sorption isotherm curve. In this study, moisture sorption isotherms were obtained at 25ºC and the data were fitted to the GAB equation. This equation was has the same assumptions of the BET model and was derived independently by Guggenheim (1966), Anderson (1946) and de Boer (1953) from a physical sorption model related to the BET (Brunauer, Emmet, and Teller) theory (Brunauer et al., 1940).

The GAB model has three constants - monolayer capacity (m_m), energy constant of monolayer sorption (C) and energy constant of multilayer sorption (k), and generally fits the entire sorption isotherm. Thus, it differs from the BET model for water sorption which is used to fit data from 0 to 0.4 water activity. The GAB equation is widely used among food scientists since it well fits sorption data for natural polymers at all water activity values (Van den Berg, 1984). This model dissects water sorption into three types of water - tightly bound water, less tightly bound water and bulk water while the BET would only dissect water sorption data into two types of water – tightly bound and bulk water. Thus, the GAB equation includes less tightly bound water which can be water that is absorbed into the polymer rather only being adsorbed at a surface.

It should be noted that the term "specific surface area" can be used only when water is not absorbed into the interior of the polymer which may cause structural changes like swelling (Zografi et al., 1984).

Figures IV-47 and IV-48 show the GAB experimental curves for water sorption, and Table IV-18 and IV-19 show the parameters derived from the GAB model for the spray-dried and wet granulated materials, respectively. Since CII is *per se* a hydrophilic material, the monolayer sorption capacity (m_m) indicates that only at the 20% level of silicification the affinity of CII for water decreased. Thus, it required up to 20% SiO_2 to equal the monolayer capacity as that of Prosolv® SMCC 50 (which contains only 2% SiO_2) because cellulose I is much less hydrophilic than cellulose II. The reduction in the monolayer sorption capacity value due to a 20% silicification was also seen in the wet granulated products (Table IV-19).

Further, although this model can estimates the energetic of the monolayer and multilayer, the resulting values will be used only for comparative purpose, since only direct measurements from calorimetry studies will give a more accurate description of these values (Sadeghnejad et al, 1986). The energy constant of monolayer sorption "C" and the resulting energetic of monolayer formation (H_1-H_m) did not change significantly with silicification. Likewise, the energy constant of multilayer sorption "k" and the energetic of the multilayer sorption were not altered with silicification (0.8 and 0.55 kJ/mol, respectively). The "k" parameter indicates the energetic difference between the liquid molecules and multilayer molecules. Since the model assumes that the multilayer molecules are less tightly bound than the bulk liquid molecules, "k" will be always less than unity (Feng, 2007).

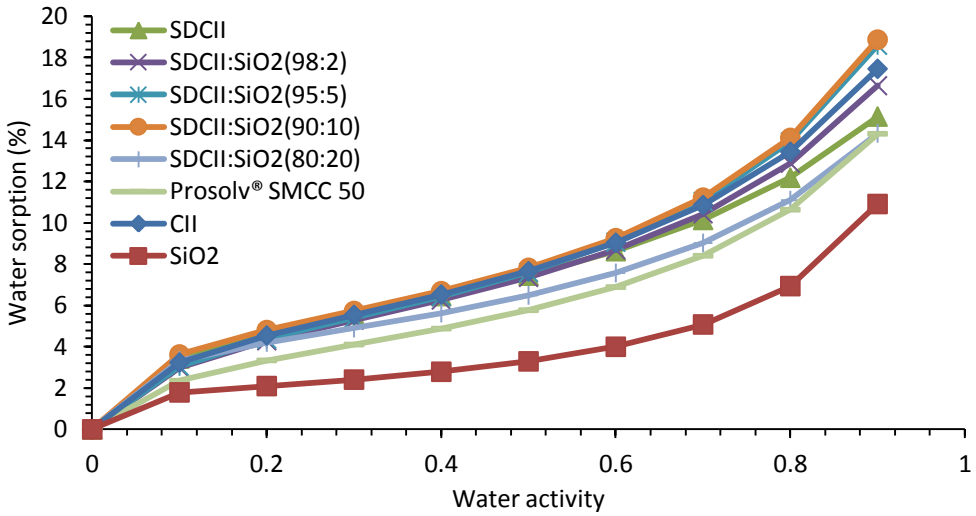

Figure IV-47. Fitted Water Sorption Isotherms of the Spray-Dried Materials According to the GAB Model.

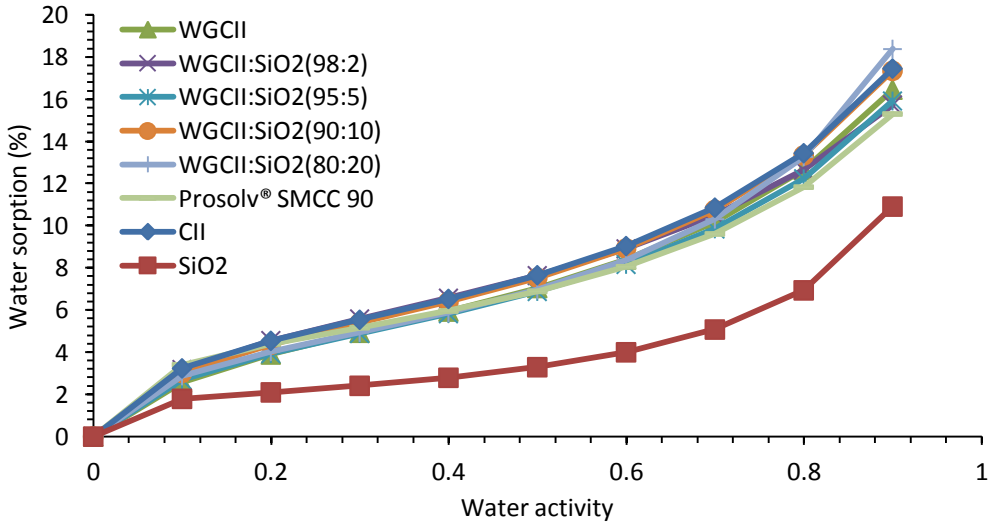

Figure IV-48. Fitted Water Sorption Isotherms of the Wet Granulated Materials According to the GAB Model.

Tablet IV-18. Parameters Obtained from the GAB Model for the Spray-Dried Materials and Prosolv® SMCC 50 (silicified microcrystalline cellulose I).

Sample	Hysteresis (%)	m_m ± SD[a*] (g/g)	C± SD[b*]	k±SD[c*]
CII	0.3	0.05 ± 0.00	16.9 ± 1.9	0.8 ± 0.0
SDCII	0.8	0.05 ± 0.00	21.3 ± 1.7	0.8 ± 0.0
SD-CII:SiO_2(98:2)	1.4	0.05 ± 0.00	14.9 ± 0.6	0.8 ± 0.0
SD-CII:SiO_2(95:5)	1.4	0.05 ± 0.00	14.9 ± 6.6	0.8 ± 0.0
SD-CII:SiO_2 (90:10)	1.5	0.05 ± 0.01	24.3 ± 3.7	0.8 ± 0.1
SD-CII:SiO_2 (80:20)	1.3	0.04 ± 0.00	35.6 ± 1.8	0.8 ± 0.0
Prosolv® SMCC 50	1.2	0.04 ± 0.00	15.8 ± 2.6	0.8 ± 0.0
Sample	(% RH monolayer®)[d]	r^2	H_m-H_L[e*] (kJ/mol)	H_1-H_m[f*] (kJ/mol)
CII	30	0.9993	0.55 ± 0.0	7.0 ± 1.6
SDCII	25	0.9988	0.55 ± 0.0	7.6 ± 1.3
SD-CII:SiO_2(98:2)	30	0.9993	0.55 ± 0.0	6.7 ± 0.0
SD-CII:SiO_2(95:5)	25	0.9987	0.55 ± 0.0	6.7 ± 4.7
SD-CII:SiO_2 (90:10)	25	0.9967	0.55 ± 0.0	7.9 ± 3.5
SD-CII:SiO_2 (80:20)	30	0.9967	0.55 ± 0.0	8.9 ± 1.5
Prosolv® SMCC 50	40	0.9994	0.55 ± 0.0	6.8 ± 2.4

*Mean of three replicate ± standard deviation.

[a] Monolayer capacity.

[b] Monolayer energetic.

[c] Multilayer energetic.

[d] Energy constant for multilayer formation.

[e] Energy constant for monolayer formation.

Tablet IV-19. Parameters obtained from the GAB Model for the Wet Granulated Materials and Prosolv® SMCC 90 (silicified microcrystalline cellulose I).

Sample	Hysteresis (%)	m_m± SD[a*] (g/g)	C± SD[b*]	k± SD[c*]
CII	0.3	0.05 ± 0.00	16.9 ± 1.9	0.80 ± 0.0
WGCII	2	0.05 ± 0.00	11.3 ± 4.0	0.80 ± 0.0
WG-CII:SiO_2(98:2)	1.4	0.05 ± 0.00	15.5 ± 3.3	0.80 ± 0.0
WG-CII:SiO_2(95:5)	1.4	0.05 ± 0.01	13.6 ± 2.3	0.80 ± 0.0
WG-CII:SiO_2 (90:10)	1.5	0.05 ±0.01	14.4 ± 2.4	0.80 ± 0.0
WG-CII:SiO_2 (80:20)	1.3	0.04 ± 0.01	16.8 ± 4.8	0.90 ± 0.0
Prosolv® SMCC 90	1.6	0.04 ± 0.00	29.9 ± 3.4	0.80 ± 0.0
Sample	(% RH monolayer®)[d]	r^2	H_m-H_L[e*] (kJ/mol)	H_1-H_m[f*] (kJ/mol)
CII	30	0.9993	0.55 ± 0.0	7.0 ± 1.6
WGCII	30	0.9982	0.55 ± 0.0	6.0 ± 3.4
WG-CII:SiO_2(98:2)	25	0.9992	0.55 ± 0.0	6.8 ± 3.0
WG-CII:SiO_2(95:5)	30	0.9992	0.55 ± 0.0	6.5 ± 2.1
WGCII:SiO_2 (90:10)	25	0.9997	0.55 ± 0.0	6.6 ± 2.2
WG-CII:SiO_2 (80:20)	30	0.9998	0.26 ± 0.0	7.0 ± 3.9
Prosolv® SMCC 90	30	0.9980	0.55 ± 0.0	8.4 ± 3.0

*Mean of three replicate ± standard deviation.

[a] Monolayer capacity.

[b] Energy constant for monolayer formation.

[c] Energy constant for multilayer formation.

[d] Relative humidity for monolayer formation.

[e] Multilayer energetic.

[f] Monolayer energetic.

For this reason, as seen for the spray-dried materials, in wet granulated products H_1-H_m > H_m-H_L indicating that the energetic for the formation of a monolayer was more favorable than multilayer, and the latter was more weakly attached. This confirms the assumptions of a first tightly bound layer and subsequent less tight bound layers made in this model.

Enthalpy values of Prosolv® SMCC 50 were in the same range as those observed for silicified materials, indicating no contribution due to the polymorphic form of cellulose on the energetic of sorption. Further, Prosolv® SMCC 50 and Prosolv® SMCC 90 had comparable m_m values (0.04 g water/g material). Reported m_m values for Avicel® PH-101, Avicel® PH-102, Prosolv® SMCC 50 and Prosolv® SMCC 90 of 0.04, 0.04, 0.04 and 0.04 g water/g cellulose, respectively, indicating that a 2% silicification in cellulose I virtually does not change the hydrophilic properties of this material (Airaksinen et al., 2005). Both Prosolv® materials are obtained from the same softwood source and produced by spray drying. Despite of the fact that CII was treated by wet granulation along with silicification at different levels, the monolayer capacity results were about the same (0.05 g/g) except for a 20% silicification (0.04 g/g). This means that the hydrophilic properties of these composites were independent of the process employed but did depend on the polymorphic form of cellulose.

Figure IV-49 and Table IV-20 show the GAB isotherms and the fitting parameters of the GAB model for the spheronized products. CP-203®, which is a cellulosic I material, presented the highest "m_m" (0.15), lowest multilayer constant "k" (0.6), and lowest monolayer constant "C" (1.0), indicating a high affinity for water. In comparison, SiO_2 showed the lowest "m_m" (0.02), highest "k" (0.9) and highest "C" (100) values, indicating a low affinity for water compared to CP-203® and silicified materials.

Figure IV-49. Fitted Water Sorption Isotherms of the Spheronized Materials According to the GAB Model.

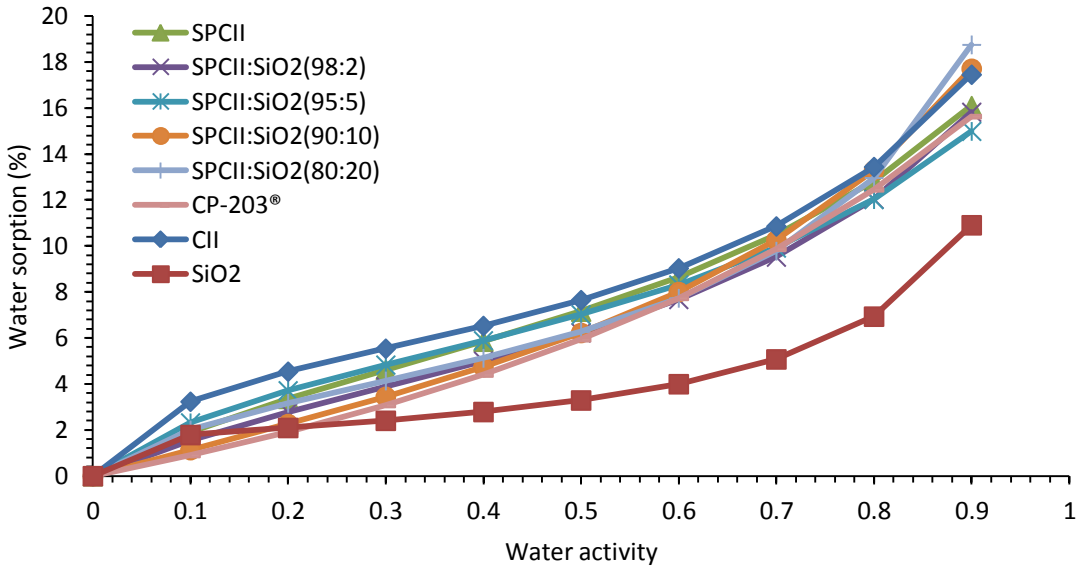

Tablet IV-20. Parameters Obtained from the GAB Model for Spheronized Materials and CP-203® (spheronized microcrystalline cellulose I).

Sample	Hysteresis (%)	m_m ± SD[a*] (g/g)	C± SD[b*]	k±SD[c*]
CII	0.3	0.05 ± 0.00	16.9 ± 1.9	0.8 ± 0.0
SPCII	0.8	0.06 ± 0.00	4.3 ± 1.7	0.7 ± 0.1
SP-CII:SiO_2(98:2)	2.1	0.05 ± 0.01	4.7 ± 0.8	0.8 ± 0.0
SP-CII:SiO_2(95:5)	1.3	0.06 ± 0.00	8.5 ± 0.9	0.7 ± 0.0
SP-CII:SiO_2 (90:10)	2.2	0.06 ± 0.00	2.3 ± 0.8	0.8 ± 0.1
SP-CII:SiO_2 (80:20)	2.2	0.04 ± 0.00	8.6 ± 0.1	0.9 ± 0.0
CP-203®	1.8	0.15 ± 0.01	1.0 ± 0.1	0.6 ± 0.1
SiO_2	-0.6	0.02 ± 0.00	100.0 ± 0.0	0.9 ± 0.0
Sample	(% RH monolayer®)[d]	r^2	H_m-H_L[e*] (kJ/mol)	H_1-H_m[f*] (kJ/mol)
CII	30	0.9993	0.55 ± 0.0	7.0 ± 1.6
SPCII	40	0.9960	0.77 ± 0.1	3.6 ± 1.3
SP-CII:SiO_2 (98:2)	40	0.9968	0.55 ± 0.0	3.8 ± 0.5
SP-CII:SiO_2 (95:5)	40	0.9961	0.77 ± 0.0	5.3 ± 0.4
SP-CII:SiO_2 (90:10)	50	0.9967	0.55 ± 0.1	2.1 ± 0.6
SP-CII:SiO_2 (80:20)	30	0.9998	0.26 ± 0.0	5.3 ± 0.0
CP-203®	90	0.9897	1.39 ± 0.1	0.0 ± 0.0
SiO_2	10	0.9842	0.17 ± 0.0	11.4 ± 0.0

*Mean of three replicate ± standard deviation.

[a] Monolayer capacity.

[b] Energy constant for monolayer formation.

[c] Energy constant for multilayer formation.

[d] Relative humidity for monolayer formation.

[e] Multilayer energetic.

[f] Monolayer energetic.

This is explained by its limited hydrogen bonding capacity compared to that of cellulosic products. These results indicate that CP-203® is so hydrophilic that the H_1-H_m energetic was very small indicating complete formation of a monolayer and multilayer with close energetics. It is more likely that most of the water was first absorbed within the particle and further incoming water molecules formed monolayer and multilayers. Conversely, dry fumed silica has a reported silanol group density of ~2 silanol/nm^2, and possibly had limited hydrogen bonding formation between the few silanol groups and water (Jonat et al., 2004). However, fumed silica presented in the CII:SiO_2 composites has already been exposed to water during the manufacturing process and hence is expected to have a larger silanol group density. It has been reported a larger silanols group density (~5 silanol/nm^2) for fumed silica stored at high relative humidities (Wang and Wunder, 2000). Thus, fumed silica is more likely to have a silanol group density > 2 OH/nm^2 in the CII:SiO_2 composites. In the manufacturing of the composites implies a mixture of the components in a wet state, in this step it is most likely that more silanols groups are formed in fumed silica and interact with CII. This might explain why only 20% silicification and not lower levels reduced the affinity of CII for water.

The estimated energetic constants can be used to compare energy values of the materials studied. The energetic of the monolayer varied as fumed silica (11.4 kJ.mol) > silicified materials > CP-203® (0.0 kJ/mol) and the energetic of the multilayer varied as CP-203® (1.39 kJ/mol) > silicified materials > SiO_2 (0.17 kJ/mol). Since fumed silica had the largest value, water is bound to the monolayer more strongly and thus, the difference between H_1-H_m will be the largest (11.4 kJ/mol). On the contrary, H_m-H_L was the lowest (0.17 kJ/mol) indicating a low interaction of multilayer molecules with the substrate and these molecules will be less firmly bound. Since the "k" value for fumed silica was close to 1 (0.95), there was almost no distinction between multilayer molecules

and liquid water, or could be interpreted to imply that the multilayer molecules are not completely structured in layers but have some characteristics as liquid water. Further, since the "C" constant of monolayer formation was the largest for fumed silica and the lowest for CP-203®, water molecules are strongly bound to the substrate in the former and less firmly attached to CP-203®. In this material, water is organized in a monolayer and water molecules in the multilayer are strongly structured, in which the water molecules do differ considerably from the bulk liquid water.

Hysteresis is defined as the difference between the amount of water desorbed and sorbed, respectively. This difference creates a loop in the isotherm and is very common for hydrophilic materials. The percentage of hysteresis between desorption and sorption isotherms was found by subtracting the desorption area from the sorption area multiplied by 100. Most materials showed a hysteresis degree of 0.3-2.2% indicating large desorption areas for the cellulosic materials. The higher moisture content obtained when a polymer is desorbing from a saturated state is due to microcapillary deformation accompanied by the creation of more permanent hydrogen bonds which are no longer attainable in subsequent re-wetting processes. This phenomenon is known in cellulose as hornification. Thus, when cellulose sorbs water it swells slightly because microcapillaries expand due to the motion of incoming water molecules forming new internal surfaces. Once water is removed, relaxation of the matrix to the original state is partially prevented. As a result, microcapillaries become greater on desorption compared to the adsorption step as reported previously (Parker et al., 2006). Conversely, this capillary deformation did not occur for fumed silica since the desorption isotherm was smaller than the sorption.

Figure IV-50 shows the change in the specific surface area obtained by the BET method with silicification. The specific surface area increased with silicification, but the

magnitude of increase varied with processing. The relationship between silicification degree and specific surface area seems to follow a linear relationship in which the slope indicates the silicification magnitude produced in each process and varied as: spray drying > wet granulation > spheronization. In this case, surface area appears to be inversely related to particle size and surface smoothness. Further, spheronized materials had the lowest porosity values and lowest specific surface area.

Ideally, the optimum moisture content for storage of pharmaceutical materials these materials should never exceed the monolayer water coverage. In the monolayer, water is in a tightly bounded state. It has been reported that this bound water is an integral part of the amorphous regions of cellulose (Zografi et al., 1984). In this scenario, the optimum relative humidity needed for a complete monolayer ranged from 20 to 30% for the spray-dried and wet granulated products altogether. On the contrary, spheronized products had complete monolayer coverage in a wider range (30-50%). This behavior might be due to the larger size and low porosity and low crystallinity of the beads since the amorphous regions required a higher relative humidity for absorbing and adsorbing water.

Fumed silica, on the contrary, due to the few silanol groups, required a very low relative humidity for a complete monolayer formation with these sorption sites, whereas CP-203®, due to the large amorphous content and hence, adsorption sites available required a high relative humidity.

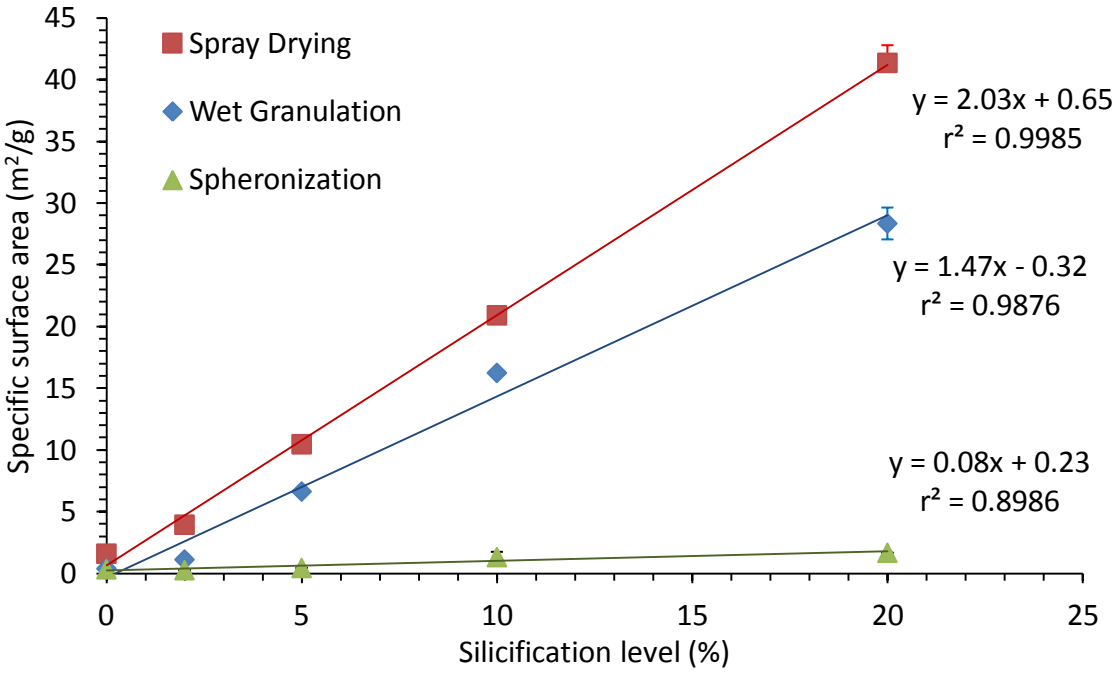

Figure IV-50. Effect of Silicification on the Specific Surface Area of CII-SiO_2.

Swelling Studies

Swelling values of the spray-dried materials in distilled water at 25°C are shown in Figure IV-51. SDCII and the material with 2% SiO_2 had comparable swelling values (~1 mL/g). However, the addition of 5-20% SiO_2 decreased swelling. A 20% SiO_2 rendered a comparable swelling to Prosolv® SMCC 50, which was the least swelling (0.25 mL/g). Swelling reduction with silicification has also been observed for microcrystalline cellulose I. For example, Avicel® PH-101 showed swelling values of 4.8 mL/g, whereas Prosolv® SMCC 50 showed a swelling value of 4.3 mL/g (Luukkonen, 2001).

The swelling values of the wet granulated materials are shown in Figure IV-52. Compared to WGCII, silicification up to 10% maintained the swelling values at ~0.65 mL/g. However, at a 20% swelling decreased to ~0.45 mL/g, which was comparable to the value obtained for Prosolv® SMCC 90. Compared to the spray-dried materials, the swelling value of the wet granulated products was below the 0.7 mL/g mark, possibly due to the so called hornification phenomenon produced by the wet granulation process which makes the material less swellable. This phenomenon happens during the drying process of cellulose in which the water hydrogen bonds are replaced by cellulose-cellulose interchain hydrogen bonds. Some of these hydrogen bonds could not reopen again upon the addition of further water (Luukkonen, 2001). Even though a 20% SiO_2 rendered materials with high porosity (0.78 and 0.83, for the spray-dried and wet granulated material, respectively), the high CII-SiO_2 interaction reduced its swelling ability.

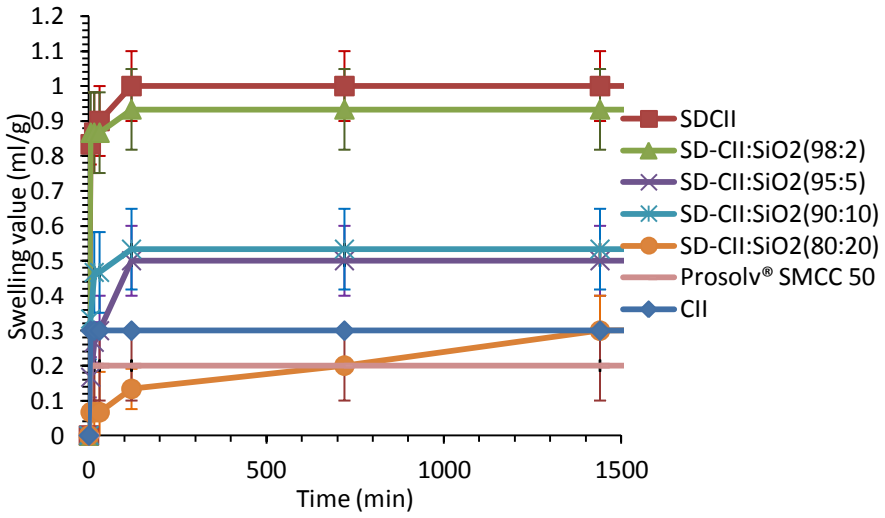

Figure IV-51. Swelling Values of CII, Spray-Dried CII:SiO_2 Materials and Prosolv® SMCC 50 (silicified microcrystalline cellulose I).

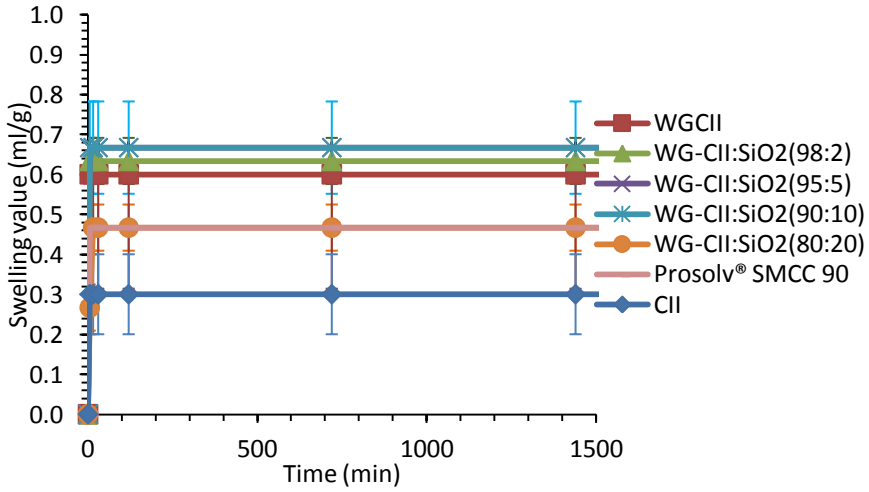

Figure IV-52. Swelling values of CII, Wet Granulated CII:SiO_2 Materials and Prosolv® SMCC 90 (silicified microcrystalline cellulose I).

The swelling values of the spheronized materials are shown in Figure IV-53. The spheronization process caused a two-fold increase in the swelling values compared to CII. CP-203® swelled as much as the spheronized materials since the former was highly hygroscopic as seen in the water sorption isotherms.

Opposed to the spray-dried and wet granulated materials, silicification levels higher than 10% had no major effect on the swelling values of SPCII due to the large swelling already achieved. In the spheronized products, the two separate trends indicate that the swelling behavior was more process-dependent, rather than silicification dependent. Likely, the very low crystallinity produced by this process allows water to penetrate in the pores of the surface, and perhaps, between the cellulose chains having a swelling which is independent of silicification. As seen for the spray-dried and wet granulated products, swelling of spheronized cellulose II materials is a fast process (~5 min), reaching an equilibrium (a plateau in the curve) within 5 min.

Tableting Properties

Compaction Characteristics

The compact tensile strength curves for the spray-dried materials obtained by the Leuenberger model are shown in Figure IV-54. In all cases, silicification caused an increase in compact tensile strength. Further, the compact tensile strength increased with increasing applied pressure, but the degree of increase varied with silicification. In this case, a 5% silicification exhibited the highest tensile strength.

On the contrary, unsilicified materials such as, SDCII and CII compacts showed the lowest tensile strength. These results indicate that fumed silica reinforced the compact strength of CII. Table IV-16 shows the parameters obtained from the Leuenberger model for compactibility. These parameters include compression susceptibility (γ_c), maximum tensile strength (T_{max}) and area under the tensile strength curve (AUTSC).

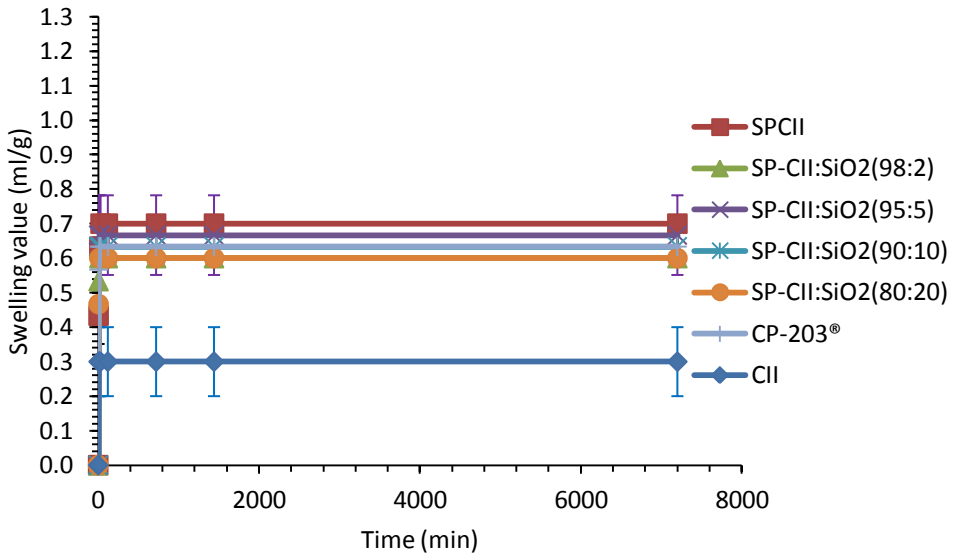

Figure IV-53. Swelling Values of CII, Spheronized Materials and CP-203® (spheronized microcrystalline cellulose I).

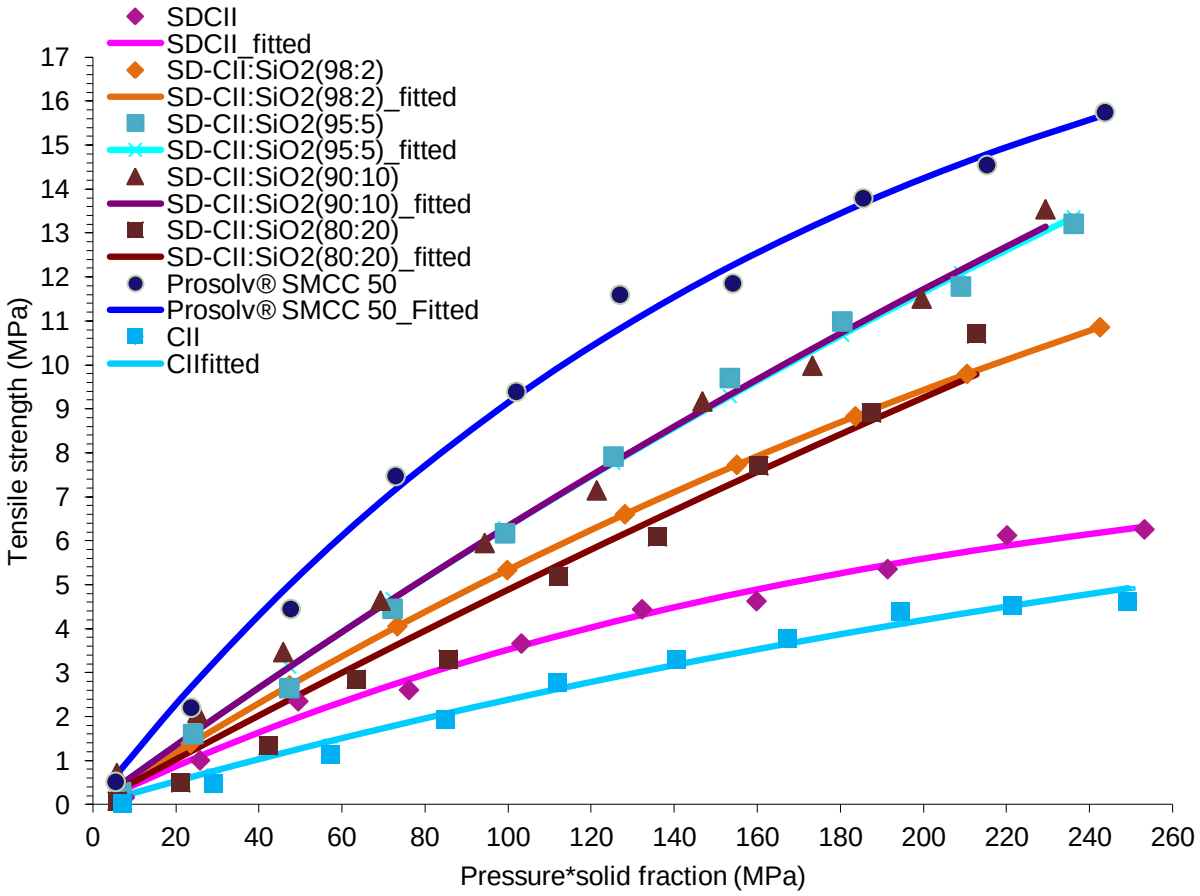

Figure IV-54. Tensile Strength of Compacts Made of CII, Spray-Dried CII:SiO_2 Materials and Prosolv® SMCC 50 (silicified microcrystalline cellulose I).

Tablet IV-16. Parameters from the Leuenberger Model for CII, Spray-Dried and Wet Granulated CII:SiO_2 and Prosolv® (silicified microcrystalline cellulose I) Materials*.

Sample	AUTSC[a] (MPa^2)	T_{max}[b] (MPa)	γ_c[c] (MPa^{-1})	r^2	CI[d] (%)	TS[e] (%)	Energy at break[f] ($J*10^{-2}$)
CII	680.5	9.9	0.003	0.9835	0.0	0.5 ±0.0	0.3 ± 0.0
SD-CII: SiO_2(80:20)	1082.5	47.0	0.001	0.9841	59.1	7.7 ± 0.0	5.8 ± 0.5
SD-CII: SiO_2(90:10)	1596.0	42.0	0.002	0.9937	134.5	6.0 ± 0.0	4.6 ± 0.4
SD-CII:SiO_2(95:5)	1683.2	40.0	0.002	0.9960	147.3	4.5 ±0.0	3.9 ± 0.3
SD-CII:SiO_2(98:2)	1460.0	22.7	0.003	0.9924	114.5	3.6 ±0.0	2.9 ± 0.7
SDCII	969.0	8.5	0.005	0.9895	42.4	2.5 ±0.0	1.0 ± 0.0
Prosolv® SMCC 50	2348.7	20.7	0.006	0.9939	N.A.	7.5 ± 0.0	14.8 ± 3.9
WG-CII: SiO_2(80:20)	632.7	51.8	0.001	0.9721	-7.0	4.4 ± 0.0	3.7 ± 1.0
WG-CII: SiO_2(90:10)	1038.9	42.6	0.001	0.9769	52.7	3.4 ± 0.0	3.0 ± 0.0
WG-CII:SiO_2(95:5)	885.0	42.2	0.001	0.9890	30.1	2.2 ± 0.0	2.6 ± 0.5
WG-CII:SiO_2(98:2)	835.2	20.2	0.002	0.9627	22.7	1.2 ± 0.0	1.4 ± 0.2
WGCII	1023.8	10.7	0.004	0.9835	50.4	1.2 ± 0.0	1.0 ± 0.1
Prosolv® SMCC 90	2229.8	21.6	0.005	0.9986	N.A.	6.9 ± 0.0	7.6 ± 0.5

[a] Area under the curve of the tensile strength.

[b] Theoretical maximum tensile strength.

[c] Compressibility parameter.

[d] Compactibility increase, based on the AUTSC.

[e] Tensile strength of compacts made at 0.2 porosity.

[f] Measured at 0.2 porosity, obtained from the load deformation curves.

* This model is given by: $TS = T_{max}*[1 - e^{(-\gamma_c * P * \rho_r)}]$, where P and ρ_r correspond to the compressive pressure and compact solid fraction, respectively.

The γ_c constant is related to the compressibility of the material. The higher the γ_c value, the faster the plateau in the curve is reached with increasing applied pressure. Highly plastic deforming materials, such as Prosolv® SMCC 50, exhibited the highest compression susceptibility (0.006 MPa^{-1}) and a plateau in the curve was reached sooner than for silicified materials. For this reason, the less plastic deforming silicified materials showed lower γ_c values (less than 0.005 MPa^{-1}) and their plots were less curved and hence, this model predicted a higher maximum tensile strength (T_{max}) values for silicified materials at infinite compression pressure (solid fraction of 1). In this case, silicification makes the rate of change of tensile strength with porosity and compression pressure slower and hence, no plateau was seen in the range of pressures used. The AUTSC indicates the overall compactibility degree and ranked as: Prosolv® SMCC 50 > SDCII:SiO_2 (95:5) > SDCII:SiO_2(90:10) > SDCII:SiO_2 (98:2) > SDCII:SiO_2(80:20) > SDCII > CII.

Figure IV-55 depicts the relationship between the radial tensile strength and the product of applied pressure and solid fraction for Prosolv® SMCC 90 and wet granulated products, according to the Leuenberger model (Leuenberger and Rohera, 1986). The fitting parameters are listed in Table IV-16. Different from the spray-dried materials, a 10% silicification rendered compacts with the highest tensile strength (~7 MPa) at a P*SF of 250 MPa. However, this value was not as high as the one maximum achieved by SD-CII:SiO_2 (95:5) (~13.5 MPa). As seen for the spray-dried materials, the theoretical maximum tensile strength (T_{max}) for the wet granulated materials increased as SiO_2 increases, being the highest for WG-CII:SiO_2(80:20).

Compared to WGCII, the compressibility parameter (γ_c) decreased as the level of silicification increased. In this case, the CII plasticity decreased as the level of silicification increased (given by a low γ_c).

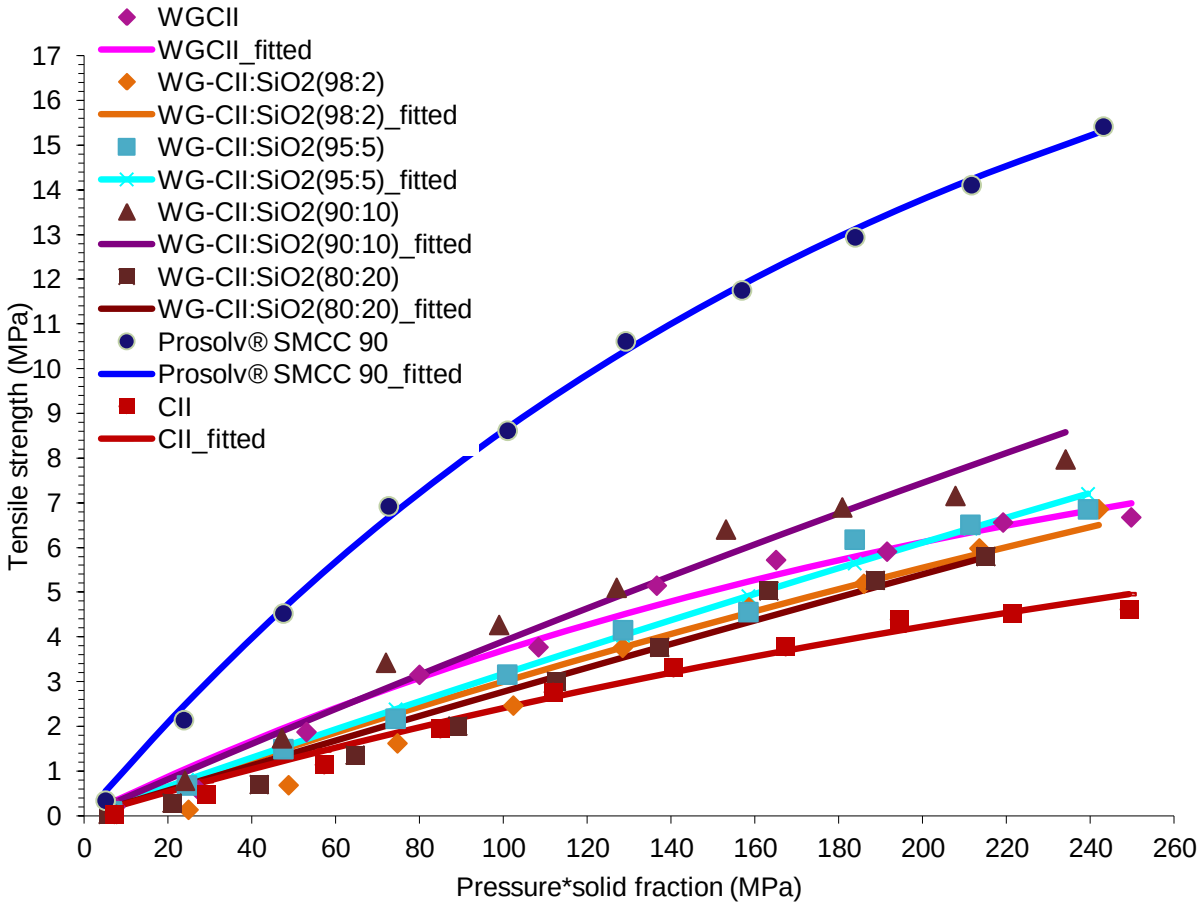

Figure IV-55. Tensile Strength of Compacts Made of CII, Wet Granulated CII:SiO_2 Materials, Prosolv® SMCC 90 (silicified microcrystalline cellulose I).

That is, from 0.005 MPa^{-1} to 0.001 MPa^{-1} and from 0.004 MPa^{-1} to 0.001 MPa^{-1} for spray-dried and wet granulated materials, respectively. Prosolv® SMCC 50 and Prosolv® SMCC 90, on the contrary, had high γ_c values of 0.006 MPa^{-1} and 0.005 MPa^{-1}, respectively proving their high plasticity. The area under the curve of tensile strength ranked compactibility of wet granulated materials as: Prosolv® SMCC 90 > WG-CII-SiO_2(90:10) > WGCII > WG-CII-SiO_2(95:5) > WG-CII-SiO_2(98:2) > CII > CII-SiO_2(80:20).

The above results indicate that silicification contributed largely to compactibility due to the modification of the particle surface roughness especially for the spray-dried products. However, silicification in wet granulated materials not only increased surface roughness, but SiO_2 could also be present inside the granules contributing to the overall granule properties. It is possible that during consolidation the increasing levels of fumed silica particles in the powder bed causes an initial large rearrangement due to SiO_2 deaggregation and probably extensive fragmentation of the particles in which small fumed silica particles fill in the void spaces between the large CII particles. At large compression pressures, more deaggregation, creation of new surfaces and movement of fumed silica particles along with the CII crystal planes dislocating may cause a larger compact rigidity than that produced by CII alone. However, the degree of compact strength varied depending on the process used, indicating that the presence of fumed silica inside the granules could make particles weak. Thus, a large surface formation is needed for particle binding, and these granules, rather than breaking, are deformed plastically without releasing all of the SiO_2 particles. Moreover, silicification levels > 10% creates a high compact porosity and thus, a larger compression pressure is needed to attain comparable porosities to SDCII and WGCII. As a result, a very rigid compact will be obtained with a larger compactibility than CII.

Surprisingly, the mere morphology modification of CII by spray drying and wet granulation also improved its compactibility (42.4% vs. 50.4% increase, respectively). The slight increase in the plastic behavior could be responsible for this finding. However, this increase was not as prominent as the one caused by a 5 and 10% silicification in spray-dried and wet granulated materials, respectively.

Figure IV-56 shows the relationship between compact crushing strength and compression pressure for silicified materials made by spheronization. In this case, a 5% silicification rendered compacts with the highest strength. However, this strength was not as high as the one achieved by CII. In fact, SP-CII:SiO_2 (95:5) compacts made at a pressure of 120 MPa were 2.4 times weaker than CII, but 21 times stronger than compacts made of CP-203®. Although it is evident than all silicified materials produced stronger compacts than those made from CP-203®, the resulting compacts were not as strong as the one achieved by CII. This could be explained by the regular semispherical and smooth surface of the beads. These characteristics might limit the surface area increase and formation of sufficient contact points needed for particle consolidation and binding under pressure, and these characteristics along with deformation are needed to form strong compacts. If a poorly compactable drug is added to these composite materials, they are expected to produce more friable compacts than those produced by CII, or perhaps very high compression forces will be needed to prepare a compact of a relative good strength. For this reason, the spheronized, silicified materials are not recommended as the first choice for direct compression and hence, further studies of the mechanical properties of these materials were not attempted.

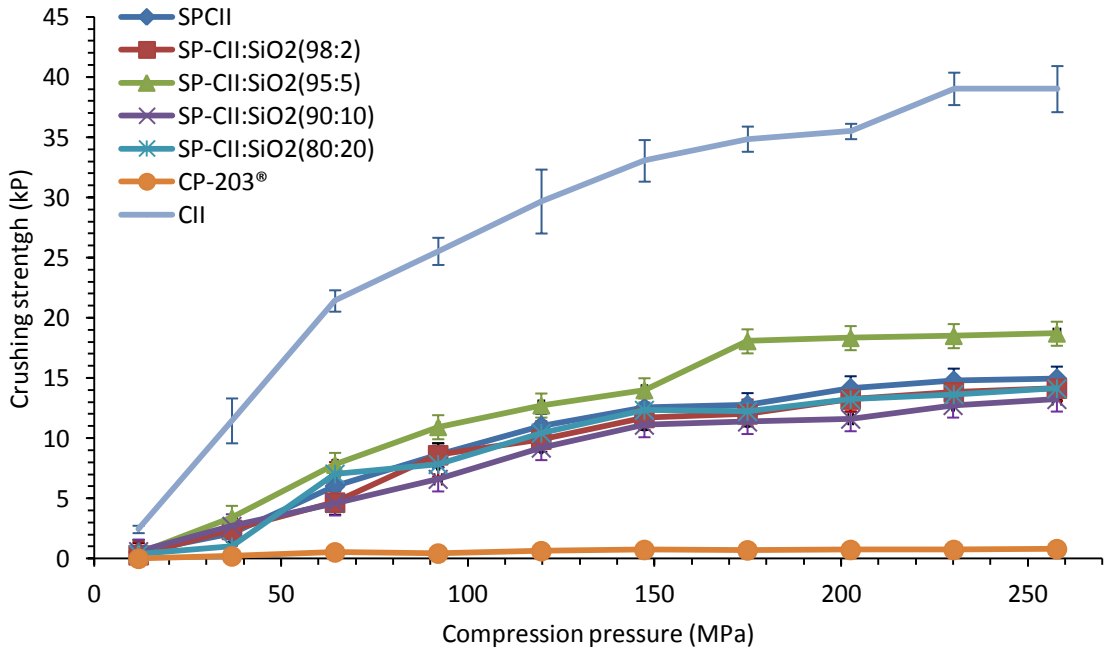

Figure IV-56. Crushing Strength of Compacts Made of CII, Spheronized CII:SiO_2 Materials and CP-203® (spheronized microcrystalline cellulose I).

Load-Deformation Curves and Diametrical Compression Test

The strength of a compact is described as its ability to withstand external forces without breaking. A load-deformation curve is a graphical representation of the relationship between the load applied to the compact and its deformation. It represents the degree of deformation of the compact when it is diametrically compressed (Rowe and Roberts, 1995). Figures IV-57 and IV-58 compare the load-deformation curves for the spray-dried, wet granulated and commercial products compacts made at 120 MPa. A large curve indicates high compact load resistance that is reflected on a high deformation before breaking occurred.

All silicified materials showed a lower deformation at break and lower breaking strength than Prosolv® SMCC 50 and Prosolv® SMCC 90. Further, all compacts are considered to have low plasticity since, beyond the elastic region of the load-deformation curves, compact broke without reaching strengths and deformations as those reported for highly plastic materials such as hydroxypropyl cellulose (HPC) (Skinner, 1998). Conversely, complete brittle materials do not show any plastic deformation but fail immediately after the elastic region.

Prosolv® SMCC 50, which was the most plastically deforming material also had the largest deformation at break (~0.5 mm). CII, on the contrary, exhibited the lowest deformation at break (0.18 mm) and load strength (0.03 kN), but it was not the least plastic deforming material. Silicified materials showed deformation values in between (0.18-0.5 mm). Results indicate that compared to CII, silicification increased the magnitude of deformation and strength of the compacts. However, there was not a direct relationship between silicification and compact strength/deformation due to the different compact porosities shown by the compacts made at 120 MPa.

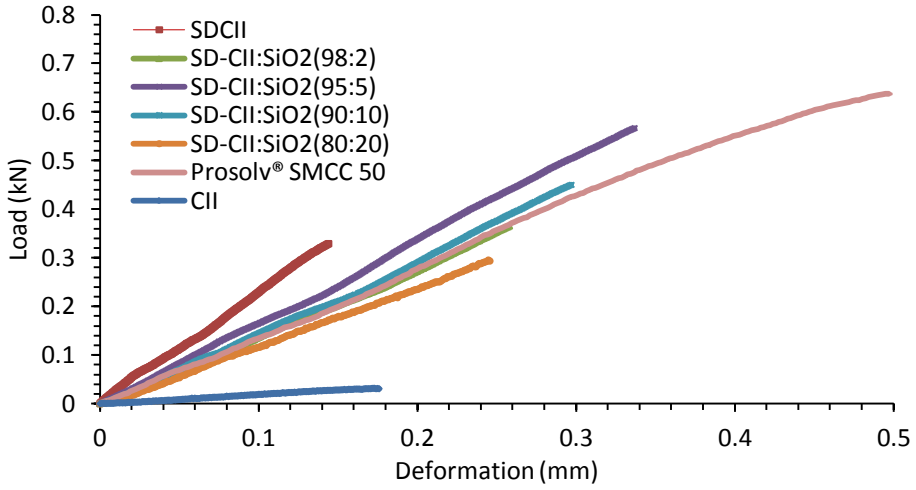

Figure IV-57. Load-Deformation Curves of CII, Spray-Dried CII:SiO_2 Materials and Prosolv® SMCC 50 (silicified microcrystalline cellulose I) Compacts Made at 120 MPa.

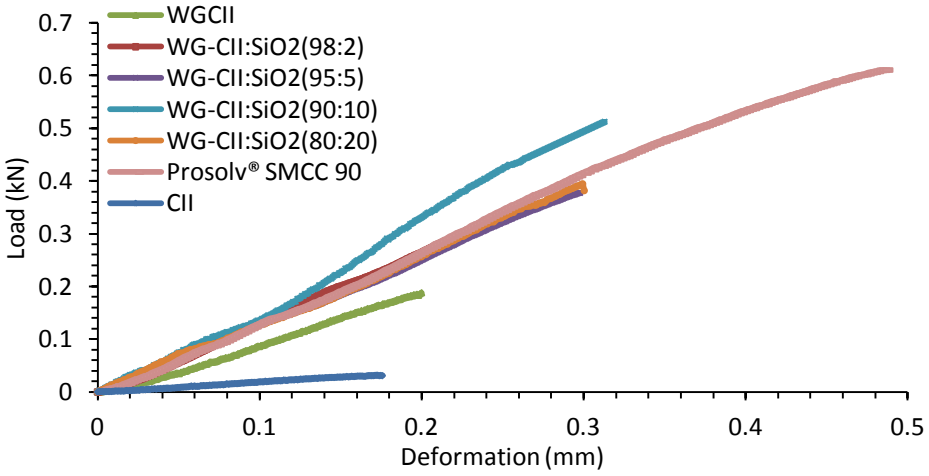

Figure IV-58. Load-Deformation Curves of CII, Wet Granulated CII:SiO_2 Materials and Prosolv® SMCC 90 (silicified microcrystalline cellulose I) Compacts Made at 120 MPa.

Thus, at this compression pressure, a 5% silicification achieved a compact with the maximum strength, followed by a strength decrease at larger silicification levels. Further, it is clear that the increase in strength given by silicification to CII also implies a deformation increase in the compacts.

Figure IV-58 shows that Prosolv® SMCC 90 had the largest deformation among wet granulated materials (0.5 mm). Moreover, silicification also increased both deformation and compact strength. For the wet granulated silicified materials, a 10% silicification rendered the highest deformation at break (~0.3 mm) and strength (~0.52 kN). In fact, these materials showed the same trend as discussed previously for compactibility (Table IV-16).

Comparing curves of Figures IV-57 and IV-58, in general, spray-dried materials showed higher compactibility in terms of load than wet granulated products. This finding was accompanied with an increase in compact deformation and can be attributed to modifications in particle size and morphology and particle interactions of CII with SiO_2. The small spray-dried particles render compacts of larger compactibility than the large wet granulated particles. This phenomenon could be explained by the increase in surface area which is related to a large creation of contact points among the particles. Particle morphology also contributed to tensile strength although this effect was less pronounced than particle size since compactibility of spray-dried materials was higher than wet granulated products. Further, spray-dried particles were more regularly-shaped than wet granulated materials. Irregular particles usually have a considerable contribution to compact strength perhaps due to the rough surface which eases formation of more contact points between particles than more smooth particles. For instance, WGCII which showed a granule with a rough surface formed stronger compacts than SDCII which had a smoother surface. Furthermore, spheronized pellets, which were highly spherical,

presented the poorest values in compact strength due to the reduced contact points between the particles.

The compact energy at break made at 0.2 porosity is shown in Table IV-16. This calculation is based on the AUC of the load-deformation curves. The stronger the compact, the higher the energy required to break it. Compacts of Prosolv® SMCC 50 and Prosolv® SMCC 90 required the highest energy at break followed by the silicified materials. It has also been reported an energy at break for Prosolv® SMCC 90 compacts of 2 J having 25 mm diameter and 6 g of weight along with a deformation of 0.96 mm and tensile strength of 11.1 MPa (Edge et al., 2000). It is reasonable that a more plastic material requires a higher energy to dislocate the crystal planes and ultimately cause a tablet failure than the energy needed for the less plastic deforming silicified materials. Wet granulated materials showed lower energy at the break values compared to spray-dried materials. Thus, in terms of compact strength, spray drying was the most effective method in producing a material with the best mechanical properties.

However, silicification and hence, partial brittleness was necessary to increase compact strength to some degree. Thus, independent of the process employed, silicification increased compactibility. This can be explained by the increasingly bulky character of CII powder with silicification, and upon compression this produced more porous compacts than unsilicified materials made at the same compression pressure. For this reason, compactibility increased to some SiO_2 level and then decreased due to its increasing contribution on compact porosity. Moreover, if all compacts are made at the same porosity, silicified materials required higher compression forces to achieve a comparable porosity than unsilicified CII. The resulting effect is that particles have better contact points due to the increased surface area available for bonding and as a result, compacts will be stronger.

Compression Characteristics

Heckel Analysis

The fundamentals of this model are briefly explained on pages 27 and 70. The linear region of these plots was determined by the number of data points that rendered the largest r^2. This method is better than selecting an arbitrary region from 50 to 150 MPa for all materials independent of the resulting r^2. Although this model was originally derived for metals, which were highly ductile, it could be used with discretion to characterize the densification behavior of pharmaceutical powders. In fact, the use of this model in these types of soft powders has been criticized. First, Heckel considered the linear region attributed to plastic deformation and considered the elastic deformation to be negligible. Further, he assumed the transition from the curve region due to particle rearrangement (absence of particle bonding) to the linear region as the minimal pressure to form a coherent compact. This assumption might be true for metals, but not necessary holds for pharmaceutical powders (Sonnergaard, 1999).

The yield pressure value, P_y, which Heckel referred as the inverse of the slope of the linear portion of the curve for metals was found to be approximately 3 times their yield stress (Heckel, 1961b). He found that a material with a lower P_y value is expected to be more ductile. The following discussion was made assuming the Heckel assumptions holds for the cellulosic materials studied. For this reason, discretion is advised for the data interpretation. Figures IV-59 and IV-60 depict the Heckel curves and Table V-17 lists the Heckel parameters for the spray-dried and wet granulated materials, respectively.

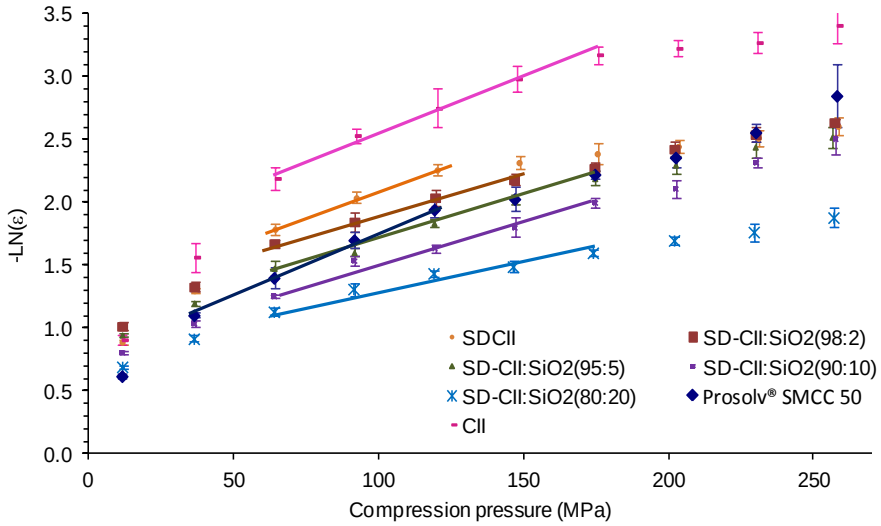

Figure IV-59. Heckel Plots for CII, Spray-Dried Materials and Prosolv® SMCC 50 (silicified microcrystalline cellulose I).

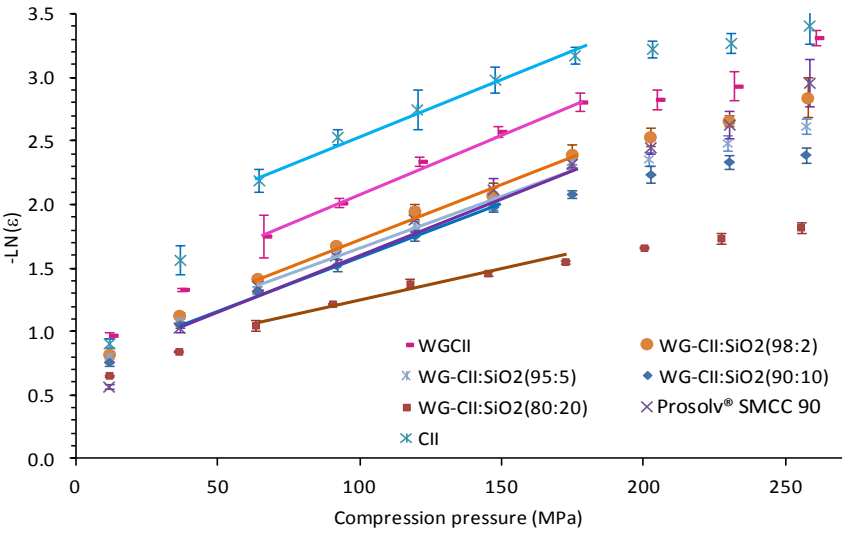

Figure IV-60. Heckel Plots for CII, Wet Granulated Materials and Prosolv® SMCC 90 (silicified microcrystalline cellulose I).

Table IV-17. Heckel Parameters for CII, Spray-Dried and Wet Granulated CII:SiO_2 Materials and Prosolv® (silicified microcrystalline cellulose I).

Product	Pressure Range (MPa)	Heckel parameters[e]					
		P_y (MPa)	A[a]	D_0[b]	D_a[c]	D_b[d]	r^2
CII	65-175	115	1.68	0.24	0.81	0.57	0.9880
SDCII	65-120	119	1.25	0.36	0.72	0.36	0.9990
SD-CII:SiO_2(98:2)	65-150	150	1.28	0.31	0.72	0.41	0.9972
SD-CII:SiO_2(95:5)	65-175	161	1.03	0.29	0.64	0.37	0.9940
SD-CII:SiO_2(90:10)	65-175	179	1.00	0.26	0.63	0.37	0.9810
SD-CII: SiO_2(80:20)	65-175	182	0.78	0.22	0.54	0.32	0.9888
Prosolv® SMCC 50	35-120	98	0.74	0.21	0.52	0.31	0.9976
WGCII	65-175	91	0.98	0.41	0.62	0.21	0.9917
WG-CII:SiO_2(98:2)	65-175	102	0.78	0.39	0.54	0.15	0.9994
WG-CII:SiO_2(95:5)	65-175	112	0.77	0.37	0.54	0.17	0.9967
WG-CII:SiO_2(90:10)	35-150	120	0.77	0.34	0.53	0.19	0.9990
WG-CII: SiO_2(80:20)	65-175	147	0.59	0.17	0.45	0.28	0.9957
Prosolv® SMCC 90	35-175	108	0.74	0.18	0.52	0.34	0.9949

[a] Powder total densification (obtained from the intercept).

[b] Relative density due to die filling (obtained from bulk density/true density).

[c] Total compact densification (obtained from $D_a = 1 - \exp^{-A}$).

[d] Relative density due to particle rearrangement/fragmentation (obtained from $D_b = D_a - D_0$).

[e] Heckel curve is given by: $\mathrm{Ln}\frac{1}{\varepsilon} = m\sigma + A$, where ε, σ, m and A corresponds to the compact porosity, compression pressure, slope and intercept, respectively.

Compared to CII and SDCII (P_y of 115 MPa and 119 MPa, respectively). , all silicified materials exhibited larger P_y values possibly due to the SiO_2 contribution This phenomenon might be caused by the SiO_2 aggregates; once compression starts, these particles deaggregate and rearrange around CII probably decreasing the apparent plastic deformation taking place in the powder bed.

The D_o value, which indicates the initial packing ability of the material in the die, suggests that as the amount of SiO_2 in the composite increases, the packing ability of CII decreases due to decreasing densification tendency. This result is in agreement with the trends observed for the bulk and tap densities (Table IV-15). Furthermore, both CII and Prosolv® SMCC 50 exhibited a low packing tendency similar to that of SDCII:SiO_2(80:20). These results are consistent considering the very low bulk density and high porosity of these materials (ρ_{bulk}, 0.32-0.38 g/cm^3 and porosity, 0.76-0.79). The parameters D_a and D_b represent the total packing and the extent of powder bed arrangement due to particle fragmentation/rearrangement at low pressures, respectively. The results shown in Table IV-17 indicate that total densification and densification by die filling (D_a and D_0, respectively) of the materials decreased as the silicification level increased. Interestingly, the fiber-like shape of CII seems to have a large effect on D_a since this material showed the largest D_b suggesting that these fibers were able to rearrange extensively, filling up the interparticle voids in the powder bed at low pressures (*vide supra*), and consequently, packed better at low applied pressures. Except for SDCII, the rearranging behavior (D_b) of silicified spray-died CII materials and Prosolv® SMCC 50 was more prevalent than the simple packing behavior (given by the D_o values). This indicates that at low pressures silicification caused particles to deaggregate extensively and rearrange/fragment in the powder bed.

Heckel parameters of the wet granulated materials are shown in Table IV-17, and the Heckel plots are depicted in Figure IV-60. Compared to WGCII, all silicified materials showed higher P_y values (91 MPa vs. 102-147 MPa), suggesting that silicification could increase brittleness in the powder bed due particle rearrangement and deaggregation of fumed silica aggregates. The process employed *per se* caused changes in the P_y value of CII. For instance, CII had a higher P_y than WGCII, but comparable P_y than SDCII. This indicates that the deformation mechanism is not altered for CII if a rapid drying is conducted as opposed to wet granulation. Perhaps part of water used during wet granulation process is not completely given up upon slow drying and hence, this non-free water could induce some apparent plasticity in CII.

Prosolv® SMCC 90 which has a 2% SiO_2 had a P_y of 108 MPa, which was higher than that of Avicel® PH-102 (73.5 MPa). Typical P_y values for cellulose I materials are between 40 to 80 MPa as reported previously (Reus, 2005; York, 1992). The yield pressure value for cellulose I materials such as Prosolv® SMCC 50 was 93 MPa. This value was close to 89.1 MPa, reported previously (Kiekens et al., 2004). Researchers have reported that a 2% SiO_2 in cellulose I virtually does not affect P_y (Habib et al., 1999; Van Veen et al., 2005).

As seen for the spray-dried materials, the total initial compact densification (D_a) decreased significantly at the 20% silicification level due to the decreasing powder densification. Moreover, the D_0 parameter, which represents the degree of initial powder packing, decreased progressively from 0.41 to 0.17 upon silicification, whereas D_b increased. For this reason, compared to spray-dried powders, wet granulated materials, due to their larger size and high particle densities, had a more prevalent densification by die filling than densification by particle rearrangement, except for the 20% silicification.

Compared to the spray-dried materials, wet granulated materials had lower D_b and P_y values, indicating that they undergo less powder rearrangement/fragmentation, probably due to their larger particle size. Likewise, D_a values of spray-dried materials were larger than those obtained for wet granulated materials, suggesting spray drying induced a high powder densification, especially due to rearrangement/fragmentation. Further, when P_y was larger than 147 MPa in silicified CII materials, D_b was larger than D_0 indicating extensive rearrangement/fragmentation taking place within the powder bed.

Kawakita Analysis

The Kawakita model describes the variation of powder volume reduction with compression pressure in a linear relationship. In this case, the inverse of the slope called "a" corresponds to the volume reduction ability of the material, whereas from the intercept the "b" parameter is obtained, and represents the ease of compression. This model is briefly discussed in pages 30 and 71. The Kawakita plots for the spray-dried materials are depicted in Figure IV-61 and the Kawakita parameters are given in Table IV-18. The compressibility parameter "a" indicates that silicification enhanced the compressible character of the materials. This could be attributed to lowering densification caused by silicification forming more void spaces between particles. Further, the "a" parameter and the total powder porosity were comparable, as reported previously (Denny, 2002). For example, CII, SD-CII-80:20, and Prosolv® SMCC 50, had bulk densities of 0.38 g/cm^3, 0.36 g/cm^3, and 0.32 g/cm^3, respectively, which translated in a high compressibility ("a" value of 0.76, 0.76, and 0.78, respectively), and porosity values (0.76, 0.78, and 0.79, respectively).

On the other hand, as discussed previously, SDCII was the least compressible material due to its high bulk density, low porosity, more regular and smoother particle surface and less fragmenting behavior. The "1/b" value obtained from the Kawakita

analysis has been related to cohesion and other type of particle interaction forces (Kuhl and Jobst, 2002; Yamashiro et al., 1983). The lowest "1/b" parameter obtained for CII suggests a low degree of interparticle interactions that oppose volume reduction, and hence, this material was the easiest to compress (volume reduction) by applied pressure. All spray-dried materials, in contrast, showed high "1/b" values (5.9 to 8.3), indicating more interparticle interactions to overcome during compression due to the combined effect of silicification and the high densification caused by spray drying.

The results presented in Table IV-18 and Figure IV-62 also show the Kawakita parameters and plots for the wet granulated materials, respectively. The "a" compressibility value progressively increased with silicification, indicating a high volume reduction with silicification, as discussed previously. It is plausible that SiO_2 aggregates rearrange and fragment in the powder bed around CII particles, leading to improved packing. Powder porosity and "a" values were comparable and inversely related to the bulk density as seen for the spray-dried materials. The "1/b" values decreased slightly with silicification especially at the 20% level suggesting that this material was the easiest to compress. Conversely, low "1/b" values were observed for spray-dried materials since there was a complete SiO_2 particle coating favoring powder compression. Therefore, for wet granulated materials, a larger degree of interparticulate interaction has to be overcome in order to get the same degree of volume reduction than spray drying. This behavior is in part due to the resulting large particle size and irregular shape.

Silicification increased the ejection forces of the upper punch in the spray-dried (0.38-0.85 kN) and wet granulated materials (0.28-0.87 kN).

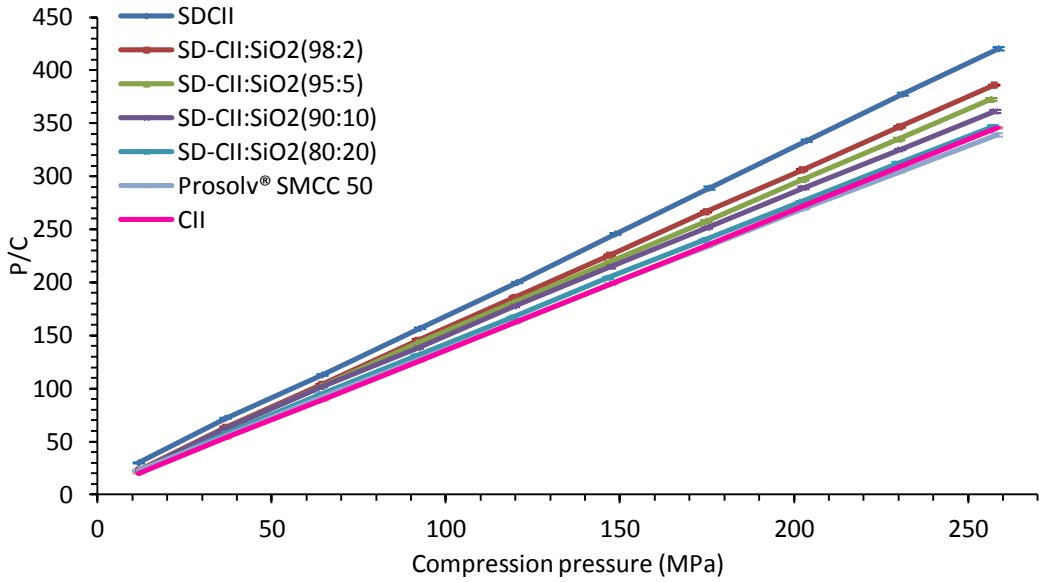

Figure IV-61. Kawakita Plots for CII, Spray-Dried Materials and Prosolv® SMCC 50 (silicified microcrystalline cellulose I).

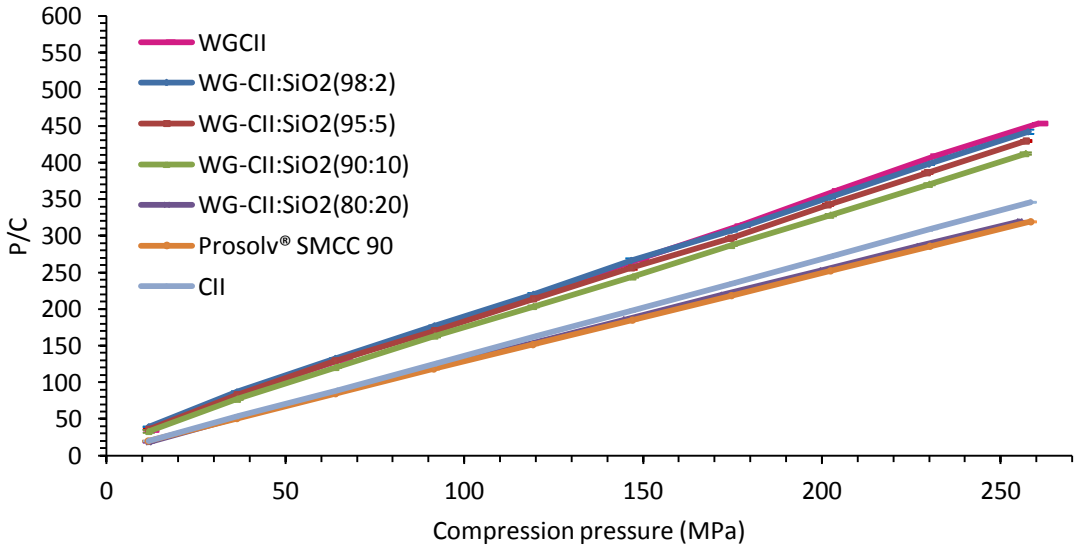

Figure IV-62. Kawakita Plots for CII, Wet Granulated Materials and Prosolv® SMCC 90 (silicified microcrystalline cellulose I).

Table IV-18. Kawakita Parameters for CII, Spray-Dried and Wet Granulated CII:SiO_2 Materials and Prosolv® (silicified microcrystalline cellulose I).

Product	Ejection Force (kN) n=3	Powder porosity	Pressure Range (MPa)	Kawakita Parameters[c]		
				a	1/b	r^2
CII	0.24 ± 0.02	0.76	90-175	0.76	3.2	1.0000
SDCII	0.59 ± 0.06	0.64	65-120	0.63	7.1	0.9999
SD-CII:SiO_2(98:2)	0.38 ± 0.05	0.69	65-150	0.68	5.9	0.9999
SD-CII:SiO_2(95:5)	0.46 ± 0.03	0.70	65-175	0.70	7.1	0.9999
SD-CII:SiO_2(90:10)	0.51 ± 0.05	0.73	90-175	0.73	8.3	0.9995
SD-CII: SiO_2(80:20)	0.85 ± 0.04	0.78	65-120	0.76	6.7	0.9998
Prosolv® SMCC 50	0.04 ± 0.01	0.79	35-125	0.78	6.7	1.0000
WGCII	0.61 ± 0.06	0.59	65-175	0.60	11.1	0.9998
WG-CII:SiO_2(98:2)	0.28 ± 0.03	0.61	35-120	0.62	16.7	0.9996
WG-CII:SiO_2(95:5)	0.33 ± 0.05	0.63	35-175	0.63	14.3	0.9995
WG-CII:SiO_2(90:10)	0.73 ± 0.05	0.66	35-150	0.65	12.5	0.9997
WG-CII: SiO_2(80:20)	0.87 ± 0.05	0.83	11-120	0.81	5.3	0.9999
Prosolv® SMCC 90	0.10 ± 0.02	0.82	90-175	0.83	5.6	1.0000

[a] Compressibility parameter (dimensionless).

[b] Measure of agglomerate shear strength during compression (dimensionless).

[c] Obtained from: $P/(1-\rho_0/\rho_a) = P/a + 1/ab$, where P, ρ_0,and ρ_a, correspond to compression pressure, bulk and compact apparent densities, respectively.

This is attributed to the frictional forces between the die wall and the brittle character of SiO_2. The addition of a lubricant should be considered for such materials. On the other hand, cellulose I materials such as Prosolv® exhibited the lowest friction, attributable to their known high plastic deforming ability and low surface area. Cellulose I materials also had high "a" compressibility values and a low degree of interparticle interactions "1/b" indicating ease of compression and thus, required lower applied compression pressures to produce a significant volume reduction. Reported data give "a" values of 0.71 and 0.80 for Prosolv® SMCC 90 and Prosolv® SMCC 50, respectively (Zhang et al, 2003).

It is well known that at the microscopic level, surface of the compacts is never completely flat and smooth, including the lateral section directly contacting the die wall. For this reason, fumed silica, which caused an increase in particle surface area and especially SiO_2 aggregates located at the compact sides, is more likely to deaggregate and create friction causing perpendicular resistant forces, impeding the axial ejection of the compact. On the other hand, the addition of a lubricant can fill the gaps between the detached fragments and reduce the contact points between the compact and the die wall surfaces easing compact ejection and decreasing die wear due to abrasion.

Compact Elastic Recovery

Elastic recovery occurs when part of the energy applied for compaction instead of causing permanent plastic or brittle deformation is released in the form of elastic rebound. In this case, the agglomerate particles expand while releasing this elastic energy leading to axial volume increase in the compact and thus, particle structural features such as lattices and dislocations move to new positions. In some cases, the original shape of the particles is partially recovered. This compact relaxation could be accompanied by the formation of microcracks which increases the separation of particles

and the amount of void space ultimately decreasing compact strength and possibly causing lamination or capping. The elastic recovery of spray-dried and wet granulated compacts is depicted in Figures IV-63 and IV-64, respectively. The data represent only the out-of-die results for compacts immediately released from the die and are compared to the respective height five days after storage under Drierite® in a desiccator at room temperature. For this reason, these data only represent the slow time-dependent elastic recovery since the in-die fast elastic component was not determined due to technical limitations.

Silicification reduced the elastic relaxation tendency of CII and this tendency was more pronounced at high silicification levels and high compression pressures. Perhaps, silicification, by increasing surface area and particle rearrangement in the powder bed, allowed more permanent particle bonding preventing energy release from CII bonded particles.

The reduction of elastic recovery was more efficient in spray-dried materials than in wet granulated products suggesting that when SiO_2 is coating completely CII particles, a stronger compact is formed due to the resulting high surface area available for bonding. Further, a low elastic recovery behavior was also characteristic for cellulose I products since they formed stronger compacts with virtually no variation of this property with compression pressure.

Lubricant Sensitivity to Magnesium Stearate

The lubricant sensitivity of all materials was tested against magnesium stearate at a 1% level in compacts made at 60 MPa. Magnesium stearate is commonly used in tablet formulations to reduce friction between the material and equipment tooling.

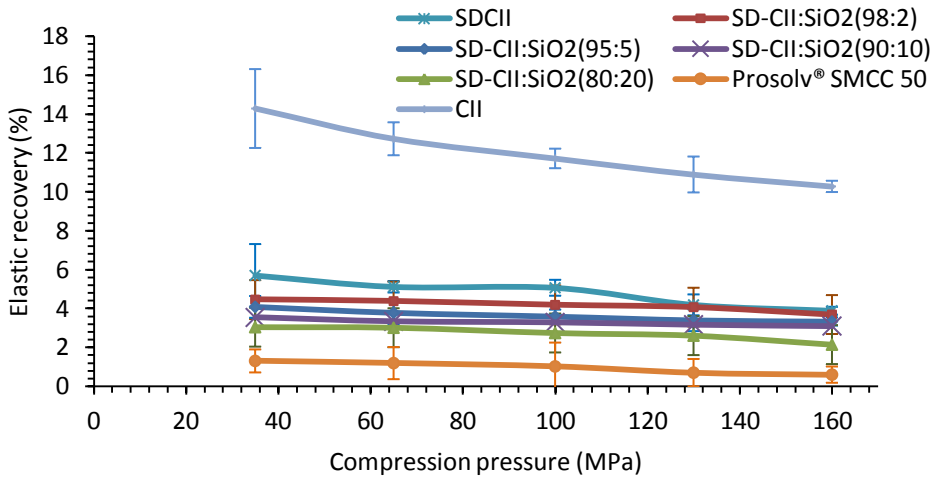

Figure IV-63. Elastic Recovery for CII, Spray-Dried CII:SiO_2 and Prosolv® SMCC 50 (silicified microcrystalline cellulose I).

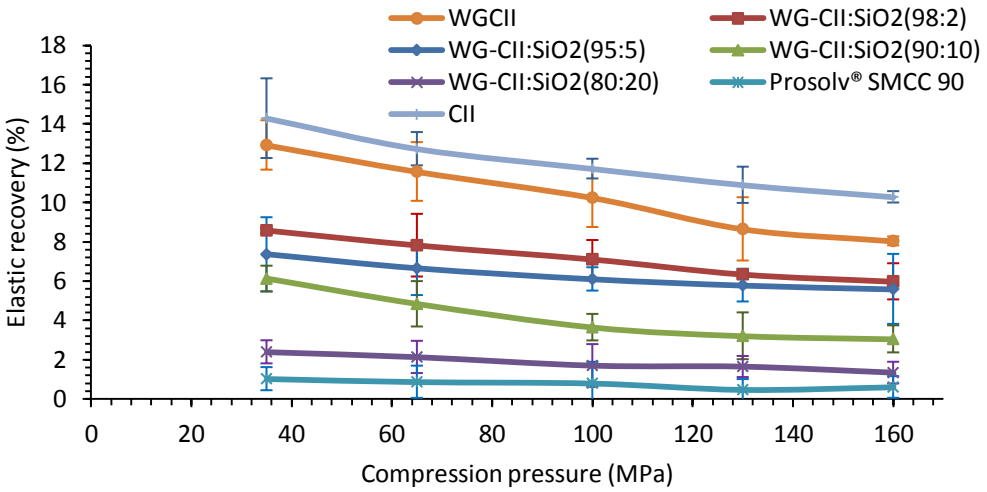

Figure IV-64. Elastic Recovery for CII, Wet Granulated CII:SiO_2 and Prosolv® SMCC 90 (silicified microcrystalline cellulose I).

As seen in Figure IV-65, the lubricant sensitivity (LSR) to magnesium stearate was low for all silicified CII composites (~0.05).On the other hand, a 2% SiO_2 in Prosolv® SMCC 50 had a minimum counteracting effect on magnesium stearate due to its known high plastic behavior. It must be remembered that this material also had a low P_y value of 98 MPa, as seen under *Heckel Analysis.* These results suggest that materials with a low P_y value such as Prosolv® SMCC 50 were more sensitive to magnesium stearate, and the sensitivity decreased as the SiO_2 level increased. Other reported studies have found an inverse relationship between plasticity and lubricant sensitivity for Avicel® products (Bolhuis and Zuurman, 1995; Vromans and Lerk, 1988). The low sensitivity of silicified CII materials to magnesium stearate is due to particle coating by SiO_2, for which magnesium stearate competes during compression. Thus, the presence of SiO_2 creates a more fragmenting behavior forming new clean surfaces available for binding with less lubricant sensitivity.

Figure IV-66 shows the sensitivity of the wet granulated materials to magnesium stearate. Opposite to the results seen for the spray-dried materials, silicification using wet granulation did not decrease lubricant sensitivity considerably except at 20% silicification. The partial surface coverage by SiO_2 compared to spray-dried materials might be responsible for this, since SiO_2 in the granules core is not completely available to interact with magnesium stearate. WGCII was more sensitive to magnesium stearate than CII. This is in agreement with the lower P_y values obtained for WGCII (91 MPa) as discussed previously with Heckel analysis.

Among CI materials, Prosolv® SMCC 90 had lower lubricant sensitivity than silicified wet granulated materials because of the fragmenting behavior of SiO_2 located on the surface which produced some free surfaces available for binding.

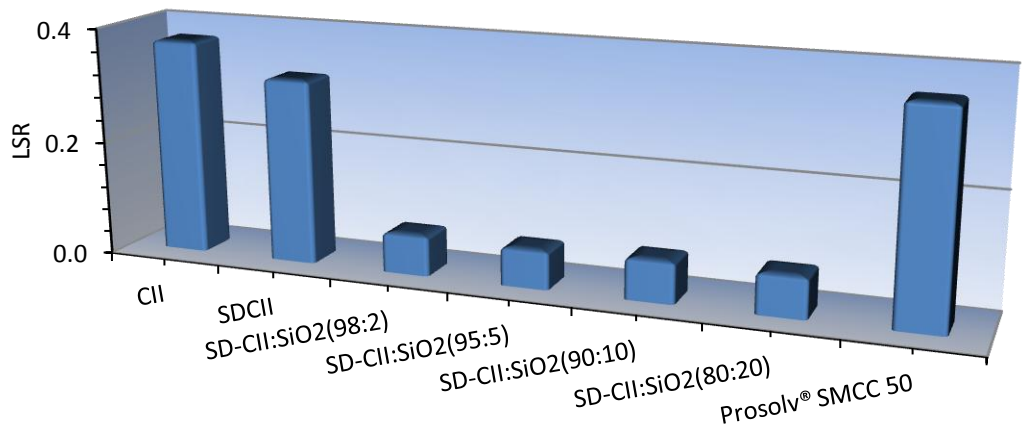

Figure IV-65. Lubricant Sensitivity (LSR) of CII, Spray-Dried Materials and Prosolv® SMCC 50 (silicified microcrystalline cellulose I).

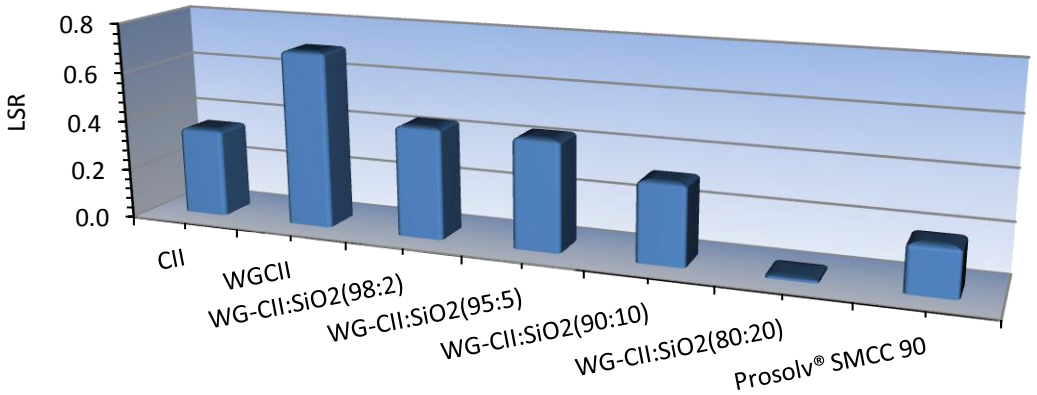

Figure IV-66. Lubricant Sensitivity (LSR) of CII, Wet Granulated Materials and Prosolv® SMCC 90 (silicified microcrystalline cellulose I).

Further, Prosolv® SMCC 90 had higher P_y than Prosolv® SMCC 50 (108 MPa vs. 98 MPa), and was less sensitive to magnesium stearate indicating an inverse relationship between yield pressure and lubricant sensitivity.

Figure IV-67 shows that highly silicified materials are virtually insensitive to magnesium stearate and that unsilicified materials require about 30 minutes of blending to reach a plateau in LSR. It seems to be that fumed silica in high plastically deforming materials, such as cellulose I, coated particles in a high degree preventing the formation of sufficient contact points during consolidation and hence, increased their LSR.

It has been reported previously that silicified cellulose I materials (Prosolv®) are less sensitive to magnesium stearate than the unsilicified ones (Muzikova and Novakova, 2007; Van Veen et al., 2005). Results suggest the use of low blending times of ~5 min (to avoid a major loss of compactibility) when magnesium stearate is added to these highly plastic materials, and longer times (15-30 min) when silicified materials are used to avoid frictional forces between the punches and die.

Compact Disintegration

Figures IV-68 and IV-69 show the fast disintegrating properties of silicified materials made by spray drying and wet granulation, respectively. Results indicate that independent of the process employed, all silicified CII materials showed faster disintegration times compared to cellulose I products. Further, silicified materials showed a critical porosity below which disintegration time increased sharply. This critical porosity increased with increasing silicification levels.

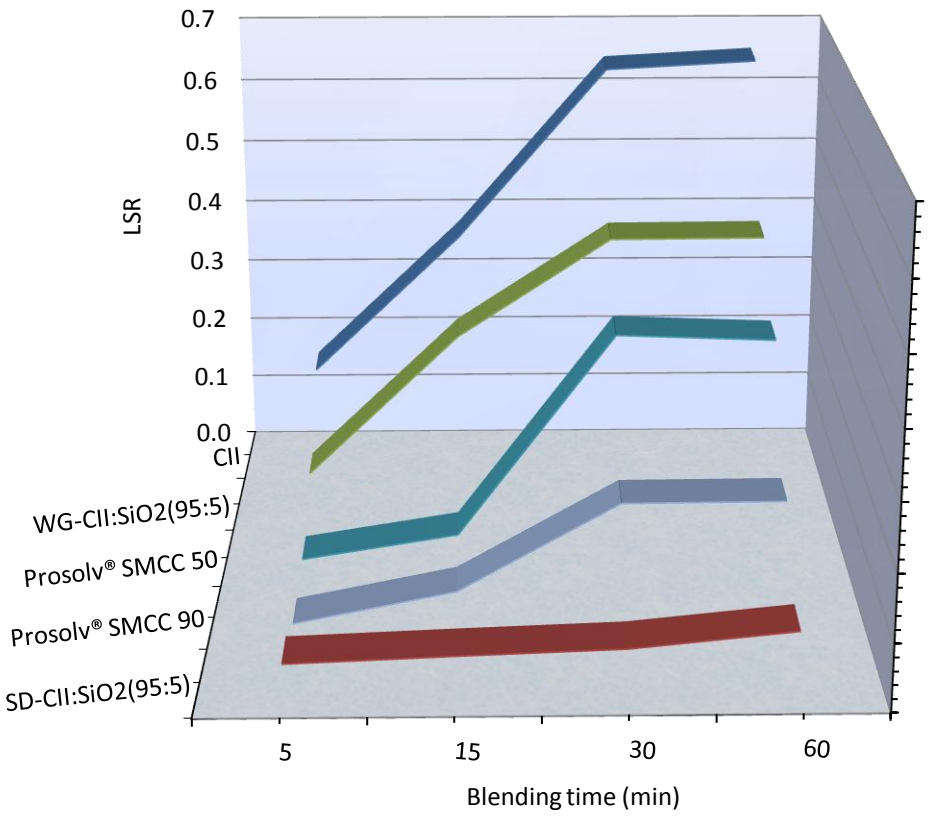

Figure IV-67. Effect of Blending Time on Lubricant Sensitivity of CII, CII:SiO_2 Materials and Prosolv® (silicified microcrystalline cellulose I).

Beyond the critical porosity, compact disintegration time increased mainly due to the high contribution of silicification on compact strength and perhaps, the decrease in water affinity caused by fumed silica (especially at 20% level) which reduced interactions with water, compared to CII particles. CII which is unsilicified, showed the lowest critical porosity (0.06) indicating that the absence of fumed silica favored compact disintegration due to the formation of less strong compacts and the high affinity of CII for water.

Prosolv® SMCC 50 and Prosolv® SMCC 90 compacts beyond 0.26 porosities presented a steady decrease of disintegration time. Below this porosity, these compacts did not disintegrate during the test period (~300 min). Long disintegration times were expected for these materials since they showed the highest compactibility by forming strong compacts with low affinity for water.

Disintegration properties of compacts made from the spheronized products are shown in Figure IV-70. Except for CII, all spheronized products had disintegration times less than 30 seconds. CII had the slowest disintegration times and CP-203® had longer times than spheronized materials.

Since CP-203® had very poor binding properties, it was not possible to make compacts at compression pressures lower than 90 MPa. With this material, individual beads came off from compacts as soon as they ejected after compression at low pressures. In general, with spheronization, silicified materials produced the weakest, but fastest disintegrating compacts. This can be explained by the regular shape, smooth surface, high compact porosity, low volume reduction (compressibility) and larger size bead produced by this technique. These characteristics did not contribute to the formation of sufficient binding sites and surface area increase in the particles which is necessary for making strong compacts.

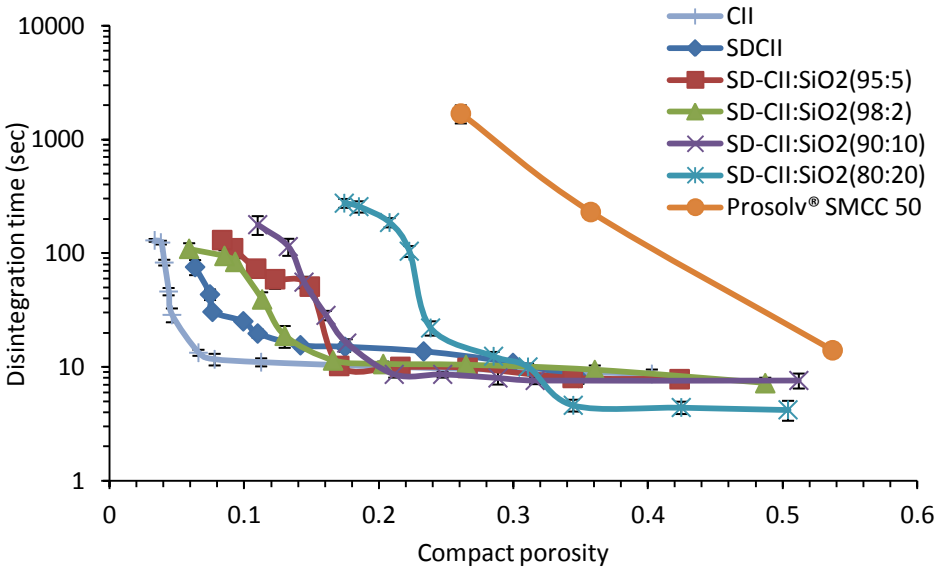

Figure IV-68. Disintegration Properties for CII, Spray-Dried CII:SiO_2 and Prosolv® SMCC 50 (silicified microcrystalline cellulose I).

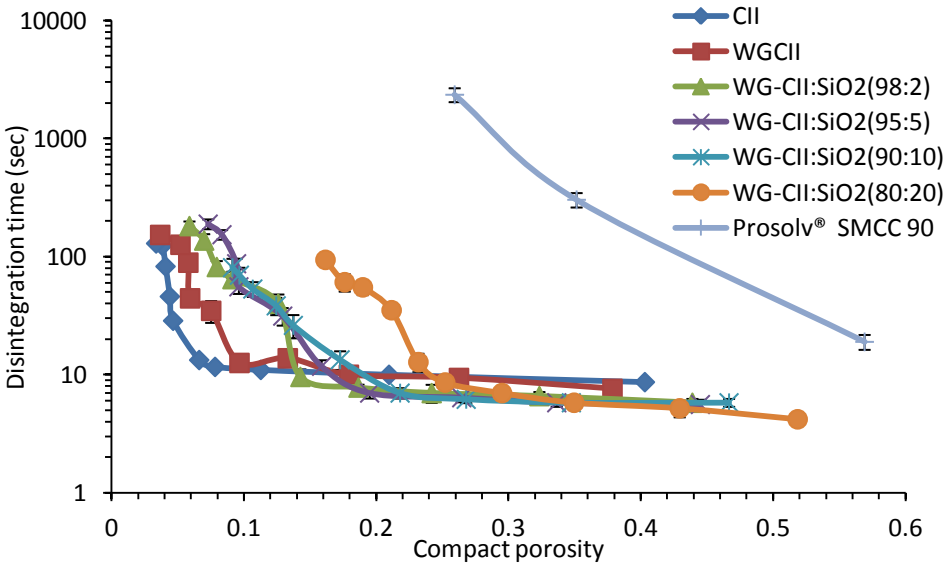

Figure IV-69. Disintegration Properties for CII, Wet Granulated CII:SiO_2 and Prosolv® SMCC 90 (silicified microcrystalline cellulose I).

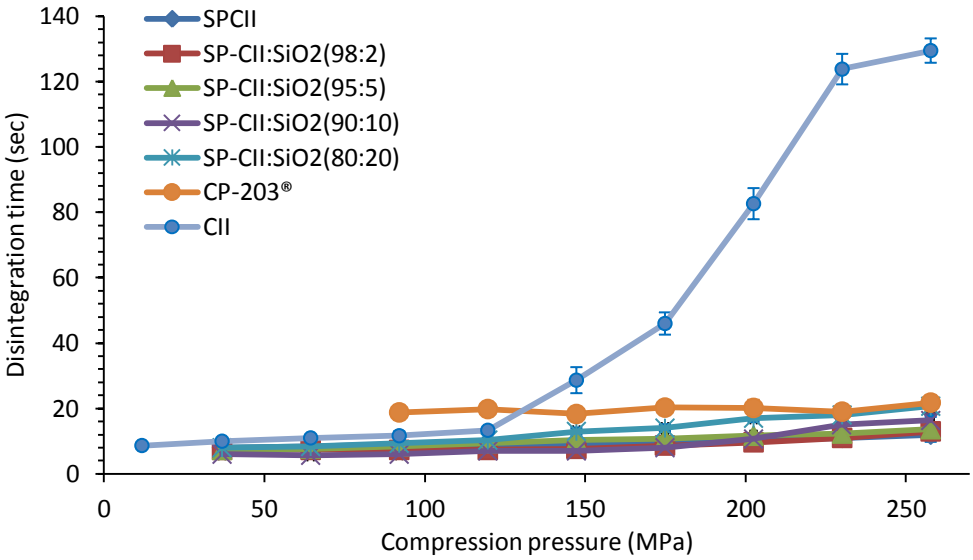

Figure IV-70. Disintegration Properties of Compacts Prepared with CII, Spheronized CII:SiO_2 and CP-203® (spheronized microcrystalline cellulose I).

Bead Friability and Disintegration

Table IV-19 lists the results of the disintegration and friability tests conducted on silicified cellulosic beads. Friability values ranged from 2.8 to 4.2% and these data did not correspond to the SiO_2 content. Further, only beads with 20% SiO_2 showed larger friability values than CP-203® possibly due to the large amount of SiO_2 detaching from the bead surface. Likewise, bead disintegration times ranged from 30 to ~39 minutes. However, CP-203® did not disintegrate during the test period of 150 minutes. This behavior was unexpected since this material was highly hydrophilic and barely formed compacts. Further, as seen in Figure IV-71, the individual CP-203® beads remained intact after 2.5 h of testing. This problem has also been reported for beads made of cellulose I leading to slow drug release and decreased bioavailability (Kranz et al., 2009; Zimm et al, 1996; Podczec et al, 2008). Silicified CII materials, on the other hand, due to their high hydrophilic properties and rapid water uptake via capillary formation and minimum swelling (explained under *evaluation of disintegration properties of CII, SDCII and commercial disintegrants*) produced beads that cracked where edges of the individual particle aggregates were formed during the spheronization process. In some cases, these cracks led to a destruction of the spherical shape and hence, the collapse of the beads. These results also showed CII and silicified products to have sufficiently low friability, and plasticity to form high density, smooth, spherical particles.

Table IV-19. Bead Friability and Disintegration of CII, Spheronized CII:SiO_2 and CP-203® (spheronized microcrystalline cellulose I).

Sample	Friability (%)	Disintegration time (min)
	n=4	n=3
SPCII	3.7 ± 1.3[a]	39.1 ± 2.1[a]
SP-CII:SiO_2(98:2)	2.8 ± 0.1	35.4 ± 1.7
SP-CII:SiO_2(95:5)	3.4 ± 0.3	31.2 ± 1.5
SP-CII:SiO_2(90:10)	3.5 ± 0.3	30.1 ± 1.7
SP-CII: SiO_2(80:20)	4.2 ± 0.2	32.1 ± 2.1
CP-203®	3.5 ± 0.4	>150 ± 0.0

[a] mean ± SD

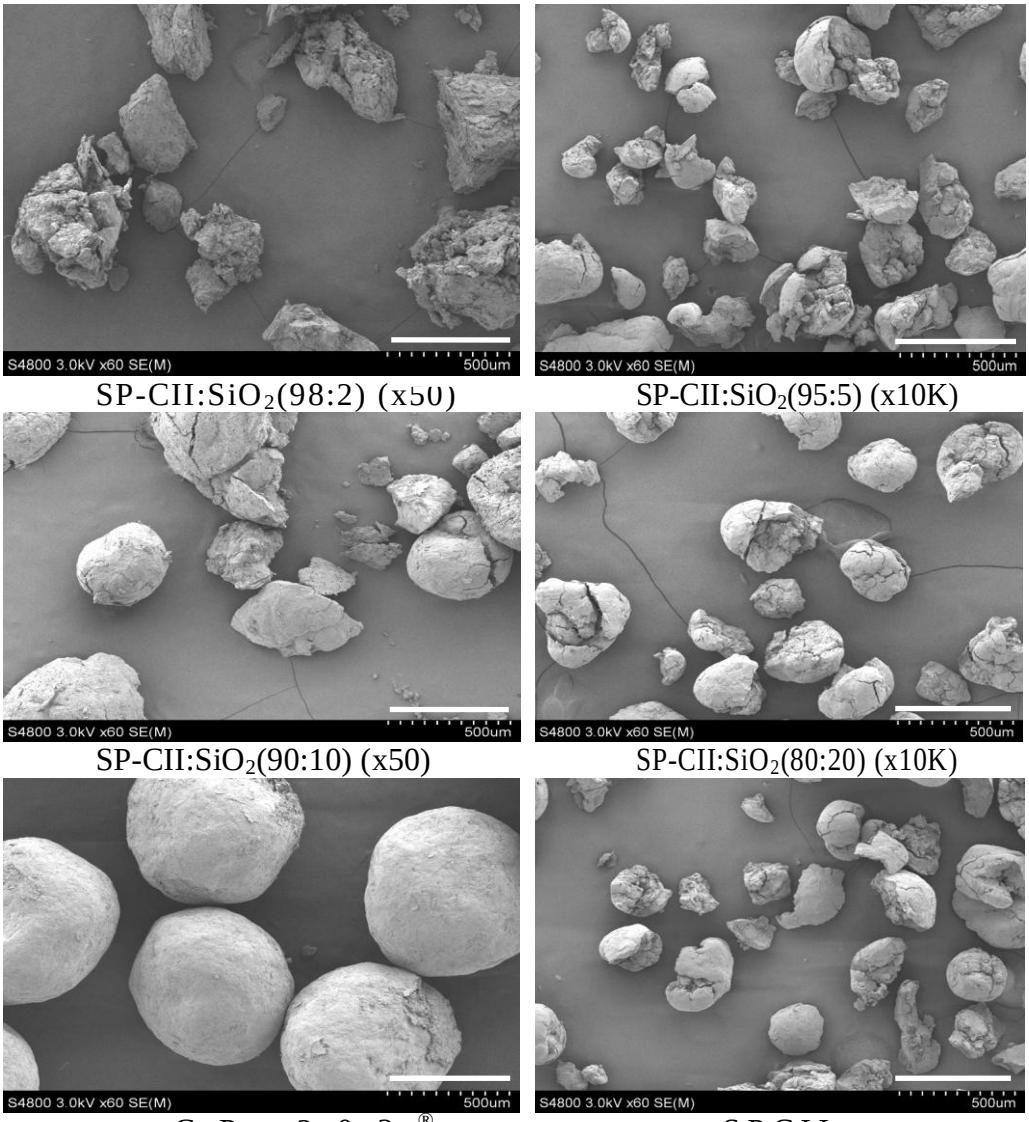

Figure IV-71. SEMs (60X) of CII, Spheronized CII:SiO_2 and CP-203® (spheronized microcrystalline cellulose I) Beads after Disintegration.

Diphenhydramine HCl and Griseofulvin Bead Preparation with Cellulosic Excipients

Since compacts from the spheronized composite materials had lower tensile strength and mechanical properties compared to CII, these materials were not employed for tableting purposes. Instead, the potential use of these materials as a hydrophilic matrix for drug delivery from beads placed in capsules was explored using diphenhydramine HCl and griseofulvin as model drugs. Diphenhydramine HCl is an example of a highly water-soluble drug, while griseofulvin is a poorly water-soluble drug. Table IV-20 gives the powder properties of these materials. All materials showed a good content uniformity indicating a homogeneous drug distribution within the beads and between filled capsules. Further, independent of the drug used, all materials presented lower porosities (0.52-0.55) as compared to spray-dried and wet granulated materials shown previously in Tables IV-15 and IV-16 (~0.64-0.8). These results are in agreement with those found for the pure excipients, indicating that the drug contribution to these parameters is low due to their low content in the formulation (16.7% for diphenhydramine HCl and 33.3% for griseofulvin, respectively). The Carr index has been widely used to measure the compressibility or volume reduction ability of powders. Further, it has also been used as an indirect measurement of flow (Lachman et al., 1986). In this case, the Carr index of the beads remained below 15% indicating an excellent to good flow property (Durgapal et al., 2010). This result is not surprising, since as seen for the spheronized composites, this process produced spherical beads with better flow, powder density and larger sizes (960-1230 μm) than the wet granulated and spray-dried materials.

Table IV-20. Properties of Diphenhydramine HCl or Griseofulvin Cellulosic Beads.

Test	Diphenhydramine HCl			
	Avicel® PH-101	CII	Prosolv® SMCC 50	Benadryl®
Content uniformity (capsule)(%), n=10	103.6 ± 1.3	108.9 ± 3.2	108.5 ± 1.2	N.A.
Content uniformity (powder)(%), n=3	103.5 ± 4.2	109 ± 9.5	103.4 ± 6.6	N.A.
Powder porosity, n=1	0.52	0.52	0.53	N.A.
Carr's index (%), n=1	9.1	7.9	14.7	N.A.
Moisture content (%), n=2	3.7 ± 1	3.2 ± 1	3.2 ± 0.2	N.A.
Geometric mean (µm) ±SE	1179 ± 89	1193 ± 63	991 ± 78	N.A.
b[a]	0.114	0.341	0.576	0.1289
a[a]	0.688	0.734	4.736	0.4021
t_{80} (min)[c]	2.5	1.6	34	0.03
r^2 (from Weibull model)	0.9959	0.9989	0.9897	0.9959
	Griseofulvin			
Uniformity of doses (capsule)(%), n=10	102.8 ± 1.3	104 ± 2.9	101.4 ± 1.7	N.A.
Uniformity of doses (powder)(%), n=5	113 ± 0.4	105 ± 1.4	116 ± 0.2	N.A.
Powder porosity, n=1	0.53	0.54	0.55	N.A.
Carr's index (%), n=1	15.0	15.1	6.1	N.A.
Moisture content (%), n=2	2.9 ± 0.5	2.7 ± 0.5	3.2 ± 0.4	N.A.
Geometric mean (µm) ±SE	1021 ± 109	1229 ± 49	960 ± 96	N.A.
d[b]	0.063	0.119	0.063	N.A
n[b]	0.588	0.606	0.6087	N.A.
r^2 (from power law model)	0.9841	0.9936	0.9934	N.A.

[a] Parameters from the Weibull model: a, time scale parameter; b, shape parameter; t_{80}, time for 80% drug dissolution.

[b] Parameters from the power law model: d, shape factor, which incorporates structural and geometric characteristics; n, indicates the release type.

Drug Release Studies from Beads of Cellulosic Excipients

Since the release properties of a drug from beads depends on its solubility in the medium and the physicochemical properties of the polymer, two drugs with two different water solubilities are expected to show different release behaviors with these cellulosic polymers. Since CII is hydrophilic, its beads could act as a non-swellable matrix which could control drug release by drug diffusion through the pores. Thus, for drugs entrapped in the cellulose matrix during extrusion/spheronization, it is likely that during dissolution, water uptake would occur through the pores forming capillaries and cracks in the beads without significant swelling as explained under *Evaluation of disintegration properties of CII, SDCII and commercial disintegrants*. Since the spherical shape, drug distribution and bead size were kept constant, variations in drug dissolution can be attributed to drug solubility and drug diffusion characteristics in the matrix.

Figure IV-72 shows the release profiles of diphenhydramine HCl beads. In order to compare the rapid release profiles, a general empirical equation described by Weibull was employed (Weibull, 1951):

$$F = 1 - exp^{\frac{\left[-(t)^b\right]}{a}} \qquad \text{Eqn. IV-1}$$

Where, "a" is the time scale of the process and "b" is curve shape parameter. This shape could be either exponential (b= 1), sigmoid (b> 1) or parabolic (b <1). This model has been used in many types of dissolution profiles. The results are given in Table IV-20. In all cases "b" values were <1 indicating a parabolic shape. However, this model has been widely criticized because it is not derived on any fundamental basis and its parameters are not related to the intrinsic dissolution rate of the drug (Pedersen and Myrick, 1977). In this case, the rate is determined by "a" and "b" together. Furthermore, this model is of

limited use when establishing *in-vitro/in-vivo* correlations. Thus, for comparison purposes, only the predicted time to release 80% of the drug (t_{80}) is shown in Table IV-20. Prosolv® SMCC 50 which was the material with the strongest mechanical properties gave beads with a slow release. In fact, it released 80% in about 30 min. This indicates that compared to CII, the low water affinity and the tight entanglement of the cellulose I chains could sufficiently restrict drug release and cause longer release times for this highly soluble drug. On the other hand, CII and Benadryl® capsules had comparably fast release profiles even though Benadryl® is formulated as a powder capsule (i.e., no beads). These results suggest that the combined effect of high drug solubility (100 mg/mL) and high water affinity of the polymer favored a fast drug dissolution through the pores without affecting the integrity of the matrix.

The Weibull model was not employed for the release studies of griseofulvin from the beads since there is not a physical meaning of the "a" and "b" parameters. Therefore, for the release studies of griseofulvin, a power law model for the drug release from spheres was employed (Peppas, 1985):

$$F = a * t^n \qquad \text{Eqn. IV-2}$$

Where, "F" is the fraction of drug release, "a" corresponds to the structural and geometric characterization of the beads and "n" indicates the release mechanism. If "n" is 0.43, drug release is Fickian. In comparison, if "n" is between 0.43 and 1, the release is non-Fickian or anomalous. Conversely, an "n" of 1 indicates a zero-order release. This model is simple and semi-empirical and relates the fraction of drug released to time raised to an exponent, "n". However, caution should be taken since Ritger and collaborators showed that this equation is only valid for the first 60% of drug release from beads (Ritger et al, 1987).

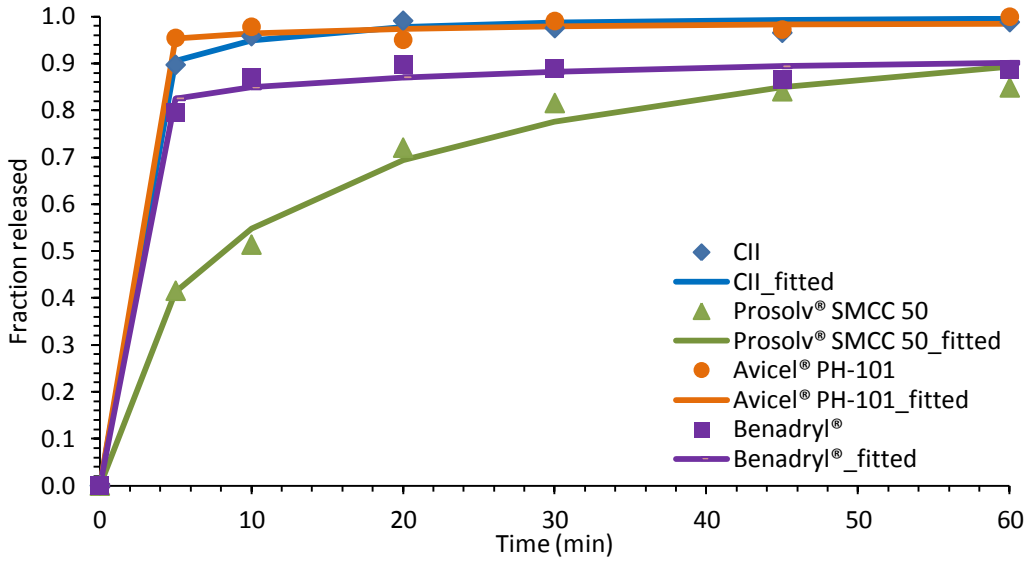

Figure IV-72. Dissolution Profiles of Diphenhydramine HCl from Cellulosic Beads. Conditions: Apparatus 1 (baskets), 100 rpm, Time of 60 Minutes in 500 mL of Distilled Water. Drug Content, 25 mg.

Table IV-20 gives the "k" and "n" parameters for griseofulvin obtained from the power law model. Surprisingly, in all cases "n" was larger than 0.43 and lower than 1 indicating a non-Fickian or anomalous release from the beads (Siepmann and Peppas, 2001). This means that the release is neither diffusion-controlled nor swelling-controlled, but rather a combination of both factors. Thus, it is possible that deviation from Fickian diffusion arises from changes in the cellulose structure upon contact with water (relaxation time). These changes could include partial pore and capillary expansion causing the surface concentration of the drug not to attain its equilibrium immediately upon polymer chains expansion. Thus, the polymer relaxation time could approximate the solvent penetration time causing a drug front (moving boundary), which separates the less wet core from the complete wet surface, possibly causing a variation of the drug diffusion coefficient with time.

Differences in the "k" parameter indicate that drug diffusivities within cellulose II beads were varied 2-fold due to the larger CII affinity for water leading to a greater pore/capillary expansion and thus, a faster griseofulvin release compared to cellulose I materials. In this case, a 2% silicification of cellulose I showed no contribution to the drug release process, probably an indication of no modification of the bead pores and cellulose's affinity towards water. For this reason, CII showed ~80% drug released within 30 h, whereas CI materials took ~72 h to release the same drug fraction (Figure IV-73). Although Grisactin® capsules were used as control, the experimental data were not fit to the power law model since it showed an essentially immediate release profile which produced meaningless fitted parameters. Grisactin® is not composed of beads, but rather is a powder mixture of griseofulvin, lactose (water soluble diluent) and sodium lauryl sulfate (surfactant) which acts as a wetting agent and in some formulations PEG 400 is also present promoting water solubility of griseofulvin.

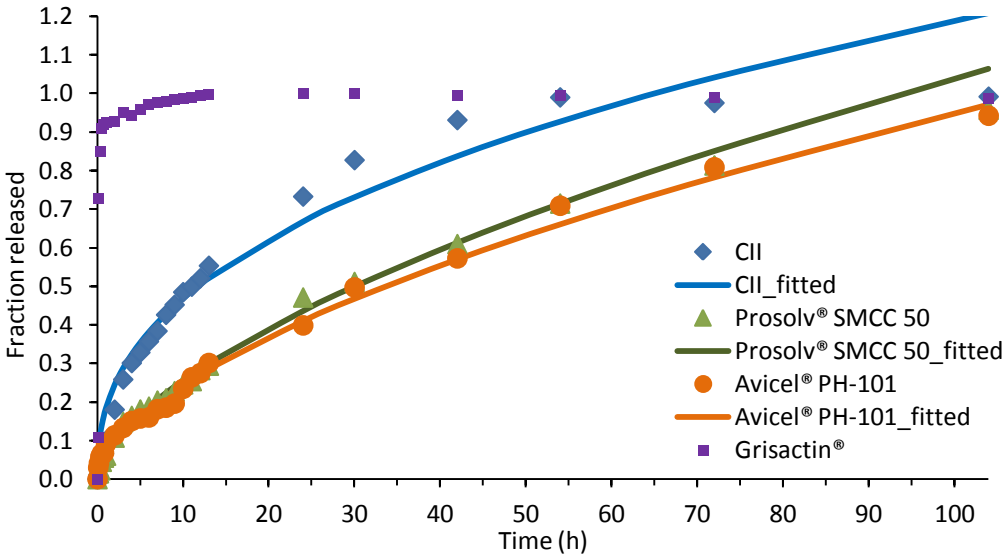

Figure IV-73. Dissolution Profiles of Griseofulvin from Cellulosic Beads. Conditions: Apparatus 2 (paddles), 50 rpm, Time of 4.5 Days in 1,000 mL of Distilled Water Containing 5.4 mg/mL of Sodium Lauryl Sulfate. Drug Content, 125 mg.

This explains why it released ~87% of the drug within 30 minutes even if the water solubility of this drug is quite low (0.018 mg/mL).

Dissolution of Diphenhydramine HCl Compacts

The dissolution profiles of diphenhydramine HCl from compacts are shown in Figure IV-74 and IV-75 for the spray-dried and wet granulated materials, respectively. Drugs were released from compacts of ~500 mg having a diameter of ~1.3 cm. The drug content per tablet was 25 mg. Since these compacts were made individually by weighing the individual drug and excipient components, drug content analysis was not needed. It is clear that silicified CII materials released more than 80% of the drug within 5 min, which was faster than Benadryl® caplets and compacts made of Prosolv® SMCC 50 (~50% release). Except for compacts with a 20% silicification (~0.25 porosity), any possible contribution of compact porosity is considered negligible since in all cases compact porosity was ~0.15. Thus, the fast drug dissolution from compacts of silicified materials can be attributed only to the cellulose II polymorph.

Since the manufacturing conditions for Benadryl® are unknown, it is possible that for this low dose drug (25 mg) wet granulation was used, in which an appropriate amount of binder/diluent and a disintegrant is needed to ensure a fast release. On the other hand, silicified CII compacts were made by employing the rapid and economical direct compression approach without including any disintegrant or lubricant. Compared to CII materials, excipients which formed stronger compacts than CII such as WGCII and WG-CII: SiO_2 (98:2) and Prosolv® SMCC 90 had also slightly longer dissolution times when produced at the same compression pressures (120 MPa). Since all silicified CII compacts exhibited a burst effect upon contact with water, it is expected that these silicified materials did not hinder compact disintegration and hence, the rapid dissolution of this highly water soluble drug.

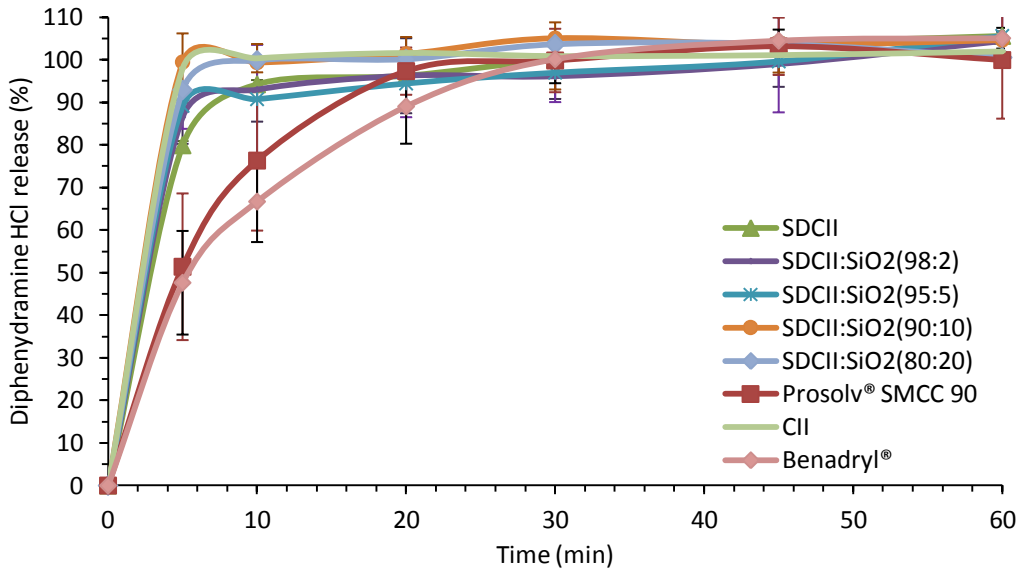

Figure IV-74. Compact Dissolution Profiles of Diphenhydramine HCl from CII, Spray-Dried Materials and Prosolv® SMCC 50. Conditions: Apparatus 1 (baskets), 100 rpm, Time of 60 Minutes in 500 mL of Distilled Water. Drug Content, 25 mg.

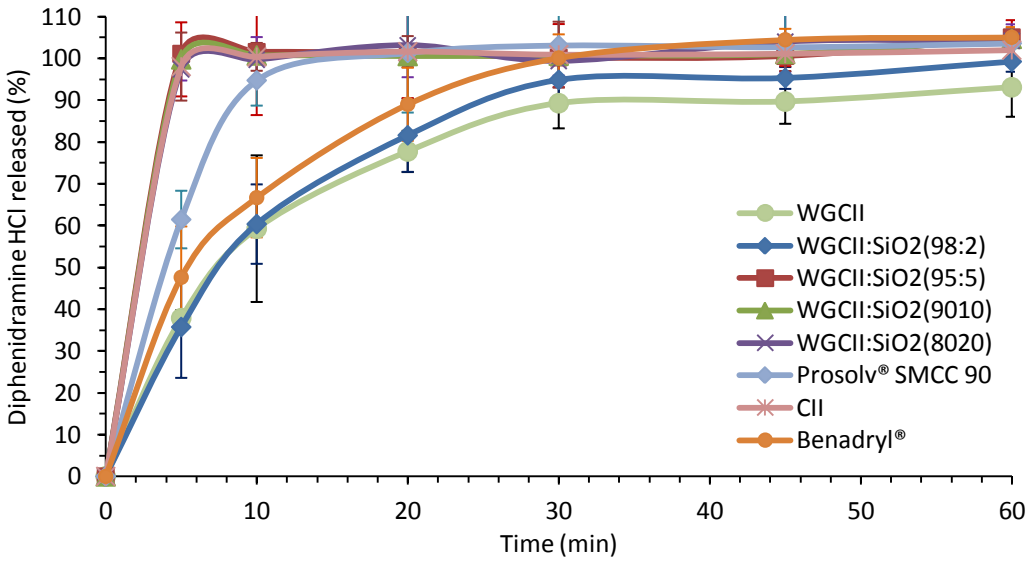

Figure IV-75. Compact Dissolution Profiles of Diphenhydramine HCl from CII, Wet Granulated Materials and Prosolv® SMCC 90. Conditions: Apparatus 1 (baskets), 100 rpm, Time of 60 Minutes in 500 mL of Distilled Water. Drug Content, 25 mg.

In fact, all silicified CII materials released a minimum of 80% of the drug within 30 min. For this reason, compacts of cellulose I materials such as Prosolv® SMCC 50 and Prosolv® SMCC 90, which are slowly disintegrating materials, after 30 minutes looked partially eroded and also passed the dissolution test. Possibly, diphenhydramine HCl easily leached out from the pores upon compact wetting.

Dissolution of Griseofulvin Compacts

Figures IV-76 and IV-77 show the griseofulvin release results for the spray-dried and wet granulated compacts, respectively. Drugs were released from compacts of ~500 mg having a diameter of ~1.3 cm. The drug content per tablet was 125 mg and the medium used was an aqueous solution of sodium lauryl sulfate at a concentration of 40 mg/mL. All silicified CII materials released more than 75% of griseofulvin within 10 minutes. On the other hand, Prosolv® SMCC 50, Prosolv® SMCC 90 and Gris-Peg® compacts released 18%, 10% and 16% within 10 min. Further, Gris-Peg® barely fulfilled the 75% release requirement specified in the USP28/NF23 within the 90 min of the test, whereas, compacts of cellulose I materials did not pass the test due to the formation of strong compacts. These results suggest that highly binding materials with less water affinity than CII are not appropriate to formulate poorly water-soluble drugs because compact disintegration and further water accessibility to the compact is restricted and delays drug dissolution. In these cases, a disintegrant, along with a non-hydrophobic lubricant is required. Since the USP recommends the use of distilled water containing 40 mg/mL of surfactant for the dissolution studies, the real *in-vivo* significance of this test is questionable.

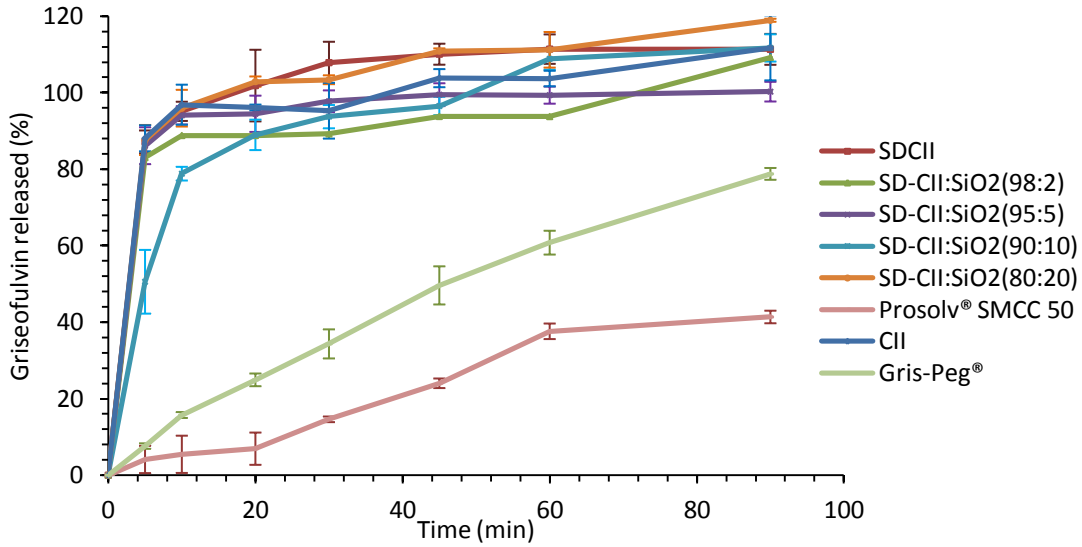

Figure IV-76. Compact Dissolution Profiles of Griseofulvin from CII, Spray-Dried Materials and Prosolv® SMCC 50. Conditions: Apparatus 2 (paddles), 75 rpm, Time of 90 Minutes in 1000 mL of 40 mg/mL Sodium Lauryl Sulfate Media. Drug Content, 125 mg.

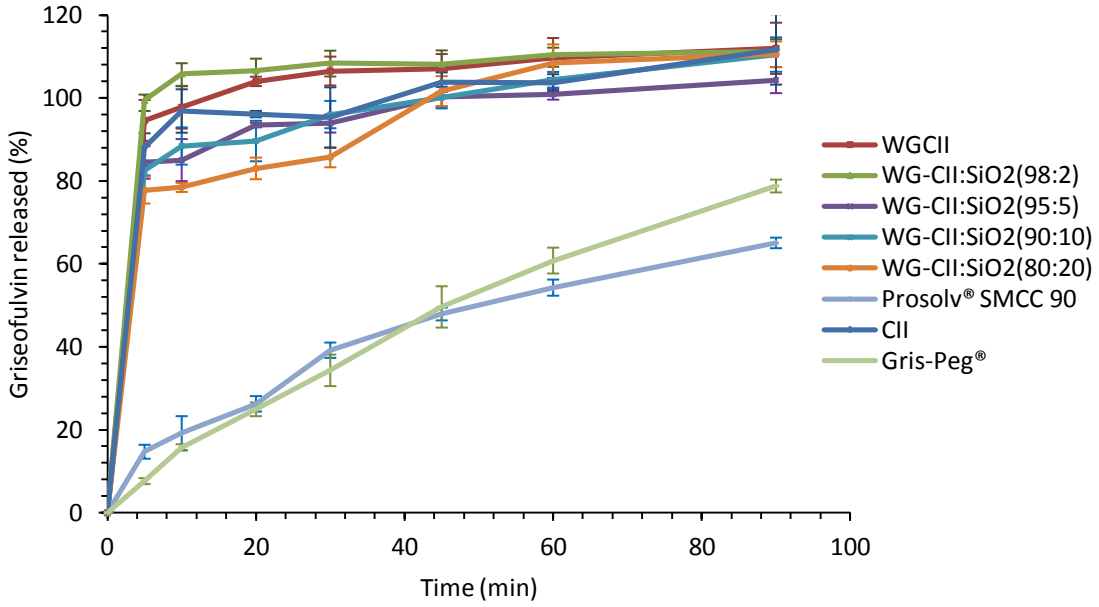

Figure IV-77. Compact Dissolution Profiles of Griseofulvin from CII, Wet granulated Materials and Prosolv® SMCC 90. Conditions: Apparatus 2 (paddles), 75 rpm, Time of 90 Minutes in 1,000 mL of 40 mg/mL Sodium Lauryl Sulfate Media. Drug Content, 125 mg.

Further Compact Studies

In the previous section, the mechanical properties of silicified CII materials were evaluated and discussed. SD-CII:SiO_2(95:5) and WG-CII:SiO_2(90:10) were selected as the materials which rendered compacts with the strongest mechanical properties when prepared at the same compression pressure. This was due to the synergistic effect of surface area increase and due to the fragmenting SiO_2 and the plastic-like deformation of CII. In this section, studies to determine the effect of relative humidity (0, 11, 22, 33, 56, 75 and 100%) and time (5, 10, 20 and 30 days) on the mechanical properties of compacts stored at 25ºC and the brittle fracture index of selected excipients were determined and discussed.

The loss of compactibility of Avicel® being higher than that of lactose has been reported by Celik et al. This effect was accompanied by an increase in porosity, bulk density and partial loss of flowability of reworked powders. In this case, excipients were used as obtained or in blends with propranolol HCl and compressed followed by milling and a further recompression (Celik et al, 1987). Moreover, if the cellulosic excipients are dry granulated or reprocessed, with or without the active ingredient, there is also a reduction in compactibility of the material. This effect is exacerbated if a hydrophobic lubricant, such as magnesium stearate (He et al., 2007) and a high particle size grade of the excipients are employed (Sun and Himmelspach, 2005). Cellulosic excipients such as Emcocel® 90 M in mixtures with paracetamol have also shown loss of compactibility (Kaerger et al., 2004).

The brittle fracture index (BFI) is obtained by comparing the tensile strength of tablets with an axially oriented hole in the center (weakening effect) with the tensile strength of tablets without a hole, both prepared at the same relative solid fraction

(Hiestand et al., 2006). Since BFI is an inverse measure of localized stress relief within the tablet (at the edge of the hole) by plastic deformation and thus, it indicates the tendency of a tablet to laminate or cap. The closer the value of BFI is to 0, the more stress relief takes place resulting in a low probability for lamination. Conversely, if this value is close to 1, the material is more likely to laminate (Hiestand and Smith, 1984).

The results of a comparative study of the effect of the moisture content on the mechanical properties of CII, SDCII, WGCII, SD-CII:SiO_2(95:5) and WG-CII:SiO_2(90:10) and cellulose I materials such as Avicel® PH-101, Avicel® PH-102, Prosolv® SMCC 50 and Prosolv® SMCC 90 are evaluated and discussed.

Compacts at Different Relative Humidities

Figures IV-78 shows the moisture sorption of 1.3 cm cellulosic round compacts stored at relative humidities from zero to a 100% for 30 days. All compacts showed a moderate water sorption up to 75% RH (7.2-9%). However, at 100% RH compacts showed a steep increase in water sorption. This effect was more pronounced for WGCII and WG-CII:SiO_2(90:10) since they had the largest increase in porosity (13%). Further, as shown in Figure IV-79, compact porosity virtually did not change from 0 to 75% RH. In general, at >75% RH the large porosity increase can be attributed to high water wicking into the cellulose particles as seen previously.

Although the presence of SiO_2 increased powder porosity, this contribution is negligible since all compacts were prepared at 0.1 porosity. Thus, only water molecules were responsible of interacting with cellulose, especially at >75% RH, resulting in a compact porosity increase.

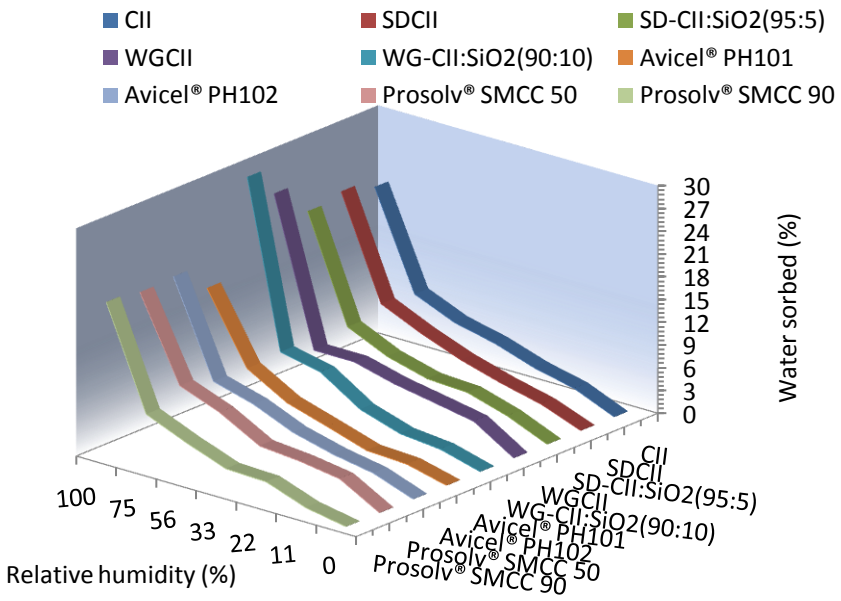

Figure IV-78. Water Sorption of 1.3 cm Round Cellulose II and Commercial Cellulose I (Avicel® and Prosolv®) Compacts Stored at Different Relative Humidities at 25º C.

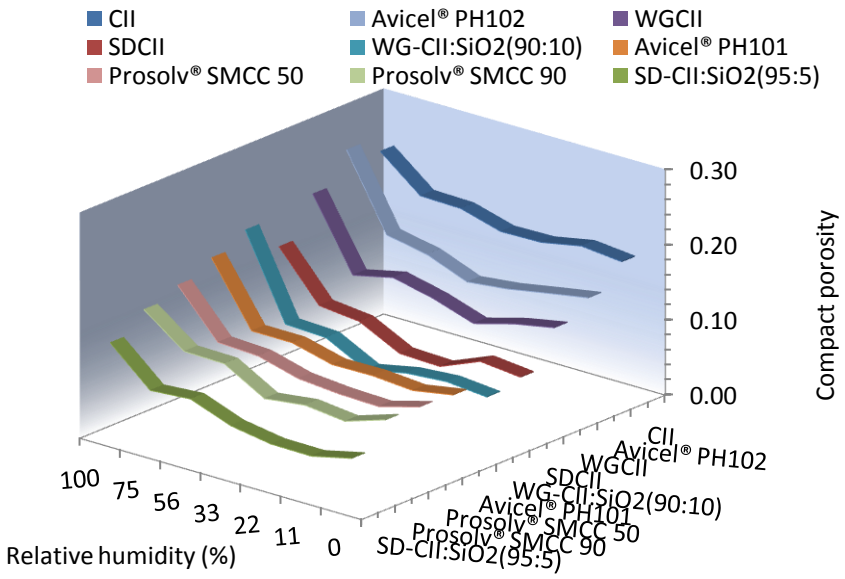

Figure IV-79. Variation of 1.3 cm Round Compact Porosity of Cellulose II and Commercial Cellulose I (Avicel® and Prosolv®) with Relative Humidity at 25ºC.

Water penetrates the compact pores through the capillaries between and within particles causing expansion of the cellulose microfibrils easing separation of the cellulose chains, and as a result, compact tensile strength decreased. Other researchers have also found a sharp decrease in compact strength when exposed to relative humidity >70% (Ladin et al., 1993; Marais et al, 2003).

Figure IV-80 shows the change of tensile strength with RH. In general, the force needed to break the compacts decreased with increasing relative humidity which was due to water sorption leading to disruption of interparticle bonding and hence, a loss in tensile strength. The water sorption properties of the excipient(s) and/or the active ingredient might cause loss of compactibility (Uhumwangho and Okor, 2005). Moreover, highly compactable materials such as Prosolv® SMCC 50, Prosolv® SMCC 90, Avicel® PH-101 and SD-CII:SiO_2(95:5) showed the highest tensile strength and a steady decrease of tensile strength with increasing relative humidity. On the other hand, CII, WGCII, SDCII showed the lowest tensile strengths and hence, their decline in tensile strength with water sorption was also small. These results suggest that an initial high tensile strength is beneficial to avoid a great loss of compactibility due to storage at high RH.

It has been reported for cellulose I that an optimum amount of moisture (~5%) is required, which limits elastic recovery after compression by the formation of hydrogen bond bridges easing the formation of strong compacts. Figures IV-78 and IV-79 show that this amount of water is achieved only if silicified CII compacts are stored at 33% RH and between 33-56 % RH for CI materials. However, Figure IV-78 shows that the highest tensile strength for cellulose I materials and SD-CII:SiO_2 (95:5) was achieved when stored at 0-11% RH, whereas for silicified CII materials the optimum ranged from 11-22% RH.

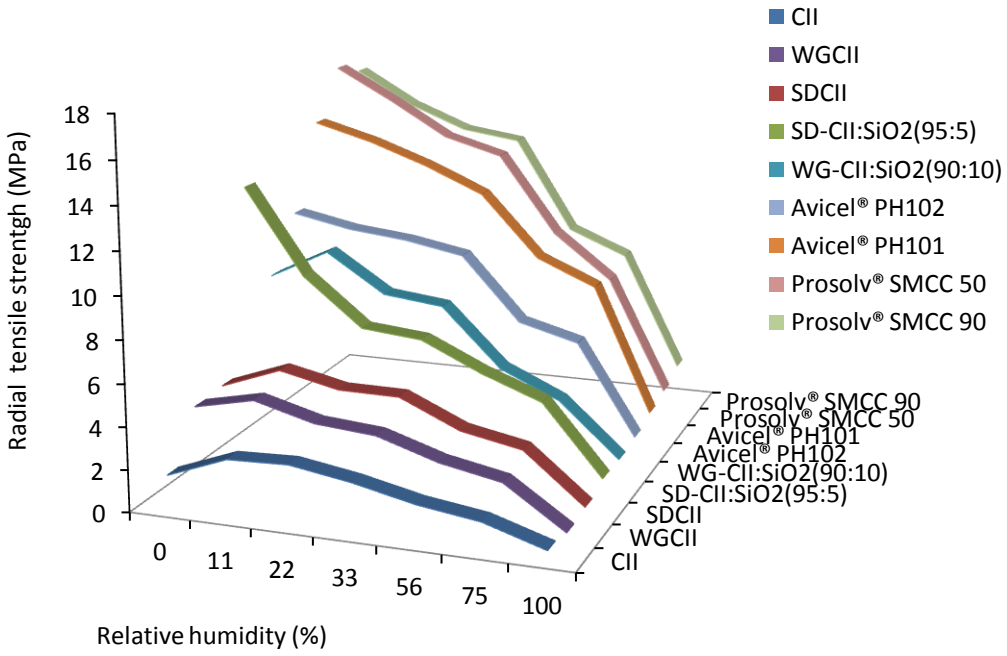

Figure IV-80. Radial Tensile Strength of 1.3 cm Round Compacts of Cellulose II and Commercial Cellulose I (Avicel® and Prosolv®) Stored at Different Relative Humidities at 25ºC.

In those cases, the moisture content of these materials was < 3%. These results show that the decrease in the mechanical properties might be due to water disrupting hydrogen bonding and crosslinking in hydroxyl groups on the cellulose chains, weakening interparticulate bonding. It is important to take into account this aspect during the drug development phase, especially when selecting the packaging system to avoid sorption of water during storage. Water vapor enters the pores of compacts to a larger extent as the relative humidity increases. As a result, after 30 days at 100% RH, compact volume expanded due to water uptake and porosity increase. It is plausible that as water penetrates the pores, binding sites between particles are weaken because of preferential hydrogen bonding with entering water molecules. The overall result is a decrease in the mechanical properties of the compacts. Further, storage of compacts prepared from these excipients should not be allowed at high relative humidities (> 75% RH). If the relative humidity cannot be well controlled after manufacture, the compacts should be packed quickly into an appropriate primary container with desiccant to minimize the loss of mechanical strength.

Brittle Fracture Index

The brittle fracture index indicates the ability of a compact to relieve stress caused by the presence of a defect region in the compact (hole in the center).

The BFI equation is:

$$BFI = 0.5\left[\left|\frac{\sigma_t}{\sigma_0}\right| - 1\right] \qquad \text{Eqn. III-31}$$

If σ_t/σ_0 (tensile strength of compact with no center hole/ tensile strength of compact with center hole) = 3, the BFI is 1 and the material does not relieve stress by plastic deformation. On the other hand, when σ_t/σ_0 is 1, the resulting BFI is 0 and the stress

relief occurs solely by plastic deformation (Hiestand and Smith, 1984). These researchers also showed that an increase in the compression pressure will increase the apparent plasticity of most pharmaceutical powders. This means that the increase in compression pressure could be associated with a decrease in BFI of the resulting tablets (Hiestand and Smith, 1984). The compact mechanical properties are given in Table IV-21. Known highly plastic deforming cellulose I materials such as Prosolv® SMCC 50 and Prosolv® SMCC 90, Avicel® PH-101 and Avicel® PH-102 had BFIs of 0.04, 0.02, 0.14, and 0.13, respectively. These results indicate that a 2% silicification reduced the capping/lamination tendency of cellulose I. Surprisingly, CII did not follow the same trend and only a silicification level of 10% rendered a large BFI (0.44).

Hiestand and Smith found the BFI for Avicel® PH-102 to be 0.04-0.09 in square compacts made at a solid fraction between 0.8-0.9 (Hiestand and Smith, 1984). Williams et al. found BFI values for Avicel® PH-101 to be 0.03-0.08 in square compacts made at a solid fraction of 0.65. Both researchers concluded that the differences were due to lot-to-lot variations (Williams et al., 1997). Likewise, Majuru and Wurster found a BFI for Avicel PH-101 of 0.11 on square compacts made at a 0.83 solid fraction (Majuru and Wurster, 1997). These studies suggest that for Avicel® a large range in solid fraction (0.65-0.9) did not affect significantly the resulting BFI (0.03-0.11) since the variability of BFI could be attributed to differences between lots. On the other hand, in this study, a solid fraction of 0.6 and 0.7 was used for cellulose I and cellulose II materials, respectively. In fact, a solid fraction larger than 0.6 was not employed for cellulose I materials due to the high values of tensile strength, which exceeded the maximum allowed limit obtained from the Q-test universal tester.

Table IV-21. Mechanical Properties Derived from the Stress-Strain Curves of Square Compacts (3.84 cm^2) of Cellulose II and Commercial Cellulose I (Avicel® and Prosolv®).

Sample	Brittle Fracture Index[a]	Toughness modulus (MPa)[b]	Young's Modulus (GPa)[c]
	n=3	n=3	n=3
CII	0.22 ± 0.00	0.017 ± 0.001	0.08 ± 0.01
SDCII	0.14 ± 0.01	0.019 ± 0.000	0.15 ± 0.02
SD-CII:SiO_2(95:5)	0.27 ± 0.03	0.042 ± 0.001	0.20 ± 0.01
WGCII	0.27 ± 0.03	0.023 ± 0.000	0.16 ± 0.02
WG-CII:SiO_2(90:10)	0.44 ± 0.11	0.027 ± 0.001	0.18 ± 0.01
Avicel® PH101	0.14 ± 0.03	0.034 ± 0.001	0.20 ± 0.01
Avicel® PH102	0.13 ± 0.01	0.034 ± 0.000	0.18 ± 0.04
Prosolv® SMCC 50	0.04 ± 0.01	0.046 ± 0.001	0.20 ± 0.00
Prosolv® SMCC 90	0.02 ± 0.00	0.049 ± 0.001	0.18 ± 0.00

[a]Obtained from 3.84 cm^2 square compacts.

[b]Obtained from the AUC of stress (GPa)-strain (%) curves.

[c]Obtained from the linear region of stress-strain curves.

Except for SDCII, cellulose II materials had a BFI of 0.20-0.44 and the highest value was found for WG-CII:SiO_2(90:10) (0.44). In this case, only a SiO_2 content of 10% increased the tendency for capping by decreasing the plasticity of CII. Nevertheless, no capping/lamination was seen when either the square compacts (3.84 cm^2) or the 1.3 cm dia. round compacts (used for the compaction studies described under *compaction characteristics*) were produced. Technological problems occurred when compromised square compacts of a highly silicified material [WG-CII:SiO_2(90:10)] were made. In this case, most of these square compacts broke into two halves when the retractable pin was removed.

Table IV-21 lists toughness modulus calculated from the area under the curve of the stress-strain curves obtained from the square compacts (Figure IV-81). Toughness measures the resistance of a material when stressed until rupture. It has been reported that cellulosic I materials behave as plastic deforming materials and hence, their mechanical properties are expected to be larger than those of less plastic deforming materials (Alderborn and Nyström, 1996; Hancock et al., 2000). The toughness values indicate that cellulose II materials can withstand less than 0.017 MPa of pressure before fracturing, except for SD-CII:SiO_2(95:5) which resisted up to 0.042 MPa. Toughness also increased with processing such as spray drying and wet granulation as seen for SDCII and WGCII, and also increased with silicification, as discussed earlier under *compaction characteristics*. The combination of cellulose's plastic deformation and the brittle component of fumed silica led to a material able to form strong compacts. The high toughness of SD-CII:SiO_2(95:5) and cellulose I materials is indicative of their high ability to absorb energy before fracturing.

Young's modulus is a measure of the resistance of a material to elastic deformation by bending, compression or stretching. In this case, the load-deformation

curves determined on the square compacts (area, 3.84 cm^2) were normalized to cross-sectional area and the percentage deformation. These normalized load-deformation curves are also called stress-strain graphs. The Young's modulus was found from the slope of the elastic linear region of the stress-strain curves. All cellulose II materials had a Young's modulus of 0.08-0.18 GPa except for SD-CII:SiO_2 (95:5) (0.20 GPa). Conversely, cellulose I materials exhibited an elastic modulus of 0.18 to 0.20 GPa. These results suggest that cellulose I materials had higher moduli of elasticity and toughness than cellulose II products. Even though SD-CII:SiO_2 (95:5) presented a high brittle fracture index, the appropriate combination of a plastic and brittle deforming material, along with increased compact surface area, due to silicification might be responsible for the formation of more binding sites for particles and perhaps dislocation or sliding of crystal planes of cellulose during compression, resulting in a material with the best mechanical properties among cellulose II materials. These results are in agreement with the tensile strength results discussed under *compaction characteristics*.

Figure IV-82 shows the change in the specific surface area (SSA) with 11 mm round compact porosity. These compacts were dried at 60 °C and at a reduced pressure of 40 mm Hg for 24 h before testing. Further, Table IV-22 list the bonding surface area found at the largest compression pressure (185 MPa). In order to analyze the surface area involved in particle bonding, the effective bonding surface area can be obtained by subtracting the initial powder surface area from the surface area of the compressed particles in a compact. Cellulose I materials and unsilicified CII materials had a small decrease of surface area upon compression.

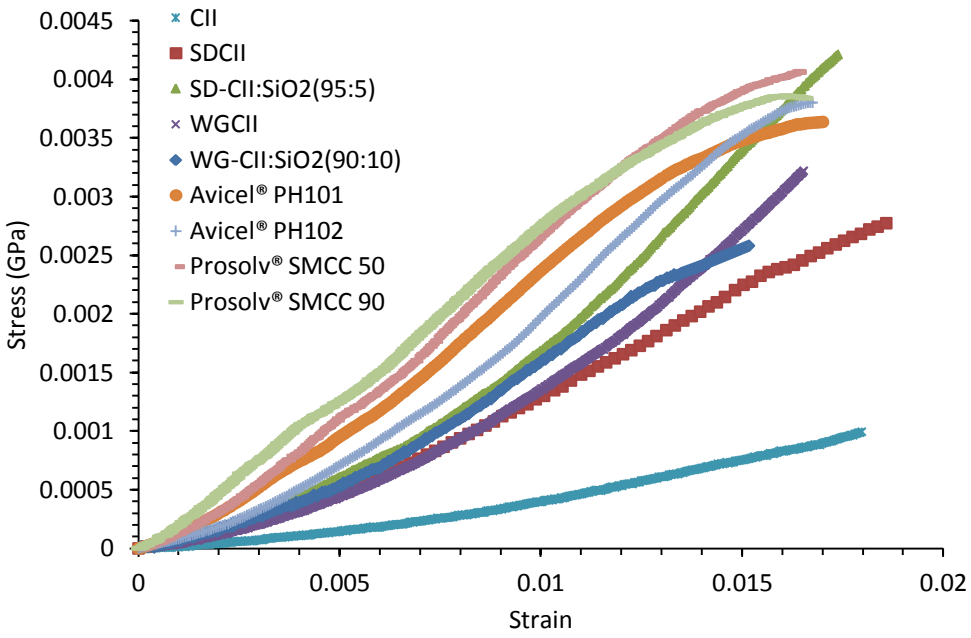

Figure IV-81. Stress-Strain Curves of Square Compacts of Cellulose II and Commercial Cellulose I (Avicel® and Prosolv®).

On the other hand, compact surface area was higher for silicified CII materials. These results revealed that the highly synergistic effect of fumed silica on CII compactibility was due to its contributing fragmenting character which was accompanied with a larger bonding surface area available for particle bonding. As seen under *compact elastic recovery*, fumed silica also prevented the typical high elastic recovery of CII, which could be explained by the increased particle surface area available for bonding.

In most cases, there was a decreasing trend of compact surface area with decreasing compact porosity. Nilsson and collaborators also reported a decrease in compact surface area with increasing compression pressures for Avicel® PH-101 by using the BET N_2 adsorption method. Nilsson used round compacts of 11.3 mm diameter and degassed those compacts at 70 °C for 8 h before testing (Nilsson et al., 2006).

Figure IV-82 also shows two trends for compact surface area, the high one formed by silicified materials such as Prosolv® SMCC 50, Prosolv® SMCC 90, SD-CII:SiO_2(95:5) and WG-CII:SiO_2(90:10) which showed a sharp decrease of compact surface area with decreasing compact porosity. These results agree with the high fragmentation tendency, low volume reduction of particles, and low apparent plastic deformation, especially found for the last two materials. On the other hand, unsilicified materials presented a low bonding surface area. For these materials it is possible that a decrease in compact porosity with increasing compression pressure involves some initial rearrangement, followed by dislocation, sliding of the crystal planes and a very low level of fragmentation.

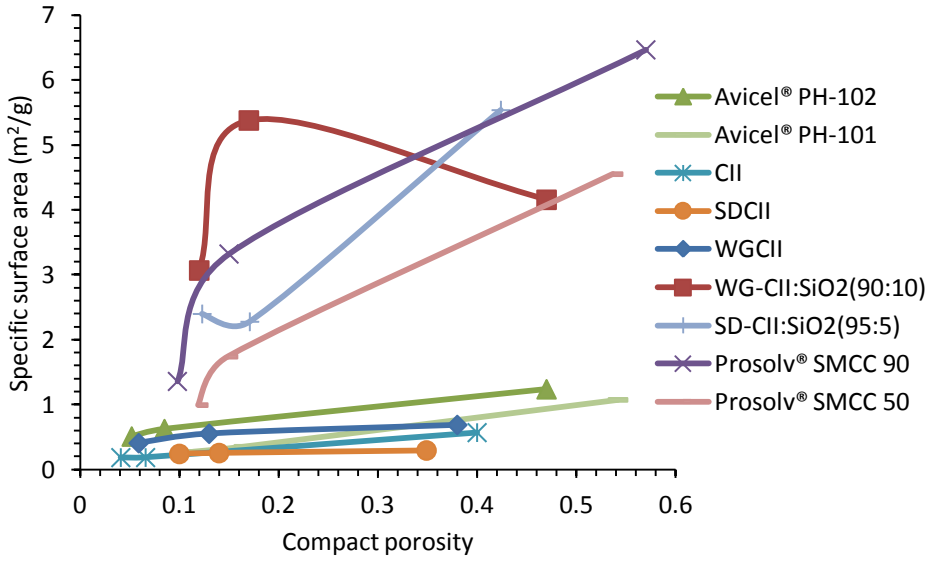

Figure IV-82. Change in Specific Surface Area with Compression Pressure (1.1 cm dia. round compacts) of Cellulose II and Commercial Cellulose I (Avicel® and Prosolv®).

Table IV-22. Bonding Specific Surface Area (1.1 cm dia. Round Compacts) of Cellulose II and Commercial Cellulose I (Avicel® and Prosolv®).

Sample	Bonding surface area (m^2/g)[a] n=1
CII	0.31
SDCII	1.36
SD-CII:SiO_2(95:5)	8.1
WGCII	0.1
WG-CII:SiO_2(90:10)	13.3
Avicel® PH101	1.22
Avicel® PH102	0.79
Prosolv® SMCC 50	5.3
Prosolv® SMCC 90	4.1

[a] Obtained by subtracting powder surface area from surface area of compacts made at 185 MPa.

CHAPTER V

CONCLUSIONS

Particle and tableting properties of CII were susceptible to processing and silicification as summarized in Figures V-1 and V-2. Spray drying and wet granulation of CII generated more regularly-shaped and more densified particles. These properties were reflected in improved flow, better compactibility and low friability. On the contrary, spheronized materials had the worse compactibility, but the best flow due to its large and densified particles.

Processing did not affect the rapid disintegration properties of CII since it did not change its water affinity and disintegration mechanism. The processed CII products and CII compacts disintegrated primarily by a water wicking mechanism similar to that of Polyplasdone® XL, whereas, a swelling mechanism was dominant for Primojel® and Ac-Di-Sol®. Disintegration times of water wicking materials such as spray-dried cellulose II (SDCII), CII and Polyplasdone® XL were faster than highly swelling materials such as Primojel® and Ac-Di-Sol®. Since SDCII and CII do not have a carboxylic acid moiety which is responsible for ionization and swelling; their disintegration was not affected in acid pH. Tablets containing the spray-dried material (SDCII) and CII (or a commercial disintegrant) and magnesium stearate alone and in combination with commonly used binders/fillers (Avicel® PH-102, Fast Flo® 316, Starch 1500®, mannitol and dicalcium phosphate) were effective at concentrations ≥ 10%. SDCII and CII had comparable functionality to commercial disintegrants different from highly swelling disintegrants in which ≥ 10% levels hindered compact disintegration. Ibuprofen release from Avicel® PH-102 compacts required disintegrant levels ≥ 10% for CII and SDCII, whereas for swelling disintegrants, levels ≤ 5% were sufficient.

Silicification increased the true density, Hausner ratio, porosity, specific surface area and ejection force of CII. Conversely, bulk and tap densities decreased with silicification. Silicification had a minimum effect on spheronized materials. Silicified products had a low sensitivity to a lubricant (magnesium stearate) due to SiO_2 competing with magnesium stearate to coat the cellulosic particles. Furthermore, silicification decreased the affinity of CII for water only at the 20% level due to the few hydroxyl groups (silanols) available for hydrogen bonding compared to CII alone.

Compressibility studies demonstrated that silicification decreased the apparent plastic behavior and relaxation tendency of CII. Further, silicification increased powder porosity and hence, the volume reduction capacity of spray-dried and wet granulated CII materials. Tensile strength and energy at break of compacts demonstrated that silicified spray-dried materials had the best compactibility followed by the wet granulated and spheronized products. The latter are not good direct compression excipients since they produced the weakest compacts.

The dissolution properties of compacts made with silicified CII were faster than those prepared with cellulose I materials (Avicel® PH-101, Avicel® PH-102, Prosolv® SMCC 50 and Prosolv® SMMCC 90) because their compacts had a higher affinity for water. Thus, the polymorphic form of cellulose, drug solubility and cellulose affinity for water played a major role in drug release.

Compact tensile strength decreased when tablets were stored at relative humidities ≥75%. This was attributed to water uptake causing partial swelling. As a result, cellulosic materials suffered from a loss of compactibility, especially cellulose II materials due to their high water affinity. For most materials, the optimum relative humidity to store compacts having the largest tensile strength was from ~11 to 22% and from 0 to 11% for cellulose II and cellulose I materials, respectively.

The brittle fracture index of silicified CII materials was higher than that of CI materials. This could indicate a higher capping tendency for these materials. Likewise, the modulus of elasticity and modulus of toughness showed that CI materials and SD-CII:SiO_2 (95:5) had the best mechanical properties, and for the latter it was due to the optimal combination of apparent plastic deformation of CII with the particle rearrangement/fragmentation caused by SiO_2.

SD-CII:SiO_2 (95:5) and WG-CII:SiO_2 (90:10) were selected as optimal excipients between spray-dried and wet granulated materials for direct compression due to their good mechanical properties, good flow, fast disintegration properties, low lubricant sensitivity and low ejection forces. These materials have a potential for use as a direct compression excipient, especially when fast compact disintegration or a double compression method is required. The co-processing technique was successful to improve the functional properties of CII avoiding the need for costly and toxic crosslinking agents.

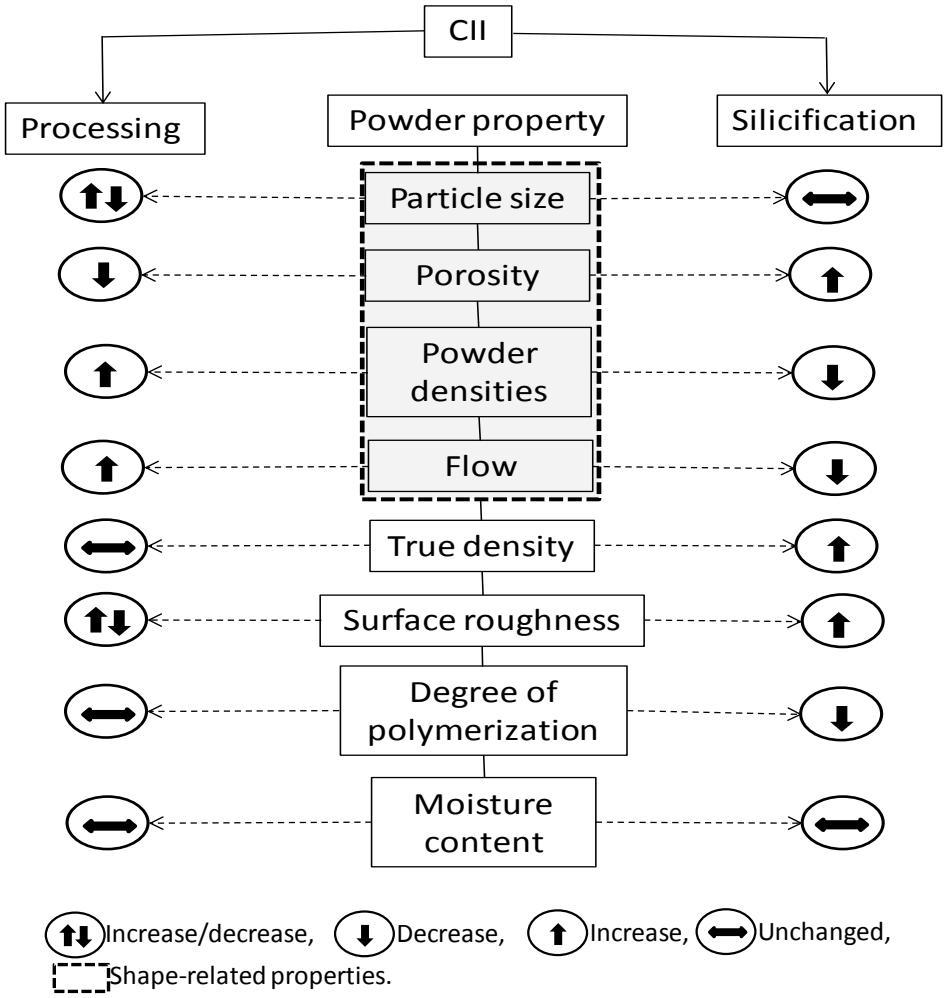

Figure V-1. Effect of Processing on the Powder Properties of CII.

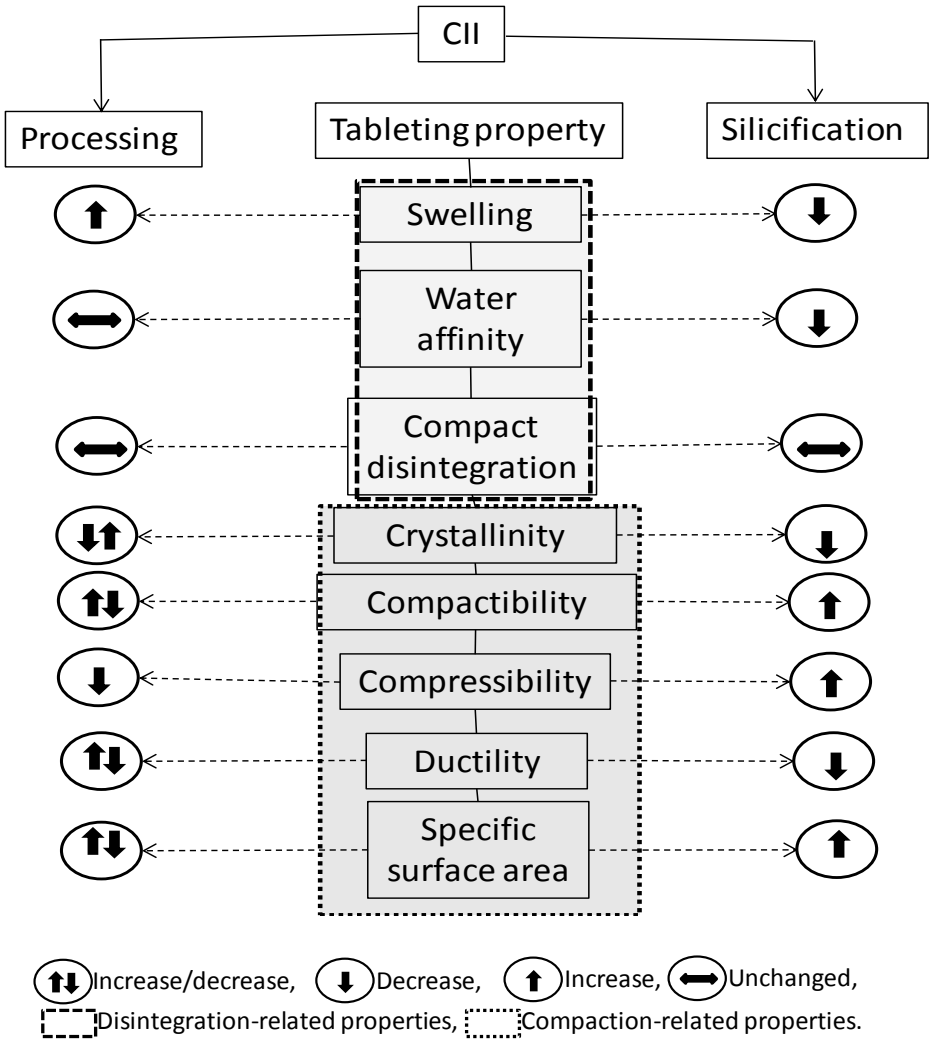

Figure V-2. Effect of Processing on the Tableting Properties of CII.

Future Directions

This study proved that processing and CII co-processing with SiO_2 can be used to improved CII functionality and showed several advantages over cellulose I. Further studies need to be conducted to get a complete understanding of the mechanisms involved on these changes. First, AFM studies are suggested to evaluate the magnitude of the adhesion forces taking place between fumed silica and CII compared to that of cellulose I and fumed silica. Likewise, studies of the shear forces taking place in the powder bed should be conducted in order to understand the magnitude of the cohesion/frictional forces of CII upon silicification. In-die studies must be carried out in a compact simulator to collect real time measurements of powder volume reduction and compression pressure altogether to determine possible contribution of elastic recovery and energy of compaction. Finally, scale-up studies should be conducted if these products want to be taken to the manufacturing industrial scale to see the reproducibility of these results.

APPENDIX A

CALIBRATION CURVES FOR DRUGS EMPLOYED IN DISSOLUTION STUDIES

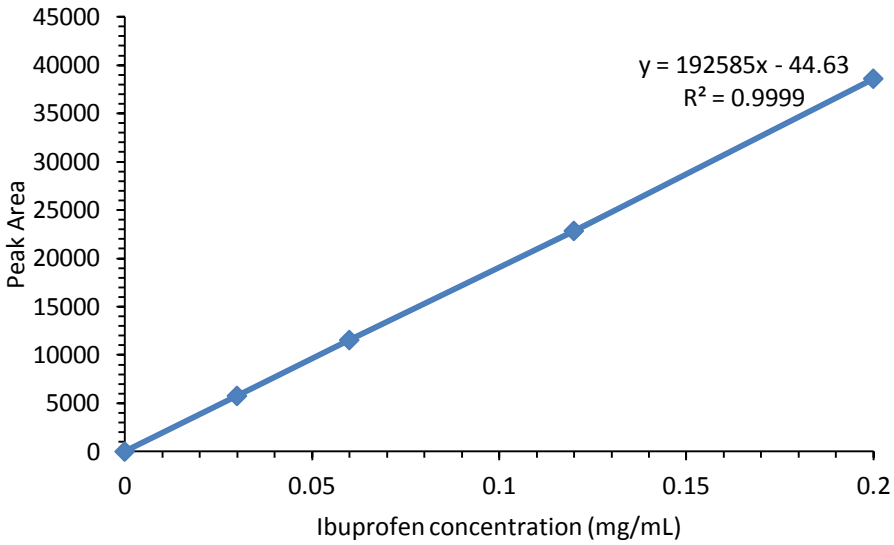

Figure A1. Ibuprofen HPLC Calibration Curve at 221 nm in pH 7.2 Phosphate Buffer.

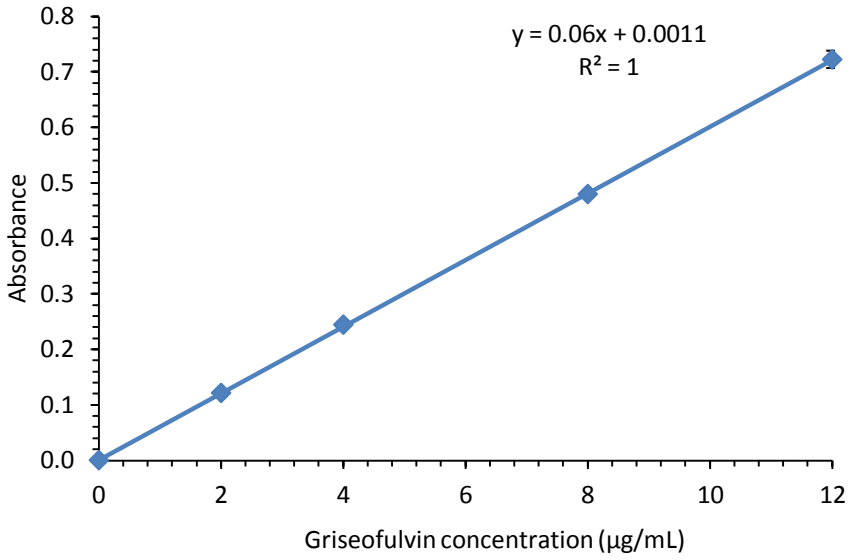

Figure A2. Griseofulvin UV Calibration Curve at 291 nm in Methanol:Water (4:1).

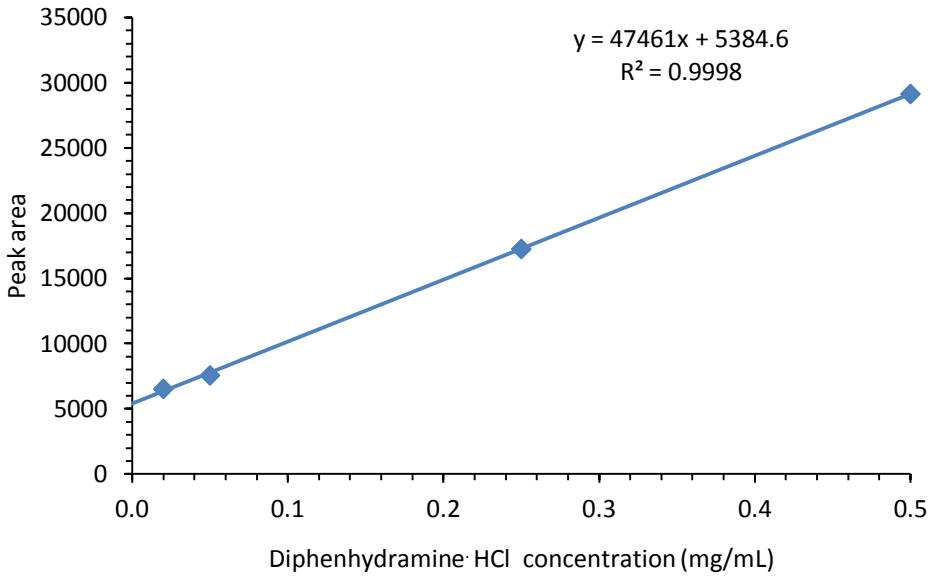

Figure A3. Diphenhydramine HCl HPLC Calibration Curve at 254 nm in Distilled Water.

APPENDIX B

ANOVA TEST FOR PARTICLE SIZE OF CII AQUEOUS DISPERSIONS

The ANOVA Test Results

The analysis of variance is used to separate the variation of data into groups with a specific variation. It tests whether the means of two groups are equal. Thus, the total variance is due to the error plus the one attributed to the treatments. The F-test decomposes variability in terms of sum of squares. The test statistic is an F-test with the ratio of two scaled sums of squares reflecting different sources of variability:

$$F = \frac{\text{explained variance}}{\text{unexplained variance}} \qquad \text{Eqn. B1}$$

According to the number of independent factors it could be one-way or two-way (orthogonal) test. The two-way ANOVA analyzes a dependent variable in terms of groups formed by two independents factors. The test is conducted using an F-distribution to test the strength of association between data. The disadvantage of the ANOVA F-test is that if the null hypothesis is rejected, we do not know which treatments are significantly different from the others. Further analysis will be needed to uncover the results. Table B1 list the results from the two-way ANOVA test to see if particle size was affected by the type of homogenization process and time employed. In this case, both, the type of homogenization and time length affected particle size. Further, the 95% interval of confidence indicate that homogenization produced the largest size followed by colloid milling at 60 aperture, and colloid milling at 6 aperture. Moreover, processing times longer than 20 minutes reduced particle size.

Table B1. ANOVA Test for Cellulosic Dispersions (See Table IV-2)

Two-way ANOVA: Geometric Mean Diameter (D_g) versus Process and Time

Source	DF	SS	MS	F	P
Process	2	19147.0	9573.49	53.34	0.000
Time	4	6539.6	1634.91	9.11	0.000
Error	38	6820.6	179.49		
Total	44	32507.2			

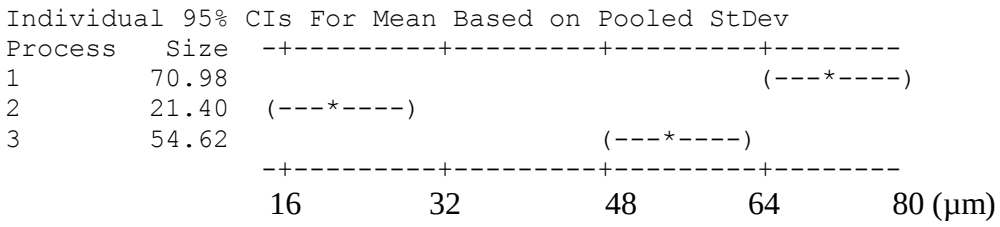

1. Homogenization
2. Colloid milling (aperture 6)
3. Colloid milling (aperture 60)

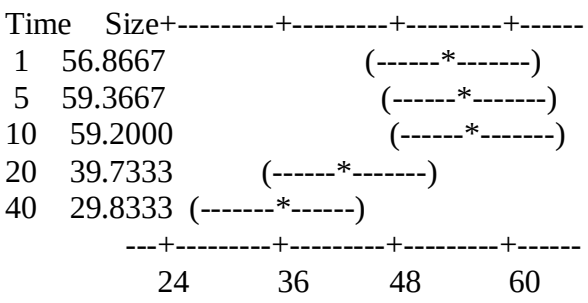

APPENDIX C
RESPONSE SURFACE ANALYSIS OF TENSILE STRENGTH AS A FUNCTION OF RELATIVE HUMIDITY AND TIME

Modeling Tensile Strength Data According to a Response Surface Methodology

In order to understand the effect of storage time and relative humidity (RH) on the tensile strength of the resulting compacts, a Response Surface Methodology was employed by using Minitab® v. 16 (Minitab Inc., State College, PA). In this method, the relationship among several explanatory variables (time and RH) and a dependent variable (tensile strength) was explored using a quadratic model fitted to the data using the least square method. In this case, a second-degree polynomial model was created for each material and these models were used to determine the optimal storage conditions of cellulosic excipients in terms of time and RH. The time levels used were 5, 10, 20 and 30 days and the levels of RH were 0, 11, 22, 33, 56, 75 and 100%, respectively. Table C1 shows the coefficients of the quadratic model for each material along with their respective correlation coefficient. Several transformations were conducted on the response data in order to get the best fit as determined by the determination coefficient and these coefficients were found by the least square method. In general, commercial cellulose I materials presented a better fit using a cubic root transformation of tensile strength ($r^2 > 0.94$). On the contrary, cellulosic II materials had the best fit using a quadratic transformation ($r^2 > 0.75$). However, none of the models used passed the lack of fit test indicating that other more complex models yet to be found. However, as a fitting exercise, these models will be sufficient to show the variation of tensile strength with time and relative humidity.

Figure C1 shows the response surface plots for cellulose II materials. In all cases, a parachute shape graph was obtained. The tensile strength initially increased between 11 to 33% RH followed by a sharp decrease with increasing RH. On the contrary, the storage time had no effect on compact tensile strength ($p > 0.05$). Thus, the tensile

strength of the CII compacts can be ranked as: SD-CII:SiO_2(95:5) ≅ WG-CII:SiO_2(90:10) >> SDCII > WGCII >> CII. This indicates that silicification not only increased the compact tensile strength of cellulose II materials, but by forming strong compacts helped resisting the weakening effect caused by water. Figure C2 shows the surface response plots for commercial cellulose I materials. Opposed to the behavior of cellulose II materials, curves showed a slide-shape. In this case, the tensile strength remained unchanged at RH from 0 to 10%, but decreased steadily after 10%. As seen for the cellulosic I materials, the effect of storage time was not significant (p> 0.05). The tensile strength of cellulosic compacts can be ranked as: Prosolv® SMCC 50 ≅ Prosolv® SMCC 90 > Avicel® PH-101 > Avicel® PH-102. The combined rank of decreasing tensile strength of cellulosic I and II materials was: Prosolv® SMCC 50 ≅ Prosolv® SMCC 90 > Avicel® PH-101 > SD-CII:SiO_2(95:5) ≅ Avicel® PH-102 > WG-CII:SiO_2(90:10) > SDCII > WGCII > CII.

The above results from the quadratic models suggest that the optimum storage condition at 25°C to maintain compacts with the highest tensile strength (i.e., by maximizing this response from the model) during the 30 days varied for each sample. For example, it was between 17 to 30% RH for CII, from 30 to 43% RH for WGCII, between 26 to 38% for SD-CII:SiO_2(95:5), from 26 to 44% for SDCII and between 33 and 49% for WG-CII:SiO_2(90:10), respectively. On the contrary, the predicted optimal storage conditions for commercial cellulose I materials was from 0 to11 % RH for cellulose I materials (Avicel® and Prosolv®). This indicates that these materials are more susceptible to the loss of tensile strength with RH than cellulosic II products.

Table C1. Coefficients of the Quadratic Model from Response Surface Analysis for Tensile Strength as a Function of RH and Time.

Term	Coef.[a]	T[b]	RH[c]	T^{2d}	RH^{2e}	T*RH[f]	r^{2g}
CII[h]	1.140	0.005	0.003	$-1E^{-4}$	$-3E^{-4}$	$-1E^{-5}$	0.7462
SDCII[h]	1.598	0.002	0.011	$-2E^{-5}$	$-1.4E^{-4}$	$-1.7E^{-4}$	0.8966
CII-CII:SiO_2(95:5)[h]	1.567	$5E^{-4}$	0.006	$-1E^{-5}$	$-8E^{-4}$	$-2E^{-4}$	0.8628
WGCII[h]	1.997	-0.002	0.015	$2E^{-4}$	$-2E^{-4}$	$-4E^{-4}$	0.8991
WG-CII:SiO_2(90:10)[h]	1.469	-0.009	0.011	$3E^{-4}$	$-1.2E^{-4}$	$-2E^{-4}$	0.8671
Avicel® PH-101[i]	168.0	-0.051	-0.637	0.04	-0.004	-0.04	0.9522
Avicel® PH-102[i]	99.08	-0.638	-0.269	0.031	-0.004	-0.017	0.9573
Prosolv® SMCC5[j]	253.5	-1.91	-1.58	0.079	0.001	-0.044	0.9576
Prosolv ®SMCC90[j]	243.5	0.132	-1.649	0.014	0.001	-0.040	0.9390

[a] Coefficient.

[b] Time.

[c] Relative humidity.

[d] Time square.

[e] Relative humidity.

[f] Interaction between time and relative humidity.

[g] Correlation coefficient.

[h] Cellulose II materials.

[I] Microcrystalline cellulose I materials.

[j] Silicified microcrystalline cellulose I materials.

Note: The predicted individual tensile strength data can be seen in the surface plots depicted in Figures C1 and C2.

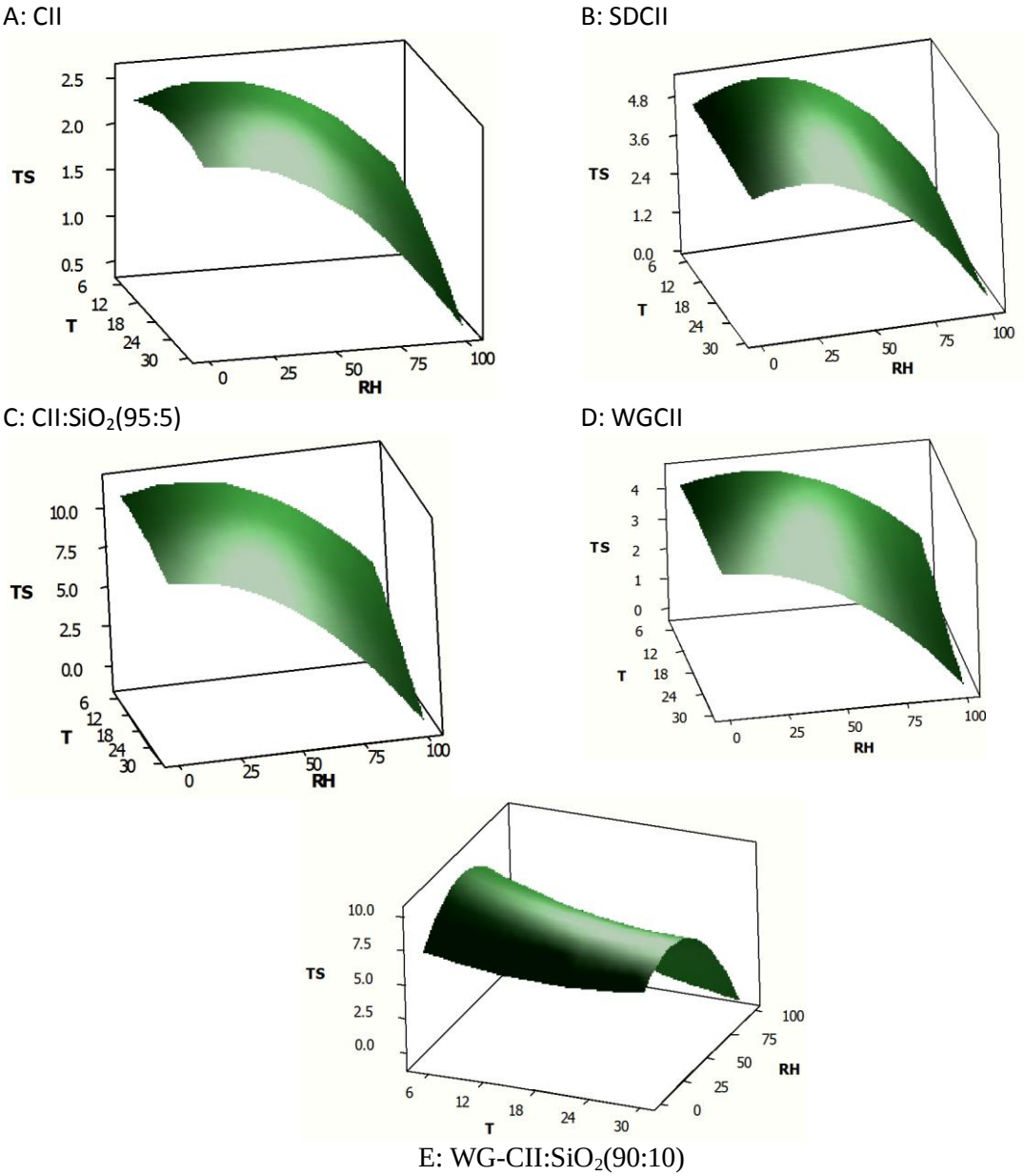

Figure C1. Response Surface Plots for Tensile Strength of the Cellulosic II Materials as a Function of RH and Time.

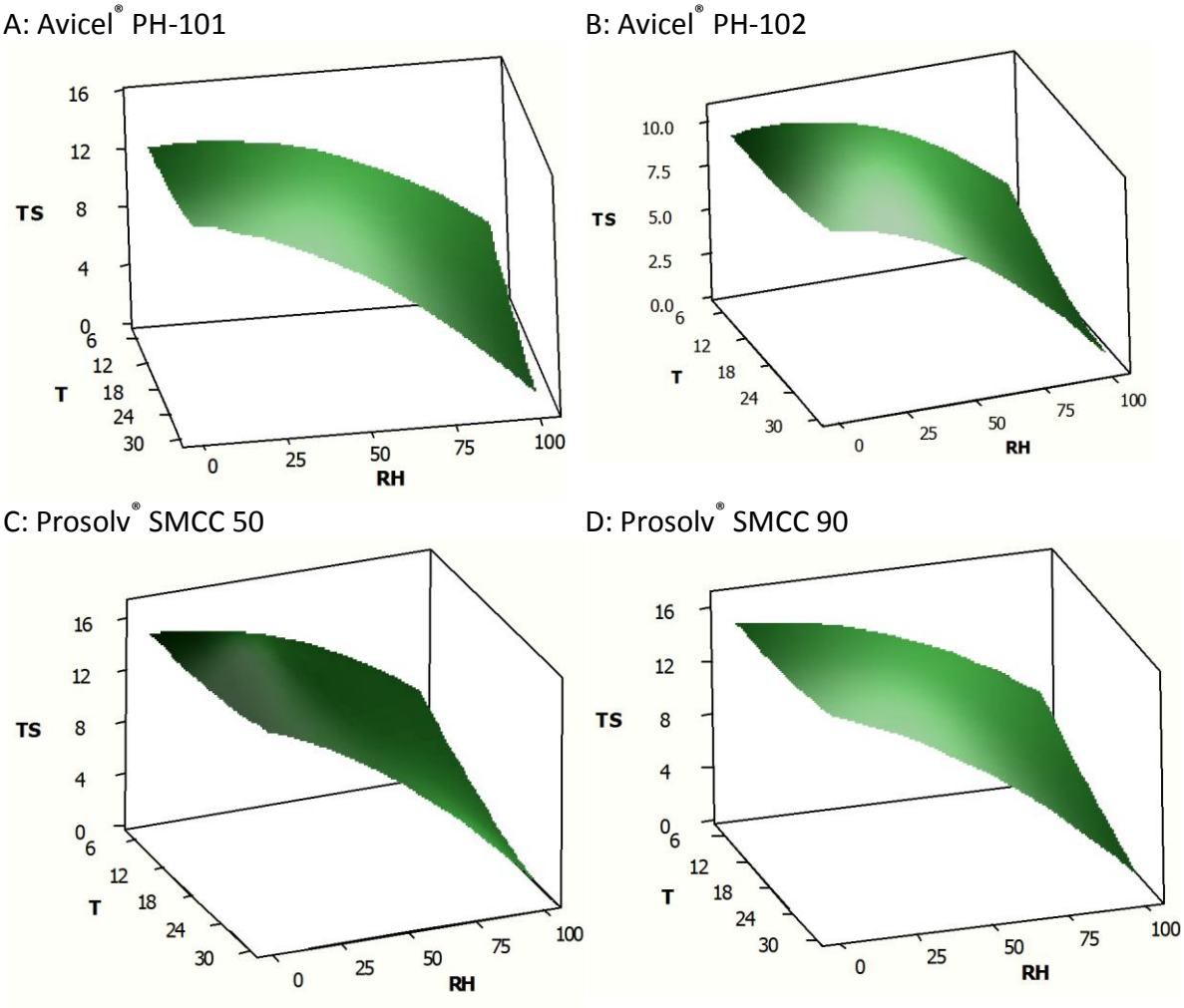

Figure C2: Response Surface Plots for Tensile Strength of Unsilicified (Avicel®) and Silicified (Prosolv®) Cellulosic I Materials as a Function of RH and Time.

Table C2. ANOVA Analysis for Response Surface Methodology for Tensile Strength as a Function of RH and Time.

CII Response Surface Regression: Tensile Strength versus Time and RH

Estimated Regression Coefficients

Term	Coef	SE Coef	T	P
Constant	1.13850	0.025164	45.243	0.000
T	0.00478	0.002981	1.602	0.113
RH	0.00296	0.000635	4.668	0.000
T*T	-0.00010	0.000081	-1.217	0.227
RH*RH	-0.00003	0.000006	-6.194	0.000
T*RH	-0.00009	0.000016	-5.287	0.000

S = 0.0481830
R-Sq = 74.62% R-Sq(pred) = 69.05% R-Sq(adj) = 73.00%

Analysis of Variance

Source	DF	Seq SS	Adj SS	Adj MS	F	P
Regression	5	0.53252	0.53252	0.106504	45.88	0.000
Linear	2	0.37513	0.05367	0.026837	11.56	0.000
Square	2	0.09250	0.09250	0.046251	19.92	0.000
Interaction	1	0.06489	0.06489	0.064891	27.95	0.000
Residual Error	78	0.18108	0.18108	0.002322		
Lack-of-Fit	22	0.13751	0.13751	0.006250	8.03	0.000
Pure Error	56	0.04358	0.04358	0.000778		
Total	83	0.71360				

Table C2 (Continued).

SDCII Response Surface Regression: Tensile Strength versus Time and RH

Estimated Regression Coefficients

Term	Coef	SE Coef	T	P
Constant	1.59802	0.047613	33.563	0.000
T	0.00146	0.005641	0.259	0.796
RH	0.01081	0.001201	8.999	0.000
T*T	-0.00002	0.000153	-0.109	0.914
RH*RH	-0.00014	0.000011	-13.539	0.000
T*RH	-0.00017	0.000031	-5.435	0.000

S = 0.0911674
R-Sq = 89.66% R-Sq(pred) = 87.97% R-Sq(adj) = 88.99%

Analysis of Variance

Source	DF	Seq SS	Adj SS	Adj MS	F	P
Regression	5	5.61993	5.61993	1.123986	135.23	0.000
Linear	2	3.85069	0.67630	0.338149	40.68	0.000
Square	2	1.52371	1.52371	0.761854	91.66	0.000
Interaction	1	0.24553	0.24553	0.245531	29.54	0.000
Residual Error	78	0.64830	0.64830	0.008311		
Lack-of-Fit	22	0.59179	0.59179	0.026899	26.66	0.000
Pure Error	56	0.05651	0.05651	0.001009		
Total	83	6.26823				

Table C2 (Continued).

SD-CII:SiO_2(95:5) Response Surface Regression: Tensile Strength versus Time and RH.

Estimated Regression Coefficients

Term	Coef	SE Coef	T	P
Constant	1.56677	0.039437	39.728	0.000
T	0.00050	0.004673	0.106	0.916
RH	0.00624	0.000995	6.274	0.000
T*T	-0.00001	0.000127	-0.104	0.918
RH*RH	-0.00008	0.000009	-9.204	0.000
T*RH	-0.00016	0.000026	-6.144	0.000

S = 0.0755121
R-Sq = 86.28% R-Sq(pred) = 83.61% R-Sq(adj) = 85.41%

Analysis of Variance

Source	DF	Seq SS	Adj SS	Adj MS	F	P
Regression	5	2.79797	2.79797	0.559594	98.14	0.000
Linear	2	2.09962	0.22589	0.112945	19.81	0.000
Square	2	0.48309	0.48309	0.241545	42.36	0.000
Interaction	1	0.21525	0.21525	0.215255	37.75	0.000
Residual Error	78	0.44476	0.44476	0.005702		
Lack-of-Fit	22	0.43398	0.43398	0.019727	102.49	0.000
Pure Error	56	0.01078	0.01078	0.000192		
Total	83	3.24273				

Table C2 (Continued).

WGCII Response Surface Regression: Tensile Strength versus Time and RH

Estimated Regression Coefficients

Term	Coef	SE Coef	T	P
Constant	1.99664	0.081997	24.350	0.000
T	-0.00221	0.009715	-0.228	0.820
RH	0.01496	0.002069	7.233	0.000
T*T	0.00016	0.000264	0.621	0.536
RH*RH	-0.00020	0.000018	-11.041	0.000
T*RH	-0.00038	0.000053	-7.085	0.000

S = 0.157004
R-Sq = 89.91% R-Sq(pred) = 87.84% R-Sq(adj) = 89.26%

Analysis of Variance

Source	DF	Seq SS	Adj SS	Adj MS	F	P
Regression	5	17.1286	17.1286	3.42572	138.97	0.000
Linear	2	12.8771	1.3111	0.65554	26.59	0.000
Square	2	3.0142	3.0142	1.50711	61.14	0.000
Interaction	1	1.2372	1.2372	1.23724	50.19	0.000
Residual Error	78	1.9227	1.9227	0.02465		
Lack-of-Fit	22	1.6974	1.6974	0.07715	19.17	0.000
Pure Error	56	0.2253	0.2253	0.00402		
Total	83	19.0513				

Table C2 (Continued).

WG-CII:SiO_2(90:10) Response Surface Regression: Tensile Strength versus Time and RH

Estimated Regression Coefficients

Term	Coef	SE Coef	T	P
Constant	1.46917	0.037242	39.449	0.000
T	-0.00867	0.004412	-1.964	0.053
RH	0.01063	0.000940	11.317	0.000
T*T	0.00028	0.000120	2.338	0.022
RH*RH	-0.00012	0.000008	-14.033	0.000
T*RH	-0.00016	0.000024	-6.483	0.000

S = 0.0713094
R-Sq = 86.71% R-Sq(pred) = 84.33% R-Sq(adj) = 85.86%
Analysis of Variance

Source	DF	Seq SS	Adj SS	Adj MS	F	P
Regression	5	2.58868	2.58868	0.517736	101.82	0.000
Linear	2	1.34585	0.69950	0.349750	68.78	0.000
Square	2	1.02911	1.02911	0.514553	101.19	0.000
Interaction	1	0.21373	0.21373	0.213728	42.03	0.000
Residual Error	78	0.39663	0.39663	0.005085		
Lack-of-Fit	22	0.37505	0.37505	0.017048	44.23	0.000
Pure Error	56	0.02158	0.02158	0.000385		
Total	83	2.98531				

Table C2 (Continued).

Avicel® PH-101 Response Surface Regression: Tensile Strength versus Time and RH

Estimated Regression Coefficients

Term	Coef	SE Coef	T	P
Constant	167.961	6.85988	24.485	0.000
T	-0.051	0.81277	-0.063	0.950
RH	-0.637	0.17305	-3.678	0.000
T*T	0.042	0.02207	1.899	0.061
RH*RH	-0.004	0.00153	-2.741	0.008
T*RH	-0.036	0.00446	-8.173	0.000

S = 13.1350
R-Sq = 95.22% R-Sq(pred) = 94.53% R-Sq(adj) = 94.91%

Analysis of Variance

Source	DF	Seq SS	Adj SS	Adj MS	F	P
Regression	5	267934	267934	53586.7	310.60	0.000
Linear	2	254492	2350	1174.8	6.81	0.002
Square	2	1918	1918	958.9	5.56	0.006
Interaction	1	11524	11524	11523.7	66.79	0.000
Residual Error	78	13457	13457	172.5		
Lack-of-Fit	22	10234	10234	465.2	8.08	0.000
Pure Error	56	3223	3223	57.6		
Total	83	281391				

Table C2 (Continued).

Avicel® PH-102 Response Surface Regression: Tensile Strength versus Time and RH

Estimated Regression Coefficients

Term	Coef	SE Coef	T	P
Constant	99.0823	3.58322	27.652	0.000
T	-0.6381	0.42454	-1.503	0.137
RH	-0.2689	0.09039	-2.974	0.004
T*T	0.0309	0.01153	2.677	0.009
RH*RH	-0.0037	0.00080	-4.698	0.000
T*RH	-0.0166	0.00233	-7.127	0.000

S = 6.86098
R-Sq = 95.73% R-Sq(pred) = 95.00% R-Sq(adj) = 95.45%

Analysis of Variance

Source	DF	Seq SS	Adj SS	Adj MS	F	P
Regression	5	82250	82250.1	16450.03	349.46	0.000
Linear	2	78483	486.4	243.21	5.17	0.008
Square	2	1376	1376.3	688.14	14.62	0.000
Interaction	1	2391	2390.9	2390.90	50.79	0.000
Residual Error	78	3672	3671.7	47.07		
Lack-of-Fit	22	2566	2566.1	116.64	5.91	0.000
Pure Error	56	1106	1105.6	19.74		
Total	83	85922				

Table C2 (Continued).

Prosolv® SMCC 50 Response Surface Regression: Tensile Strength versus Time and RH

Estimated Regression Coefficients

Term	Coef	SE Coef	T	P
Constant	253.460	8.73735	29.009	0.000
T	-1.908	1.03521	-1.843	0.069
RH	-1.580	0.22042	-7.167	0.000
T*T	0.079	0.02811	2.805	0.006
RH*RH	0.001	0.00195	0.358	0.721
T*RH	-0.044	0.00568	-7.744	0.000

S = 16.7299
R-Sq = 95.76% R-Sq(pred) = 95.04% R-Sq(adj) = 95.49%
Analysis of Variance

Source	DF	Seq SS	Adj SS	Adj MS	F	P
Regression	5	493368	493368	98673.6	352.55	0.000
Linear	2	474344	14748	7374.1	26.35	0.000
Square	2	2238	2238	1119.0	4.00	0.022
Interaction	1	16786	16786	16786.2	59.97	0.000
Residual Error	78	21831	21831	279.9		
Lack-of-Fit	22	18380	18380	835.5	13.56	0.000
Pure Error	56	3451	3451	61.6		
Total	83	515199				

Table C2 (Continued).

Prosolv® SMCC 90 Response Surface Regression: Tensile Strength versus Time and RH

Estimated Regression Coefficients

Term	Coef	SE Coef	T	P
Constant	243.508	10.4554	23.290	0.000
T	0.132	1.2388	0.107	0.915
RH	-1.649	0.2638	-6.253	0.000
T*T	0.014	0.0336	0.412	0.681
RH*RH	0.001	0.0023	0.427	0.670
T*RH	-0.040	0.0068	-5.920	0.000

S = 20.0195
R-Sq = 93.90% R-Sq(pred) = 92.96% R-Sq(adj) = 93.51%

Analysis of Variance

Source	DF	Seq SS	Adj SS	Adj MS	F	P
Regression	5	481203	481203.3	96240.7	240.13	0.000
Linear	2	467018	15879.2	7939.6	19.81	0.000
Square	2	141	141.3	70.6	0.18	0.839
Interaction	1	14044	14044.4	14044.4	35.04	0.000
Residual Error	78	31261	31260.8	400.8		
Lack-of-Fit	22	22900	22899.8	1040.9	6.97	0.000
Pure Error	56	8361	8361.0	149.3		
Total	83	51246				

APPENDIX D

TENSILE STRENGTH OF REPROCESSED MATERIALS

Reprocessing Susceptibility

Figure D1 shows the tensile strength of ~1 g of round size compacts prepared at ~0.1 porosity with acetaminophen:excipient mixtures (1:1) before and after reprocessing or recompression. In general, reprocessing had a negative impact on the compact tensile strength since the binding ability of the particles was reduced after the first compaction (p= 0.00). It has been reported that the loss of compactibility is due to the increase in the yield pressure. In other words, materials become less plastic after compression followed by milling (Kochhar, 1994). Tensile strength of these compacts showed the rank: Prosolv® SMCC 50 ≅ SD-CII:SiO_2 (95:5) (p= 0.99) > Avicel® PH-102 ≅ Avicel® PH-101 (p= 0.99) > Prosolv® SMCC 90 ≅ WG-CII:SiO_2(90:10) ≅ SDCII (p= 0.24 and p= 0.33) > CII ≅ WGCII (p= 1.00). The loss of compactibility was more pronounced for cellulose I materials. For instance, Prosolv® SMCC 90 and Prosolv® SMCC 50 had initially different tensile strength, but upon reprocessing their tensile strength were comparable. It is possible that the P_y of these highly plastically deforming materials increased due the loss of plasticity of cellulose I and the contributing brittle character of acetaminophen. Some studies suggest the work of hardening as the cause for the loss of compactibility. For this reason, the pre-compression process also contributed to a decrease in compactibility similar to that reported for dry granulation (Herting and Kleinebudde, 2008). After recompression the tensile strength of Avicel® PH-101, Avicel® PH-102, Prosolv® SMCC 50 and Prosolv® SMCC 90, SDCII and WG-CII:SiO_2(90:10) were comparable. After the second compression process only SD-CII:SiO_2(95:5) showed comparable values to the unprocessed material suggesting that a 5% SiO_2 counteracts the acetaminophen ability to induce relaxation and loss of compact strength of cellulose compacts. However, this protective effect was not seen for WG-CII:SiO_2(90:10) due to the large SiO_2 component

which also interacted with the brittle deforming acetaminophen resulting in weak compacts after recompression.

Figure D2 depicts the percentage of loss of compactibility with reprocessing. In this case, the loss of compactibility is defined as the inverse of reworkability. Reworkability refers to the capacity of the materials to withstand reprocessing without losing their compactibility. Two major trends for the loss of compactibility are shown. The first one composed by Avicel® PH-102, CII, Prosolv® SMCC 50 and Avicel® PH-101 which lost from 60 to 70% of their original compactibility. The second trend is composed by Prosolv® SMCC 90, SD-CII:SiO_2(95:5), WGCII, WG-CII:SiO_2(90:10) and SDCII which lost from 15 to 30% of compactibility. It is reported that the loss of reworkability is due to the "work hardening". This theory establishes that during compression or roller compaction a great amount of defects in the particles and entanglement of new dislocations occurs while being deformed plastically. These defects harden particles and makes plastic deformation more difficult for the subsequent compaction process (He et al., 2007; Sun and Himmelspach, 2005). The overall trend of compactibility loss was Avicel® PH-102 > CII > Prosolv® SMCC 50 ≅ Avicel® PH-101 >> Prosolv® SMCC 90 > SD-CII:SiO_2(95:5) ≅ WGCII > WG-CII:SiO_2(90:10) > SDCII. Thus, most plastic deforming materials which exhibited a high initial tensile strength presented a high loss of compactibility except for CII. Results indicate that the reinforcing role of SiO_2 was very important to avoid a major loss of compactibility due to reprocessing. Since SiO_2 makes materials less plastic, the impact of work hardening produced by reprocessing will be less pronounced than that of unsilicified materials.

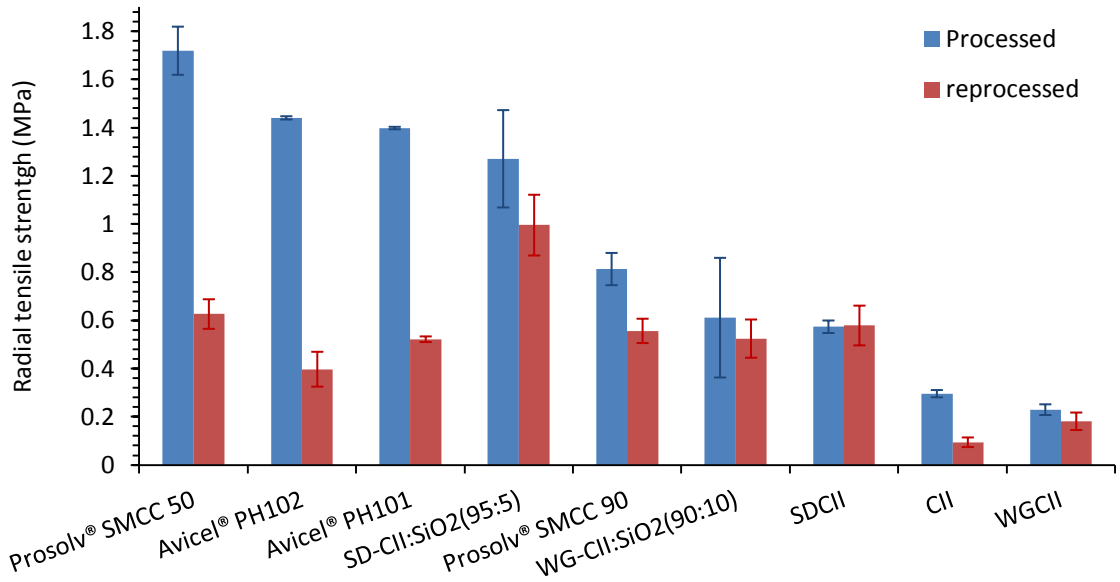

Figure D1. Radial Tensile Strength of Processed and Reprocessed Round Compacts of Acetaminophen:Excipient (1:1) for Cellulose II and Commercial Cellulose I (Avicel® and Prosolv®) Materials.

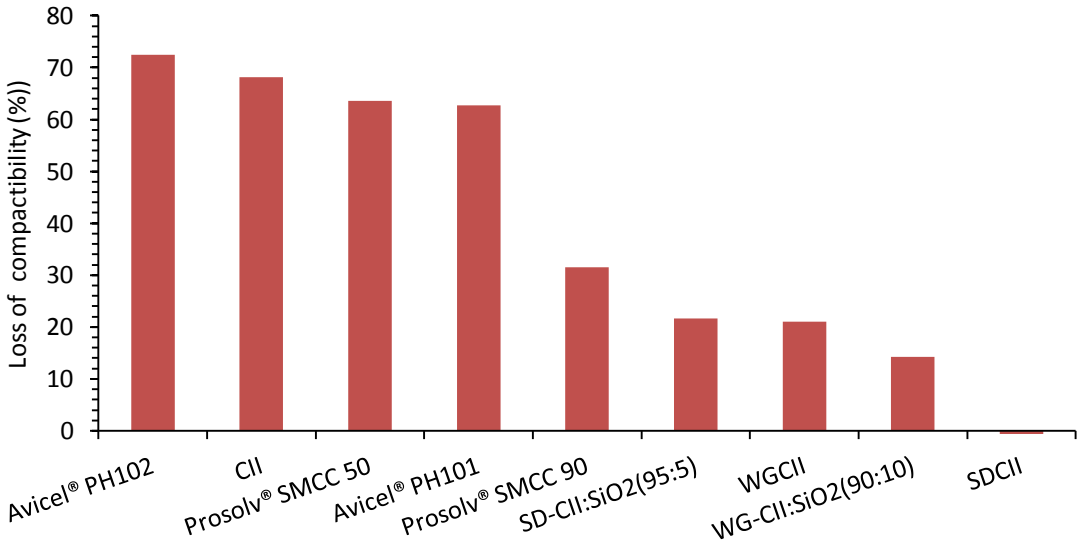

Figure D2. Decrease in Compact Tensile Strength with Reprocessing for Cellulose II and Commercial Cellulose I (Avicel® and Prosolv®) Materials.

Tukey Test for the Tensile Strength of Reprocessed Materials.

The Tukey test for equal sample sizes is a *post hoc* test which is used after the ANOVA test has been conducted. This test builds confidence intervals for all pairwise differences between factor level means maintaining a family error constant (usually 0.05). Thus, the mean of each factor level is compared with the others and if the *p*-value is <0.05, there is a significant difference between the two means. Further, confidence intervals can be constructed for the difference of the two means and if this interval contains the zero value, there is no statistical difference between the two sample means. This test assumes that the two sample groups are independent and that there is an equal variation among all observations. The Tukey statistic and the interval of confidence for the difference of the means of the two groups are found by:

$$t = \frac{\mathrm{Y_i} - \mathrm{Y_j}}{\mathrm{SE}}$$

$$Y_i - \mathrm{Y_j} \pm \frac{\mathrm{t}\alpha, \mathrm{r}, (\mathrm{N} - \mathrm{r})}{\sqrt{2}} - \sigma\sqrt{\frac{2}{N}}$$

Where t is the studentized distribution, $\mathrm{Y_i}$ and $\mathrm{Y_j}$ are the means of groups i and j, respectively. SE is the standard error, α is the confidence level, N and r are the population size and the group size, respectively.

Table D1. ANOVA Table and Tukey Test for Tensile Strength of Reprocessed Cellulose II and Commercial Cellulose I (Avicel® and Prosolv®) Materials.

Source	Degree of freedom	Sum squares	Mean squares	F	p-value
Reprocessing	1	3.34	3.34	392.24	0.00
Sample	8	8.46	1.06	124.27	0.00
Reprocessing and sample	8	3.15	0.39	46.22	0.00
Error	54	0.46	0.01		
Total	71				

Prosolv® SMCC 50 and:	Difference of Means	SE	t-Value	p-Value
Avicel® PH-102	-0.25	0.05	-5.50	0.00
Avicel® PH-101	-0.21	0.05	-4.61	0.00
SD-CII:SiO_2(95:5)	-0.04	0.05	-0.86	0.99
Prosolv® SMCC 90	-0.49	0.05	-10.58	0.00
WG-CII:SiO_2(90:10)	-0.60	0.05	-13.11	0.00
SDCII	-0.60	0.05	-12.93	0.00
CII	-0.98	0.05	-21.19	0.00
WGCII	-0.97	0.05	-20.97	0.00
Avicel® PH-102 and:				
Avicel® PH-101	0.04	0.05	0.89	0.99
SD-CII:SiO_2(95:5)	0.21	0.05	4.64	0.00
Prosolv® SMCC 90	-0.23	0.05	-5.08	0.00
WG-CII:SiO_2(90:10)	-0.35	0.05	-7.61	0.00
SDCII	-0.34	0.05	-7.43	0.00
CII	-0.72	0.05	-15.69	0.00
WGCII	-0.71	0.05	-15.47	0.00
Avicel® PH-101 and:				
SD-CII:SiO_2(95:5)	0.17	0.05	3.75	0.01
Prosolv® SMCC 90	-0.28	0.05	-5.97	0.00
WG-CII:SiO_2(90:10)	-0.39	0.05	-8.50	0.00
SDCII	-0.38	0.05	-8.32	0.00
CII	-0.77	0.05	-16.58	0.00
WGCII	-0.75	0.05	-16.36	0.00

Table D1 (Continued).

SD-CII:SiO_2(95:5) and:				
Prosolv® SMCC 90	-0.45	0.05	-9.72	0.00
WG-CII:SiO_2(90:10)	-0.57	0.05	-12.25	0.00
SDCII	-0.56	0.05	-12.07	0.00
CII	-0.94	0.05	-20.33	0.00
WGCII	-0.93	0.05	-20.11	0.00
Prosolv® SMCC 90 and				
WG-CII:SiO_2(90:10)	-0.12	0.05	-2.53	0.24
SDCII	-0.11	0.05	-2.35	0.33
CII	-0.49	0.05	-10.61	0.00
WGCII	-0.48	0.05	-10.39	0.00
WG-CII:SiO_2(90:10) and:				
SDCII	0.01	0.05	0.18	1.00
CII	-0.37	0.05	-8.08	0.00
WGCII	-0.36	0.05	-7.86	0.00
SDCII and:				
CII	-0.38	0.05	-8.26	0.00
WGCII	-0.37	0.05	-8.04	0.00
CII and:				
WGCII	0.01	0.05	0.22	1.00

REFERENCES

Adolfsson A and Nystrom C. 1996. Tablet strength, porosity, elasticity and solid state structure of tablets compressed at high loads. Int J Pharm 132:95-106.

Agrawal AM, Howard MA, Neau SH. 2004. Extruded and spheronized beads containing no microcrystalline cellulose: influence of formulation and process variables. Pharm Dev Technol 9:197-217.

Ahmad AA, Chatterji A, Shah NA, Sandhu HK. 2009. Functional performance of silicified microcrystalline cellulose versus microcrystalline cellulose: a case study. Drug Dev Ind Pharm 35:1066-1071.

Ahuja S and Scypinski S, editors. 2011. Handbook of Modern Pharmaceutical Analysis. Burlington: Academic Press. pp.39-42.

Airaksinen S, Karjalainen M, Schevchenko A, Westermarck S, Leppanen E, Rantanen J, Yliruusi, J. 2005. Role of water in the physical stability of dosage formulations. J Phar Sci 94:2147-2165.

Alderborn G and Nyström C. 1996. Pharmaceutical Powder Compaction Technology. New York: Marcel Dekker Inc.615 p.

Allen LV, Popovich NG, Ansel HC, editors. 1999. Ansel's Pharmaceutical Dosage Forms and Drug Delivery Systems. 8th ed. Philadelphia: Lippicont Williams and Wilkins. 423 p.

Almaya A and Aburub A. 2008. Effect of particle size on compaction of materials with different deformation mechanisms with and without lubricants. AAPS PharmSciTech 9:414-418.

Arida AI and Al-Tabakha MM. 2008. Cellactose a co-processed excipient: A comparison study. Pharm Dev Technol 13:165-175.

Ashish A and Neves S. 2006. From commodities to specialized excipients. Pharm Health News 4:5-8.

Ashok K and Mahesh VC. 2006. A comparison of physical and mechanical properties of common tabeting diluents. In: Excipient Development for Pharmaceutical, Biotechnology and Drug Delivery. 1st ed. New York: CRC Press. pp.146-149.

Auguello M, Ruszkay T, Reier G, inventors; Co-processed microcrystalline cellulose and calcium carbonate. EP 0942950. 1998a.

Auguello M, Ruszkay TA, Reier GE, inventors; Co-processed products. US Pat. 5,747,067. 1998b.

Avachat A and Ahire V. 2007. Characterization and evaluation of spray dried co-processed excipients and their application in solid dosage forms. Indian J Pharm Sci 69:85-90.

Badwan A, Al-remawi M, Rashid I, inventors; Starch silica co-precipitate, method for preparing the same and use thereof. EP 1 886 671 A1. 2008.

Banker GS and Rhodes CT, editors. 2002. Modern Pharmaceutics. 4th ed. New York: Marcel Dekker. 628 p.

Bassam F, York P, Rowe R, Roberts R. 1990. Young's modulus of powders used as pharmaceutical excipients. Int J Pharm 64:55-60.

Battista OA, Hill D, Smith PA, inventors; Level-off D.P. Cellulose products. US Pat, 2,978,446. 1957.

Battista O, inventor; Shaped particles containing cellulose crystallite aggregates having an average level-off. US 3357845. 1966.

Battista O. 1965. Colloidal macromolecular phenomena. J Polym Sci Pol Sym 9:135-155.

Battista O and Smith P, inventors; Level-off degree of polymerization cellulose products. US 2978446. 1961.

Belda P and Mielck J. 1996. Tableting behavior of Cellactose compared with mixtures of celluloses with lactoses. Eur J Pharm Biopharm 42:325-330.

Behzadi SS, Ölzant S, Länger R, Koban C, Unger FM, Viernstein H. 2006. Investigation of the stability of tablets prepared from sucrose and citric acid anhydride utilizing response surface methodology. Eur Food Res Technol 223:238-245.

Beso A and Sirca J, inventors; Rapidly disintegrating orodispersible composition containing nonfilamentous coprocessed polyols particles and silicified microcrystalline cellulose. EP 1773292. 2006.

Bhargava HN, Shah D, Anaebonam A, Oza B. 1991. An evaluation of smecta as a tablet disintegrant and dissolution aid. Drug Dev Ind Pharm 17:2093-2102.

Bi YX, Sunada H, Yonezawa Y, Danjo K. 1999. Evaluation of rapidly disintegrating tablets prepared by a direct compression method. Drug Dev Ind Pharm 95:571-581.

Billon A, Bataille B, Maury L, Terol A, Jacob M. 1999. Physicochemical investigation of the interaction between cellulose derivatives and plasticizers in controlled release forms: Application to spray-dried acetaminophen microparticulate systems. STP Pharma Sci 9:169-174.

Blackwell J and Kolpak F. 1975. The cellulose microfibril as an imperfect array of elementary fibrils. Macromolecules 8:322-326.

Block LH, Moreton RC, Apte SP, Wendt RH, Munson EJ, Creekmore JR, Persaud IV, Sheehan C, Wangc H. 2009. Co-processed excipients. Pharm Forum 35:1026-1028.

Bolhuis GK and Armstrong AN. 2006. Excipients for direct compaction-an update. Pharm Dev Technol 11:111-124.

Bolhuis GK and Chowhan ZT. 1996. Materials for direct compression. In: Pharmaceutical Powder Compaction Technology. Alderborn G and Nystrom C, editors. New York: Dekker. pp.419-500.

Bolhuis G and Zuurman K. 1995. Tableting properties of experimental and commercially available lactose granulations for direct compression. Drug Dev Ind Pharm 21:2057-2071.

Bolhuis GK, Arends-Scholte AW, Stuut GJ, De Vries JA,. 1994. Disintegration efficiency of sodium starch glycolates, prepared from different native starches. Eur J Pharm Biopharm 40:317-320.

Bolhuis G, Kussendrager K, Langridge J. 2004. New developments in spray-dried lactose. Pharm Technol:26-31.

Bolhuis GK, Rexwinkel EG, Zuurman K. 2009. Polyols as filler-binders for disintegrating tablets prepared by direct compaction. Drug Dev Ind Pharm 35:671-677.

Bos CE, Bolhuis GK, Lerk CF, Duineveld CAA. 1992. Evaluation of modified rice starch, e new excipient for direct compression. Drug Dev Ind Pharm 18:93-106.

Boyer HE, editor. 1987. Atlas of Stress-Strain Curves. 1st ed. American Society for Metals. Metals Park, Ohio. 630 p.

Bowe K, Billig J, Schwartz J, Moore J, Wang A. 1997. Crystalline maltose: A direct-compression pharmaceutical excipient. Pharm Technol:44-50.

Broadhead J, Rouan ESK, Rhodes CT. 1992. The spray drying of pharmaceuticals. Drug Dev Ind Pharm 18:1169-1206.

Brunauer S, Deming LS, Deming WE, Teller E. 1940. On a theory of the Van der Waals adsorption of gases. J Am Chem Soc 62:1723-1732.

Cabot. 2008a. CAB-o-Sil M-5DP untreated fumed silica is a synthetic, amorphous silica that complies with the pharmacopoeia monographs. Cabot Corp PDS-147:1-4.

Cabot. 2008b. CAB-o-Sil M-5DP: Higher bulk density fumed silica for tableting. Cabot Corp TD-255:1-2.

Cabot. 2004. Influence of Cab-o-Sil M5P on the angle of repose and flow rates of pharmaceutical powders. Cabot Corp TD-176:1-10.

Cabot. 1987. CAB-o-Sil Fume silica properties and functions. Cabot CGen-8:1-36.

Carlin B. 2008. Direct compression and the role of filler-binders. In: Pharmaceutical Dosage Forms: Tablets, Volume 2: Rational Design and Formulation. Augsburger AL and Hoag SW, editors. 3rd ed. New York, USA: Informa Healthcare. pp.173-216.

Carr RL. 1965. Evaluating flow properties of solids. Chem Eng 72: 163-168.

Carrillo F, Colom X, Sunol JJ, Saurina J. 2004. Structural FT-IR analysis and thermal characterization of lyocel and viscose-type fibers. Eur Polym J 40:229-234.

Casalderrey M, Souto C, Concheiro A, Gómez-Amoza JL, Martínez-Pacheco R. 2004. A comparison of drug loading capacity of Cellactose with two *ad hoc* processed lactose-cellulose direct compression excipients. Chem Pharm Bull 52:398-401.

Celik, M., Mollan, M.J., Chang, N. 1987. The reworkability of microcrystalline cellulose formulations. In: Pharmaceutical Technology: Tableting Technology (Compression). Wells J and Rubinstein M., editors. 1st ed. Chichester, Great Britain: Ellis Horwood. pp.44-60.

Chang D and Chang R. 2007. Review of current issues in pharmaceutical excipients. Pharm Technol 31:56.

Chow K, Tong HHY, Lum S, Chow AHL. 2008. Engineering of pharmaceutical materials: An industrial perspective. J Pharm Sci 97:2855-2877.

Chowdary KPR and Srinivasa SK. 2000. Investigation of dissolution enhancement of itraconazole by solid dispersion in superdisintegrants. Drug Dev Ind Pharm 26:1207-1211.

Chowhan CT and Chow YP. 1980. Compression behavior of pharmaceutical powders. Int J Pharm 5:139-148.

Clerch AV. 2008. Aportacion al diseno de un nuevo excipient tipo "coprocessed product" para compresion directa. Barcelona: University of Barcelona, 235p.

Corrigan OI and Crean AM. 2002. Comparative physicochemical properties of hydrocortisone-PVP composites prepared using supercritical carbon dioxide by the gas anti-solvent recrystallization process, by coprecipitation and by spray drying. Int J Pharm 245:75-82.

Crisp JL, Dann SE, Edgar M, Blatchford CG. 2010. The effect of particle size on the dehydration /rehydration behaviour of lactose. Int J Pharm 391:38-47.

David S and Augsburger L. 1977. Plastic flow during compression of directly compressible fillers and its effect on tablet strength. J Pharm Sci 66:155-159.

Davis JR. 2004. Tensile Testing. 2nd ed. Materials Park, OH: Asm Intl. 283 p.

Denny PJ. 2002. Comparison equations: A comparison of the Heckel and Kawakita equations. Powder Technol 127:162-172.

DMV Fonterra excipients. 2008. Primojel and Primellose superdisintegrants. DMV GmBh & Co. 3:1-6.

Doldan C, Souto C, Concheiro A, Martinez-Pacheco R, Gomez-Amoza J. 1995. Dicalcium phosphate dihydrate and anhydrous dicalcium phosphate for direct compression: a comparative study. Int J Pharm 124:69-74.

Drapier-Beche N, Fanni J, Parmentier M. 1999. Physical and chemical properties of molecular compounds of lactose. J. Dairy Sci. 82:2558-2563.

Durgapal S, Das A, Das S, Ghosh A, Deb J, Tyagi G, Upadhyay M, Saha S. 2010. Formulation, evaluation, and optimization of floating microparticulate system of ofloxacin for oral controlled delivery system. Int J Pharm Sci Bio 2:86-92.

Edge S, Steele DF, Chen A, Tobyn MJ, Staniforth JN. 2000. The mechanical properties of compacts of microcrystalline cellulose and silicified microcrystalline cellulose. Int J Pharm 200:67-72.

Edge S, Steele FD, Tobyn M, Staniforth JN, editors. 1999. Polysaccharide engineering: Silicified microcrystalline cellulose as a novel high-functionality pharmaceutical material in: ACS Symposium series # 737: Polysaccharides Applications: cosmetics and Pharmaceuticals. Washington D.C. American Chemical Society. 368 p.

Edge S, Steele DF, Staniforth JN, Chen A, Woodcock P. 2002a. Powder compaction properties of sodium starch glycolate disintegrants. Drug Dev Ind Pharm 28:989-999.

Edge S, BeluA M, Potter UJ, Steele DF, Young PM, Price R, Staniforth JN. 2002b. Chemical characterisation of sodium starch glycolate particles. Int J Pharm 240:67-78.

El-Barghouthi M, Eftaiha A, Rashid I, Al-Remawi M, Badwan A. 2008. A novel superdisintegrating agent made from physically modified chitosan with silicon dioxide. Drug Dev Ind Pharm 34:373-383.

Elversson J and Millqvist-Fureby A. 2005. Particle size and density in spray drying-effects of carbohydrate properties. J Pharm Sci 94:2049-2060.

Eroma OP, Nygren J, Heikkila H, Sorensen PB, Sarkki ML, Fairs I, Gros H, inventors; Crystallization of polyol compositions, crystalline polyol composition product and use thereof. EP 1539664. 2003.

Esezobo S and Pilpel N. 1987. Effects of applied load and particle size on the plastoelasticity and tablet strength of some directly compressible powders. J Pharm Pharmacol 39:303-304.

Faroongsarng D and Peck G. 1991. The swelling of core tablets during aqueous coating: A simple model describing extent of swelling and water penetration for insoluble tablets containing a superdisintegrant. Drug Dev Ind Pharm 17:2439-2455.

Fassihi AR. 1988. Consolidation behavior of polymeric substances in non-disintegrating solid matrices. Int J Pharm 44:249-256.

Fell JT and Newton JM. 1968. The tensile strength of lactose tablets. J Pharm Pharmacol 20:657-758.

Felton LA, Garcia DI, Farmer R. 2002. Weight and weight uniformity of hard gelatin capsules filled with microcrystalline cellulose and silicified microcrystalline cellulose. Drug Dev Ind Pharm 28:467-472.

Feng H. 2007. Modeling of vapor sorption in glassy polymers using new dual model based on multilayer sorption theory. Polymer 48:2988-3002.

Ferrari F, Bertoni M, Bonferni MC, Rossi S, Caramella C. 1996. Disintegration efficiency of several sodium carboxymethyl celluloses in paracetamol tablets. STP Pharma Sci 6:285-291.

Flores LE, Arellano RL, Diaz Esquivel JJ. 2000. Study of load capacity of Avicel PH-200 and Cellactose, two direct compression excipients, using experimental design. Drug Dev Ind Pharm 26:465-469.

Fukami J, Yonemochi E, Yoshihashi Y, Terada K. 2006. Evaluation of rapidly disintegrating tablets containing glycine and carboxymethylcellulose. Int J Pharm 310:101-109.

Gabaude CM, Gillot M, Gautier JC, Saudemon P, Chulia D. 1999. Effects of true density, compacted mass, compression speed, and punch deformation on the mean yield pressure. J Pharm Sci 88:725-730.

Garcia J and Ghaly E. 2001. Evaluation of bioadhesive glipizide spheres and compacts from spheres prepared by extruder/marumerizer technique. Pharm Dev Technol 6:407-417.

Garr JSM and Rubinstein MH. 1991. Compaction properties of a cellulose-lactose direct compression excipient. Pharm Techol Int 55:24-27.

Garratt-Reed AJ and Bell DC. 2003. Energy-dispersive X-ray Analysis in the Electron Microscope. BIOS, Oxford. 86 p.

Gonnissen Y, Goncalves SIV, Remon JP, Vervaet C. 2008. Mixture design applied to optimize a directly compressible powder produced via cospray Drying. Drug Dev Ind Pharm 34:248-257.

Gonnissen Y, Remon JP, Vervaet C. 2008. Effect of maltodextrin and superdisintegrant in directly compressible powder mixtures prepared via co-spray drying. Eur J Pharm Biopharm 68:277-282.

Gordon RE, Peck GE, Kildsig DO. 1984. A thermodynamic study of the Ac-Di-Sol-water and CLD-2-water surface interaction. Drug Dev Ind Pharm 10:833-860.

Greenspan L. 1977. Humidity fixed points of binary saturated aqueous solutions. J Res Nat Bur Stand 81A:89-96.

Guo M, Muller FX, Augsburger LL. 2002. Evaluation of the plug formation process of silicified microcrystalline cellulose. Int J Pharm 233:99-109.

Gupta P, Nachaegari SK, Bansal AK. 2006. Improved excipient functionality by coprocessing. In: Excipient Development for Pharmaceutical, Biotechnology and Drug Delivery Systems. New York: Informa Healthcare USA Inc. pp.109-127.

Gustafsson C. 2000. Solid state characterization and compaction behavior of pharmaceutical materials. Upssala (Sweden): Uppsala University, 179p.

Guyot-Hermann A and Draguet-Brughmans M. 1985. Gamma sorbitol as a diluent in tablets. Drug Dev Ind Pharm 11:551-564.

Habib YS, Abramowitz R, Jerzewski RL, Jain NB, Agharkar SN. 1999. Is silicified wet-granulated microcrystalline cellulose better than original wet-granulated microcrystalline cellulose?. Pham Dev Technol 4:431-437.

Habib Y, Augsburger L, Reier G, Wheatley T, Shangraw R. 1996. Dilution potential: A new perspective. Pham Dev Technol 1:205-212.

Hancock BC, Clas SD, Christensen K. 2000. Micro-scale measurement of the mechanical properties of compressed pharmaceutical powders. 1: The elasticity and fracture behavior of microcrystalline cellulose. Int J Pharm 209:27-35.

Harden JW, Glover D, Redding Jr BK, inventors; Method for increasing the active loading of compressible composition forms. US Pat, 6,716,453. 2004.

Hausner, HH.1967. Friction conditions in a mass of metal powder. Inter J Powder Metal 3:7-13.

He X, Secreast PJ, Amidon GE. 2007. Mechanistic study of the effect of roller compaction and lubricant on tablet mechanical strength. J Pharm Sci 96:1342-1355.

Hebeda RE, Holik DJ, Leach HW, inventors; Dextrose production with immobilized glucoamylase. US Pat, 4,132,595. 1979.

Heckel RW. 1961a. An analysis of powder compaction phenomena. Trans Metal Sci AIME 221:1001-1008.

Heckel RW. 1961b. Density-pressure relationship in powder compaction. Trans Metal Sci AIME 221:671-675.

Hedden DB, Brone DL, Clement S, McCall M, Olsofsky A, Patel PJ, Prescott J, Hancock BC. 2006. Development of an improved fluidization segregation tester for use with pharmaceutical powders. Pharm Technol 30:54-64.

Hengel VC. 2001. Stress-strain curve. In: Fibre Metal Laminate: An Introduction. Vlot, A.D., Gunnink, J.W., editors. Dordrecht, Netherlands: Kuwer Academic Publisher. pp.101-108.

Herman J, Remon JP, De Vilder J. 1989. Modified starches as hydrophilic matrices for controlled oral delivery. I. Production and characterization of thermally modified starches. Int J Pharm 56: 51-63.

Herting MG and Kleinebudde P. 2008. Studies on the reduction of tensile strength of tablets after roll compaction/dry granulation. Eur J Pharm Biopharm 70:372-379.

Hidaka A, Yasui S, Kuwata A, Takeuchi H. 2009. Improving powder flow properties of a direct compression formulation using a two-step glidant mixing process. Chem Pharm Bull 57:647-652.

Hiestand EN. 1997. Principles, tenets and notions of tablet bonding and measuring of strength. Eur J Pharm Biopharm 44:229-242.

Hiestand E, Wells J, Peot C, Ochs J. 1977. Physical processes of tableting. J Pharm Sci 66:510-518.

Hiestand H and Smith D. 1984. Indices of tableting performance. Powder Technol 38:145-159.

Hou H and Changquan CS. 2008. Quantifying effects of particulate properties on powder flow properties using a ring shear tester. J Pharm Sci 97:4030-4039.

Isogai A and Atalla R. 1998. Dissolution of cellulose in aqueous NaOH solutions. Cellulose 5:309-319.

ISP Corp. 2009. Polyplasdone, Crospovidone. Superdisintegrants for orally disintegrating and chewable tablets. ISP PH5284-I1-07/2009:1-4.

Jacob S, Shirwaikar A, Joseph A, Srinivasan K. 2007. Novel co-processed excipients of mannitol and microcrystalline cellulose for preparing fast dissolving tablets of glipizide. Indian J Pharm Sci 69:633-639.

Jahn T and Steffens KJ. 2005. Press chamber coating as external lubrication for high speed rotary presses: Lubricant spray rate optimization. Drug Dev Ind Pharm 31:951-957.

Jivraj M, Martini LG, Thomson CM. 2000. An overview of the different excipients useful for the direct compression of tablets. Pharm Sci Technol Today 3:58-63.

Jonat S. 2005. The mechanism of hydrophilic and hydrophobic colloidal silicon dioxide types as glidants. Tubingen, Germany: University of Tubingen, 165p.

Jonat S, Hasenzahl S, Drechler M, Albers P, Wagner KG, Schmidt PC. 2004. Investigation of compacted hydrophilic and hydrophobic colloidal silicon dioxides as glidants for pharmaceutical excipients. Powder Technol 141:31-43.

Jumaa H, El-Saleh F, Hassan I, Muller BW, Kleinebudde P. 2000. Influence of cellulose type on the properties of extruded pellets. Part I: Physicochemical characterization of the cellulose types after homogenization. Colloid Polym Sci 278:597-607.

Kachrimanis K, Nikolakakis I, Malamataris S. 2003. Tensile strength and disintegration of tableted silicified microcrystalline cellulose: Influences of interparticle bonding. J Pharm Sci 92:1489-1501.

Kaerger JS, Edge S, Price R. 2004. Influence of particle size and shape on flowability and compactibility of binary mixtures of paracetamol and microcrystalline cellulose. Eur J Pharm Biopharm 22:173-179.

Kawakita K and Ludde KH. 1971. Some considerations on powder compression equations. Powder Techn 4:61-68.

Kennedy T, Yaginuma Y, Hampshire S. 1996. The compression mechanism of powders. J Mater Process Eng 56:581-588.

Kiekens F, Debunne A, Vervaet C, Baert L, Vanhoutte F, Assche IV, Menard F, Remon JP. 2004. Influence of the punch diameter and curvature on the yield pressure of MCC-compacts during Heckel analysis. Eur J Pharm Sci 22:117-126.

Kim AI, Akers MJ, Nail SL. 1998. The physical state of mannitol after freeze-drying: effects of mannitol concentration, freezing rate, and a noncrystallizing cosolute. J Pharm Sci 87:931-935.

Klemm D, Philipp B, Heinze T, Heinze U. 1998a. Comprehensive Cellulose Chemistry: Functionalization of Cellulose. New York, USA: John Wiley. 389 p.

Klemm D, Philipp T, Heinze U, Wagenknecht W, editors. 1998b. Comprehensive Cellulose Chemistry: Fundamental and Analytical Methods. John Willey. pp.107-249.

Klinger R, Meuser F, Niediek E. 1986. Depolymerization of starch by high pressure extrusion. Starch/Starke 38:40-44.

Kochhar K. 1994. Slugging and recompression characterisation of some blends of pharmaceutical excipients. Int J Pharm 112:225-231.

Kolpak F and Blackwell J. 1976. Determination of the structure of cellulose II. Macromolecules 9:273-278.

Kothari SH, Kumar V, Banker GS. 2002. Comparative evaluation of powder and mechanical properties of low crystallinity celluloses, microcrystalline celluloses, and powdered celluloses. Int J Pharm 232:69-80.

Kottke MK and Rhudic EM. 2002. Tablet dosage forms. In: Modern Pharmaceutics. Rhodes CT and Banker GS, editors. New York: Marcel Dekker. pp.437-511.

Kranz H, Jürgens K, Pinier M, Siepmann J. 2009. Drug release from MCC-and carrageenan-based pellets: Experiment and theory. Eur J Pharm Biopharm 73:302-309.

Krassig H, editor. 1996. Cellulose, Structure, Accessibility and Reactivity. Asterdam: Gordon and Breach. 371 p.

Kroon-Batenburg L, Bouma B, Kroon J. 1996. Stability of cellulose structures studied by MD simulations. Could mercerized cellulose II be parallel? Macromolecules 29:5695-5699.

Krueger C, Thommes M, Kleinebudde P. 2010. MCC SANAQ burst"-A new type of cellulose and its suitability to prepare fast disintegrating pellets. J Pharm Innov 5:45-57.

Kuentz M and Leuenberger H. 2000. A new theoretical approach to tablet strength of a binary mixture consisting of a well and a poorly compactable substance. Eur J Pharm Biopharm 49:151-159.

Kuhl P and Jobst M. 2002. Tableting of pellet-matrix systems: ability of parameters from dynamic and kinetic models to eliminate the densification of matrix formers of pellets. Int J Pharm 10:101-114.

Kumar V, Reus M, Yang D. 2002. Preparation, characterization, and tabletting properties of a new cellulose-based pharmaceutical aid. Int J Pharm 235:129-140.

Lachman L, Lieberman HA, Kanig JL. 1986. The Theory and Practice of Industrial Pharmacy. 3rd ed. Philadelphia: Lea and Febiger. pp.1317-1318.

Ladin M, Ramirez-Pacheco R, Gomez-almoza JL, Souto C, Concheiro A, Rowe RC. 1993. Influence of microcrystalline cellulose source and batch variation on the tableting behavior and stability of prednisolone formulations. Int J Pharm 91:143-149.

Lahdenpaa E, Antikainen O, Yliruusi J. 2001. Direct compression with silicified and non-silicified microcrystalline cellulose: Study of some properties of powders and tablets. STP Pharm Sci 11:129-135.

Lanz M. 2005. PhD thesis. Pharmaceutical powder technology: Towards a science based understanding of the behavior of powder systems. Basel: University of Basel, 162p.

Laovachirasuwana P, Peerapattanaa J, Srijesdarukb V, Chitropasa P, Otsukac M. 2010. The physicochemical properties of a spray dried glutinous rice starch biopolymer. Colloids Surf , B 78:30-35.

Larner G, Schoneker D, Sheehan C, Uppoor R, Walsh P, Wiens R. 2006. Pharmaceutical excipient testing and control strategies. Pharm Technol 1:1-7.

Lerk C, Bolhuis G, De Boer A. 1974. Comparative evaluation of excipients for direct compression, II. Pharm Weekbl 109:945–955.

Lerk CF. 1993. Consolidation and compaction of lactose. Drug Dev. Ind. Pharm. 19:2359-2398.

Leuenberger H and Rohera BD. 1986. Fundamentals of powder compression. I. The compactibility and compressibility of pharmaceutical powders. Pharm Res 3:12-22.

Leuenberger H and V K. 2004. Comparative evaluation of the powder properties and compression behavior of a new cellulose-based direct compression excipient and Avicel PH102. J Pharm Pharmacol 56:951-956.

Levin M. 2006. Wet Granulation: End-point determination and scale-up. Encyclopedia of Pharmaceutical Technology. New York: Marcel Dekker: pp.4078-4098.

Lieberman HA, Lachman L, Schwartz JB. 1990. Pharmaceutical Dosage Forms: Tablets. New York: Marcel Dekker. 562 p.

Li X, WenYang G, Wang Y, Huang L, Liu C. 2010. Preparation and physicochemical properties of carboxymethyl *Fritillaria ussuriensis maxim*. starches. Carbohyd Polym 80:768-773.

Lide DR. 2003. CRC Handbook of Chemistry and Physics. 84th Ed. Boca Raton, USA: CRC Press LLC. 179 p.

Limwong V, Sutanthavibul N, Kulvanich P. 2004. Spherical composite particles of rice starch and microcrystalline cellulose: a new coprocessed excipient for direct compression. AAPS PharmSciTech 5:40-49.

Lin JH, Chang YH, Hsu YH. 2009. Degradation of cotton cellulose treated with hydrochloric acid either in water or in ethanol. Food Hydrocoll 23:1548-1553.

Lizuka K and Aishima T. 1999. Starch gelation process observed by FTIR/ATR spectrometry with multivariate data analysis. J Food Sci 64:653-658.

Luukkonen P. 2001. PhD thesis. Rheological properties and the state of water of microcrystalline cellulose and silicified microcrystalline cellulose wet masses. Helsinki, Finland: University of Helsinki, 190p.

Majuru S, Wurster DE. 1997. The effect of composition on the tableting indices of binary mixtures. Pharm Dev Technol 2:313-321.

Marais AF, Song M, Villiers MM. 2003. Effect of compression force, humidity and disintegrant concentration on the disintegration and dissolution of directly compressed furosemide tablets using crosscarmellose sodium as disintegrant. Trop J Pharm Res 2:125-135.

Martin A, Bustamante P, Chun, ACH. 1993. Physical pharmacy. Physical Chemical Principles in the Pharmaceutical Sciences. Philadelphia: Lean & Febiger. pp.426-430.

Martinez-Pacheco R, Gomez Amoza JL, Vil-Jato JL. 1987. Los modelos de compresion: su utilidad en la obtencion de comprimidos. Cienc Ind Farm 6:13-20.

Marwaha M, Sandhu D, Marwaha R. 2010. Coprocessing of excipients: A review on excipient development for improved tableting performance. Int J Appl Pharm 2:41-47.

Massimo G, Catellani PL, Santi P, Bettini R, Vaona G, Bonfanti A, Maggi L, Colombo P. 2000. Disintegration propensity of tablets evaluated by means of disintegrating force kinetics. Pharm Dev Technol 5:163-169.

Master K, editor. 1991. Spray drying Handbook. 5th ed. New York: Longman. 725 p.

Mattson S, Bredenberg C, Nystronm C. 2001. Formulation of high tensile strength rapidly disntegrating tablets. Evaluation of some binder properties. STP Pharm Sci 11:211-220.

Maury M, Murphy K, Kumar S, Shi L, Lee G. 2005. Effect of process variables on the powder yield of spray-dried trehalose on a laboratory spray-drier. Eur J Pharm Biopharm 59:565-573.

McCormick D. 2005. Evolutions in direct compression. Pharm Technol 1:52-62.

Meyer V, editor. 2006. Annual Book of American Society of Testing and Materials. Section 6. Paints Related Coatings and Aromatics. West Conshhocken, PA: ASTM International. 403 p.

Miao S and Ross Y. 2005. Crystallization kinetics and X-rays diffraction of crystals formed in amorphous lactose, trehalose and lactose/trehalose mixtures. J Food Sci 70:350-358.

Michrafy A, Michrafy M, Kadiri MS, Dodd JA. 2007. Predictions of tensile strength of binary tablets using linear and power law mixing rules. Int J Pharm 333:118-126.

Mihranyan A, Edsman K, Strømme M. 2007. Rheological properties of cellulose hydrogels prepared from *Cladophora* cellulose powder. Food Hydrocoll 21:267-272.

Mishra DN, Bindal M, Singh SK, Vijaya Kumar SG. 2006. Spray dried excipient base: A novel technique for the formulation of orally disintegrating tablets. Chem Pharm Bull 54:99-102.

Mitrevej A, Faroongsarng D, Sinchaipanid N. 1996. Compression behavior of spray dried rice starch. Int J Pharm 140:61-68.

Mitrevej A, Sinchaipanid N, Faroongsarng D. 1996. Spray-dried rice starch: comparative evaluation of direct compression fillers. Drug Dev Ind Pharm 22: 587-594.

Mittal KL, editor. 2008. Contact angle, Wettability and Adhesion. Leiden, Netherlands: Brill Academic. 300 p.

Miyazaki T, Sivaprakasam K, Tantry J, Suryanarayanan R. 2009. Physical characterization of dibasic calcium phosphate dihydrate and anhydrate. J Pharm Sci 98:905-916.

Modliszewski JJ and Ballard DA, inventors; Coprocessed galactomannan-glucomannan. US Pat 5,498,436. 1996.

Moreton R. 1996. Tablet excipients to the year 2001: A look into the crystal ball. Drug Dev Ind Pharm 22:11-23.

Moreton RC. 2008. Disintegrants in tableting. In: Pharmaceutical Dosage Forms:Tablets. Ausburger L and Hoag S, editors. 3rd ed. New York: Informa Healthcare. pp. 217-250.

Mullarney MP, Hancock BC, Carlson GT, Ladipo DD, Langdon BA. 2003. The powder flow and compact mechanical properties of sucrose and three high-intensity sweeteners used in chewable tablets. Int J Pharm 257:227-236.

Muzikova J and Novakova P. 2007. A study of the properties of compacts from silicified microcrystalline celluloses. Drug Dev Ind Pharm 33:775-781.

Muzikova J and Balharkova J. 2008. A study of the properties of tablets made of directly compressible maltose. Ceska Slov Farm 57:21-27.

Nachaegari SK and Bansal AK. 2004. Coprocessed excipients for solid dosage forms. Pharm Technol 28:52-65.

Nada AAMA, El-Kady MY, El-Sayed ESA, Amine FM. 2009. Preparation and characterization of microcrystalline cellulose (MCC). BioResources 4:1359-1371.

Narayan P and Hancock B. 2003. The relationship between the particle properties, mechanical behavior, and surface roughness of some pharmaceutical excipient compacts. Mater Sci Eng , A 355:24-36.

Nehete P, Shah N, Ramamurthy V, Kothari R. 1992. An optimized protocol for the production of high purity maltose. World J Microb Biot 8:446-450.

Nicklasson F, Johansson B, Alderborn G. 1999. Tabletting behaviour of pellets of a series of porosities-a comparison between pellets of two different compositions. Eur J Pharm Sci 8:11-17.

Nilsson M, Mihranyan A, Valizadeh S, Stromme M. 2006. Mesopore structure of microcrystalline cellulose tablets characterized by nitrogen adsorption and SEM: The influence on water-induced ionic conduction. J Phys Chem B 110:15776-15781.

Nanochemistry from Renewable Biomaterial for Various Applications [Internet]. Aalto, Finland; c2010 [cited 2009 05/09]. Available from: http://www.umk.fi/en/newsletter_Newsletter_0207_Paakko_more.htmL.

Olmo IG and Ghaly ES. 1999. Compressional characterization of two dextrose-based directly compressible excipients using an instrumented tablet press. Pharm Dev Technol 4:221-231.

Parker, M.E, Bronlund JE, Mawson. 2006. Moisture sorption isotherms for paper and paperboard in food chain conditions. Packag Technol Sci 19:193-209.

Parikh D, Thibodeaux D, Condon B. 2007. X-ray crystallinity of bleached and crosslinked cottons. Text Res J 77:612.

Patel S, Kaushal AM, Bansal AK. 2007. Effect of particle size and compression force on compaction behavior and derived mathematical parameters of compressibility. Pharm Res 24:111-124.

Direct compression (DC) [Internet]. Netherlands: DOMO; c2010 [cited 2009 06/23]. Available from: www.lactose.com/.../direct_compression.htmL.

Pedersen PV and Myrick JW. 1978. Versatile kinetic approach to analysis of dissolution data. J Pharm Sci 67:1450-1455.

Peppas NA. 1985. Analysis of Fickian and non-Fickian drug release from polymers. Pharm Acta Helv 60:110-111.

Picker K. 2000. A new theorical model to characterize the densification behavior of tableting materials. Eur J Pharm Biopharm 49:267-273.

Picker KM. 2004. The 3D model: explaining densification and deformation mechanisms by using 3D parameter plots. Drug Dev Ind Pharm 30:413-425.

Pisecky J, editor. 1997. Handbook of Milk Powder Manufacture. Denmark: Soeborg Niro A.S. 580 p.

Plaizier-vercammen JA and Van den Bossche H. 1992. Evaluation of the tableting properties of a new excipient for direct compression. Die Pharma 54:973-977.

Podczeck F, Knight P, Newton J. 2008. The evaluation of modified microcrystalline cellulose for the preparation of pellets with high drug loading by extrusion/spheronization. Int J Pharm 350:145-154.

Portmann C, Ziolko T, Wiprachtiger A, Kleinhan S, Schonenberger G., editors. 2007. The Laboratory Assistant. Switzerland: Buchi Labortechnik. pp.68-87.

Pourkavoos N and Peck GE. 1994. Effect of aqueous film coating conditions on water removal efficiency and physical properties of coated tablet ores containing superdisintegrants. Drug Dev Ind Pharm 20:1535-1554.

Pourkavoos N and Peck GE. 1993. The effect of swelling characteristics of superdisintegrants on the aqueous coating solution penetration into the tablet matrix during the film coating process. Pharm Res 10:1363-1371.

Pushpadars H, Marx D, Hanna M. 2008. Effect of extrusion temperature and plasticizer on the physical and functional properties of starch films. Starch 60:527-538.

Quadir A and Kolter K. 2006. A comparative study of current superdisintegrants. PharmTech 10:1-4.

Qui Rijns EJ, Van Boxtel AJB, Van Loon WKO, Van Straten G. 2005. Sorption isotherms, GAB parameters and isosteric heat of sorption. J Sci Food Agri 85:1805-1814.

Rabek JF. 1980. Experimental Methods in Polymer Chemistry. Bristol, UK: John Wiley. 861 p.

Rahmouni M, Lenaerts V, Massuelle D, Doelker E, Leroux JC. 2002. Influence of physical parameters and lubricants on the compaction properties of granulated and non-granulated cross-linked high amylose starch. Chem Pharm Bull 50:1155-1162.

Rashid I, Al-Remawi M, Eftaiha A, Badwan A. 2008. Chitin-silicon dioxide coprecipitate as a novel superdisintegrant. J Pharm Sci 97:4955-4969.

Rasmussen KE and Albrechtsen J. 1974. Glutaraldehyde. The influence of pH, temperature, and buffering on the polymerization rate. Histochem Cell Biol 38:19-26.

Rees JE and Rue PJ. 1978. Time-dependent deformation of some direct compression excipients. J Pharm Pharmacol 30:601-607.

Reiff F, Hartner H, Basedow A, Hugenbusch HW, Schmidt PC, Bardonner H, inventors; Sorbitol, process for its preparation, and use thereof. US Pat 4,605,794. 1986.

Reimerdes D. 1993. The near future of tablet excipients. Manuf Chem 64:14-15.

Reimerdes D and Aufmuth KP. 1992. Tableting with coprocessed lactose-cellulose excipients. Manuf Chem 63:21-24.

Reus M. 2005. PhD thesis. Preparation, characterization and tableting properties of cellulose II powders. Iowa City: The University of Iowa, 335p.

Reus M and Kumar V. 2007. Modified cellulose II powder: Preparation, characterization, and tableting properties. J Pharm Sci 96:408-420.

Ritger P, Peppas N. 1987. A simple Fickian equation for description of solute release. I. Fickian and non-Fickian release from non-swellable devices in the form of slabs, spheres, cylinders or discs. J Controlled Rel 5:23-26.

Roberts RJ and Rowe RC. 1986. The effect of the relationship between punch velocity and particle size on the compaction behavior of materials with varying deformation mechanisms. J Pharm Pharmacol 38:567-571.

Rowe RC and Roberts RJ. 1995. Mechanical properties. In: Pharmaceutical Powder Compaction Technology. Alderborn G and C. Nystrom C, editors. New York: Marcel Dekker, Inc. pp. 283-402.

Saha S and Shahiwala AF. 2009. Multifunctional coprocessed excipients for improved tabletting performance. Expert Opin Drug Deliv 6:197-208.

Saigal N, Baboota S, Ahuja A, Ali J. 2009. Microcrystalline cellulose as a versatile excipient in drug research. J Young Pharmacists 1:6.

Sadeghnejad GR, York P, Stanley-Wooda NG. 1986. Water vapor interaction with pharmaceutical cellulose powders. Drug Dev Ind Pharm 12:2171-21192.

Schmidt PC and Rubensdörfer CJW. 1994. Evaluation of Ludipress as a "multipurpose excipient" for direct compression: Part I: Powder characteristics and tableting properties. Drug Dev Ind Pharm 20:2899-2925.

Schwarz E, Fitchner V, Irlinger B, Haeusler O. 2006. Influence of lubricants on the tableting and disintegration times of tablets made up of coprocessed excipients vs the physical blends Roquette-Pharma:1-2.

Sebhatu T, Elamin AA, Ahlneck C. 1994. Effect of moisture sorption on tabletting characteristics of spray dried (15% amorphous) lactose. Pharm Res 11:1233-1238.

Sekar V and Chellan VR. 2008. Immediate release tablets of telmisartan using superdisintegrant- formulation, evaluation and stability studies. Chem Pharm Bull 56:575-577.

Shangraw R, Mitrevej A, Shah M, Niazi S, editors. 1979. Textbook of Biopharmaceutics and Clinical Pharmacokinetics. 1st ed. New York: Appleton-Century-Crofts. 332 p.

Shangraw R and Demarest D. 1993. A survey of current industrial practices in the formulation and manufacture of tablets and capsules. Pharm Technol 17:32-33.

Sherwood B and Becker J. 1998. A new class of high-functionality excipients: Silicified microcrystalline cellulose. Pharm Technol 22:78-88.

Sherwood BE, Staniforth JH, Hunter EA, inventors; Pharmaceutical excipient having improved compresibility. US Pat 5,725,883. 2004.

Shlantha S and Milosovich G. 1964. Compression of pharmaceutical powders I. J Pharm Sci 53:562-564.

Siepmanna J, Peppas NA. 2001. Modeling of drug release from delivery systems based on hydroxypropyl methylcellulose (HPMC). Adv Drug Del Rev. 48:139-157.

Sindhu M, Brahmakumar T, Abraham E. 2006. Microstructural imaging and characterization of the mechanical, chemical, thermal and swelling properties of starch-chitosan blend films. Biopolymers 82:176-187.

Singh N, Belton P, Georget D. 2009. The effects of iodine on kidney beans starch: film and plastic properties. Int J Pharm 45:116-119.

Skinner GW. 1998. Correlating the ejection force of tablets with the toughness of binders in the solid dosage forms. Aqualon PTR-009:1-9.

Soh Lay Peng J. 2006. PhD thesis. Preformulation studies on microcrystalline cellulose for grouping and predicting their preformance in extrusion-spheronization. Singapur: National University of Singapur, 248p.

Soh JLP, Yang L, Liew CV, Cui FD, Heng PWS. 2008. Importance of small pores in microcrystalline cellulose for controlling water distribution during extrusion-spheronization. AAPS PharmSciTech 9:972-981.

Stout P, Howard S, Mouger J. 1991. Dissolution of pharmaceutical suspensions. In: Encyclopedia of Pharmaceutical Technology. Swarbrick J and Boylan J, editors. New York, USA: Marcel Dekker. pp.169-192.

Steele DF, Edge S, Tobyn MJ, Moreton RC, Staniforth N. 2003. Adsorption of an amine drug onto microcrystalline cellulose and silicified microcrystalline cellulose samples. Drug Dev Ind Pharm 29:475-487.

Sun CC and Himmelspach MW. 2005. Reduced tabletability of roller compacted granules as a result of granule size enlargement. J Pharm Sci 95:200-206.

Szepes A, Fiebig A, Ulrich J, Szabó-Révész P. 2007. Structural study of alpha lactose monohydrate subjected to microwave irradiation. J Therm Anal Calorim 89:757-760.

Taylor MK, Ginsburg J, Hickey AJ, Gheyas F. 2000. Composite method to quantify powder flow as a screening method in early tablet or capsule formulation development. AAPS PharmSciTech 1:1-11.

Te Wierik G, Bergsma J, Arends-Scholte A, Boersma T, Eissens A, Lerk C. 1996. A new generation of starch products as excipient in pharmaceutical tablets. I. Preparation and binding properties of high surface area potato starch products. Int J Pharm 134:27-36.

Tho I, Sande SA, Kleinebudde P. 2002. Pectinic acid, a novel excipient for production of pellets by extrusion/spheronization: Preliminary studies. Eur J Pharm Biopharm 54:95-99.

Thoorens G, Leclercq B, Carlin B, Riley P, Garcia M, It P, inventors; Dry granulation binders, products, and use thereof. WO/2008/057266. 2008.

Troy DV and Hauber MJ, editors. 2005. Remington, the Science and Practice of Pharmacy. 21st ed. Washington D.C.: Lippincott Williams and Wilkins. pp. 893.

Uhumwangho MU and Okor RS. 2005. Effect of humidity on the disintegrant property of alpha cellulose. Acta Pol Pharm 62:39.

US Pharmacopoeia. 2005. General chapters: Disintegration, loss on drying, viscosity and friability. In: USP. Rockville, MD: USP28-NF23. pp.2411-2748.

Van den Berg C. 1984. Description of water activity of foods for engineering purposes by means of the GAB model of sorption. In B.M. McKenna, Engineering and foods. New York: Elsevier. pp. 119-131.

Van der Voort Maarschalk, K., Vromans H, Groenendijk W, Bolhuis GK, Lerk CF. 1997. Effect of water on deformation and bonding of pregelatinized starch compacts. Eur J Pharm Biopharm 44:253-260.

Van Veen B, Bolhuis GK, Wu YS, Zuurman K, Frijlink HW. 2005. Compaction mechanism and tablet strength of unlubricated and lubricated (silicified) microcrystalline cellulose. Eur J Pharm Biopharm 59:133-138.

Vehring R. 2008. Pharmaceutical particle engineering via spray drying. Pharm Res 25:999-1022.

Vehring R, Foss WR, Lechuga-Ballesteros D. 2007. Particle formation in spray drying. J Aerosol Sci 38:728-746.

Vidal P, Basora N, Overend R, Chornet E. 1991. A pseudouniversal calibration procedure for the molecular weight determination of cellulose. J Appl Polym Sci 42:1659-1664.

Vromans H and Lerk C. 1988. Densification properties and compactibility of mixtures of pharmaceutical excipients with and without magnesium stearate. Int J Pharm 46:183-192.

Vromans H, Bolhuis G, Lerk C, Van de Biggelaar H, Bosch H. 1987. Studies on tableting properties of lactose. VII: The effect of variations in primary particle size and

percentage of amorphous lactose in spray dried lactose products. Int J Pharm 35:29-37.

Vromans H, Bolhuis GK, Lerk CF, Kussendrager KD. 1986. Studies on tableting properties of lactose. VI. Consolidation and compaction of spray-dried amorphous lactose. Acta Pharm Suec 23:231-240.

Wang R and Wunder SL. 2000. Effects of silanol density, distribution, and hydration state of fumed silica on the formation of self-assembled monolayers of *n*-octadecyltrichlorosilane. Langmuir, 16: 5008-5016.

Weibull W. 1951. Dissolution of fludrocortisone from phospholipid coprecipitates. J Applied Mech 18: 293-297.

Westermarck S, Juppo AM, Kervinen L, Yliruusi J. 1999. Microcrystalline cellulose and its microstructure in pharmaceutical processing. Eur J Pharm Biopharm 48:199-206.

Whiteman M and Yarwood R. 1988. The evaluation of six lactose-based materials as direct compression tablet excipients. Drug Dev Ind Pharm 14:1023-1040.

Williams RO, Sriwongjanya M, Barron MK. 1997. Compaction properties of microcrystalline cellulose using tableting indices. Drug Dev Ind Pharm 23:695-704.

Wong LW and Pilpel N. 1990. The effect of particle shape on the mechanical properties of powders. Int J Pharm 59:145-154.

World Health Organization expert committee. 1974. WHO Food Additives Series No. 5. Wld Hlth Org Techn Rep Ser 53.

Xiang Q, Lee YY, Pettersson PO, Torget RW. 2003. Heterogeneous aspects of acid hydrolysis of α-cellulose. Appl Biochem Biotechnol 107:505-514.

Yamashiro M, Yuasa Y, Kawakita K. 1983. An experimental study on the relationships between compressibility, fluidity and cohesion of powder solids at small tapping numbers. Powder Technol 34:225-231.

York P. 1992. Crystal engineering and particle design for the powder compaction process. Drug Dev Ind Pharm 18:677-721.

Young PM, Edge S, Staniforth JN, Steele DF, Price R. 2005. Dynamic vapor sorption properties of sodium starch glycolate disintegrants. Pharm Dev Technol 10:249-259.

Yoshinari T, Forbes RT, York P, Kawashima Y. 2003. The improved compaction properties of mannitol after a moisture-induced polymorphic transition. Int J Pharm 258:121-131.

Yu L, Milton N, Groleau EG, Mishra DS, Vansickle RE. 1999. Existence of a mannitol hydrate during freeze-drying and practical implications. J Pharm Sci 88:196-198.

Zeleznik JA and Renak J. 2005. High functionality excipients (HFE)-ProSolv SMCC as an effective strategy for generic drug formulation. Tech Serv:1-4.

Zhang Y, Law Y, Chakrabarti S. 2003. Physical properties and compact analysis of commonly used direct compression binders. AAPS PharmSciTech 4:1-11.

Zhao N and Augsburger LL. 2006. The influence of product brand-to-brand variability on superdisintegrant performance: A case study with croscarmellose sodium. Pharm Dev Technol 11:179-185.

Zhao N and Augsburger LL. 2005. The influence of swelling capacity of superdisintegrants in different pH media on the dissolution of hydrochlorothiazide from directly compressed tablets. AAPS PharmSciTech 6:E120-E126.

Zhbankov RG, editor. 1964. Infrared Spectra of Cellulose and its Derivatives. New York: Consultants Bureau. 333 p.

Zimm KR, Schwartz JB, O'Connor RE. 1996. Drug release from a multiparticulate pellet system. Pharm Dev Technol 1:37-42.

Zografi G, Kontny MJ, Yang I, Brenner GS. 1984. Surface area and water vapor sorption of microcrystalline cellulose *Int* J Pharm 18: 99-116.